NUMERICAL SOLUTION OF PARTIAL DIFFERENTIAL EQUATIONS FOR LID-DRIVEN FLUID FLOW AND HEAT TRANSFER ANALYSIS WITH NO-SLIP AND FREE-SLIP EFFECTS

WONG HON FEI

FACULTY OF SCIENCE
UNIVERSITI MALAYA
KUALA LUMPUR

2021

Universiti Malaya

NUMERICAL SOLUTION OF PARTIAL DIFFERENTIAL EQUATIONS FOR LID-DRIVEN FLUID FLOW AND HEAT TRANSFER ANALYSIS WITH NO-SLIP AND FREE-SLIP EFFECTS

WONG HON FEI

THESIS SUBMITTED IN FULFILMENT OF THE REQUIREMENTS FOR THE DEGREE OF DOCTOR OF PHILOSOPHY

INSTITUTE OF MATHEMATICAL SCIENCES
FACULTY OF SCIENCE
UNIVERSITI MALAYA
KUALA LUMPUR

2021

Universiti Malaya

UNIVERSITI MALAYA

ORIGINAL LITERARY WORK DECLARATION

Name of Candidate: **WONG HON FEI**

Matric No: **SHB160001**

Name of Degree: **Doctor of Philosophy**

Title of Project Paper/Research Report/Dissertation/Thesis ("this Work"):

NUMERICAL SOLUTION OF PARTIAL DIFFERENTIAL EQUATIONS FOR LID-DRIVEN FLUID FLOW AND HEAT TRANSFER ANALYSIS WITH NO-SLIP AND FREE-SLIP EFFECTS

Field of Study: **FLUID MECHANICS**

I do solemnly and sincerely declare that:

(1) I am the sole author/writer of this Work;
(2) This Work is original;
(3) Any use of any work in which copyright exists was done by way of fair dealing and for permitted purposes and any excerpt or extract from, or reference to or reproduction of any copyright work has been disclosed expressly and sufficiently and the title of the Work and its authorship have been acknowledged in this Work;
(4) I do not have any actual knowledge nor do I ought reasonably to know that the making of this work constitutes an infringement of any copyright work;
(5) I hereby assign all and every rights in the copyright to this Work to the University of Malaya ("UM"), who henceforth shall be owner of the copyright in this Work and that any reproduction or use in any form or by any means whatsoever is prohibited without the written consent of UM having been first had and obtained;
(6) I am fully aware that if in the course of making this Work I have infringed any copyright whether intentionally or otherwise, I may be subject to legal action or any other action as may be determined by UM.

Candidate"s Signature Date: 13-7-2021

Subscribed and solemnly declared before,

Witness"s Signature Date: 13.07.2021

Name:

Designation:

University of Malaya

NUMERICAL SOLUTION OF PARTIAL DIFFERENTIAL EQUATIONS FOR LID-DRIVEN FLUID FLOW AND HEAT TRANSFER ANALYSIS WITH NO-SLIP AND FREE-SLIP EFFECTS

ABSTRACT

Thermal fluid is a branch of science and engineering that covers the application of experimental research and mathematical modeling based on fundamental laws from physics, heat transfer and fluid dynamics. The great significance of thermal fluids can be seen in phase transition and chemical reactions. Perhaps two-dimensional lid-driven model is the simplest model to demonstrate the study of the thermal fluids. The behavior of fluid that filled inside the lid-driven cavity when subject to different boundary conditions (free-slip and no-slip), different aspect ratios and different steady-state criteria are studied extensively. The partial differential equations of time-dependent vorticity-stream function and thermal energy equation are discretized and solved using finite difference method. All the codes were written and solved inside Matlab® environment and the results were verified using commercial engineering simulation software named Ansys Fluent®. For the first study, an analysis of time dependent stream-function of fluid to identify patterns of forming, merging and unmerging of additional eddy is presented when steady-state condition with different criteria are achieved. Due to numerical error, it is also observed that the value of stream function begins to drop and streamline distribution changes shape after achieving steady-state criterion of $e \leq 10^{-6}$. Also, damage of merging and formation of additional eddy happens until the free-slip boundary condition effect passes the threshold value. For the second study, the iteration process focuses on dissipation of viscous-heating through a transient conduction process of the entire liquid filled inside the lid-driven

cavity. The time–dependent fluid flow and heat transfer with viscous heating process are depicted by contour plot and image plot inside Matlab® environment. For the third study, Robin boundary condition is adopted rather than Neumann boundary condition which employed in the second study. Moreover, heat transfer analysis is extended to cooling process in the third study. The effects of viscous heating coupled with several other physical parameters, namely Reynolds, Prandtl, Peclet and other numbers are examined. Finally, a simple graphical user interface is developed using Matlab® to facilitate the end user in analyzing the fluid flow.

Keywords: Lid-driven, free-slip, vorticity-stream function, viscous heating, finite difference method.

Universiti Malaya

PENYELESAIAN BERANGKA PERSAMAAN TERBITAN SEPARA BAGI ALIRAN BENDALIR PEMANDUAN TERTUTUP DAN ANALISIS PEMINDAHAN HABA DENGAN KESAN TANPA TERGELINCIR DAN TERGELINCIR

ABSTRAK

Bendalir terma ialah cabangan sains dan kejuruteraan yang meliputi aplikasi penyelidikan eksperimen dan pemodelan matematik berdasarkan hukum-hukum asas dari fizik, pemindahan haba dan dinamik bendalir. Kepentingan yang nyata dalam bendalir terma dapat dipantau dalam peralihan fasa dan tindak balas kimia. Model aliran berongga dalam pemanduan tertutup dua dimensi mungkin adalah model paling mudah untuk menunjukkan kajian bendalir terma. Tingkah laku bendalir yang diisi di dalam pemanduan rongga tertutup apabila tertakluk kepada keadaan sempadan yang berbeza (keadaan tergelincir dan bebas daripada keadaan tergelincir), nisbah aspek yang berbeza dan kriteria keadaan mantap yang berbeza dikaji secara terperinci. Persamaan pembezaan separa daripada fungsi aliran-kepusaran yang bergantung pada masa dan persamaan tenaga terma yang terasing dan diselesaikan menggunakan kaedah pembezaan terhingga. Semua kod telah ditulis dan diselesaikan di dalam persekitaran Matlab® dan keputusannya disahkan dengan menggunakan perisian ringan simulasi kejuruteraan komersial yang bernama Ansys Fluent®. Untuk kajian pertama, analisis aliran masa fungsi arus untuk mengenalpasti corak pembentukan, penggabungan dan perpecahan olakan tambahan ditunjukkan apabila keadaan mantap dengan kriteria yang berbeza dicapai. Disebabkan ralat yang terhasil daripada kaedah berangka, juga dapat diperhatikan bahawa nilai fungsi arus mula dijatuhkan dan perubahan bentuk

Universiti Malaya

pengedaran garis aliran selepas mencapai kriteria keadaan mantap pada $e \leq 10^{-6}$. Juga, kerosakan penggabungan dan pembentukan olakan tambahan berlaku sehingga kesan bebas daripada keadaan tergelincir melampaui nilai ambang. Untuk kajian kedua, proses lelaran menumpukan kepada pelesapan haba daripada proses pemanasan kelikatan bendalir melalui proses pemindahan haba sementara bagi keseluruhan bendalir yang diisi di dalam rongga pemanduan tertutup. Aliran bendalir yang bergantung pada masa dan pemindahan haba dengan proses pemanasan kelikatan bendalir dapat ditunjukkan dengan plot kontur dan plot imej di dalam persekitaran Matlab®. Untuk kajian ketiga, keadaan sempadan Robin diterima pakai dan bukannya keadaan sempadan Neumann seperti yang digunakan dalam kajian kedua. Malahan, analysis pemindahan haba dilanjutkan ke proses penyejukan dalam kajian ketiga. Pemanasan kelikatan bendalir digabungkan dengan beberapa parameter fizikal yang lain, iaitu nombor Reynolds, Prandtl, Peclet dan nombor yang lain-lain turut diperiksa. Akhirnya, antara muka pengguna grafik mudah dibangunkan dengan menggunakan Matlab® untuk memudahkan pengguna dalam menganalisis aliran bendalir.

Kata-kata kunci: Pemanduan tertutup, bebas daripada keadaan tergelincir, fungsi aliran-kepusaran, pemanasan kelikatan, kaedah pembezaan terhingga.

Universiti Malaya

ACKNOWLEDGEMENTS

First and foremost, I would like to extend my deepest gratitude and appreciation to my supervisor, Dr. Noor Fadiya Binti Mohd Noor for her invaluable generosity and kindness for giving me a lot of chance and guidance to contribute my energy to this project and complete this project.

Secondly, I would like to express my special thanks to Malaysian Rubber Board (MRB) especially my head of department of UKRP, Dr. Nazirah bt Ahmad for her consistent encouragement, assistance, helpful advice and guidance throughout this project.

I am also very grateful to other MRB‟s members, Dr. Marina Fernando (based in Tun Abdul Razak Research Centre, UK) and Dr. Julia Gough who had contributed their dedication in this project so that I could contribute the ample knowledge and effort in this project.

Finally, I would like to express my thankfulness to my former physics teacher, Mr. Moay Choo Hwa as he has triggered my interest in learning physics when I was in secondary school. Last but not the least, the continual encouragement, constant support and profound concern of my dearest family and all my friends are deeply and sincerely appreciated.

Universiti Malaya

TABLE OF CONTENTS

ABSTRACT iii

ABSTRAK v

ACKNOWLEDGEMENT vii

LIST OF FIGURES xi

LISF OF TABLES xvi

LIST OF ABBREVIATIONS xviii

LIST OF SYMBOLS xviii

CHAPTER 1: INTRODUCTION 1

1.1 Introduction 1

1.2 Background of Problem 2

1.3 Statement of the Problems 4

1.4 Objectives of Study 5

1.5 Importance of the Study 5

1.6 Scope of the Study 6

1.7 Organization of Thesis 7

CHAPTER 2: LITERATURE REVIEWS 9

2.1 A Review of Lid-driven Model 9

2.2 Viscous Heating and Other Effects 11

2.3 Derivation of Navier-Stoke Equations 15

2.3.1 Conservation of Mass 16

2.3.2 The Material Derivative 18

2.3.3 Description of Forces Acting on the Differential Element 20

2.3.4 Viscous Flow (Stress-Deformation Relationship) 24

2.4 Analytical and Numerical Solution 27

Universiti Malaya

2.4.1 Method of Separation of Variables 27

2.4.2 Finite Difference Method 28

2.5 Solution of NSEs by Other Authors 31

2.6 Lid-driven Trapezoidal Cavity Model 34

2.7 Implementation of FDM in Other Applications 36

2.8 Summary of Literature Reviews 40

CHAPTER 3: METHODOLOGY 42

3.1 Overview 42

3.2 Methodology Process 44

3.3 Derivation of Vorticity-stream Function 45

3.4 Numerical Method in Solving Vorticity Stream Function Equation 53

3.5 Lid-driven in 2D Fluid Flow Analysis 59

3.5.1 Discretization of BCs for Lid-driven Cavity 62

3.5.2 Discretization of free-slip BCs for Lid-driven Cavity 68

3.6 Lid-driven in 2D Thermal Analysis 71

3.6.1 Thermal Analysis with Neumann BC 72

3.6.2 Thermal Analysis with Robin BC 75

3.7 Stability Criteria Analysis 79

3.8 Derivation and Discretization of non-Newtonian Governing Equations 81

3.8.1 Discretization of non-Newtonian Governing Equations 93

3.8.2 Discretization Using Implicit FDM 100

3.9 Boundary Layer Model (Non-Newtonian Model) 107

3.10 Programming on Lid-driven Model 109

3.11 Graphical User Interface 112

3.12 Comparison with Finite Element Analysis Result 129

Universiti Malaya

CHAPTER 4: RESULTS AND DISCUSSIONS 133

4.1 Different BCs and Different AR in Different Steady-state Criterion 133

4.2 Lid-driven Cavity Fluid Subject to Neumann BC 148

4.3 Lid-driven Cavity Fluid Subject to Robin BC 162

CHAPTER 5: CONCLUSION & RECOMMENDATIONS 173

5.1 Conclusion 173

5.2 Recommendations 175

REFERENCES 178

LIST OF PUBLICATIONS AND PAPERS PRESENTED 185

Universiti Malaya

LIST OF FIGURES

Figure 2.1 : Differential element for the development of conservation of mass equation 17

Figure 2.2 : Velocity and position of particle *A* at time *t* 19

Figure 2.3 : Component of force acting on an arbitrary differential area 21

Figure 2.4 : Normal and shear stresses 22

Figure 2.5 : Surface forces in the *x*-direction acting on a fluid element 22

Figure 2.6 : Nodal network and finite difference approximation 29

Figure 2.7 : Alternating direction implicit method 32

Figure 2.8 : Trapezoidal lid-driven model 34

Figure 2.9 : Application of finite difference method 41

Figure 3.1 : Methodology flow chart 43

Figure 3.2 : Two-dimensional flow field 46

Figure 3.3 : Rotational fluid particle 46

Figure 3.4 : Angular velocity 47

Figure 3.5 : Grid used for the finite-difference solution 54

Figure 3.6 : Finite difference in explicit form 57

Figure 3.7 : Lid-driven in two-dimensional analysis 60

Figure 3.8 : Schematic drawing of lid-driven in two-dimensional fluid flow analysis 61

Figure 3.9 : Lid-driven in two-dimensional analysis 61

Figure 3.10 : Boundary condition at the bottom 62

Figure 3.11 : No-slip boundary condition 63

Figure 3.12 : Boundary condition at the top 64

Figure 3.13 : Boundary condition at the left 65

Universiti Malaya

Figure 3.14 : No-slip boundary condition on the left wall 66

Figure 3.15 : Boundary condition at four sides 67

Figure 3.16 : Boundary condition of stream function, ψ 68

Figure 3.17 : Free-slip boundary condition 69

Figure 3.18 : Schematic drawing of lid-driven flow in two-dimensional with Neumann boundary condition..... 73

Figure 3.19 : Schematic drawing of Neumann boundary condition 74

Figure 3.20 : Schematic drawing of lid-driven in two-dimensional with Robin .... boundary condition..... 75

Figure 3.21 : Energy balance method use for third kind of boundary condition..... 76

Figure 3.22 : 4×4 grids system 93

Figure 3.23 : Computational solution strategy 110

Figure 3.24 : Graphical user interface 113

Figure 3.25 : Input panel 115

Figure 3.26 : Error message on entering negative numeric data 117

Figure 3.27 : Error message on entering invalid or empty input 117

Figure 3.28 : Schematic drawing of nodes 118

Figure 3.29 : Allow for data entry in number of nodes" column 119

Figure 3.30 : Minimum value of number of nodes 119

Figure 3.31 : Error dialog box (non-integer input) 119

Figure 3.32 : Sequence of data entry..... 121

Figure 3.33 : Warning dialog box (maximum time increment)..... 122

Figure 3.34 : Warning dialog box (adjusted total time) 122

Figure 3.35 : Sequence to push button 123

Figure 3.36 : Error dialog box (plot button) 124

Universiti Malaya

Figure 3.37 : Flow status as insufficient input 124

Figure 3.38 : Flow status: Ready to flow 125

Figure 3.39 : Plot button 125

Figure 3.40 : Radio button 125

Figure 3.41 : Contour plot of stream function distribution 126

Figure 3.42 : Contour plot of *u*- and *v*-velocity distribution 127

Figure 3.43 : Velocity vector distribution 127

Figure 3.44 : Computational time and percentage of completion 128

Figure 3.45 : Simulation is running 128

Figure 3.46 : Result panel 129

Figure 3.47 : Finite element model 130

Figure 3.48 : Meshing with about 1000 elements 130

Figure 3.49 : Quadrilateral meshing 132

Figure 4.1 : Comparison of contour plot at steady-state condition (a) *u*-velocity distribution via FDM (in-house Matlab® code) (b) *u*-velocity distribution via FEM (Ansys Fluent®) (c) *v*-velocity distribution via FDM (in-house Matlab® code) (d) *v*-velocity distribution via FEM (Ansys Fluent®) 136

Figure 4.2 : Contour plot of stream function distribution 137

Figure 4.3 : Contour plot of streamline distribution at steady-state condition (free-slip BC) 138

Figure 4.4 : Contour plot of evolution of *u*- and *v*-velocity distribution at steady-state condition (free-slip BC) 139

Figure 4.5 : Contour plot of evolution of streamline distribution at (a) t = 5.50 s (b) t = 24.90 s (c) t= 51.60 s (d) t = 65.60 s (e) t = 67.30 s (f) t = 152.90 s and (g) t = 36.60 s (Re = 325.8 with no-slip BC) 143

Figure 4.6 : Maximum value of stream function along the iteration (a) Standard view (b) Zoomed view around coordinate $(t(\psi_{\max}),\psi_{\max})$ 144

Universiti Malaya

Figure 4.7 : Contour plot of streamline distribution at steady-state condition (Re = 325.8 with significant free-slip BC)..... 146

Figure 4.8 : Contour plot of evolution of *u*- and *v*-velocity distribution at steady-state condition (Re = 325.8 with significant free-slip BC)..... 147

Figure 4.9 : Comparison of contour plot at t = 2.00 s (a) *u*-velocity using FDM in Matlab® (b) *u*-velocity using FEM in Ansys Fluent® (c) *v*-velocity using FDM in Matlab® (d) *v*-velocity using FEM in Ansys Fluent 151

Figure 4.10 : Comparison of image plot of temperature distribution at t = 2.00 s (a) using FDM in Matlab® (b) using FEM in Ansys Fluent®..... 152

Figure 4.11 : Stream function distribution at t = 2.00 s 153

Figure 4.12 : Stream function profile at point A 154

Figure 4.13 : Centre vertical line and centre horizontal line..... 154

Figure 4.14 : Comparison of results using FDM and FEM (a) *u*-velocity profile (b) *v*-velocity profile..... 155

Figure 4.15 : Comparison of temperature profile at point A between FDM and FEM..... 156

Figure 4.16 : (a) Stream function and (b) Temperature distribution for the 2nd test case..... 157

Figure 4.17 : Temperature profile at point A along the iteration for the 1st test case (no-slip) and 2nd test case (free-slip)..... 158

Figure 4.18 : Temperature profile at point A ($\mathrm{Re}L = 100$ VS $\mathrm{Re}L = 50$)..... 159

Figure 4.19 : Temperature profile at point A ($Pr = 1$ VS $Pr = 2$) 159

Figure 4.20 : Schematic drawing of viscous heating inside the insulated BC 161

Figure 4.21 : Temperature profile at point A (1st test case at prolonged period).... 162

Figure 4.22 : Comparison of image plot of temperature distribution at t = 2.00 s using (a) FDM in Matlab® (b) FEM in Ansys Fluent®..... 164

Figure 4.23 : Temperature distribution at t = 2.80 s 165

Figure 4.24 : Comparison of temperature profile at point A for the 1st and 2nd test cases..... 165

Universiti Malaya

Figure 4.25 : Comparison of temperature profile at point A for the 1st, 3rd, 5th, 7th and 9th test cases..... 166

Figure 4.26 : Comparison of temperature profile at point A for the 2nd, 4th, 6th, 8th and 10th test cases..... 169

Figure 4.27 : Increase of temperature due to inertial force (4th test case)..... 170

Figure 5.1 : Rotational lid-driven model..... 176

Universiti Malaya

LIST OF TABLES

Table 2.1 : FDM applications 36

Table 3.1 : Properties of FDM 55

Table 3.2 : Forward and centered finite difference formulas 94

Table 3.3 : Mesh properties 131

Table 4.1 : Value and location of ψ_{max} at different steady-state criteria (AR=1.629) 145

Table 4.2 : Flow conditions of six test cases 149

Table 4.3 : Flow conditions of ten test cases 163

Table 4.4 : Value of different type of convection heat transfer coefficient 167

Table 4.5 : Advantages of GUI and FEA 171

Table 4.6 : Disadvantages of GUI and FEA 172

Universiti Malaya

LIST OF ABBREVIATIONS

ADI	:	Alternating direction implicit
AR	:	Aspect ratio
BC	:	Boundary condition
CCS	:	Cartesian coordinate system
CS	:	Control surface
FDE	:	Finite difference equation
FDM	:	Finite difference method
FEM	:	Finite element method
FEA	:	Finite element analysis
GUI	:	Graphical user interface
NSEs	:	Navier-Stoke equations
TEE	:	Thermal energy equation
2D	:	Two-dimensional

Universiti Malaya

LIST OF SYMBOLS

A	: Material properties
$A_{i,j}^{n}$	: Three-dimensional matrix of stream function dependent material property
a, b	: Unknowns
$a, b, c, s, \gamma, d, \alpha, \delta, \mu, \varepsilon$	: Positive constants
$a_A, \bar{a}, a_x, a_y, a_z$	: Acceleration field
B, b	: Reynolds transport theorem
Bi_{bottom}	: Biot number at bottom
Bi_{side}	: Biot number at side
Bi_{top}	: Biot number at top
CV	: Control volume
C	: Column vector
CS	: Control system
c	: Specific heat
dA	: Control area
$d\forall$	: Finite volume
e	: Steady-state criterion
g	: Sufficient smoothness
g, g_x, g_y, g_z	: Gravity acceleration
H	: Height
h_{top}	: Convection heat transfer coefficient at top
h_{bottom}	: Convection heat transfer coefficient at bottom

Universiti Malaya

$h, \Delta x, \Delta y, \Delta z$	: Step size
h_{side}	: Convection heat transfer coefficient at side
I	: Identity matrix
i, j, k	: Unit vector
i, j	: Node
j	: Row
k_{air}	: Prandtl number of ambient air
k	: Thermal conductivity
L	: Length
l_s	: Slip length
M_{sys}	: System mass
$\dot{m}_{in}$	: Inflow mass flow rate
$\dot{m}_{out}$	: Outflow mass flow rate
m	: Consistency index
N	: Maximum time step
$\hat{n}$	: Normal vector
n	: Iteration steps, power-law index
$O(h^3)$	: Higher order
Pr_{air}	: Prandtl number of ambient air
p_t	: Function of underlying
p	: Pressure
R	: Radius
Ra_L	: Rayleigh number of ambient air

Universiti Malaya

Re	: Reynolds number
r	: Risk-free instantaneous interest rate
S	: Vector of prices, asset price
S_1	: Asset price
s	: Slowness parameter
T	: Temperature
T_∞	: Ambient temperature
T_i	: Initial temperature
$T_{\max}$	: Maximum temperature
$T_{\min}$	: Minimum temperature
t	: Time, travel time, step time, current step time
$t+1$	: New step time
U_{wall}	: Applied velocity at top lid
u	: Electrical potential, amplitude
u, v	: Surface of tapering cylinder
u_s	: Slip velocity
u, v, w	: Velocity component in Cartesian coordinate system
$V, \overline{V}$	: Velocity vector
V_A	: Particle"s velocity
V	: Velocity
X, Y	: Function
x, y, z	: Cartesian coordinate system
x_A, y_A, z_A	: Location of moving particle
x_{cavity}	: Length of cavity

Universiti Malaya

y_{cavity}	: Height of cavity
α, λ	: Thermal diffusivity
α_{air}	: Thermal diffusity of ambient air
β	: Volumetric thermal expansion coefficient
$\dot{\gamma}$	: Rate of shearing strain
$\dot{\gamma} : \dot{\gamma}$	: Magnitude of the rate-of-strain tensor
$\delta F_{sx}, \delta F_{sy}, \delta F_{sz}, \delta F_s$	: Surface force
$\delta F_{bx}, \delta F_{by}, \delta F_{bz}, \delta F_b$	: Body force
$\delta F_n, \sigma_{xx}, \sigma_{yy}, \sigma_{zz}, \sigma_n$	: Normal force
$\delta F_1, \delta F_2$	: Shearing force
δ	: Thickness of velocity boundary layer
δ_t	: Thickness of thermal boundary layer
$\frac{\partial \overline{V}}{\partial t}$	: Time derivative
$\Delta t, l$	: Step time
$\Delta t_{\max}$	: Maximum allowable step time
∇	: Operator
∇V	: Gradient operator
∇V^T	: Transpose of gradient operator
ζ	: Vorticity
$\zeta^*, x^*, y^*, u^*, v^*, t^*, \psi^*,$ $\delta x^*, \delta y^*, h^*, \delta t^*, \Delta t^*$	: Dimensionless parameter
ζ_{bottom}	: Vorticity at bottom

Universiti Malaya

ζ_{top}	: Vorticity at top
ζ_{left}	: Vorticity at left
ζ_{right}	: Vorticity at right
$\zeta_{i,j}^{t}$	: Two-dimensional matrix of vorticity at current step time
$\zeta_{i,j}^{t+1}$	: Two-dimensional matrix of vorticity at new step time
$\eta\left(\dot{\gamma}\right)$	: Non-Newtonian viscosity
θ	: Angle
μ	: Dynamic viscosity
ν	: Kinematic viscosity
ν_{air}	: Kinematic viscosity of ambient air
π	: Momentum flux tensor
ρ	: Density
$\rho_{ij}, \sigma_{i,j}$	: Correlation coefficient
σ	: New grid function, electric conductivities
τ	: Torque, shear stress
τ_{xx}, τ_{yy}	: Stress tensor
$\tau_{xy}, \tau_{yx}, \tau_{yz}, \tau_{zy}, \tau_{zx}, \tau_{xz}, \tau_1, \tau_2$	: Shearing stress
ψ	: Stream function
$\psi_{i,j}^{n+1}$	: Stream function at current step time
$\psi_{i,j}^{n}$	: Stream function at previous step time
$\psi_{\min}$	: Minimum stream function
Ω	: Head

Universiti Malaya

ω, ω_z	: Rotational speed in z-direction
:	: Frobenius norm

Universiti Malaya

CHAPTER 1: INTRODUCTION

1.1 Introduction

Fluid flow and heat transfer prediction have been carried out using finite element analysis (FEA) simulation e.g. Moldflow®, Ansys Fluent®, Abaqus® and etc. over the years. However, there are many industries unable to procure such pricey software which may cost about few hundred thousand Ringgit Malaysia to simulate the behavior of fluid flow and heat transfer processes during the process of injection molding to ensure the rubber can fill in all the cavities in the mold. Moreover, to train the trainee is also another cost factor and this may give a heavy burden to rubber and plastic industries. Thus, many rubber and plastic industries always fail to cure a rubber product correctly at exact and optimum curing pressure and temperature. As a result, it may create a cured and injected defect or imperfection where some of the cavities of the rubber and plastic product are not fully filled which can diminish the properties of the rubber/plastic and inconsistence in the production of rubber and plastic products. Besides of this, this problem may waste a lot of time and money because of the disposal of the defect rubber and plastic products. Also, it is quite tedious to justify the optimum curing pressure and temperature to cure and inject the rubber/plastic product correctly using trial and error method.

Nevertheless, there is a method that can justify the correct curing/injection pressure and temperature to perfectly cure and inject the rubber/plastic products. The mentioned method above is called numerical method using finite difference approximation to solve the governing equations i.e. Navier-Stokes equations (NSEs) for fluid flow of rubber and governing transient heat transfer equation for heat transfer process. By implementing these governing equations, the resultant fluid flow and heat transfer processes can be well described by giving the independent variables i.e. curing pressure and temperature to the equation.

Universiti Malaya

It is not easy to understand the mechanism of thermal-fluid problem in 3D model due to its complexity. Thus, we always start with analytical solution, rule of thumb or 1D model but their results are still far deviate from the 3D model. In order to get a closer solution to 3D model and to have a better understanding of its mechanism, finite difference method (FDM) in 2D model can be compromised to predict and understand the mechanism of thermal-fluid problem. Because of the general complexity of the NSEs (nonlinear of the equation, second order, partial differential equations) and thermal energy equation (TEE), it is not amenable to exact solution. There are various techniques available for the numerical solution of the governing differential equations of fluid flow namely, FDM, finite element method (FEM), boundary element method and etc. By using these methods, differential equations are replaced by a set of algebraic equations.

The FDM typically is the most easily understood and widely used of the mentioned methods listed above. The flow and temperature fields are dissected into a set of grid points and the continuous functions (temperature, velocity, pressure and etc) are approximated by discrete values of these functions calculated at the grid points in this method. The differential equations are thereby transferred into a set of algebraic equations, which is solved by appropriate numerical techniques. The larger the number of grid points used, the larger the number of equations that must be solved. It is usually necessary to increase the number of grid points where large gradients are to be expected, such as in the boundary layer near a solid surface. In this case, NSEs and TEE will be solved in two-dimensional lid-driven cavity model to demonstrate the fluid flow and heat transfer results.

1.2 Background of Problem

This project is aimed to create a simple graphical user interface (GUI) by exploring the two-dimensional unsteady-state Newtonian fluid flow and heat transfer analyses in two-

Universiti Malaya

dimensional lid-driven cavity flow using FDM. Lid-driven cavity flow is defined primarily from the NSEs and due to the complex nature of these NSEs and TEE, there is a need for researchers to create a program and to write a code to solve those equations directly without making specific assumptions as the analytical solutions are not easily obtainable. Since it is not easy to track the trajectory and heat transfer of the fluid flow by naked eyes, investigation on stream function and temperature distribution are very crucial and can be done using the GUI.

Moreover, there is no study that specifically discussed the forming, merging and split of additional eddies when the analysis is subject to different steady-state criteria and different aspect ratios. Also, free-slip boundary condition (BC) is applied to the lid-driven model to differentiate the fluid flow and heat transfer behavior with no-slip BC. Then the lid-driven is assumed perfectly thermally insulated (Neumann or BC of second kind) to study the temperature profile at the location with maximum value of stream function. Some parameters are scrutinized to delineate their influences on temperature distribution in lid-driven cavity flow. To make this model close to reality, this model is reconstructed by using Robin BC and exposed to natural convection. If significant free-slip BC would influence the stream function distribution, it will engender a change in temperature distribution of lid-driven model in whatever thermal BC. Thus, it is important to compare thermo-fluid study of lid-driven model in no-slip and free-slip BCs.

The existing Newtonian fluid filled inside the lid-driven cavity can be substituted with any other non-Newtonian fluid model. In this case, the simplest power law as the non-Newtonian model is adopted. The rate-of-strain-tensor, magnitude of the rate-of-strain tensor, constitutive stress tensor and total stress tensor based on the power law are studied. These four components are combined with Cauchy momentum equation to derive the two-dimensional governing fluid flow equation for power law model. The lid-driven model can be easily reduced to boundary layer model by ignoring all the terms in x-direction diffusion of momentum in fluid flow governing equations.

Universiti Malaya

1.3 Statement of the Problems

This project is aimed to create a fundamental study and provide some comprehensive solutions to the previous study. 2D lid-driven model is the simplest model to investigate the fluid flow and heat transfer analyses over the past years. However, the lid-driven models studied in the previous researches are without free-slip effect or mixed with different types of heat transfer BCs. Besides, many researchers discovered a new numerical method in solving NSEs and implemented the new numerical method in lid-driven model to verify it. Those new discovered numerical methods are used to solve Newtonian and non-Newtonian fluid in lid-driven model. Most of the studies in non-Newtonian fluid model are based on generalized Newtonian model. Finally, the flow pattern of fluid such as the evolution of secondary main cell happened at which steady-state criterion is not mentioned in lid-driven model when achieving aspect ratio, AR = 1.629. Despite a lot of works have been done in lid-driven model, there is still lack of study in free-slip effect and cooling process of the lid-driven model once the applied force is removed. Many papers and journals do not reveal the final or exact governing fluid flow equation for non-Newtonian model that used in the lid-driven model. Thus, it is hard for student or novice who wanted to study the non-Newtonian fluid model. All the mentioned difficulties need to be overcome and improved. To conquer the problems, it is momentous to carry the study of lid-driven model in different steady-state criteria to investigate the evolution of flow pattern, and then it can be combined with certain type of heat transfer BC to investigate the temperature profile. Because of this trend, thermal fluid study will be carried out in free-slip and no-slip BCs and couple with heat transfer analysis and extent it even after the applied force is removed on the lid-driven model. The fundamental study on generalized Newtonian model will be studied extensively to discover the final fluid flow governing equation of non-Newtonian model in 2D shear flow system. Thus, students or researchers can read this thesis and learn how to derive any other non-Newtonian fluid model for their study. Finally, an in-house Matlab® code will be

Universiti Malaya

developed and incorporated in a simple GUI to illustrate the fluid flow and temperature profile throughout the two-dimensional lid driven model n both free-slip and no-slip BCs.

1.4 Objectives of Study

(a) To derive the governing equations of two-dimensional Newtonian and non-Newtonian fluid flows and transforms them into equivalent finite difference equation (FDE).

(b) To derive the governing equation of non-Newtonian fluid in a boundary layer model by reducing the 2D simple shear flow system.

(c) To verify an in-house Matlab® code with commercial engineering simulation software Ansys Fluent® and develop a simple GUI for lid-driven model.

(d) To examine the different aspect ratios, different steady-state criteria and free-slip BC in fluid flow analysis in lid-driven model. Then compare the thermal fluid analysis in both no-slip and free-slip BCs.

(e) To include the thermal energy equation in the lid-driven model and solve it in Neumann and Robin BC respectively. Then extent the thermal fluid study even after the applied force is removed.

1.5 Importance of the Study

As mentioned earlier, this project aims to create a simple GUI (in Matlab® environment), which is user interactive and user friendly to facilitate the end user to conduct the fluid flow and thermal analyses. Besides, this in-house Matlab code can include free-slip BC in lid-driven model and to the best of our knowledge, Ansys Fluent® doesn‟t provide this parameter. Besides,

Universiti Malaya

writing this in-house code can help other users to have a better understanding in doing thermal-fluid analysis and hence increase their interest in learning thermal-fluid problem. This GUI is designed and written based on FDM in solving the time dependent NSEs and TEE govern the time and spatial effect. One function of FDM is to reduce higher mathematics to basic arithmetic operations, enables to get at the „nuts and bolts" of some otherwise obscure topics. During the using of this GUI, it will guide the end user step by step and enable the end user to key-in the correct data. Besides, end user is not required to be equipped with fundamental knowledge of heat transfer, fluid mechanics, numerical method and programming skills when using this GUI. Thus, training is not required for the end user but only with a simple explanation of how to use this GUI.

1.6 Scope of the Study

The limitation of the boundary of each research, solution and method is discussed. The comprised scopes such as fundamentals of heat transfer and fluid mechanics are studied extensively especially those theories involving lid-driven problem and fundamentals of governing fluid flow equation of non-Newtonian fluid. All the derivation of governing equation of non-Newtonian is shown clearly and in step-by-step based. Numerical method such as FDM is employed to solve the NSEs and TEE. All the governing partial differential equations are converted into their equivalent FDEs to enable the solutions. Finally, it is followed by programming and designing the GUI to ease the end-user to solve all the governing equations, to envisage and to interpret those results.

Universiti Malaya

1.7 Organization of Thesis

The content of each chapter is summarized briefly and shown as below:

(a) Chapter 1 describes the overall of this research, problem statement, importance and scope of study. Hence, this chapter tries to give a big picture to the readers.

(b) Chapter 2 reviews those literature reviews about the pass researches that involved this particular mathematical model and their governing equations. A step-by-step in deriving NSEs is shown in a comprehensive way (conversation of mass, material derivative, forces acting on the finite element and stress-deformation relationship). Besides, all the analytical and numerical methods in solving NSEs are considered. Some information about the application of FDM in other applications is briefly mentioned.

(c) Chapter 3 describes the whole methodology process in detail in running this project. This chapter is a very technical and lengthy chapter as it shows how to derive vorticity-stream function, fluid flow in free-slip and no-slip BCs, heat transfer analysis in Neumann and Robin BCs, non-Newtonian equation in 2D shear flow system and non-Newtonian boundary layer model. It is followed by FDM in solving all the equation and their associated stability criteria. A simple in-house developed GUI is designed to solve the fluid flow in no-slip and free-slip BCs.

(d) Chapter 4 presents and interprets all the relevant results. This chapter reveals the results for three models i.e. fluid flow in different aspect ratio of lid-driven and in different steady-state criteria, fluid flow combines with Neumann BC and fluid flow incorporates with Robin BC. These three models are executed in no-slip and free-slip BCs respectively.

Universiti Malaya

(e) Chapter 5 gives an overall conclusion and recommendation of this project. In addition, this chapter gives some important information and tries to relate the fundamental study with engineering applications via scientific proven data.

Universiti Malaya

CHAPTER 2: LITERATURE REVIEWS

2.1 A Review of Lid-driven Model

Lid-driven cavity flow can be defined as dynamics of fluid within an empty space surrounded by connected walls. It is the simplest two-dimensional model to demonstrate how certain fluid behaves when it is subject to different BCs, different aspect ratios (AR), different steady-state criteria and different fluid properties. There are two important dimensionless parameters which are often used namely Reynolds number, $\mathrm{Re}\left(=\frac{\rho UL}{\mu}\right)$ and the AR, $\mathrm{A}\left(=\frac{H}{L}\right)$ of the cavity (Sousa et al., 2016). Another important parameter that is often used in lid-driven heat transfer analysis and it is known as Prandtl number, $\mathrm{Pr}\left(=\frac{\upsilon}{\alpha}\right)$ (Incropera et al., 2006). The model contemplated in this project is known as "singular driven cavity" as there are two discontinuities in the BC at the top lid (Botella & Peyret, 1998). In order to avoid costly experiment and troubles related to primitive variable approach (velocity-pressure), vorticity-stream function and vorticity-velocity function of the NSEs are broadly employed (Moshkin & Poochinapan, 2009) to solve the two-dimensional partial differential equations directly. Because of general difficulty of the NSEs by its nonlinear second-order term (Munson et al., 2002), numerical solution of the NSEs is preferred and FDM as one of the established numerical schemes is often used.

The study of free-slip BC is important at certain occasions in order to imitate or to assess its impact on the whole fluid flow pattern especially at a very low pressure (Shu et al.,

Universiti Malaya

2016) or when immersion or penetration of bubble or fluid particle into solid interface happens and results as surface contamination. Thus, a large viscosity ratio of the fluid and near the solid boundary happens and causes a rise in the tangential velocity near the solid boundary (Shu et al., 2016). This defines dissimilarity between free-slip and no-slip effects where the fluid tangential velocity at a solid wall is zero for no-slip BC. In some cases, no-slip BC is well-posed in modeling of viscous flow without penetration condition but in analysis of highly inviscid flows, it can lead to indiscretion. Free-slip is measured by a so-called slip length physical parameter (Kempe et al., 2015) that can be measured experimentally such as via instruments of rheometry and particle imaging or by using theoretical calculation of effective slip length and data fitting. Abundant researches have been devoted in this practical area of study especially for fluid flow and heat transfer problems in micro channel where the effect of free-slip cannot be simply disregarded (Sauli et al., 2010) and no-slip BC is not suitable for flows at the microchannel (Tretheway et al., 2002). However, the study of free-slip BC inside a large cavity such as lid-driven model was not known especially the fluid content inside of it is polymer (Black, 2000). In some cases, partial slip effect is applied to lid-driven model with mixed convection (Ismail et al., 2014).

Eddy is a swirling motion of a mass of fluid in the direction apart from the fluid flow main streamlines. Mainly caused by pressure difference between the cavity walls, disturbance in the flow due to changes in AR, Reynolds number, applied velocity and density can be very much significant. According to Moffatt (1964) for Stokes flow, two corner eddies at the bottom merge to form a secondary main cell at a critical aspect AR of 1.629 in no-slip BC besides a primary main cell which is formed at the beginning of the unsteady-state simulation. In the present study, we found the primary main cell is rotating in clockwise direction while the two corner eddies at the bottom are rotating in counter-clockwise

direction with infinitesimal negative stream function value even after they have formed a secondary main cell (negative stream function value means rotating in counter-clockwise direction). We also found the secondary main cell is formed when iteration is terminated at steady-state condition with criterion of $e \leq 10^{-8}$ (Moshkin & Poochinapan, 2009) is achieved in no-slip BC. Then, it is noticeable that the additional eddies disappear and appear again in different locations by further increasing the AR. Due to numerical error, we will discuss what happen to the secondary main cell if iteration is extended beyond the prescribed steady-state condition.

2.2 Viscous Heating and Other Effects

Viscous heating is generated by fluid viscous friction when the fluid is sheared by the external motion, provided the fluid is not inviscid and sluggish (Zhang et al., 2010). Viscous heating process is important in creating energy sources, cooling process and many studies have been carried out to delineate the temperature profile. Viscous heating is studied in a slip flow region or free-slip BC by Mohamed (1999). His study shows a momentous effect on the heat transfer and fluid flow peculiarity in microchannel studies eventhough the fluid has tenuous viscous flow and possesses a tiny value of hydraulic diameter (Koo & Kleinstreuer, 2004). Koo and Kleinstreneur (2004) discovered that viscous dissipation is effectively influenced by Reynolds number and geometrical aspect ratio. Moreover, its influence is more prone to microchannel with small aspect ratio. The viscous dissipation effect on free-slip BC is also discussed by Rij et al. (2009) in a 3D microchannel gas flow where it is dependent on the amount of rarefaction and other factors.

Universiti Malaya

Another important study of viscous dissipation when merged with Joule heating carried out by Kumar et al. (2017) shows an upward trend of temperature distribution in a non-Newtonian fluid flow. The effect of viscous dissipation especially in a fully-developed region cannot be disregarded due to the temperature dependent viscosity in broad manipulating conditions (Giudice et al., 2007). The heat transfer process of a Newtonian fluid which takes the viscous dissipation into account in a fully-developed region was performed using explicit numerical method (Coelho & Pinho, 2006). One more significant effect of viscous dissipation in Newtonian fluid was observed in a large-scale piping system. It shows that the temperature distribution is dependent on the viscous dissipation in a fully-developed flow and in a thermal developing region (Aydin, 2005a; Aydin, 2005b). Other consideration of viscous dissipation in heat transfer process of a Newtonian fluid between two parallel plates was analyzed (Rij et al., 2009). The variation of the heat transfer process presented an unusual degree in both hydro dynamically and thermally fully-developed region due to the thermal energy balance in between the heat wall and the viscous induced heat (Aydin & Avci, 2006; Aydin & Avci, 2007). The catastrophe such as the source of heat in storm or hurricane is derived from the viscous dissipation near the surface (Albright et al., 1995) and can be estimated via turbulent kinetic energy (Kraus & Businger, 1994). The reported viscous dissipation of heat is a cubic function of the wind speed.

Some simple mixed convection in lid-driven models were carried out previously (Khanafer & Chamkha, 1999; Chamkha, 2002). In order to increase the feasibility of lid-driven model, some authors utilized non-Newtonian fluid such as nanofluid in the said models (Abu-Nada & Chamkha, 2010; Nasrin et al., 2014; Abu-Nada & Chamkha, 2014; Rashad et al., 2016; Alsabery et al., 2018; Chamkha & Abu-Nada, 2012). Complexity of the lid-driven model can be enhanced by incorporating porous square cavity (Basak et al., 2012;

Universiti Malaya

Muthukumar et al., 2019) and impose partial slip effect on the enclosure on the lid-driven model (Chamkha et al., 2017a; Chamkha et al, 2017b). Besides, some extra features like triangular solid or cavity (Ismail et al., 2018; Chamkha et al., 2018; Alsabery et al., 2020a), conductive rotating circular or solid cylinder (Mirzakhanlari et al., 2017; Alsabery et al., 2019a; Alsabery et al., 2020b) and conductive inner block (Alsabery et al., 2019b) can be positioned inside the lid-driven model to enhance the thermo fluid performance.

In some cases such as in magnetohydrodynamic (MHD) and mixed convection study (Oğlakkaya & Bozkaya, 2018; Manchanda & Gangawane, 2018; Selimefendigil & Chamkha, 2016), the electrically conducting fluid motion is retarded by the magnetic field (Selimefendigil et al., 2017; Chamkha & Ismail, 2016; Alsabery et al., 2019c) and hence produces an insignificant viscous heating if compared with the amount of heat generated by buoyancy force. The study of MHD was also conducted in a thermal-fluid analysis where three modes of convection specifically referred to as free, forced and Marangoni convections are taken into consideration (Biswas & Manna, 2018). Besides, Zhou et al. (2018) merely considered the Boussinesq approximation (Incropera et al., 2006) in TEE when Newtonian fluid is subject to mixed convection heat transfer process with different heat sources in a lid-driven cavity. Rahman et al. (2011) revealed that the behaviour and temperature profile of the lid-driven flow with wall of semi-circular heater are independent of viscous heating when subject to magnetic field and Joule heating. Mixed convection is often applied when the magnitude of natural convection and forced convection are comparable. Buoyancy effect often happens in mixed convection and can be evaluated using the Boussinesq‟s approximation. Buoyancy force exerts upwardly from the bottom heated lid will generate a large temperature gradient. Thus, it is necessary to couple the heat transfer and fluid flow analyses in the lid-driven cavity flow in the buoyancy forces. Those parameters in governing

the coupling analysis are Reynolds number, Grashof number and Prandtl number. While Richardson number gives a relative magnitude of forced and natural convection in mixed convection flow.

In the astrometry study of surface temperature of meteorites, they are very cold in space and its surface temperature increases abruptly when meteorites arrive atmosphere (Lynn, 2015). Some literatures (Arthur, 2000; Yirka, 2017) reported the surface temperature of meteorites could be as high as 1650 ^{o}C to 2370 ^{o}C when they hit the ground. During the free-fall of their descent, much heat is generated from the compressed air in front of it and very little frictional heating or viscous heating due to the atmospheric air. This is because the viscous boundary layer thickness during the free-fall is only 1/90 of the characteristic length of meteorite (Yirka, 2017). Anderson (2003) derived the thermal energy equation for viscous high temperature flow which includes the viscous terms to estimate the meteorite surface temperature. With regard to the heat retention of the Newtonian fluid created by viscous heating process inside the lid-driven, rubber is chosen as the container to fill the Newtonian fluid because rubber is a good thermal insulator (Admin, 2016). Besides, rubber is often used as capacitors and high voltage insulators (Mahdi et al., 2017).

Robin BC (Markus & Mahamadi, 2009) or also known as third kind of BC due to natural or forced convection is always experienced in engineering applications such as turbo machinery, injection moulding process, food and beverage processing, hydraulic and lubrication system. In order to ensure those engineering components operate safely and efficiently within the optimum temperature range, it is momentous to remove generated heat from the operating system to its ambient air. One of the suitable and low cost cooling mechanism is using natural convection and can be modeled using Robin BC. A simple mathematical cooling process had been modeled and derived (Wu, 1974).

Universiti Malaya

There are few methods available to study the heat transfer across Newtonian fluid, rubber and to environment i.e. control-volume approach (Lobbia, 2014), finite volume and FEM (Chapra & Canale, 2006). FEM employs interpolation functions and divides the model into elements while FDM divides the model into a grid of discrete points. Perhaps, FDM is the most easily graspable method and can be applied to heat transfer in multiple materials provided the model is simple or regular geometry. Yau et al. (2012) utilized FDM combined with energy balance method to study the two-dimensional heat loss from the press across rubber, mould and to the environment. Then this solution was verified using FEA software i.e. Abaqus. Finally, two-dimensional governing fluid flow and thermal energy equations that employed in lid-driven model can be easily reduced to boundary layer model for non-Newtonian Sisko nanofluid by ignoring all the terms in x-direction diffusion of momentum and thermal energy (Incropera et al., 2006). Sisko fluid model (Hayat et al., 2017) is an extension and more comprehensive version of power law model and often used in MHD study.

2.3 Derivation of NSEs

This section briefly discusses how to derive NSEs using conservation of mass, the material derivative, description of forces acting on the differential element and stress-strain relation.

Universiti Malaya

2.3.1 Conservation of Mass

The first principle that used in derivation of NSEs is conservation of mass or also known as the continuity equation (Munson et al., 2002). The principle for the system is stated as:

Time rate of change of the system mass= 0

$$\frac{DM_{sys}}{Dt} = 0\,, \tag{2.1}$$

$$M_{sys} = \int_{sys} \rho d\forall\,, \tag{2.2}$$

where M_{sys} is the system mass, ρ is density, t is time and $d\forall$ is finite volume.

For a system and fixed, non-deforming control volume that are coincident at an instant of time, the Reynolds transport theorem with B = mass and b = 1 denotes that:

$$\frac{D}{Dt}\int_{sys} \rho d\forall = \frac{\partial}{\partial t}\int_{cv} \rho d\forall + \int_{cs} \rho \overline{V} \cdot \hat{n}\, dA\,, \tag{2.3}$$

where $\hat{n}$ is the normal vector, dA is control volume and $\overline{V}$ is velocity vector.

In other words, the time rate of change of the mass of the coincident system is equal to time rate of change of the mass of the contents of the coincident control volume plus net rate of flow of mass through the control surface. Control volume is an Eulerian description and control surface (or system) is Lagrangian description. Because the flow is steady, all field properties including density remain constant with time, i.e:

$$\frac{\partial}{\partial t}\int_{cv}\rho d\forall + \int_{cs}\rho\overline{V}\cdot\hat{n}\,dA = 0 \quad . \tag{2.4}$$

By considering the control volume as a small, stationary cubical element is given by:

$$\frac{\partial}{\partial t}\int_{cv}\rho d\forall = \frac{\partial\rho}{\partial t}\delta x\delta y\delta z \quad . \tag{2.5}$$

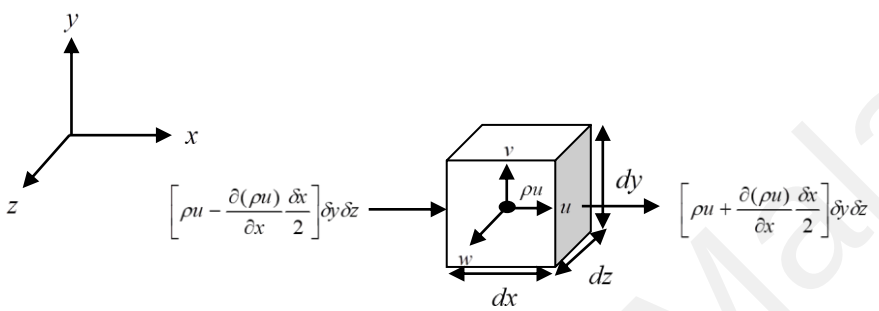

where x, y and z are the fixed set of Cartesian axes
u, v and w are the velocity component parallel to the x, y and z axes

Figure 2.1: Differential element for the development of conservation of mass equation (Munson et al., 2002)

The net mass flow rate through the control surface (CS) is given by:

$$\int_{cs}\rho\overline{V}\cdot\hat{n}\,dA = \sum\dot{m}_{out} - \dot{m}_{in} \ , \tag{2.6}$$

where $\dot{m}_{out}$ is the outflow mass flow rate and $\dot{m}_{in}$ is the inflow mass flow rate.

Thus, net rate of mass outflow in x - direction is given by:

$$\left[\rho u + \frac{\partial(\rho u)}{\partial x}\frac{\delta x}{2}\right]\delta y\delta z - \left[\rho u - \frac{\partial(\rho u)}{\partial x}\frac{\delta x}{2}\right]\delta y\delta z = \frac{\partial(\rho u)}{\partial x}\delta x\delta y\delta z \ . \tag{2.7}$$

Similarly, net rate of mass outflow in y - direction= $\frac{\partial(\rho v)}{\partial y}\delta x\delta y\delta z$. (2.8)

Similarly, net rate of mass outflow in z - direction= $\frac{\partial(\rho w)}{\partial z}\delta x\delta y\delta z$. (2.9)

From Equation (2.4), the differential equation for conservation of mass is given by:

$$\left[\frac{\partial\rho}{\partial t}+\frac{\partial(\rho u)}{\partial x}+\frac{\partial(\rho v)}{\partial y}+\frac{\partial(\rho w)}{\partial z}\right]\delta x\delta y\delta z=0. \quad (2.10)$$

For steady and incompressible flow, fluid density is constant throughout the flow field and Equation (2.10) reduces to:

$$\frac{\partial u}{\partial x}+\frac{\partial v}{\partial y}+\frac{\partial w}{\partial z}=0. \quad (2.11)$$

Equation (2.11) applies to both steady and unsteady flow of incompressible fluids.

2.3.2 The Material Derivative

The particle"s velocity, V_A is a function of its location and time (Munson, Young, Okiishi, 2002). That is:

$$V_A=V_A(r_A,t)=V_A[x_A(t),y_A(t),z_A(t),t], \quad (2.12)$$

where $x_A=x_A(t), y_A=y_A(t), z_A=z_A(t)$ are the location of the moving particle.

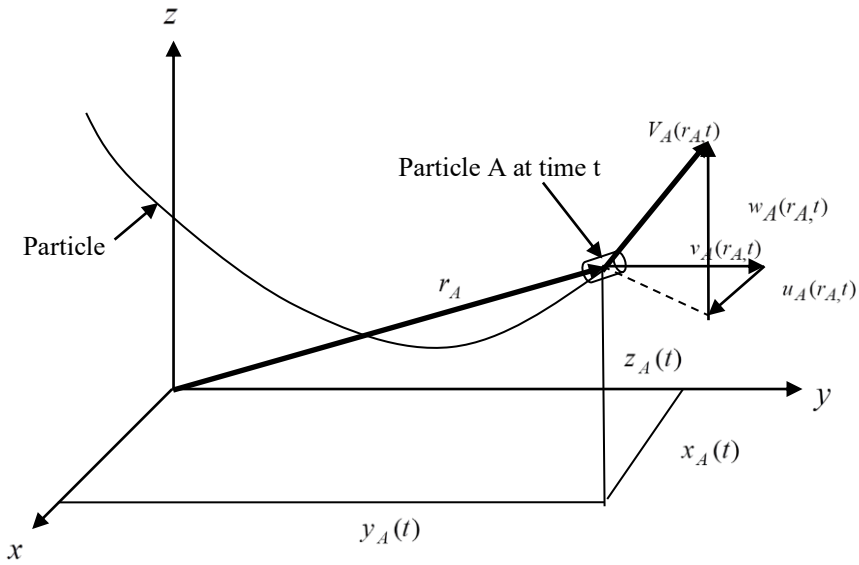

Figure 2.2: Velocity and position of particle *A* at time *t* (Munson et al., 2002)

By using chain rule of differentiation to obtain the acceleration of particle *A*:

$$a_A = \frac{dV_A}{dt} = \frac{\partial V_A}{\partial t} + \frac{\partial V_A}{\partial x}\frac{dx_A}{dt} + \frac{\partial V_A}{\partial y}\frac{dy_A}{dt} + \frac{\partial V_A}{\partial z}\frac{dz_A}{dt}, \tag{2.13}$$

$$a_A = \frac{\partial V_A}{\partial t} + u_A\frac{\partial V_A}{\partial x} + v_A\frac{\partial V_A}{\partial y} + w_A\frac{\partial V_A}{\partial z}. \tag{2.14}$$

Thus the acceleration field is given by:

$$\bar{a} = \frac{\partial \bar{V}}{\partial t} + u\frac{\partial \bar{V}}{\partial x} + v\frac{\partial \bar{V}}{\partial y} + w\frac{\partial \bar{V}}{\partial z}, \tag{2.15}$$

where $\frac{\partial \bar{V}}{\partial t}$ is time derivative (also called as local derivative or local acceleration) represents the unsteadiness of the flow.

For a steady flow, time derivative is equal to zero. $u\frac{\partial \overline{V}}{\partial x}+v\frac{\partial \overline{V}}{\partial y}+w\frac{\partial \overline{V}}{\partial z}$ is the convective derivative or spatial derivative or convective acceleration. Those components can be written as:

$$a_x=\frac{\partial u}{\partial t}+u\frac{\partial u}{\partial x}+v\frac{\partial u}{\partial y}+w\frac{\partial u}{\partial z}, \tag{2.16}$$

$$a_y=\frac{\partial v}{\partial t}+u\frac{\partial v}{\partial x}+v\frac{\partial v}{\partial y}+w\frac{\partial v}{\partial z}, \tag{2.17}$$

and $$a_z=\frac{\partial w}{\partial t}+u\frac{\partial w}{\partial x}+v\frac{\partial w}{\partial y}+w\frac{\partial w}{\partial z}. \tag{2.18}$$

2.3.3 Description of Forces Acting on the Differential Element

There are two types of forces acting on the fluid particle namely surface forces which act on the surface of the differential element and body forces which are distributed throughout the element. Finite element of body forces are given by:

$$\delta \overline{F}_b=\delta m\overline{g}. \tag{2.19}$$

In component form:

$$\delta F_{bx}=\delta m g_x, \tag{2.20}$$

$$\delta F_{by}=\delta m g_y, \tag{2.21}$$

$$\delta F_{bz}=\delta m g_z. \tag{2.22}$$

Universiti Malaya

Normally, acceleration of gravity, g is the same in all directions.

Surface force, δF_s acts on the element as a result of its interaction with its surrounding. Figure 2.3 shows the surface force, δF_s can be resolved into three components. δF_n is normal force, δF_1 and δF_2 are shearing forces and perpendicular to each other.

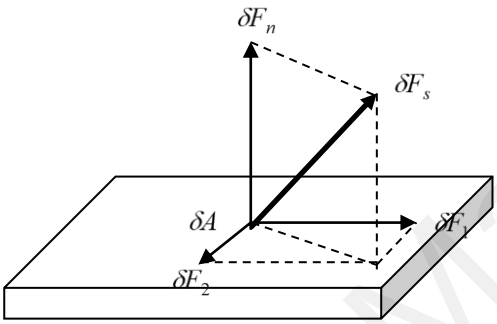

Figure 2.3: Component of force acting on an arbitrary differential area (Munson et al., 2002)

Based on Figure 2.3, the forces are given by:

Normal stress, $\sigma_n = \lim_{\delta A \to 0} \frac{\delta F_n}{\delta A}$, (2.23)

Shearing stress, $\tau_1 = \lim_{\delta A \to 0} \frac{\delta F_1}{\delta A}$, (2.24)

Shearing stress, $\tau_2 = \lim_{\delta A \to 0} \frac{\delta F_2}{\delta A}$. (2.25)

y

x

Universiti Malaya

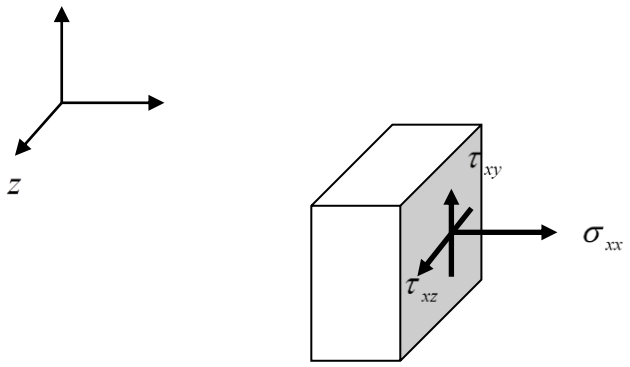

Figure 2.4: Normal stress and shear stresses (Munson et al., 2002)

Surface forces acting on a small cubical element of fluid in terms of the stresses acting on the element in *x*-direction are shown in Figure 2.5.

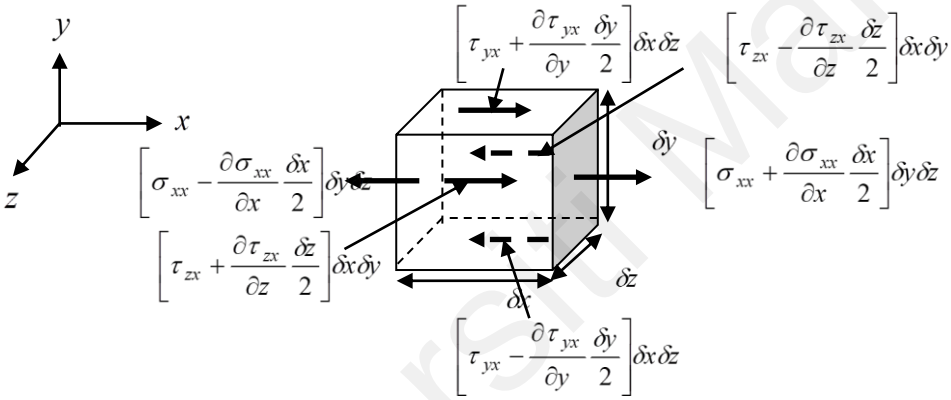

Figure 2.5: Surface forces in the *x*-direction acting on a fluid element (Munson et al., 2002)

Summing all the forces in *x*-direction:

$$\delta F_{sx}=\left[\sigma_{xx}+\frac{\partial\sigma_{xx}}{\partial x}\frac{\delta x}{2}\right]\delta y\delta z-\left[\sigma_{xx}-\frac{\partial\sigma_{xx}}{\partial x}\frac{\delta x}{2}\right]\delta y\delta z+\left[\tau_{yx}+\frac{\partial\tau_{yx}}{\partial y}\frac{\delta y}{2}\right]\delta x\delta z$$
$$-\left[\tau_{yx}-\frac{\partial\tau_{yx}}{\partial y}\frac{\delta y}{2}\right]\delta x\delta z+\left[\tau_{zx}+\frac{\partial\tau_{zx}}{\partial z}\frac{\delta z}{2}\right]\delta x\delta y-\left[\tau_{zx}-\frac{\partial\tau_{zx}}{\partial z}\frac{\delta z}{2}\right]\delta x\delta y$$

Universiti Malaya

$$
\begin{aligned}
&= \sigma_{xx}\delta y\delta z + \frac{\partial \sigma_{xx}}{\partial x}\frac{\delta x}{2}\delta y\delta z - \sigma_{xx}\delta y\delta z + \frac{\partial \sigma_{xx}}{\partial x}\frac{\delta x}{2}\delta y\delta z + \tau_{yx}\delta x\delta z + \frac{\partial \tau_{yx}}{\partial y}\frac{\delta y}{2}\delta x\delta z \\
&\quad - \tau_{yx}\delta x\delta z + \frac{\partial \tau_{yx}}{\partial y}\frac{\delta y}{2}\delta x\delta z + \tau_{zx}\delta x\delta y + \frac{\partial \tau_{zx}}{\partial z}\frac{\delta z}{2}\delta x\delta y - \tau_{zx}\delta x\delta y + \frac{\partial \tau_{zx}}{\partial z}\frac{\delta z}{2}\delta x\delta y
\end{aligned}
$$

$$
= \left[\frac{\partial \sigma_{xx}}{\partial x} + \frac{\partial \tau_{yx}}{\partial y} + \frac{\partial \tau_{zx}}{\partial z} \right] \delta x\delta y\delta z \,. \tag{2.26}
$$

Similarly, summing all the forces in *y*-direction:

$$
\delta F_{sy} = \left[\frac{\partial \tau_{xy}}{\partial x} + \frac{\partial \sigma_{yy}}{\partial y} + \frac{\partial \tau_{zy}}{\partial z} \right] \delta x\delta y\delta z \,. \tag{2.27}
$$

Summing all the forces in z-direction yields:

$$
\delta F_{sz} = \left[\frac{\partial \tau_{xz}}{\partial x} + \frac{\partial \tau_{yz}}{\partial y} + \frac{\partial \sigma_{zz}}{\partial z} \right] \delta x\delta y\delta z \,. \tag{2.28}
$$

Thus,

$$
\delta \overline{F}_s = \delta F_{sx}\,\hat{i} + \delta F_{sy}\,\hat{j} + \delta F_{sz}\,\hat{k} \,. \tag{2.29}
$$

By applying the body and surface forces with conjunction with Newton‟s second law,

$$
\delta \overline{F} = \delta m \overline{a} \,. \tag{2.30}
$$

By combining Equation (2.15), (2.19) and (2.30) yields:

$$
\delta \overline{F}_s + \delta \overline{F}_b = \delta m \left[\frac{\partial \overline{V}}{\partial t} + u\frac{\partial \overline{V}}{\partial x} + v\frac{\partial \overline{V}}{\partial y} + w\frac{\partial \overline{V}}{\partial z} \right], \tag{2.31}
$$

Universiti Malaya

$$\delta \overline{F}_s + \delta \overline{F}_b = \rho \delta x \delta y \delta z \left[\frac{\partial \overline{V}}{\partial t} + u \frac{\partial \overline{V}}{\partial x} + v \frac{\partial \overline{V}}{\partial y} + w \frac{\partial \overline{V}}{\partial z} \right] \ldots 2.32$$

Based on Figure 2.5, equation of motion in components form (in *x*-direction),

$$\left[\frac{\partial \sigma_{xx}}{\partial x} + \frac{\partial \tau_{yx}}{\partial y} + \frac{\partial \tau_{zx}}{\partial z} \right] \delta x \delta y \delta z + \rho \delta x \delta y \delta z g_x = \rho \delta x \delta y \delta z \left[\frac{\partial u}{\partial t} + u \frac{\partial u}{\partial x} + v \frac{\partial u}{\partial y} + w \frac{\partial u}{\partial z} \right]$$

$$\rho g_x + \frac{\partial \sigma_{xx}}{\partial x} + \frac{\partial \tau_{yx}}{\partial y} + \frac{\partial \tau_{zx}}{\partial z} = \rho \left[\frac{\partial u}{\partial t} + u \frac{\partial u}{\partial x} + v \frac{\partial u}{\partial y} + w \frac{\partial u}{\partial z} \right]. \quad (2.33)$$

Similarly in *y*-direction,

$$\rho g_y + \frac{\partial \tau_{xy}}{\partial x} + \frac{\partial \sigma_{yy}}{\partial y} + \frac{\partial \tau_{zy}}{\partial z} = \rho \left[\frac{\partial v}{\partial t} + u \frac{\partial v}{\partial x} + v \frac{\partial v}{\partial y} + w \frac{\partial v}{\partial z} \right]. \quad (2.34)$$

Similarly in *z*-direction,

$$\rho g_z + \frac{\partial \tau_{xz}}{\partial x} + \frac{\partial \tau_{yz}}{\partial y} + \frac{\partial \sigma_{zz}}{\partial z} = \rho \left[\frac{\partial w}{\partial t} + u \frac{\partial w}{\partial x} + v \frac{\partial w}{\partial y} + w \frac{\partial w}{\partial z} \right]. \quad (2.35)$$

2.3.4 Viscous Flow (Stress-Deformation Relationship)

For incompressible Newtonian fluids, normal stresses are linearly related to the rates of deformation as shown below:

$$\sigma_{xx} = -p + 2\mu \frac{\partial u}{\partial x}, \quad (2.36)$$

Universiti Malaya

$$\sigma_{yy} = -p + 2\mu \frac{\partial v}{\partial y}, \tag{2.37}$$

$$\sigma_{zz} = -p + 2\mu \frac{\partial w}{\partial z}. \tag{2.38}$$

Shearing stresses:

$$\tau_{xy} = \tau_{yx} = \mu\left(\frac{\partial u}{\partial y} + \frac{\partial v}{\partial x}\right), \tag{2.39}$$

$$\tau_{yz} = \tau_{zy} = \mu\left(\frac{\partial v}{\partial z} + \frac{\partial w}{\partial y}\right), \tag{2.40}$$

$$\tau_{zx} = \tau_{xz} = \mu\left(\frac{\partial w}{\partial x} + \frac{\partial u}{\partial z}\right), \tag{2.41}$$

where μ is dynamic viscosity.

By substituting Equation (2.36), Equation (2.39) and Equation (2.41) into Equation (2.33), it results:

$$\begin{aligned}
&\rho g_x + \frac{\partial\left(-p + 2\mu\left[\frac{\partial u}{\partial x}\right]\right)}{\partial x} + \frac{\partial\left(\mu\left[\frac{\partial u}{\partial y} + \frac{\partial v}{\partial x}\right]\right)}{\partial y} + \frac{\partial\left(\mu\left[\frac{\partial w}{\partial x} + \frac{\partial u}{\partial z}\right]\right)}{\partial z} = \rho\left[\frac{\partial u}{\partial t} + u\frac{\partial u}{\partial x} + v\frac{\partial u}{\partial y} + w\frac{\partial u}{\partial z}\right] \\
&\rho g_x - \frac{\partial p}{\partial x} + 2\mu\frac{\partial^2 u}{\partial x^2} + \mu\frac{\partial^2 u}{\partial y^2} + \mu\frac{\partial^2 v}{\partial x \partial y} + \mu\frac{\partial^2 w}{\partial x \partial z} + \mu\frac{\partial^2 u}{\partial z^2} = \rho\left[\frac{\partial u}{\partial t} + u\frac{\partial u}{\partial x} + v\frac{\partial u}{\partial y} + w\frac{\partial u}{\partial z}\right] \\
&\rho g_x - \frac{\partial p}{\partial x} + \mu\left(\frac{\partial^2 u}{\partial x^2} + \frac{\partial^2 u}{\partial y^2} + \frac{\partial^2 u}{\partial z^2}\right) + \mu\frac{\partial^2 u}{\partial x^2} + \mu\frac{\partial^2 v}{\partial x \partial y} + \mu\frac{\partial^2 w}{\partial x \partial z} = \rho\left[\frac{\partial u}{\partial t} + u\frac{\partial u}{\partial x} + v\frac{\partial u}{\partial y} + w\frac{\partial u}{\partial z}\right] \\
&\rho g_x - \frac{\partial p}{\partial x} + \mu\left(\frac{\partial^2 u}{\partial x^2} + \frac{\partial^2 u}{\partial y^2} + \frac{\partial^2 u}{\partial z^2}\right) + \mu\frac{\partial}{\partial x}\left(\frac{\partial u}{\partial x} + \frac{\partial v}{\partial y} + \frac{\partial w}{\partial z}\right) \\
&= \rho\left[\frac{\partial u}{\partial t} + u\frac{\partial u}{\partial x} + v\frac{\partial u}{\partial y} + w\frac{\partial u}{\partial z}\right]
\end{aligned}. \tag{2.42}$$

Universiti Malaya

From Equation (2.11),

$$\frac{\partial u}{\partial x}+\frac{\partial v}{\partial y}+\frac{\partial w}{\partial z}=0$$

Thus,

$$\rho\left[\frac{\partial u}{\partial t}+u\frac{\partial u}{\partial x}+v\frac{\partial u}{\partial y}+w\frac{\partial u}{\partial z}\right]=-\frac{\partial p}{\partial x}+\rho g_x+\mu\left(\frac{\partial^2 u}{\partial x^2}+\frac{\partial^2 u}{\partial y^2}+\frac{\partial^2 u}{\partial z^2}\right). \tag{2.43}$$

Similarly in *y*-direction:

$$\rho\left[\frac{\partial v}{\partial t}+u\frac{\partial v}{\partial x}+v\frac{\partial v}{\partial y}+w\frac{\partial v}{\partial z}\right]=-\frac{\partial p}{\partial y}+\rho g_y+\mu\left(\frac{\partial^2 v}{\partial x^2}+\frac{\partial^2 v}{\partial y^2}+\frac{\partial^2 v}{\partial z^2}\right). \tag{2.44}$$

Similarly in *z*-direction:

$$\rho\left[\frac{\partial w}{\partial t}+u\frac{\partial w}{\partial x}+v\frac{\partial w}{\partial y}+w\frac{\partial w}{\partial z}\right]=-\frac{\partial p}{\partial z}+\rho g_z+\mu\left(\frac{\partial^2 w}{\partial x^2}+\frac{\partial^2 w}{\partial y^2}+\frac{\partial^2 w}{\partial z^2}\right). \tag{2.45}$$

Or in term of vector, Equation (2.43) till Equation (2.45) can be expressed as:

$$\rho\left[\frac{\partial \tilde{V}}{\partial t}+\tilde{V}\bullet\nabla\tilde{V}\right]=-\nabla p+\rho\,\tilde{g}+\mu\nabla^2\tilde{V}\,. \tag{2.46}$$

Equation (2.43), (2.44) and (2.45) are known as NSEs, named in the honor of the French mechanician Claude Lewis Marie Henri Navier (1758-1836) and the English mathematician Sir. George Gabrielle Stokes (1819-1903). NSEs have four equations and four unknowns. It has a general complexity as they are nonlinear, second-order, partial differential

equations; they are not amenable to exact mathematical solutions. NSEs are considered to be the governing differential equations of motion for incompressible Newtonian fluids.

2.4 Analytical and Numerical Solutions

There are some analytical and numerical methods respectively to solve NSEs. In this section, the shortcomings of analytical solution and the reason why numerical solution should be adopted will be discussed and outlined respectively.

2.4.1 Method of Separation of Variables

This is an analytical solution to solve most of the second order partial differential equations such as wave equation, one and two-dimensional heat flow, radio equation and so on (Dass, 1988). However, this method can only solve those equations when the dependent variable is the product of two functions only and each of the dependent variables involves only one of the independent variables. It is done by forming two ordinary differential equations. Besides, it is only valid for linear partial differential equations. For example:

$$u(x, y) = X(x) \bullet Y(y), \tag{2.47}$$

where X is a function of x only and Y is a function of y only.

NSEs as shown in Equation (2.43) till Equation (2.45) are nonlinear because of those nonlinear convective acceleration terms $u\frac{\partial u}{\partial x}$, $v\frac{\partial u}{\partial y}$, $w\frac{\partial u}{\partial z}$, $u\frac{\partial v}{\partial x}$, $v\frac{\partial v}{\partial y}$, $w\frac{\partial v}{\partial z}$, $u\frac{\partial w}{\partial x}$ $v\frac{\partial w}{\partial y}$

and $w\frac{\partial w}{\partial y}$. $\frac{\partial \psi}{\partial x}\frac{\partial \zeta}{\partial y}$. Moreover, there are four independent variables as shown in Equation (2.43) till Equation (2.45) which are ∂t, ∂x, ∂y and ∂z. Another limitation of method of separation of variables is it only can solve up to two independent variables (Dass, 1988).

However, in some cases, there are some approximate or exact solutions of NSEs. For an instance, NSEs can be reduced to Euler‟s equation if the viscosity of fluid is negligible. Another scenario is to presume a slow flow (where the viscous force become dominant), so that all the convective terms can be neglected and the NSEs become linear. Thus, the resultant equation is amenable to analytical solutions to these „slow flow‟ or „creeping flow‟ (Munson, Young, Okiishi, 2002).

2.4.2 Finite Difference Method (FDM)

Finite difference method is a part of numerical methods. It‟s used rather than analytical method as analytical solutions to NSEs are restricted to inviscid and slow flows. However, in many cases these assumptions are impractical. Thus, recourse must be made to numerical method such as FDM. Some of the FDMs will be discussed in this section.

a.) Explicit Method:

NSEs require approximations for the second derivative in space and the first derivative in time. To obtain the finite difference form for Equation (2.43) till Equation (2.45), the central-difference approximations to the spatial derivatives might be applied and is shown as figure below:

Universiti Malaya

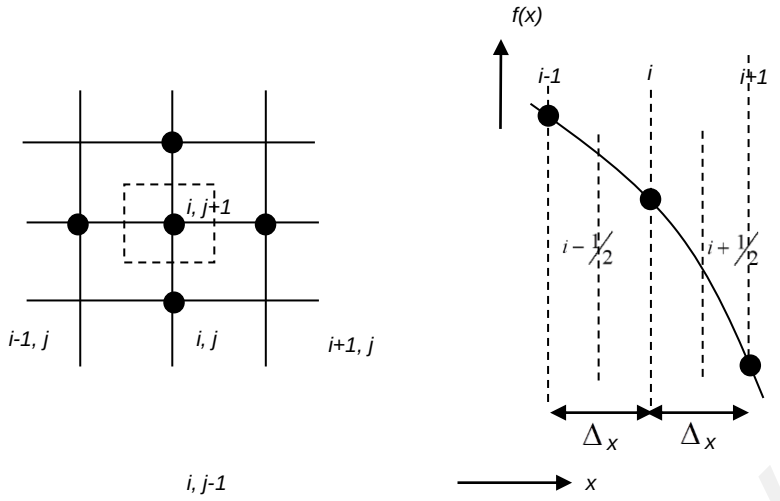

Figure 2.6: Nodal network and finite difference approximation (Incropera et al., 2006)

Based on the Figure 2.6, *i* and *j* are used to designate *x* and *y* locations of discrete nodal points. In this method, the independent variables shown in Equation (2.43) till Equation (2.45) are evaluated at the previous time. Hence, this method is considered as forward-difference approximation to the time derivative. However, due to its stability requirement, the value of time step, Δt should be chosen to avoid the numerical oscillations.

b.) Implicit Method:

In the explicit method, the function of any node at a new step time may be calculated from knowledge of function at the same and neighboring nodes for the preceding time. Although it offers computational convenience, it has problem related to stability. Implicit method can overcome this difficulty but with the expense of more complicated algorithms. This method is a backward-difference approximation to the time derivative. The new function of the *i*, *j* node depends on the function on new step time of its adjoining nodes which are

unknown. Thus, the corresponding nodal equations must be solved simultaneously. A suggested method is to form all the simultaneous equations into the form of a matrix and solve the matrix by using Gauss Seidel method or any other methods. Implicit formulation has the important advantage of being unconditionally stable. On the other hand, there is no restrictions on step size, Δx and step time, Δt. In order to maximize accuracy, step time should be sufficiently small to ensure that the results are independent of further reductions in its value.

c.) The ADI Scheme:

The alternating-direction implicit (ADI) scheme provides a means for solving parabolic equations in two spatial dimensions using tridiagonal matrices. It is based on the Crank-Nicolson method (Chapra & Canale, 2006) by averaging the value of mixture between implicit method and explicit method. It is constructed by two steps. For the first step, $\frac{d^2 f(x)}{dx^2}$ is written explicitly at the base point t^l where values of function are known while $\frac{d^2 f(x)}{dy^2}$ is written implicitly at the base point $t^{l+\frac{1}{2}}$. The finite difference equations for the nodes must be solved simultaneously for each time increment. By rearranging the equations into a matrix form, the first half step time is given by:

$$\begin{bmatrix} A_{11} & \cdots & \cdots & A_{i1} \\ \vdots & \ddots & & \vdots \\ \vdots & & \ddots & \vdots \\ A_{1j} & \cdots & \cdots & A_{ij} \end{bmatrix} \begin{bmatrix} f(x)_{i,1}^{l+1/2} \\ \vdots \\ \vdots \\ f(x)_{i,j}^{l+1/2} \end{bmatrix} = \begin{bmatrix} C_{1,1} \\ \vdots \\ \vdots \\ C_{i,j} \end{bmatrix}, \tag{2.48}$$

or it also can be expressed as:

$$[A][f(x)] = [C], \tag{2.49}$$

where matrix A depends on material properties, matrix $f(x)$ is the nodal function at the subsequent time $l + 1/2$ and matrix C is the column vector which is evaluated at previous step time, l.

For the second step, from $t^{l+1/2}$ to t^{l+1}, $\frac{d^2 f(x)}{dx^2}$ is written implicitly at the base point t^{l+1}. Similarly, by rearranging the equations into a matrix form, the second half step time is given by:

$$\begin{bmatrix} A_{11} & \cdots & \cdots & A_{i1} \\ \vdots & \ddots & & \vdots \\ \vdots & & \ddots & \vdots \\ A_{1j} & \cdots & \cdots & A_{ij} \end{bmatrix} \begin{bmatrix} f(x)_{i,1}^{l+1} \\ \vdots \\ \vdots \\ f(x)_{i,j}^{l+1} \end{bmatrix} = \begin{bmatrix} C_{1,1} \\ \vdots \\ \vdots \\ C_{i,j} \end{bmatrix}, \tag{2.50}$$

where the second half step time is denoted as $l+1$ while the matrix A keeps unchanged along the analysis as it merely depends on material properties.

There are a number of methods can be used to solve the matrix shown in Equation (2.48) and Equation (2.50). Gauss-Seidel iteration is suggested and it can be written as a

Universiti Malaya

logical source code in any programmable software. The iteration process keeps going on by calculating the new value of *f(x)* at a new step time from the old value of *f(x)* at the previous step time, *l*. The iteration is terminated until the prescribed criterion is satisfied. Any other method such as Gauss-Jordan, Gauss elimination or any analytical solution can be used to invert the matrix *A*. Programmable software such as Matlab® provides the built-in function to invert the matrix. Figure 2.7 shows the methods clearer.

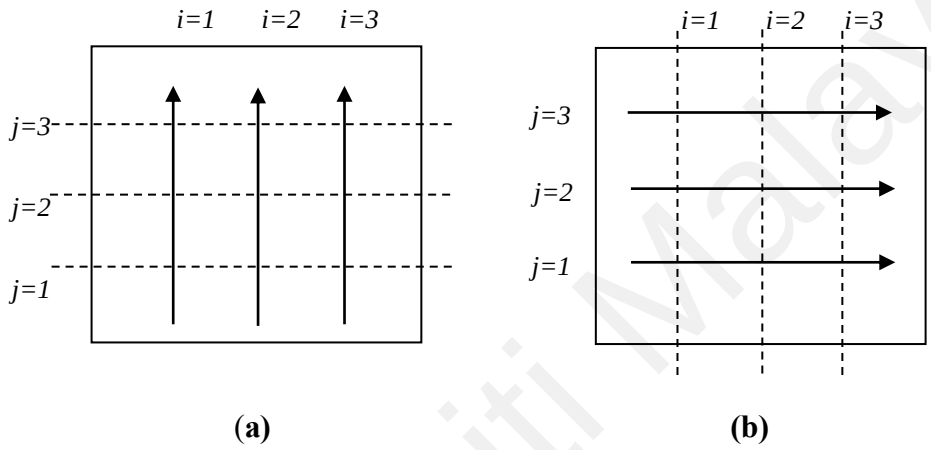

Figure 2.7: ADI method with a) First direction and b) second direction

Similarly, this scheme is limited by a stringent stability criterion similar to explicit method.

d.) The Energy Balance Method:

The methods mentioned above can only be used for fluid flow or heat transfer problem involving single material. As will become evident, this method enables the analysis to be done for many different phenomena such as problems involving multiple materials. The

Universiti Malaya

energy balance equation can be generated by applying conservation of energy to a control volume about the nodal region so that it can be applied to such a complicated BC.

e.) The Control-Volume Approach:

This approach (Chapra & Canale, 2006) offers an alternative method to solve a system with multiple materials and mixed BCs. However, this method becomes a more difficult endeavor for irregularly shaped boundaries. This approach resembles the point-wise approach where the points are determined across the domain. In other words, this approach is applied to a volume surrounding the point. The formulation of equation of this approach is the same with method mentioned in the preceding section by considering the conservation of energy.

2.5 Solution of NSEs by Other Authors

There are many authors who have successfully solved NSEs using various FDMs in the past. A novel form of NSEs in 2D lid-driven was done by Moshkin et al. (2009). This novel finite difference scheme was performed on a 2D square lid-driven cavity flow with no slip BCs up to $Re < 1000$. Subsequently, they compared the obtained value of minimum stream function, $\psi_{\min}$ of the primary eddy and secondary eddy from his novel finite difference scheme with the value obtained by other authors. Besides, the authors also suggested that if the iterations need to be run until a steady-state criterion is reached, then the suggested criterion:

$$\frac{\max_{i,j}\left|\sigma_{i,j}^{N+1}-\sigma_{i,j}^{N}\right|}{\max_{i,j}\left|\sigma_{i,j}^{N+1}\right|} \leq 10^{-8}, \tag{2.51}$$

should be satisfied, where σ is the new grid function, N is time step, i and j are the coordinates in nodal system.

Another comparison work have been done by Carlos Henrique Marchi, *et al.* (2009). The solution of NSEs was attempted by finite volume method with 1024×1024 grids. They outlined the problem of analytical solution on calculating velocity, u and veloctiy, v. Afterward, they compared the value of minimum stream function, $\psi_{\min}$, velocity, u and veloctiy, v with other authors. Typically, they employed a very small time step, Δt (range from $5.0 \times 10^{-4} s$ to 0.5 s) in solving the NSEs and the computation time needed to complete the calculation range from 1 day 9 hours to 9 days 1 hour. However, author didn't outline the reason why an extremely small value of time step, Δt should be employed to solve the iteration.

An efficient FDM was employed to solve 3D Navier-Stokes equation by Abd-El Hafiz S. K. *et al.* (2004). The authors (Abd-El-Hafiz et al., 2004) presume:

$$\mathrm{Re} = \frac{1}{\upsilon}, \tag{2.52}$$

where *Re* is Reynolds number and υ is kinematic viscosity.

The authors outlined the maximum allowable time step for 3D NSEs in order to fulfill the stability requirement which is:

$$\Delta t \leq \frac{\mathrm{Re}}{2\left[\dfrac{1}{(\Delta x)^2 + (\Delta y)^2 + (\Delta z)^2}\right]}, \tag{2.53}$$

where Δx, Δy and Δz are step sizes in *x*-direction, *y*-direction and *z*-direction respectively.

2.6 Lid-driven Trapezoidal Cavity Model

Lid-driven model can be modeled as trapezium rather than square or rectangle to increase its complexity. In this case, this trapezoidal model which consisted of circular obstacle may exclude the use of FDM and lead to the necessity of FEM. Mixed convection heat transfer and fluid flow analysis inside this model were studied extensively (Ismail & Chamkha, 2015; Ababaei et al., 2018). Certain wall was insulated while other walls were maintained isothermally at different temperature to investigate the heat transfer process. Figure 2.8 shows the trapezoidal lid-driven model.

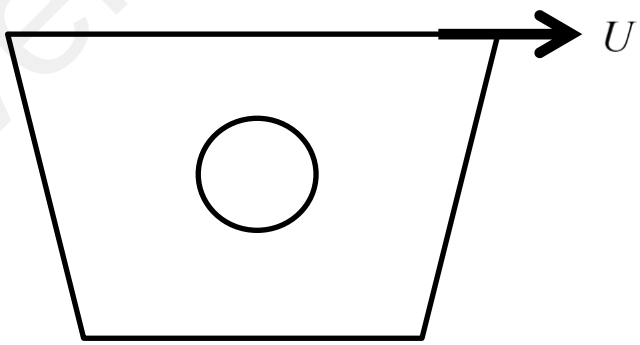

Figure 2.8: Trapezoidal lid-driven model

Similarly, the problem can be formulated using the stream function–vorticity procedure but solved using FEM. The inclination angle of the side walls are considered as pertinent parameters and investigated (Aly et al., 2016).

Universiti Malaya

2.7 Implementation of FDM in Other Applications

FDM is widely used in other applications besides of NSEs. Its application can be found in solving the mathematical model, wave equation in biology, chemistry and fluid mechanics applications, diffusion transport application, food study, heat and mass transfer and etc.

Table 2.1: FDM applications

Application Field	Details
Mathematics	a) FDM, finite element method (FEM) and finite volume methods had been applied to solve the two-point boundary value problem (Fang et al., 2002). The equation is shown as: $$-\frac{d}{dx}\left(p(x)\frac{du}{dx}\right)=f(x). \quad (2.54)$$ b) Implementation of FDM in solving the differential-algebraic equations and ordinary differential equations (Wu & White, 2004). c) The split-step FDM was used to solve nonlinear Schrodinger (NLS) equations. This NLS describes the dynamics of Bose-Einstein Condensate at very low temperature (Wang, 2005). d) FDM was used to solve fractional partial differential equation such as space-time fractional convection-diffusion equation which involves in fluid flow problem (Zhang, 2009). The equation is shown as below:

Universiti Malaya

	$$\frac{\partial^{\alpha} u(x,t)}{\partial t^{\alpha}} = -b(x)\frac{\partial u(x,t)}{\partial x} + a(x)\frac{\partial^{\beta} u(x,t)}{\partial x^{\beta}} - c(x)u(x,t) + q(x,t) \quad . \qquad (2.55)$$ e) The Burgers equation as an approach to NSEs is widely used in fluid dynamic problem. It had been solved by using explicit FDM (Kutluay et al., 1999). The equation is: $$\frac{\partial u}{\partial t} + u\frac{\partial u}{\partial x} = v\frac{\partial^2 u}{\partial x^2} \, . \qquad (2.56)$$ It is also known as linear parabolic partial differential equation.
Biology and Chemistry	a) FDM is used to calculte the X-ray Absorption Fine Structure (XAFS) for copper. This FDM enables the high accuracy of XAFS theory in the near edge regoin can be obtained (Bourke & Chantler, 2010). b) Fully implicit FDM was used to solve the fourth- and second-order partial differetial equations membrane-mediated protein-protein interactions and heat and magnetic field diffusion in plasma by using rectangular grid (Gennady et al., 2006). c) A three-dimensional of FDM is employed to solve the forward problem in electroencephalography (EEG) for calculating the electric potential in human head (Veronique, 2004). The electromagnetic field generators in the brain is the major problem in neuro-logical pathologies such as epilopsy. The equation of three-dimensional boundary problem is given as: $$-\nabla.(\sigma\nabla u) = f \, , \qquad (2.57)$$ where u represents the electrical potential, Ω is head and σ the electric conductivities. d) The explicit, fully implicit and semi implicit (Crank-Nicolson)

Universiti Malaya

	used to calculate non-steady state ion transfer due to diffusion and convection in unidimensional electrochemical systems. This method is also used to decouple the coupled continuity equations (Volgin et al., 2003). e) The formation of animal coat patterns had been solved by Peace-Rachford FDM until a steady-state value was obtained (Basiri et al., 2009). The mathematical model is shown in Equation 58: $$\begin{aligned} u_t &= \nabla^2 u + \gamma f(u,v), \\ v_t &= d\nabla^2 v + \gamma g(u,v) \end{aligned}, \quad (2.58)$$ where u and v are defined on the surface of tapering cylinder, s, γ and d are the positive constants.
Wave	a) A compact ADI scheme was used to solve the two-dimensional nonhomogeneous wave differential equation (Qin, 2009). The wave equation is: $$\frac{\partial^2 u}{\partial t^2} - (a\frac{\partial^2 u}{\partial x^2} + b\frac{\partial^2 u}{\partial y^2}) + cu = g(x,y,t), \quad (2.59)$$ where a, b and c are positive constants, g is the given functions with sufficient smoothness. Its ADI equations are: $$\begin{aligned} &(1-\frac{a\Delta t^2}{4A}\delta_x^2)(V_{i,j}^{n+1/2} - V_{i,j}^n) = \frac{\Delta t^2}{2A}(a\delta_x^2 + b\delta_y^2)V_{i,j}^n \\ &-\frac{c\Delta t^2}{2A}V_{i,j}^n + \frac{\Delta t}{A}(a\delta_x^2 + b\delta_y^2 - c)U_{i,j}^n + \frac{\Delta t}{A}g_{i,j}^{n+1/2} \end{aligned}, \quad (2.60)$$ $$(1-\frac{b\Delta t^2}{4A}\delta_y^2)(V_{i,j}^{n+1} - V_{i,j}^n) = V_{i,j}^{n+1/2} - V_{i,j}^n, \quad (2.61)$$ where Equation 60 is referred as first half step time and

Universiti Malaya

	Equation 61 is referred as second half step time. b) The wavefront propagation based on Eikonal, Fermat‟s and Huygen‟s principal had been solved by using FDM and written in FORTRAN 77 environment. It results in an accurate, efficient, stable and friendly computer code in travetime calculation (Zhao, 1996). The wavefront equation is: $$\left(\frac{dt}{dx}\right)^2 + \left(\frac{dt}{dy}\right)^2 = s^2, \quad (2.62)$$ where t is traveltime, x and y are coordinates, s is slowness parameter. c) The equal width (EW) and regularized long-wave (RLW) equation were used to investigate the creation of secondary solitary wave or radiation to get insight into corresponding process of the particle physics (Ramos, 2006). The equation is: $$u_t + \alpha u_x + \varepsilon (u_p)_x = \mu u_{xx} + \delta u_{xx}, \quad (2.63)$$ where u, t and x denote the amplitude, time and spatial coordinate respectively, $\alpha, \delta, \mu, \varepsilon$ are positive constants.
Finance	a) Explicit FDM and ADI are implemented to evaluate the multivariate contingent claims such as compensation plans, risk-sharing contracts, multifactor interest rate, pricing of foreign currency debts and so on (Manfred et al., 2002). The Euporean-style derivatives on the three risky assets is modelled as a linear parabolic partial differential equation: $$\frac{\partial C}{\partial t} = -\sum_{i=1}^{3} rS_i \frac{\partial C}{\partial S_i} - \frac{1}{2}\sum_{i,j=1}^{3} \frac{\partial^2 C}{\partial S_i S_j} \rho_{ij}\sigma_i\sigma_j + rC, \quad (2.64)$$ where S_i is the vector of prices, ρ_{ij} and $\sigma_{i,j}$ are the correlation

Universiti Malaya

	coefficients, r is the risk-free instantaneous interest rate. b) The compact FDM is used to solve the problem of pricing of American option. The simplest financial option is the European option (Zhao et al., 2007). It can be modelled by Black-Scholes partial differential equation as stated in Equation (2.65): $$p_t + \frac{\sigma^2}{2} S_1^{\,2} p_{SS} + (r - D) S_1 p_S - rp = 0\,, \qquad (2.65)$$ where S_1 is asset price, t is time, p_t is a function of underlying of S and t, r are the risk-free interest rates

2.8 Summary of Literature Reviews

Based on the study of the literature reviews, NSEs was successfully derived and shown using conservation of mass, the material derivative, description of forces acting on the differential element and stress-strain relation. Due to the difficulty in solving the NSEs as shown in Equation 43 till Equation 45 (also known as primitive variable formulation) as there is no evolution equation to calculate the pressure term, NSEs will be transformed into a vorticity-stream formulation by calculating the curl of NSEs as shown in the next chapter. Subsequently, all the available analytical and numerical solutions are studied extensively to investigate which method is suitable to be employed to solve the vorticity-stream formulation. Some literatures on those similar works were done by other authors to study which type of numerical method to be used to solve the designated scheme of NSEs. Finally, due to its impressive and powerful solution, FDM can also be applied in many other fields such as in solving the complicated partial differential equations, fluid mechanics, biology and chemistry, wave equation, financial problem and so on. Implementation of FDM has been

Universiti Malaya

proved for its accuracy and convenience. Figure 2.9 shows the application of FDM in multi-field which discussed in Section 2.7.

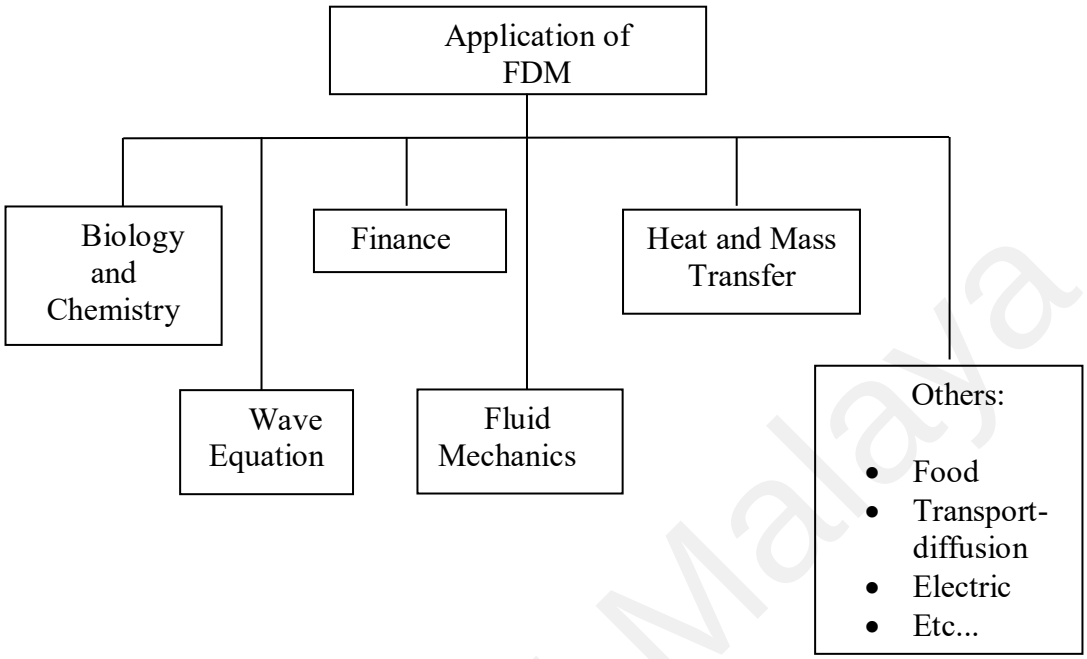

Figure 2.9: Application of FDM

Universiti Malaya

CHAPTER 3: METHODOLOGY

3.1 Overview

The flow chart of methodology throughout this thesis is shown in Figure 3.1. With reference to the flow chart as shown in Figure 3.1, this chapter describes the methodology of the project in Section 3.2. In Section 3.3, derivation of vorticity-stream formulation equation will be demonstrated by evaluating the curl of NSEs. After the appropriate assumptions and the equations had been defined, the suitable FDM has been chosen to solve the NSEs and viscous heating equation in the following section. In Section 3.5 and Section 3.6, vorticity-stream formulation equation and TEE will be discretized and employed to solve the lid-driven 2D analysis. Subsequently, Neumann and Robin BC will be adopted respectively in our work and their associated equation along the BC will be derived based on energy balance method. Stability criteria analysis will be carried out based on every single equation which obtained in Section 3.5 and Section 3.6. Derivation using generalized Newtonian model which proposed by Bird et al. (2002) and discretization of non-Newtonian governing equation will be shown in Section 3.8. In Section 3.9, equation of boundary layer model can be generated based on a 2D shear flow system. In Section 3.10, all the involved equations will be written as a source code in Matlab® and a graphical user interface (GUI) will be designed to facilitate the analysis of Newtonian fluid flow in Section 3.11. In the final section, verification of in-house Matlab® code will be provided using standard FEM software i.e. Ansys Fluent® which employing finite element method (FEM). The entire 2D model and its meshing properties in Ansys Fluent® were created and analysed.

Universiti Malaya

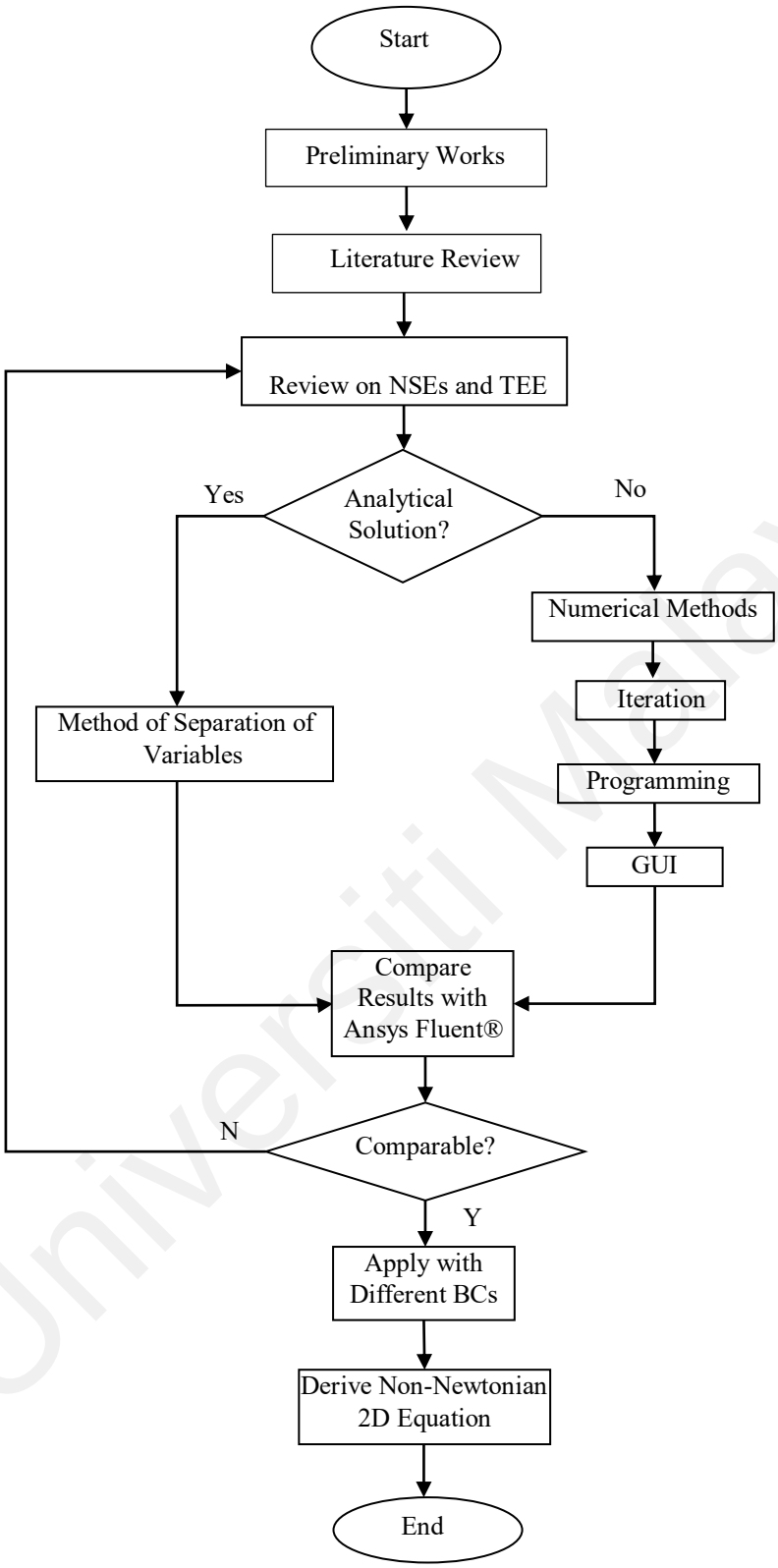

Figure 3.1: Methodology flow chart

Universiti Malaya

3.2 Methodology Process

Initially, preliminary works are to be carried out. These would include setting the objectives, planning and scheduling the tasks such as creating a Gantt chart, as well as defining the scope of work and the justification for the project. In our project, we only focus on laminar flow region. This is because for shear-thinning fluid (non-Newtonian fluid), low shear rate region will have high viscosity. Low shear rate also means laminar flow (or Stokes flow). Thus, laminar flow is important in low shear rate region for shear thinning fluid.

Once the preliminary works are done, literature review would be carried out to identify other researches in similar areas and also to conduct investigations regarding areas of interest in the title subject.

Numerical method also has been reviewed after the fundamental of NSEs had been studied. Some of the FDMs have been identified in term of their pro and con and the suitable method has been adopted in solving the complicated equations.

NSEs is only limited for Newtonian fluid flow analysis. To cater the fluid flow of non-Newtonian model, a governing non-Newtonian fluid flow momentum equation is need. Thus, it is necessary to study the incompressible generalized Newtonian model which proposed by Bird et al. (2002). Discretization of the non-Newtonian equation will be demonstrated as well.

All the finite difference equations (FDEs) of vorticity-stream formulation and TEE will be used to solve the 2D lid-driven cavity flow problem. This includes those finite difference equations of the boundary condition of the mentioned model.

Universiti Malaya

Programmable software such as Matlab® has been chosen in writing all the equations as the logical source code. Matlab® is a highly technical language and provides many built-in functions. GUI will be designed to facilitate the end user in analyzing the stream function and velocity profile as it was designed to provide the contour plot of stream function and velocity throughout the cavity flow.

All the results generated using in-house Matlab® code will be compared with commercial engineering simulation software i.e. Ansys Fluent®. Ansys Fluent® is utilizing FEM and it is able to provide a reliable result.

3.3 Derivation of Vorticity-stream Function

There are few types of schemes for the solution of NSEs which are velocity-pressure (also known as primitive variables), vorticity-stream function (Moshkin & Poochinapan, 2010), stream function and vorticity-velocity formulation. In this context, vorticity-stream formulation will be discussed in detail because it is widely used. We assume a two-dimensional flow field as shown in Figure 3.2:

Universiti Malaya

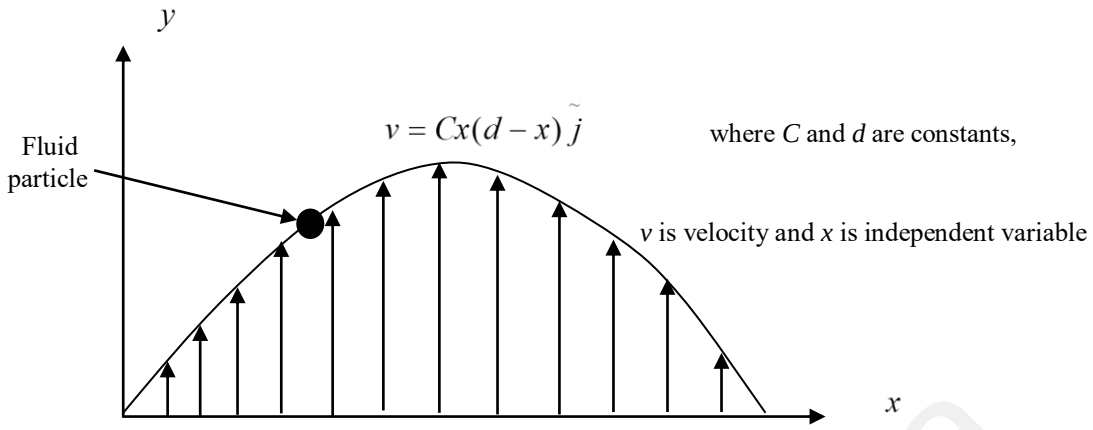

Figure 3.2: Two-dimensional flow field

Every fluid particle will rotate because of its viscosity (Munson et al., 2002) as shown in Figure 3.3. Viscous fluid will support shear stress and shear stress will create a torque, τ . The coupling of torque will make the fluid particle to rotate in *z*-axis only.

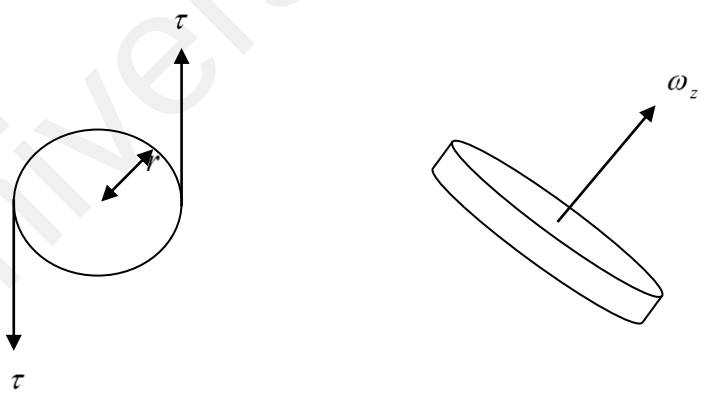

Figure 3.3: **Rotational fluid particle**

Thus, NSEs will reduce to:

$$\rho\left[\frac{\partial u}{\partial t}+u\frac{\partial u}{\partial x}+v\frac{\partial u}{\partial y}\right]=-\frac{\partial p}{\partial x}+\rho g_x+\mu\left(\frac{\partial^2 u}{\partial x^2}+\frac{\partial^2 u}{\partial y^2}\right), \text{ (in } x\text{-direction)} \tag{3.1}$$

$$\rho\left[\frac{\partial v}{\partial t}+u\frac{\partial v}{\partial x}+v\frac{\partial v}{\partial y}\right]=-\frac{\partial p}{\partial y}+\rho g_y+\mu\left(\frac{\partial^2 v}{\partial x^2}+\frac{\partial^2 v}{\partial y^2}\right), \text{ (in } y\text{-direction)} \tag{3.2}$$

where u and v are independent in z-direction.

Vorticity-stream function can be obtained by calculating the curl (Dass, 1988) of Equation (3.1) and Equation (3.2). The fluid particle subjected to rotation in z-axis is shown in Figure 3.4.

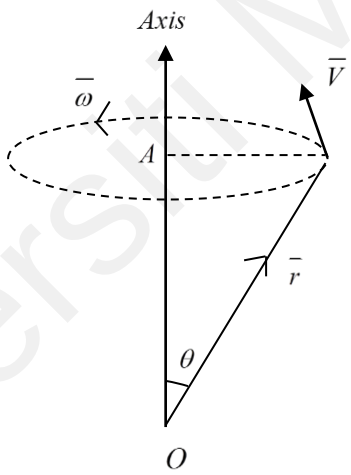

Figure 3.4: **Angular velocity**

$$Curl(NSEs)=\nabla\times\tilde{\omega}\times\tilde{r}\,,$$

$$=\nabla\times NSEs\,, \tag{3.3}$$

$$
= \begin{vmatrix} i & j & k \\ \frac{\partial}{\partial x} & \frac{\partial}{\partial y} & \frac{\partial}{\partial z} \\ \rho\left[\frac{\partial u}{\partial t} + u\frac{\partial u}{\partial x} + v\frac{\partial u}{\partial y}\right] = & \rho\left[\frac{\partial v}{\partial t} + u\frac{\partial v}{\partial x} + v\frac{\partial v}{\partial y}\right] = & \\ -\frac{\partial p}{\partial x} + \rho g_x + \mu\left(\frac{\partial^2 u}{\partial x^2} + \frac{\partial^2 u}{\partial y^2}\right) & -\frac{\partial p}{\partial y} + \rho g_y + \mu\left(\frac{\partial^2 v}{\partial x^2} + \frac{\partial^2 v}{\partial y^2}\right) & 0 \end{vmatrix},
$$

$$
= 0i + 0j + \begin{vmatrix} \frac{\partial}{\partial x}\left[\rho\left(\frac{\partial v}{\partial t} + u\frac{\partial v}{\partial x} + v\frac{\partial v}{\partial y}\right) = -\frac{\partial p}{\partial y} + \rho g_y + \mu\left(\frac{\partial^2 v}{\partial x^2} + \frac{\partial^2 v}{\partial y^2}\right)\right] - \\ \frac{\partial}{\partial y}\left[\rho\left[\frac{\partial u}{\partial t} + u\frac{\partial u}{\partial x} + v\frac{\partial u}{\partial y}\right] = -\frac{\partial p}{\partial x} + \rho g_x + \mu\left(\frac{\partial^2 u}{\partial x^2} + \frac{\partial^2 u}{\partial y^2}\right)\right] \end{vmatrix} k, \quad (3.4)
$$

Now we split Equation (3.4) into two separate equations:

$$
\frac{\partial}{\partial x}\left[\rho\left(\frac{\partial v}{\partial t} + u\frac{\partial v}{\partial x} + v\frac{\partial v}{\partial y}\right) = -\frac{\partial p}{\partial y} + \rho g_y + \mu\left(\frac{\partial^2 v}{\partial x^2} + \frac{\partial^2 v}{\partial y^2}\right)\right], \quad (3.5)
$$

$$
-\frac{\partial}{\partial y}\left[\rho\left[\frac{\partial u}{\partial t} + u\frac{\partial u}{\partial x} + v\frac{\partial u}{\partial y}\right] = -\frac{\partial p}{\partial x} + \rho g_x + \mu\left(\frac{\partial^2 u}{\partial x^2} + \frac{\partial^2 u}{\partial y^2}\right)\right]. \quad (3.6)
$$

By combining Equation (3.5) and Equation (3.6) yields,

$$
\frac{\partial}{\partial x}\left[\rho\left(\frac{\partial v}{\partial t} + u\frac{\partial v}{\partial x} + v\frac{\partial v}{\partial y}\right)\right] - \frac{\partial}{\partial y}\left[\rho\left(\frac{\partial u}{\partial t} + u\frac{\partial u}{\partial x} + v\frac{\partial u}{\partial y}\right)\right] =
$$

$$
\frac{\partial}{\partial x}\left[-\frac{\partial p}{\partial y} + \rho g_y + \mu\left(\frac{\partial^2 v}{\partial x^2} + \frac{\partial^2 v}{\partial y^2}\right)\right] - \frac{\partial}{\partial y}\left[-\frac{\partial p}{\partial x} + \rho g_x + \mu\left(\frac{\partial^2 u}{\partial x^2} + \frac{\partial^2 u}{\partial y^2}\right)\right],
$$

Universiti Malaya

$$\rho\frac{\partial^2 v}{\partial x\partial t}+\rho\frac{\partial u}{\partial x}\frac{\partial v}{\partial x}+\rho u\frac{\partial^2 v}{\partial x^2}+\rho\frac{\partial v}{\partial x}\frac{\partial v}{\partial y}+\rho v\frac{\partial^2 v}{\partial x\partial y}-\rho\frac{\partial^2 u}{\partial y\partial t}-\rho\frac{\partial u}{\partial y}\frac{\partial u}{\partial x}-\rho u\frac{\partial^2 u}{\partial x\partial y}-\rho\frac{\partial v}{\partial y}\frac{\partial u}{\partial y}$$
$$-\rho v\frac{\partial^2 u}{\partial y^2}=-\frac{\partial p}{\partial y\partial x}+\frac{\partial\rho g_x}{\partial x}+\mu\frac{\partial}{\partial x}\left(\frac{\partial^2 v}{\partial x^2}+\frac{\partial^2 v}{\partial y^2}\right)+\frac{\partial p}{\partial x\partial y}-\frac{\partial\rho g_y}{\partial x}-\mu\frac{\partial}{\partial y}\left(\frac{\partial^2 u}{\partial x^2}+\frac{\partial^2 u}{\partial y^2}\right),$$

$$\rho\left(\frac{\partial^2 v}{\partial x\partial t}-\frac{\partial^2 u}{\partial y\partial t}\right)+\rho\left(v\frac{\partial^2 v}{\partial x\partial y}-u\frac{\partial^2 u}{\partial x\partial y}\right)+\rho\left(\frac{\partial u}{\partial x}\frac{\partial v}{\partial x}-\frac{\partial u}{\partial y}\frac{\partial u}{\partial x}\right)+\rho\left(u\frac{\partial^2 v}{\partial x^2}-v\frac{\partial^2 u}{\partial y^2}\right)$$
$$+\rho\left(\frac{\partial v}{\partial x}\frac{\partial v}{\partial y}-\frac{\partial v}{\partial y}\frac{\partial u}{\partial y}\right)=\mu\frac{\partial}{\partial x}\left(\frac{\partial^2 v}{\partial x^2}+\frac{\partial^2 v}{\partial y^2}\right)-\mu\frac{\partial}{\partial y}\left(\frac{\partial^2 u}{\partial x^2}+\frac{\partial^2 u}{\partial y^2}\right),$$

$$\rho\frac{\partial}{\partial t}\left(\frac{\partial v}{\partial x}-\frac{\partial u}{\partial y}\right)+\rho\left(v\frac{\partial^2 v}{\partial x\partial y}-v\frac{\partial^2 u}{\partial y^2}\right)+\rho\left(\frac{\partial u}{\partial x}\frac{\partial v}{\partial x}-\frac{\partial u}{\partial y}\frac{\partial u}{\partial x}\right)+\rho\left(u\frac{\partial^2 v}{\partial x^2}-u\frac{\partial^2 u}{\partial x\partial y}\right)$$
$$+\rho\left(\frac{\partial v}{\partial x}\frac{\partial v}{\partial y}-\frac{\partial v}{\partial y}\frac{\partial u}{\partial y}\right)=\mu\frac{\partial}{\partial x}\left(\frac{\partial^2 v}{\partial x^2}\right)+\mu\frac{\partial}{\partial x}\left(\frac{\partial^2 v}{\partial y^2}\right)-\mu\frac{\partial}{\partial y}\left(\frac{\partial^2 u}{\partial x^2}\right)-\mu\frac{\partial}{\partial y}\left(\frac{\partial^2 u}{\partial y^2}\right),$$

$$\rho\frac{\partial}{\partial t}\left(\frac{\partial v}{\partial x}-\frac{\partial u}{\partial y}\right)+\rho v\frac{\partial}{\partial y}\left(\frac{\partial v}{\partial x}-\frac{\partial u}{\partial y}\right)+\rho\left(\frac{\partial u}{\partial x}\frac{\partial v}{\partial x}+\frac{\partial v}{\partial x}\frac{\partial v}{\partial y}\right)+\rho u\frac{\partial}{\partial x}\left(\frac{\partial v}{\partial x}-\frac{\partial u}{\partial y}\right)$$
$$-\rho\left(\frac{\partial u}{\partial y}\frac{\partial u}{\partial x}+\frac{\partial v}{\partial y}\frac{\partial u}{\partial y}\right)=\mu\frac{\partial}{\partial x}\left(\frac{\partial^2 v}{\partial x^2}\right)+\mu\frac{\partial}{\partial x}\left(\frac{\partial^2 v}{\partial y^2}\right)-\mu\frac{\partial}{\partial y}\left(\frac{\partial^2 u}{\partial x^2}\right)-\mu\frac{\partial}{\partial y}\left(\frac{\partial^2 u}{\partial y^2}\right),$$

$$\rho\frac{\partial}{\partial t}\left(\frac{\partial v}{\partial x}-\frac{\partial u}{\partial y}\right)+\rho v\frac{\partial}{\partial y}\left(\frac{\partial v}{\partial x}-\frac{\partial u}{\partial y}\right)+\rho\frac{\partial v}{\partial x}\left(\frac{\partial u}{\partial x}+\frac{\partial v}{\partial y}\right)+\rho u\frac{\partial}{\partial x}\left(\frac{\partial v}{\partial x}-\frac{\partial u}{\partial y}\right)-\rho\frac{\partial u}{\partial y}\left(\frac{\partial u}{\partial x}+\frac{\partial v}{\partial y}\right)$$
$$=\mu\frac{\partial}{\partial x}\left[\frac{\partial}{\partial x}\left(\frac{\partial v}{\partial x}\right)\right]+\mu\frac{\partial}{\partial x}\left[\frac{\partial}{\partial y}\left(\frac{\partial v}{\partial y}\right)\right]-\mu\frac{\partial}{\partial y}\left[\frac{\partial}{\partial x}\left(\frac{\partial u}{\partial x}\right)\right]-\mu\frac{\partial}{\partial y}\left[\frac{\partial}{\partial y}\left(\frac{\partial u}{\partial y}\right)\right],$$

$$\rho\frac{\partial}{\partial t}\left(\frac{\partial v}{\partial x}-\frac{\partial u}{\partial y}\right)+\rho v\frac{\partial}{\partial y}\left(\frac{\partial v}{\partial x}-\frac{\partial u}{\partial y}\right)+\rho u\frac{\partial}{\partial x}\left(\frac{\partial v}{\partial x}-\frac{\partial u}{\partial y}\right)+\rho\left(\frac{\partial v}{\partial x}-\frac{\partial u}{\partial y}\right)\left(\frac{\partial u}{\partial x}+\frac{\partial v}{\partial y}\right)$$
$$=\mu\frac{\partial}{\partial x}\left[\frac{\partial}{\partial x}\left(\frac{\partial v}{\partial x}\right)\right]+\mu\frac{\partial}{\partial x}\left[\frac{\partial}{\partial y}\left(\frac{\partial v}{\partial y}\right)\right]-\mu\frac{\partial}{\partial y}\left[\frac{\partial}{\partial x}\left(\frac{\partial u}{\partial x}\right)\right]-\mu\frac{\partial}{\partial y}\left[\frac{\partial}{\partial y}\left(\frac{\partial u}{\partial y}\right)\right].$$

Since for two-dimensional flow, the continuity equation is given by Equation (2.11):

$$\frac{\partial u}{\partial x}+\frac{\partial v}{\partial y}=0,$$

From Equation (2.11) and there is no component *w*, the above equation can be further reduced to:

$$\rho\frac{\partial}{\partial t}\left(\frac{\partial v}{\partial x}-\frac{\partial u}{\partial y}\right)+\rho v\frac{\partial}{\partial y}\left(\frac{\partial v}{\partial x}-\frac{\partial u}{\partial y}\right)+\rho u\frac{\partial}{\partial x}\left(\frac{\partial v}{\partial x}-\frac{\partial u}{\partial y}\right)$$
$$=\mu\frac{\partial^2}{\partial x^2}\left(\frac{\partial v}{\partial x}\right)+\mu\frac{\partial}{\partial y}\left[\frac{\partial}{\partial y}\left(\frac{\partial v}{\partial x}\right)\right]-\mu\frac{\partial}{\partial x}\left[\frac{\partial}{\partial x}\left(\frac{\partial u}{\partial y}\right)\right]-\mu\frac{\partial^2}{\partial y^2}\left(\frac{\partial u}{\partial y}\right),$$

$$\rho\frac{\partial}{\partial t}\left(\frac{\partial v}{\partial x}-\frac{\partial u}{\partial y}\right)+\rho v\frac{\partial}{\partial y}\left(\frac{\partial v}{\partial x}-\frac{\partial u}{\partial y}\right)+\rho u\frac{\partial}{\partial x}\left(\frac{\partial v}{\partial x}-\frac{\partial u}{\partial y}\right)$$
$$=\mu\frac{\partial^2}{\partial x^2}\left(\frac{\partial v}{\partial x}\right)+\mu\frac{\partial^2}{\partial y^2}\left(\frac{\partial v}{\partial x}\right)-\mu\frac{\partial^2}{\partial x^2}\left(\frac{\partial u}{\partial y}\right)-\mu\frac{\partial^2}{\partial y^2}\left(\frac{\partial u}{\partial y}\right),$$

$$\rho\frac{\partial}{\partial t}\left(\frac{\partial v}{\partial x}-\frac{\partial u}{\partial y}\right)+\rho v\frac{\partial}{\partial y}\left(\frac{\partial v}{\partial x}-\frac{\partial u}{\partial y}\right)+\rho u\frac{\partial}{\partial x}\left(\frac{\partial v}{\partial x}-\frac{\partial u}{\partial y}\right)$$
$$=\mu\frac{\partial^2}{\partial x^2}\left(\frac{\partial v}{\partial x}\right)-\mu\frac{\partial^2}{\partial x^2}\left(\frac{\partial u}{\partial y}\right)+\mu\frac{\partial^2}{\partial y^2}\left(\frac{\partial v}{\partial x}\right)-\mu\frac{\partial^2}{\partial y^2}\left(\frac{\partial u}{\partial y}\right),$$

$$\rho\frac{\partial}{\partial t}\left(\frac{\partial v}{\partial x}-\frac{\partial u}{\partial y}\right)+\rho v\frac{\partial}{\partial y}\left(\frac{\partial v}{\partial x}-\frac{\partial u}{\partial y}\right)+\rho u\frac{\partial}{\partial x}\left(\frac{\partial v}{\partial x}-\frac{\partial u}{\partial y}\right)$$
$$=\mu\frac{\partial^2}{\partial x^2}\left(\frac{\partial v}{\partial x}-\frac{\partial u}{\partial y}\right)+\mu\frac{\partial^2}{\partial y^2}\left(\frac{\partial v}{\partial x}-\frac{\partial u}{\partial y}\right), \tag{3.7}$$

By substituting vorticity, $\zeta=\frac{\partial v}{\partial x}-\frac{\partial u}{\partial y}$, (3.8)

Equation (3.7) becomes:

$$\frac{\partial\zeta}{\partial t}+v\frac{\partial\zeta}{\partial y}+u\frac{\partial\zeta}{\partial x}=\frac{\mu}{\rho}\left(\frac{\partial^2\zeta}{\partial x^2}+\frac{\partial^2\zeta}{\partial y^2}\right), \tag{3.9}$$

where $\zeta=2\omega_z$ (Munson et al., 2002) and

$$\omega_z=\frac{1}{2}\left(\frac{\partial v}{\partial x}-\frac{\partial u}{\partial y}\right). \tag{3.10}$$

Universiti Malaya

For two-dimensional flow, the stream function relates to the following velocities:

$$u = \frac{\partial \psi}{\partial y}, \tag{3.11}$$

$$v = -\frac{\partial \psi}{\partial x}. \tag{3.12}$$

Equation (3.9) becomes:

$$\frac{\partial \zeta}{\partial t} - \frac{\partial \psi}{\partial x}\frac{\partial \zeta}{\partial y} + \frac{\partial \psi}{\partial y}\frac{\partial \zeta}{\partial x} = \frac{\mu}{\rho}\left(\frac{\partial^2 \zeta}{\partial x^2} + \frac{\partial^2 \zeta}{\partial y^2}\right). \tag{3.13}$$

Equation (3.13) is also known as vorticity-transport equation. Equation (3.13) can be modified so that a dimensionless quantity, Reynolds number (Re) exists in these NSEs. We adopt the following dimensionless variables:

$$x^* = \frac{x}{L}, \quad y^* = \frac{y}{L}, \quad u^* = \frac{u}{V}, \quad v^* = \frac{v}{V}, \quad t^* = \frac{t}{L/V}, \tag{3.14}$$

where L is characteristic length, V is velocity, x^*, y^*, u^*, v^* and t^* are dimensionless quantities.

By substituting all the dimensionless quantities into Equation (3.13), we get:

$$\frac{\partial}{\partial(t^* \times \frac{L}{V})}\left(\frac{\partial(v^*V)}{\partial(x^*L)} - \frac{\partial(u^*V)}{\partial(y^*L)}\right) + (v^*V)\frac{\partial}{\partial(y^*L)}\left(\frac{\partial(v^*V)}{\partial(x^*L)} - \frac{\partial(u^*V)}{\partial(y^*L)}\right) + (u^*V)\frac{\partial}{\partial(x^*L)}\left(\frac{\partial(v^*V)}{\partial(x^*L)} - \frac{\partial(u^*V)}{\partial(y^*L)}\right),$$
$$= \frac{\mu}{\rho}\left[\frac{\partial}{\partial(x^*L)}\left(\frac{\partial}{\partial(x^*L)}\left(\frac{\partial(v^*V)}{\partial(x^*L)} - \frac{\partial(u^*V)}{\partial(y^*L)}\right)\right) + \frac{\partial}{\partial(y^*L)}\left(\frac{\partial}{\partial(y^*L)}\left(\frac{\partial(v^*V)}{\partial(x^*L)} - \frac{\partial(u^*V)}{\partial(y^*L}\right)\right)\right]$$

$$\frac{V^2}{L^2}\left[\frac{\partial}{\partial t^*}\left(\frac{\partial v^*}{\partial x^*}-\frac{\partial u^*}{\partial y^*}\right)+v^*\frac{\partial}{\partial y^*}\left(\frac{\partial v^*}{\partial x^*}-\frac{\partial u^*}{\partial y^*}\right)+u^*\frac{\partial}{\partial x^*}\left(\frac{\partial v^*}{\partial x^*}-\frac{\partial u^*}{\partial y^*}\right)\right]$$
$$=\frac{V}{L^3}\left[\frac{\mu}{\rho}\left[\frac{\partial}{\partial x^*}\left(\frac{\partial}{\partial x^*}\left(\frac{\partial v^*}{\partial x^*}-\frac{\partial u^*}{\partial y^*}\right)\right)+\frac{\partial}{\partial y^*}\left(\frac{\partial}{\partial y^*}\left(\frac{\partial v^*}{\partial x^*}-\frac{\partial u^*}{\partial y^*}\right)\right)\right]\right],$$

$$\frac{\partial}{\partial t^*}\left(\frac{\partial v^*}{\partial x^*}-\frac{\partial u^*}{\partial y^*}\right)+v^*\frac{\partial}{\partial y^*}\left(\frac{\partial v^*}{\partial x^*}-\frac{\partial u^*}{\partial y^*}\right)+u^*\frac{\partial}{\partial x^*}\left(\frac{\partial v^*}{\partial x^*}-\frac{\partial u^*}{\partial y^*}\right)$$
$$=\frac{1}{VL}\times\frac{\mu}{\rho}\left[\frac{\partial}{\partial x^*}\left(\frac{\partial}{\partial x^*}\left(\frac{\partial v^*}{\partial x^*}-\frac{\partial u^*}{\partial y^*}\right)\right)+\frac{\partial}{\partial y^*}\left(\frac{\partial}{\partial y^*}\left(\frac{\partial v^*}{\partial x^*}-\frac{\partial u^*}{\partial y^*}\right)\right)\right],$$

$$\frac{\partial}{\partial t^*}\left(\frac{\partial v^*}{\partial x^*}-\frac{\partial u^*}{\partial y^*}\right)+v^*\frac{\partial}{\partial y^*}\left(\frac{\partial v^*}{\partial x^*}-\frac{\partial u^*}{\partial y^*}\right)+u^*\frac{\partial}{\partial x^*}\left(\frac{\partial v^*}{\partial x^*}-\frac{\partial u^*}{\partial y^*}\right)$$
$$=\frac{\mu}{V\rho L}\left[\frac{\partial}{\partial x^*}\left(\frac{\partial}{\partial x^*}\left(\frac{\partial v^*}{\partial x^*}-\frac{\partial u^*}{\partial y^*}\right)\right)+\frac{\partial}{\partial y^*}\left(\frac{\partial}{\partial y^*}\left(\frac{\partial v^*}{\partial x^*}-\frac{\partial u^*}{\partial y^*}\right)\right)\right]. \tag{3.15}$$

By substituting $\mathrm{Re}=\frac{V\rho L}{\mu}$ and $\zeta^*=\frac{\partial v^*}{\partial x^*}-\frac{\partial u^*}{\partial y^*}$ into Equation (3.15),

$$\frac{\partial\zeta^*}{\partial t^*}+v^*\frac{\partial\zeta^*}{\partial y^*}+u^*\frac{\partial\zeta^*}{\partial x^*}=\frac{1}{\mathrm{Re}}\left[\frac{\partial^2\zeta^*}{\partial x^{*2}}+\frac{\partial^2\zeta^*}{\partial y^{*2}}\right]. \tag{3.16}$$

From Equation (3.11) and Equation (3.12), the dimensionless of the stream function can be derived as follows:

$\partial\psi=u\partial y$, from Equation (3.11)

Dividing by VL,

$$\frac{\partial\psi}{VL}=\frac{u}{V}\frac{\partial y}{L},$$

$\partial\psi^* = u^*\partial y^*$,

Rearranging the above equation,

$$u^* = \frac{\partial\psi^*}{\partial y^*}. \tag{3.17}$$

Similarly, the dimensionless of Equation (3.12) becomes:

$$v^* = -\frac{\partial\psi^*}{\partial x^*}. \tag{3.18}$$

Substituting Equation (3.17) and Equation (3.18) into Equation (3.16) yields:

$$\frac{\partial\zeta^*}{\partial t^*} - \frac{\partial\psi^*}{\partial x^*}\frac{\partial\zeta^*}{\partial y^*} + \frac{\partial\psi^*}{\partial y^*}\frac{\partial\zeta^*}{\partial x^*} = \frac{1}{\mathrm{Re}}\left[\frac{\partial^2\zeta^*}{\partial x^{*2}} + \frac{\partial^2\zeta^*}{\partial y^{*2}}\right] \ldots 3.19$$

Equation (3.19) is known as dimensionless vorticity stream-function equation.

3.4 Numerical Method in Solving Vorticity Stream-function Equation

Because of the general complexity of the vorticity stream-function formulation (second order nonlinear terms $\frac{\partial\psi}{\partial y}\frac{\partial\zeta}{\partial x}$ and $\frac{\partial\psi}{\partial x}\frac{\partial\zeta}{\partial y}$ on the left hand side of the equation, partial differential equations), it is not amenable to exact solution. Moreover, there are three independent variables as shown in Equation (3.9) which are ∂t, ∂x and ∂y. They are various techniques available for the numerical solution of the governing differential equations of fluid flow namely as discussed in Section 2.4: FDM, finite element, boundary element method and

Universiti Malaya

etc. By using these methods, differential equations are replaced by a set of algebraic equations.

The FDM typically is the most easily understood and widely used of the mentioned methods listed above. The flow field is dissected into a set of grid points and the continuous functions (velocity, pressure, etc) are approximated by discrete values of these functions calculated at the grid points in this method. The differential equations are thereby transferred into a set of algebraic equations, which is solved by appropriate numerical techniques. The larger the number of grid points used, the larger the number of equations that must be solved. It is usually necessary to increase the number of grid points where large gradients are to be expected, such as in the boundary layer near a solid surface (Munson et al., 2002). Figure 3.5 shows the grid system used for the finite difference solution of parabolic partial difference equation in two independent variables.

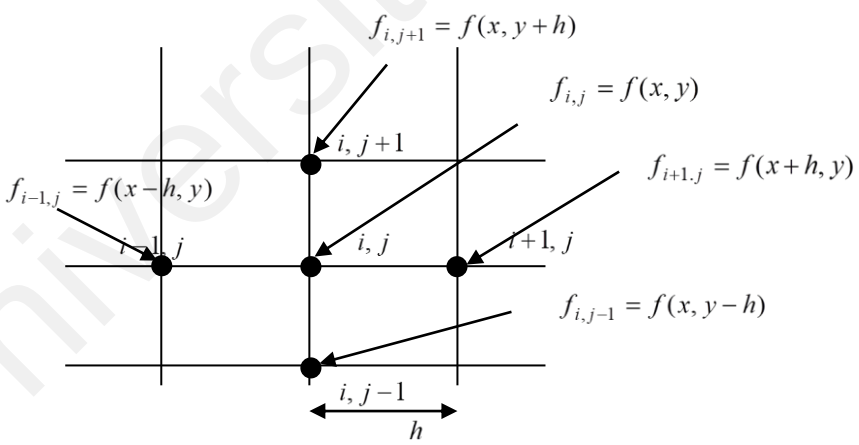

Figure 3.5: Grid used for the finite-difference solution (Chapra & Canale, 2006)

Universiti Malaya

The properties of the different types of FDM which discussed in Section 2.4.2 are analyzed in this section. The table below shows the advantages and disadvantages of each of the methods:

Table 3.1: Properties of FDM

	Explicit	**Implicit**	**ADI scheme**
Advantage	Calculation of unknown temperature is straightforward. No formation of matrices is needed.	No stability problem. Thus the solution remains stable for all space and time intervals. Can reduce the computation time and computational effort.	Retain properties of tridiagonal matrices in solving two-dimensional governing equation.
Disadvantage	Stability problem, oscillation increases with larger step time. Value of step time may not be chosen independently but determined by stability requirement. Computational effort	It involves more complicated algorithms. Need to form matrices and invert the matrices by Gauss-Seidel method or other methods. The matrices lose the valuable property of	Same with explicit method, it retains the stability problem since it is based on Crank-Nicolson method. Larger computational effort as it is consisted of two steps.

Universiti Malaya

	increases with decreasing step time to ensure accuracy.	being tridiagonal when solving two or three-dimensional model problem.	
Remark	It is a forward finite difference approximation. The unknown variable for the new step time are determined exclusively by known variable at the previous time.	It is a backward finite difference approximation. Need to form the corresponding nodal equations and solved simultaneously. Matrix is needed	It is constructed by two steps. The first step implicitly solves in one direction only while the second step implicitly solves in another direction only.

Based on the analysis shown in the Table 3.1, explicit and central FDM has been adopted in solving the two-dimensional NSEs in this analysis such as Equation (3.21) and Equation (3.47). This is because it is the simplest method and no matrices are needed to be formed like what the other two methods do, whereas the number of terms in the equations is too large to be solved efficiently if implicit method is applied. However, the maximum allowable step time needs to be determined from the stability criterion and it results in a longer computation time and more effort is needed. Figure 3.6 shows the explicit method with nodes that constitute the spatial and temporal approximations.

Universiti Malaya

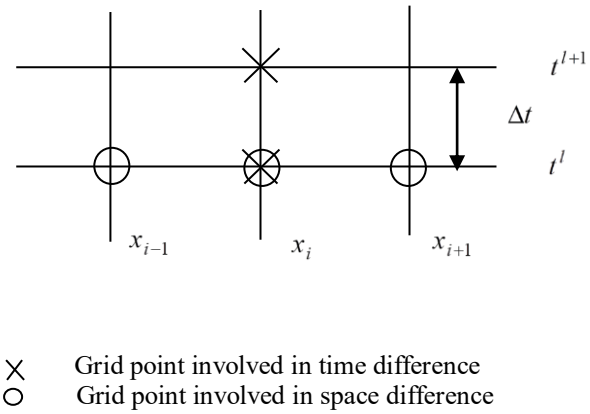

Figure 3.6: Finite difference in explicit form (Chapra & Canale, 2006)

Equation (3.13) can be transferred into a finite difference equation (FDE) using forward and centered finite-divided-difference formula:

$$\begin{aligned}\frac{\zeta_{i,j}^{t+1}-\zeta_{i,j}^{t}}{\Delta t} &= -\left(\frac{\psi_{i,j+1}^{t}-\psi_{i,j-1}^{t}}{2h}\right)\left(\frac{\zeta_{i+1,j}^{t}-\zeta_{i-1,j}^{t}}{2h}\right)+\left(\frac{\psi_{i+1,j}^{t}-\psi_{i-1,j}^{t}}{2h}\right)\left(\frac{\zeta_{i,j+1}^{t}-\zeta_{i,j-1}^{t}}{2h}\right), \\ &+\frac{\mu}{\rho}\left(\frac{\zeta_{i+1,j}^{t}+\zeta_{i-1,j}^{t}+\zeta_{i,j+1}^{t}+\zeta_{i,j-1}^{t}-4\zeta_{i,j}^{t}}{h^2}\right)\end{aligned} \tag{3.20}$$

where h is step size.

Rearrange Equation (3.20) yields:

$$\begin{aligned}\zeta_{i,j}^{t+1} &= -\Delta t\left[\left(\frac{\psi_{i,j+1}^{t}-\psi_{i,j-1}^{t}}{2h}\right)\left(\frac{\zeta_{i+1,j}^{t}-\zeta_{i-1,j}^{t}}{2h}\right)-\left(\frac{\psi_{i+1,j}^{t}-\psi_{i-1,j}^{t}}{2h}\right)\left(\frac{\zeta_{i,j+1}^{t}-\zeta_{i,j-1}^{t}}{2h}\right)\right]. \\ &+\Delta t\times\frac{\mu}{\rho}\left(\frac{\zeta_{i+1,j}^{t}+\zeta_{i-1,j}^{t}+\zeta_{i,j+1}^{t}+\zeta_{i,j-1}^{t}}{h^2}\right)+\left(1-\frac{4\upsilon\Delta t}{h^2}\right)\zeta_{i,j}^{t}\end{aligned} \tag{3.21}$$

The criterion is determined by requiring that the coefficient associated with the node of interest at the previous time is greater than or equal to zero (Incropera et al., 2006).

$$\left(1-\frac{4\upsilon\Delta t}{h^2}\right)\geq 0 \text{ or } \Delta t \leq \frac{h^2}{4\upsilon}, \tag{3.22}$$

where $\upsilon = \frac{\mu}{\rho}$ (or known as kinematic viscosity).

Equation (3.22) is the stability criterion because of its conditional stability.

Substitute Equation (3.11) and Equation (3.12) into Equation (3.8) yields:

$$-\zeta = \frac{\partial^2\psi}{\partial x^2} + \frac{\partial^2\psi}{\partial y^2}. \tag{3.23}$$

Equation (3.23) is called Poisson Equation (Chapra & Canale, 2006). Similarly, Equation (3.23) can be discretized using the finite difference as shown in Figure 3.5.

$$-\zeta_{i,j}^{n} = \frac{\psi_{i+1,j}^{n} + \psi_{i-1,j}^{n} + \psi_{i,j+1}^{n} + \psi_{i,j-1}^{n} - 4\psi_{i,j}^{n}}{h^2}. \tag{3.24}$$

Rewrite Equation (3.24) gives:

$$\psi_{i,j}^{n+1} = \frac{1}{4}\left(\psi_{i+1,j}^{n} + \psi_{i-1,j}^{n} + \psi_{i,j+1}^{n} + \psi_{i,j-1}^{n} + h^2\zeta_{i,j}^{n}\right), \tag{3.25}$$

where n is the iteration steps, h is step size.

Equation (3.25) can be solved by using Gauss-Seidel method (Dass, 1988). By equating ∂x^* and ∂y^* as shown in Equation (3.14), the FDE of Equation (3.19) can be obtained:

$$\partial x^* = \partial y^* = h* \text{ and } \partial t^* = \Delta t^*, \tag{3.26}$$

Universiti Malaya

$$\frac{\zeta^{*t+1}_{i,j}-\zeta^{*t}_{i,j}}{\Delta t^*}=-\left(\frac{\psi^{*t}_{i,j+1}-\psi^{*t}_{i,j-1}}{2h^*}\right)\left(\frac{\zeta^{*t}_{i+1,j}-\zeta^{*t}_{i-1,j}}{2h^*}\right)+\left(\frac{\psi^{*t}_{i+1,j}-\psi^{*t}_{i-1,j}}{2h^*}\right)\left(\frac{\zeta^{*t}_{i,j+1}-\zeta^{*t}_{i,j-1}}{2h^*}\right)$$
$$+\frac{1}{\mathrm{Re}}\left(\frac{\zeta^{*t}_{i+1,j}+\zeta^{*t}_{i-1,j}+\zeta^{*t}_{i,j+1}+\zeta^{*t}_{i,j-1}-4\zeta^{*t}_{i,j}}{h^{*2}}\right).$$

(3.27)

Rearrange Equation (3.27):

$$\zeta^{*t+1}_{i,j}=-\Delta t^*\left[\begin{array}{l}\left(\frac{\psi^{*t}_{i,j+1}-\psi^{*t}_{i,j-1}}{2h^*}\right)\left(\frac{\zeta^{*t}_{i+1,j}-\zeta^{*t}_{i-1,j}}{2h^*}\right)-\\ \left(\frac{\psi^{*t}_{i+1,j}-\psi^{*t}_{i-1,j}}{2h^*}\right)\left(\frac{\zeta^{*t}_{i,j+1}-\zeta^{*t}_{i,j-1}}{2h^*}\right)\end{array}\right]$$
$$+\frac{\Delta t^*}{\mathrm{Re}}\left(\frac{\zeta^{*t}_{i+1,j}+\zeta^{*t}_{i-1,j}+\zeta^{*t}_{i,j+1}+\zeta^{*t}_{i,j-1}}{h^{*2}}\right)+\left(1-\frac{4\Delta t^*}{\mathrm{Re}.h^{*2}}\right)\zeta^{*t}_{i,j}. \quad (3.28)$$

Thus, $\left(1-\frac{4\Delta t^*}{\mathrm{Re}.h^{*2}}\right)\geq 0$ or $\Delta t^*\leq\frac{\mathrm{Re}.h^{*2}}{4}$. (3.29)

Equation (3.29) is known as stability criterion in dimensionless analysis.

3.5 Lid-driven in 2D Fluid Flow Analysis

The discretized vorticity transport equation will be employed here to solve the lid-driven 2D analysis. Figure 3.7 shows the model of the lid-driven laminar flow in a 2D cavity.

Universiti Malaya

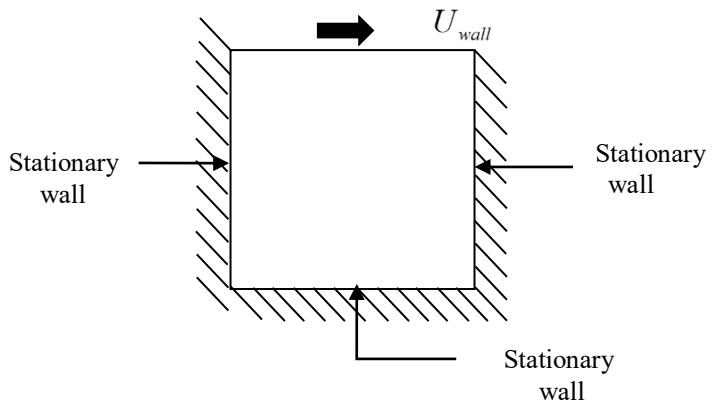

Figure 3.7: Lid-driven in 2D analysis

The BC of all the walls, applied force, Newtonian fluid properties are depicted in Figure 3.8. In this case, the applied velocity, U_{wall} is imposed on the top lid, u and v are the velocity vectors in $x-$and $y-$directions, ρ and μ are fluid density and dynamic viscosity, $\left.\frac{\partial u}{\partial y}\right|_{x=0}$, $\left.\frac{\partial u}{\partial y}\right|_{x=L}$ and $\left.\frac{\partial v}{\partial x}\right|_{y=0}$ are the velocity gradient along the fixed wall in $x-$and $y-$directions, H and L are the height and length of the cavity. The fluid flow analysis is carried out first and then followed by heat transfer analysis. The schematic drawing of a two-dimensional lid-driven cavity model within the Cartesian coordinate system used in the fluid flow and heat transfer analyses are shown in Figure 3.8.

Universiti Malaya

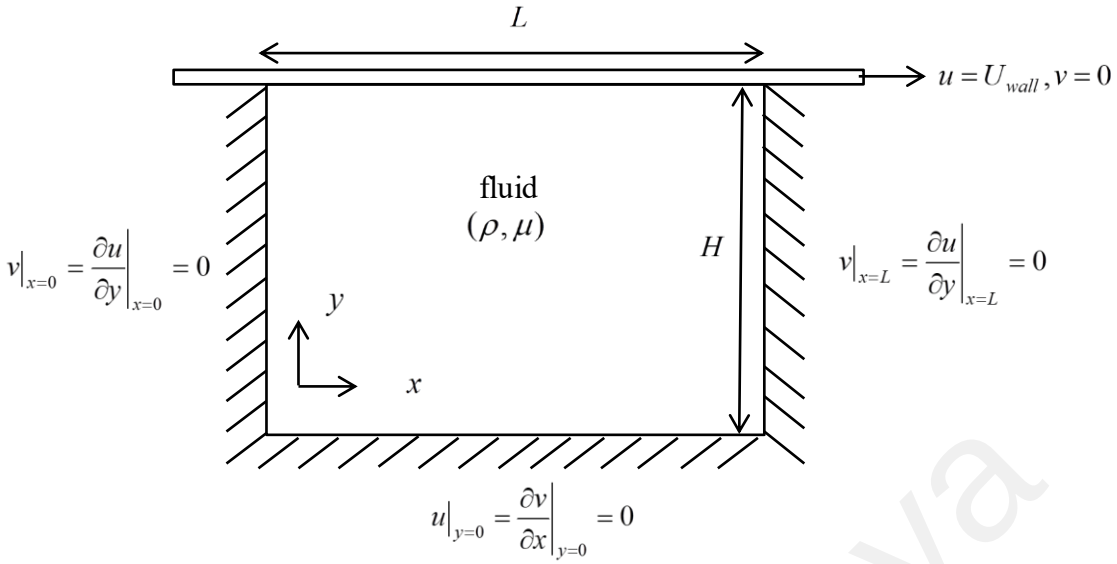

Figure 3.8: Schematic drawing of lid-driven in 2D fluid flow analysis

The schematic drawing of the above model is shown in Figure 3.9 which includes all the nodal points.

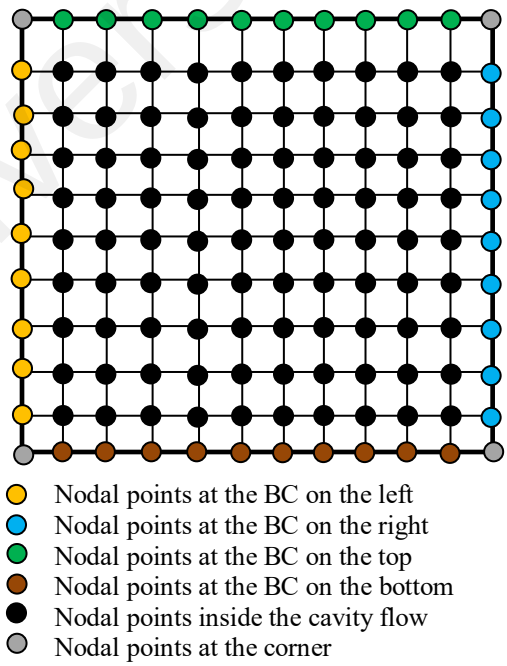

Figure 3.9: Lid-driven in 2D analysis

All the nodal points shown in the Figure 3.9 represent its finite difference nodes that used in each region respectively. Each of the finite difference nodes comprises one finite difference equation. However, there are only finite difference equations represented by the nodal points inside the cavity flow was obtained by far. In order to obtain the FDE on each of the BCs, Taylor series expansion is required (University department in Dortmund, Germany, 2017). Uniform mesh is adopted in this thesis as we want to make the algorithm simpler. Our in-house coding can be modified so that non-uniform mesh can be adopted but this will lead to a more complicated algorithm. In order to correctly capture the thermal analysis near the boundary layer, we can use a very fine uniform mesh for the whole lid-driven model (very fine mesh should be utilized near the boundary layer because the velocity and thermal gradient is large if compared to other region).

3.5.1 Discretization of BCs for Lid-driven Cavity

Figure 3.10 shows the BC of the stream function at the bottom.

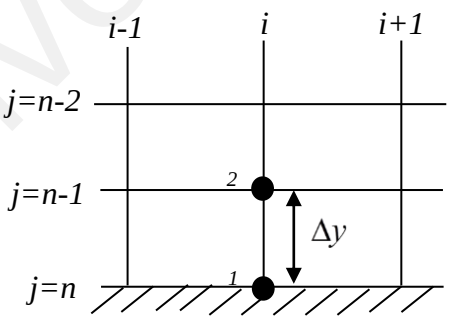

Figure 3.10: BC at the bottom

Stream function at the bottom can be expanded using Taylor series expansion which leads to:

$$\psi(y) = \sum_{n=0}^{\infty}\left[\frac{(y-y_i)^n}{n!}\left(\frac{\partial^n \psi}{\partial y^n}\right)_i\right], \tag{3.30}$$

$$\psi_{i,j=ny} = \psi_{i,j=ny-1} + \frac{\partial \psi_{i,j=ny-1}}{\partial y} h + \frac{\partial^2 \psi_{i,j=ny-1}}{\partial y^2}\frac{h^2}{2} + O(h^3), \tag{3.31}$$

where $O(h^3)$ is of higher order and can be ignored.

Figure 3.11 shows the no-slip BC (Munson et al., 2002) in laminar flow. This BC is true whether the fluid is relatively inviscid air or a very viscous fluid because the viscous effect causes it to stick to the wall.

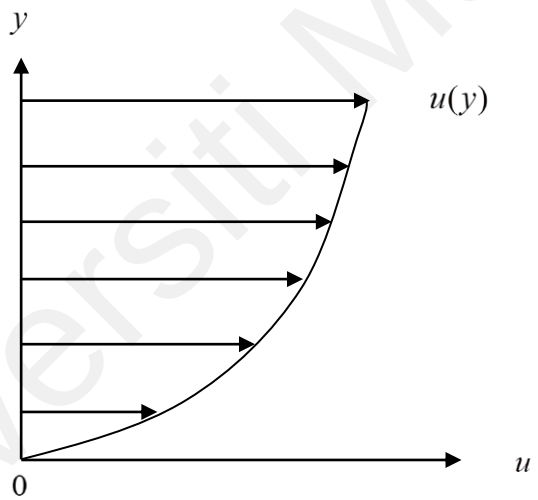

Figure 3.11: No-slip BC (Munson et al., 2002)

Velocity of fluid at the wall is zero and the velocity profile does not vary with *x*. Thus *u(0)=0* and $\frac{\partial v}{\partial x} = 0$. From Equation (3.11),

$\frac{\partial \psi}{\partial y} = u_1(y) = u_1(0) = U_{wall} = 0$ and also from Equation (3.23), $\zeta_{bottom} = -\frac{\partial u}{\partial y} = -\frac{\partial^2 \psi}{\partial y^2}$

Thus, $-\zeta_{bottom} = \frac{\partial^2 \psi}{\partial y^2}$. By substituting $\frac{\partial \psi}{\partial y} = 0$ and $-\zeta_{bottom} = \frac{\partial^2 \psi}{\partial y^2}$ into Equation (3.31), this will lead to:

$$\psi_{i,j=ny} = \psi_{i,j=ny-1} - \zeta_{bottom} \frac{\Delta y^2}{2} \quad \text{or}$$

$$\zeta_{bottom} = \frac{-2(\psi_{i,j=ny-1} - \psi_{i,j=ny})}{\Delta y^2}, \tag{3.32}$$

where $\Delta y = h$.

Similarly, the same procedure can be applied to BC of the stream function at the top wall. Figure 3.12 shows BC of the stream function at the top wall.

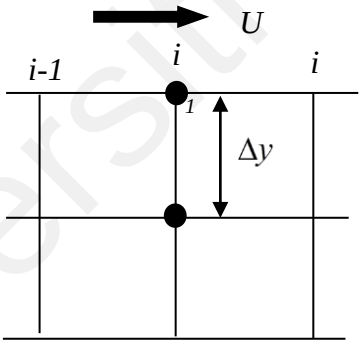

Figure 3.12: BC at the top

Velocity of fluid at the wall is U_{wall} and the velocity profile does not vary with x. Thus $\frac{\partial v}{\partial x} = 0$, $\frac{\partial \psi}{\partial y} = U_{wall}$, $\zeta_{top} = -\frac{\partial u}{\partial y} = -\frac{\partial^2 \psi}{\partial y^2}$ and $\Delta y = h$. From Equation (3.31),

$$\psi_{i,j=2} = \psi_{i,j=1} + U_{wall}(\Delta y) + (-\zeta_{top})\frac{\Delta y^2}{2} + 0, \tag{3.33}$$

Rearranging Equation (3.33) will yield:

$$\zeta_{top} = \frac{-2(\psi_{i,j=2} - \psi_{i,j=1})}{\Delta y^2} + \frac{2U_{wall}}{\Delta y}. \tag{3.34}$$

The BCs for the left and right walls are a little bit different if compared to top and bottom walls. Figure 3.13 shows the BC at the left wall.

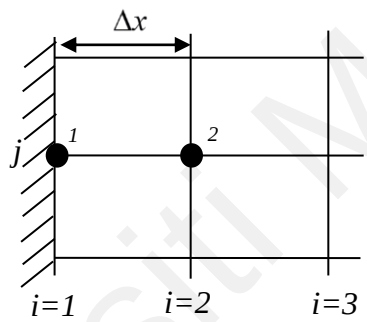

Figure 3.13: BC at the left

Figure 3.14 shows the no-slip BC at the left wall. In this case, velocity of fluid at the left wall is zero and the velocity profile does not vary with *y*. Thus *v(0)=0* and $\frac{\partial u}{\partial y} = 0$ based on Figure 3.14. From Equation (3.12),

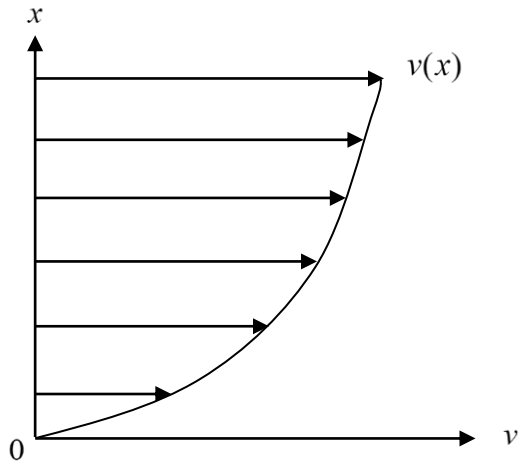

Figure 3.14: No-slip BC on the left wall

$\frac{\partial \psi}{\partial x} = v_1(x) = v_1(0) = V_{wall} = 0$ and also from Equation (3.23),

$$\zeta_{left} = \frac{\partial v}{\partial x} = -\frac{\partial^2 \psi}{\partial x^2}$$

Thus, $-\zeta_{left} = \frac{\partial^2 \psi}{\partial x^2}$.

Similarly, the stream function in *x*-direction can be expressed as:

$$\psi_{i=2,j} = \psi_{i=1,j} + \frac{\partial \psi_{i=1,j}}{\partial x}\Delta x + \frac{\partial^2 \psi_{i=1,j}}{\partial x^2}\frac{\Delta x^2}{2}, \qquad \text{from (3.31)}$$

By substituting $\frac{\partial \psi}{\partial x} = 0$ and $-\zeta_{left} = \frac{\partial^2 \psi}{\partial x^2}$ into Equation (3.31), this will lead to:

$$\psi_{i=2,j} = \psi_{i=1,j} - \zeta_{left}\frac{\Delta x^2}{2}. \qquad (3.35)$$

By rearranging Equation (3.35), it will lead to:

$$\zeta_{left} = \frac{-2(\psi_{i=2,j} - \psi_{i=1,j})}{\Delta x^2}. \tag{3.36}$$

Similarly, the BC of at the right wall is given by:

$$\zeta_{right} = \frac{-2(\psi_{i=nx-1,j} - \psi_{i=nx,j})}{\Delta x^2}. \tag{3.37}$$

Figure 3.15 shows the overall BCs at four sides.

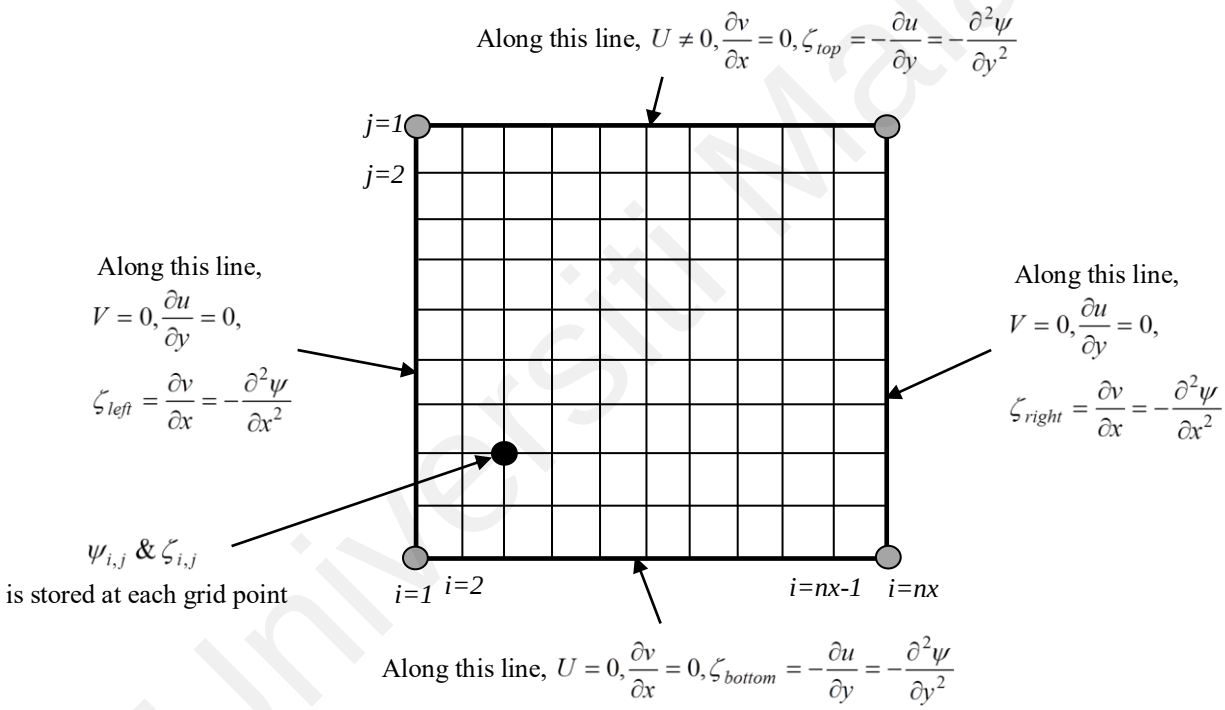

Figure 3.15: BC at four sides

There is a need to acknowledge that those four nodal points located at the four corners are not in used along the calculation. Also, Figure 3.16 shows the stream function, ψ is zero on the entire boundary anytime and at every interior nodes at the beginning. Once the fluid starts

Universiti Malaya

moving, the value of stream function, ψ at the BCs are evaluated using Equation (3.32), Equation (3.34), Equation (3.36) and Equation (3.37). Then, the values of stream function, ψ at the interior nodes are calculated via Equation (3.25). The whole iteration process in calculating stream function, ψ is repeated until steady-state condition is achieved or at any desired period of time. Equation (3.25) can be evaluated using Gauss-Seidel method or successive over-relaxation (SOR) method by setting the weighting factor in between 1 and 2 (Chapra & Canale, 2006).

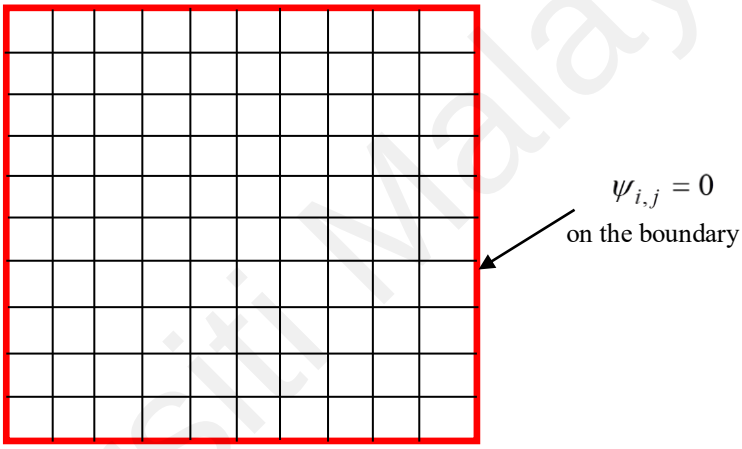

Figure 3.16: BC of stream function, ψ

3.5.2 Discretization of free-slip BCs for Lid-driven Cavity

The free-slip BC will be derived in the similar way. Figure 3.17 shows the diagram of free-slip BC.

Universiti Malaya

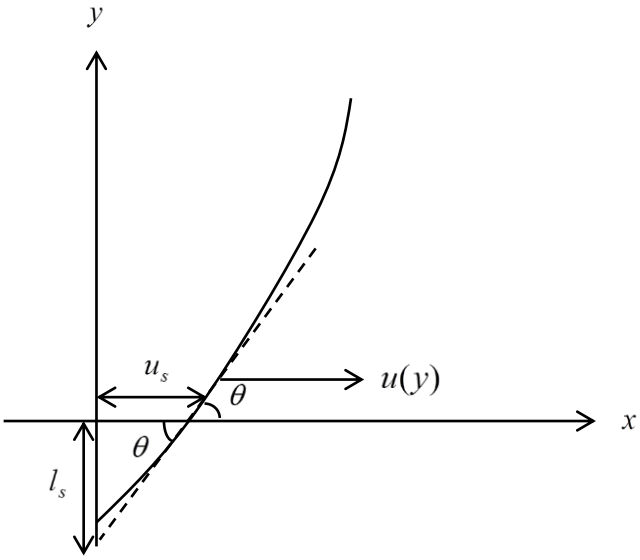

where l_s is slip length, u_s is slip velocity, u is applied velocity, $\theta = \tan^{-1}\left(\frac{l_s}{u_s}\right)$

Figure 3.17: Free-slip BC

Stream function for free-slip BC at each of the walls can be expanded using Taylor series expansion based on Equation (3.31). Based on Figure 3.17, it shows that:

$$\tan\theta = \frac{l_s}{u_s} = \left.\frac{\partial y}{\partial u}\right|_{wall} . \tag{3.38}$$

And thus, $u_s = l_s \left.\frac{\partial u}{\partial y}\right|_{wall}$ and $u_s = \frac{\partial \psi}{\partial y}$.

Substituting Equation (3.38) into Equation (3.31),

$$\psi_{i,j=ny} = \psi_{i,j=ny-1} + l_s \left.\frac{\partial u}{\partial y}\right|_{wall} \Delta y + \left.\frac{\partial u}{\partial y}\right|_{wall} \frac{\Delta y^2}{2} + O(h^3) ,$$

$$\psi_2 = \psi_1 + \left(l_s \Delta y + \frac{\Delta y^2}{2} \right) \frac{\partial u}{\partial y},$$

where $O(h^3)$ is of higher order and can be ignored, and from Equation (3.23),

$$\zeta = -\frac{\partial u}{\partial y},$$

$$\psi_2 = \psi_1 + \left(l_s \Delta y + \frac{\Delta y^2}{2} \right)(-\zeta) \cdot \tag{3.39}$$

Rearranging Equation (3.39), it yields:

$$\zeta = \frac{\psi_1 - \psi_2}{l_s \Delta y + \frac{\Delta y^2}{2}} \cdot \tag{3.40}$$

Vorticity, ζ at each wall becomes:

Bottom BC, $\zeta_{bottom} = \dfrac{-(\psi_{i,j=ny-1} - \psi_{i,j=ny})}{l_s \Delta y + \frac{\Delta y^2}{2}}$, (3.41)

Left BC: $\zeta_{left} = \dfrac{-(\psi_{i=2,j} - \psi_{i=1,j})}{l_s \Delta x + \frac{\Delta x^2}{2}}$, (3.42)

Right BC: $\zeta_{right} = \dfrac{-(\psi_{i=nx-1,j} - \psi_{i=nx,j})}{l_s \Delta x + \frac{\Delta x^2}{2}}$, (3.43)

where $\Delta x = \Delta y$ is step size, j is row and i is column, U_{wall} is applied velocity.

Equation (3.41) till Equation (3.43) can be applied for no-slip BC by simply setting $l_s = 0$.

Universiti Malaya

3.6 Lid-driven in 2D Thermal Analysis

Two-dimensional and unsteady-state of thermal energy equation (TEE) (Incropera et al., 2006) which includes the effect of viscous dissipation is given by:

$$\frac{\partial T}{\partial t}+u\frac{\partial T}{\partial x}+v\frac{\partial T}{\partial y}=\frac{k}{\rho c}\left(\frac{\partial^2 T}{\partial x^2}+\frac{\partial^2 T}{\partial y^2}\right)+\frac{\mu}{\rho c}\left[\left(\frac{\partial u}{\partial y}+\frac{\partial v}{\partial x}\right)^2+2\left(\frac{\partial u}{\partial x}\right)^2+2\left(\frac{\partial v}{\partial y}\right)^2\right], \tag{3.44}$$

where T is temperature.

By substituting Equation (3.11) and Equation (3.12) into Equation (3.44) will result:

$$\frac{\partial T}{\partial t}+\frac{\partial \psi}{\partial y}\frac{\partial T}{\partial x}-\frac{\partial \psi}{\partial x}\frac{\partial T}{\partial y}=\frac{k}{\rho c}\left(\frac{\partial^2 T}{\partial x^2}+\frac{\partial^2 T}{\partial y^2}\right)+\frac{\mu}{\rho c}\left[\left(\frac{\partial^2 \psi}{\partial y^2}-\frac{\partial^2 \psi}{\partial x^2}\right)^2+4\left(\frac{\partial^2 \psi}{\partial x \partial y}\right)^2\right]. \tag{3.45}$$

The resultant FDE for the TEE is given by:

$$\begin{aligned}\frac{T_{i,j}^{t+1}-T_{i,j}^{t}}{\Delta t}&=-\left(\frac{\psi_{i,j+1}^{t}-\psi_{i,j-1}^{t}}{2h}\right)\left(\frac{T_{i+1,j}^{t}-T_{i-1,j}^{t}}{2h}\right)+\left(\frac{\psi_{i+1,j}^{t}-\psi_{i-1,j}^{t}}{2h}\right)\left(\frac{T_{i,j+1}^{t}-T_{i,j-1}^{t}}{2h}\right)\\&+\frac{k}{\rho c}\left(\frac{T_{i+1,j}^{t}+T_{i-1,j}^{t}+T_{i,j+1}^{t}+T_{i,j-1}^{t}-4T_{i,j}^{t}}{h^2}\right)\\&+\frac{\mu}{\rho c}\left[\left(\frac{\psi_{i,j+1}^{t}+\psi_{i,j-1}^{t}-\psi_{i+1,j}^{t}-\psi_{i-1,j}^{t}}{h^2}\right)^2+4\left(\frac{\psi_{i+1,j+1}^{t}+\psi_{i-1,j-1}^{t}-\psi_{i+1,j-1}^{t}-\psi_{i-1,j+1}^{t}}{4h^2}\right)^2\right]\end{aligned}. \tag{3.46}$$

Rearranging Equation (3.46) yields:

$$T_{i,j}^{t+1} = \Delta t \left[\begin{array}{l} -\left(\dfrac{\psi_{i,j+1}^{t} - \psi_{i,j-1}^{t}}{2h}\right)\left(\dfrac{T_{i+1,j}^{t} - T_{i-1,j}^{t}}{2h}\right) + \left(\dfrac{\psi_{i+1,j}^{t} - \psi_{i-1,j}^{t}}{2h}\right)\left(\dfrac{T_{i,j+1}^{t} - T_{i,j-1}^{t}}{2h}\right) \\ + \dfrac{k}{\rho c}\left(\dfrac{T_{i+1,j}^{t} + T_{i-1,j}^{t} + T_{i,j+1}^{t} + T_{i,j-1}^{t}}{h^2}\right) \\ + \dfrac{\mu}{\rho c}\left[\begin{array}{l} \left(\dfrac{\psi_{i,j+1}^{t} + \psi_{i,j-1}^{t} - \psi_{i+1,j}^{t} - \psi_{i-1,j}^{t}}{h^2}\right)^2 \\ + \left(\dfrac{\psi_{i+1,j+1}^{t} + \psi_{i-1,j-1}^{t} - \psi_{i+1,j-1}^{t} - \psi_{i-1,j+1}^{t}}{2h^2}\right)^2 \end{array} \right] \end{array} \right] . \tag{3.47}$$

$$+\left(1 - 4\frac{k\Delta t}{\rho c h^2}\right) T_{i,j}^{t}$$

From Equation (3.47), the criterion is determined by requiring that the coefficient associated with the node of interest at the previous time is greater than or equal to zero (Incropera et al., 2006), such that

$$\left(1 - \frac{4k\Delta t}{\rho c h^2}\right) \geq 0 \text{ or } \Delta t \leq \frac{\rho c h^2}{4k} . \tag{3.48}$$

3.6.1 Thermal Analysis with Neumann BC

The schematic drawing of a two-dimensional lid-driven model within the Cartesian coordinate system used in heat transfer analyses with Neumann BC (Chapra & Canale, 2006) or insulated BC is shown in Figure 3.18. Subsequently, k and c are thermal conductivity and specific heat of fluid, $\left.\dfrac{\partial T}{\partial x}\right|_{x=0}$, $\left.\dfrac{\partial T}{\partial x}\right|_{x=L}$, $\left.\dfrac{\partial T}{\partial y}\right|_{y=0}$ and $\left.\dfrac{\partial T}{\partial y}\right|_{y=L}$ are the temperature gradient along the fixed wall in $x-$ and $y-$ directions. The fluid flow process is presumed as two-

dimensional, incompressible, laminar and the Newtonian fluid properties are not in the function of temperature or they behave as constants. Then the buoyancy force is excluded from the heat transfer analysis as the heat flux (due to viscous heating) is generated from the moving top lid. Therefore, there is no convection occurs from the bottom fixed lid to the top moving lid and Boussinesq approximation is not included in TEE. The top moving lid is presumed fully insulated.

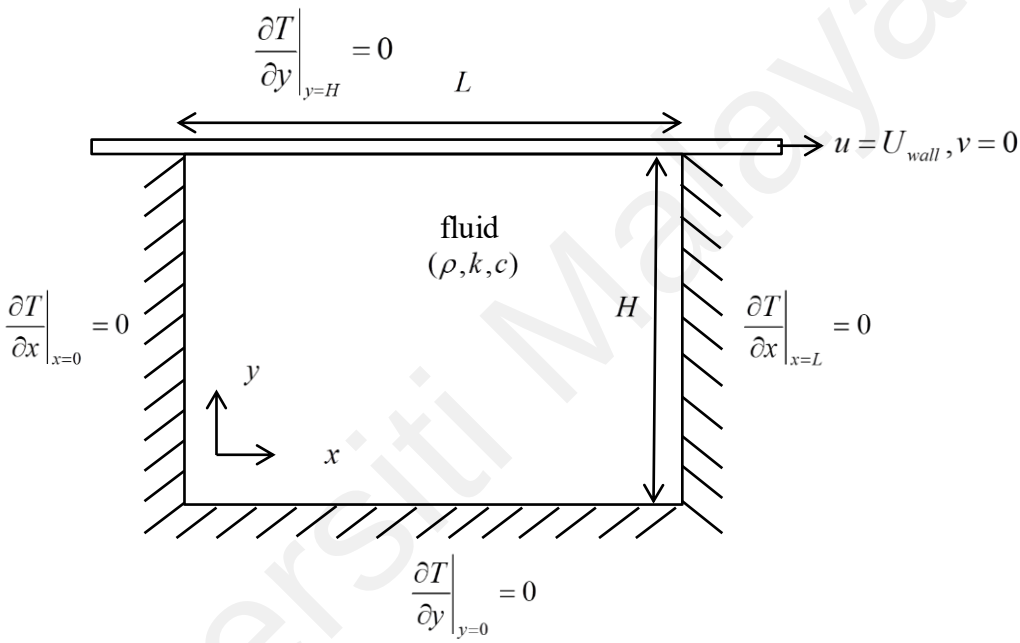

Figure 3.18: Schematic drawing of lid-driven in 2D with Neumann BC

The temperature, T at each of the walls and each of the corners can be obtained by introducing Neumann BC in unsteady-state condition. Schematic drawing of Neumann BC is shown in Figure 3.19:

Universiti Malaya

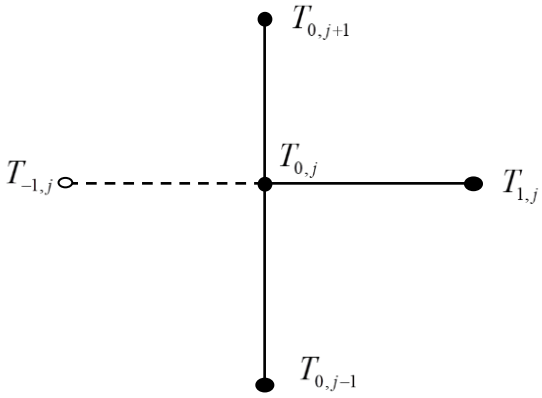

Figure 3.19: Schematic drawing of Neumann BC (Chapra & Canale, 2006)

The governing equations for Neumann BC are shown as below:

top moving lid BC: $$T_{i,j=1}^{t+1} = \lambda(2T_{i,j+1}^{t} + T_{i-1,j}^{t} + T_{i+1,j}^{t}) + (1-4\lambda)T_{i,j=1}^{t}, \quad (3.49)$$

bottom BC: $$T_{i,j=ny}^{t+1} = \lambda(2T_{i,j-1}^{t} + T_{i-1,j}^{t} + T_{i+1,j}^{t}) + (1-4\lambda)T_{i,j=ny}^{t}, \quad (3.50)$$

left BC: $$T_{i=1,j}^{t+1} = \lambda(2T_{i+1,j}^{t} + T_{i,j+1}^{t} + T_{i,j-1}^{t}) + (1-4\lambda)T_{i=1,j}^{t}, \quad (3.51)$$

right BC: $$T_{i=nx,j}^{t+1} = \lambda(2T_{i-1,j}^{t} + T_{i,j+1}^{t} + T_{i,j-1}^{t}) + (1-4\lambda)T_{i=nx,j}^{t}, \quad (3.52)$$

top left corner BC: $$T_{i=1,j=1}^{t+1} = 2\lambda(T_{i+1,j}^{t} + T_{i,j+1}^{t}) + (1-4\lambda)T_{i=1,j=1}^{t}, \quad (3.53)$$

top right corner BC: $$T_{i=nx,j=1}^{t+1} = 2\lambda(T_{i-1,j}^{t} + T_{i,j+1}^{t}) + (1-4\lambda)T_{i=nx,j=1}^{t}, \quad (3.54)$$

bottom left corner BC: $$T_{i=1,j=ny}^{t+1} = 2\lambda(T_{i+1,j}^{t} + T_{i,j-1}^{t}) + (1-4\lambda)T_{i=1,j=ny}^{t}, \quad (3.55)$$

bottom right corner BC: $$T_{i=nx,j=ny}^{t+1} = 2\lambda(T_{i-1,j}^{t} + T_{i,j-1}^{t}) + (1-4\lambda)T_{i=nx,j=ny}^{t}, \quad (3.56)$$

Universiti Malaya

where $\lambda = \dfrac{k\Delta t}{\rho c h^2}$, Δt is step time, $t+1$ is new step time and t is current step time

3.6.2 Thermal Analysis with Robin BC

Figure 3.20 shows the schematic drawing of lid-driven with Robin BC (Markus & Mahamadi, 2009) or insulated BC.

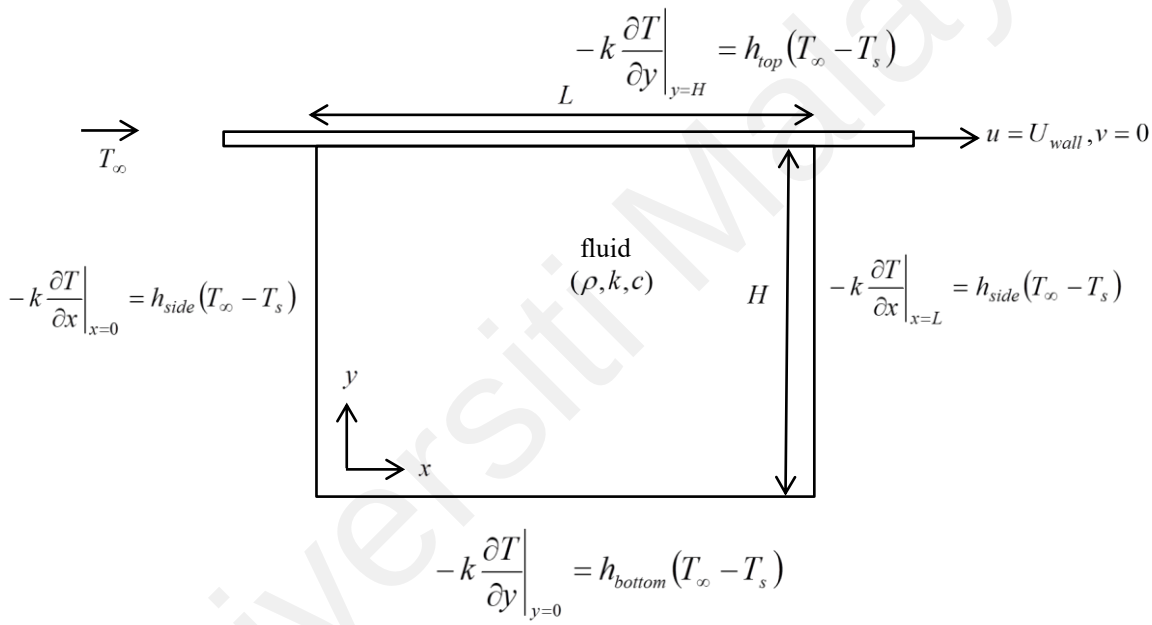

Figure 3.20: Schematic drawing of lid-driven in 2D with Robin BC

The temperature, T at each of the walls and each of the corners can be obtained by introducing Robin BC in unsteady-state condition and can be derived using energy balance method (Incropera et al., 2006) as shown in Figure 3.21.

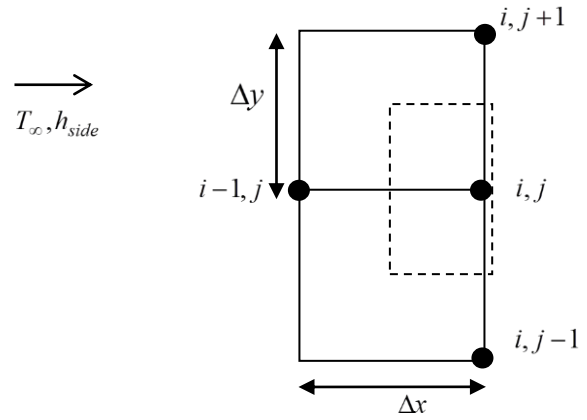

Figure 3.21: Energy balance method use for third kind of BC (Incropera et al., 2006)

All the unsteady-state governing equations of these boundaries are shown as below:

top moving lid BC:
$$\begin{aligned} T_{i,j=1}^{t+1} &= \lambda(2T_{i,j+1}^{t} + T_{i-1,j}^{t} + T_{i+1,j}^{t} + 2Bi_{top}T_\infty) \\ &+ (1 - 4\lambda - 2Bi_{top}\lambda)T_{i,j=1}^{t} \end{aligned}, \quad (3.57)$$

bottom BC:
$$\begin{aligned} T_{i,j=ny}^{t+1} &= \lambda(2T_{i,j-1}^{t} + T_{i-1,j}^{t} + T_{i+1,j}^{t} + 2Bi_{bottom}T_\infty) + \\ &(1 - 4\lambda - 2Bi_{bottom}\lambda)T_{i,j=ny}^{t} \end{aligned}, \quad (3.58)$$

left BC:
$$T_{i=1,j}^{t+1} = \lambda(2T_{i+1,j}^{t} + T_{i,j+1}^{t} + T_{i,j-1}^{t} + 2Bi_{side}T_\infty) + (1 - 4\lambda - 2Bi_{side}\lambda)T_{i=1,j}^{t}, \quad (3.59)$$

right BC:
$$T_{i=nx,j}^{t+1} = \lambda(2T_{i-1,j}^{t} + T_{i,j+1}^{t} + T_{i,j-1}^{t} + 2Bi_{side}T_\infty) + (1 - 4\lambda - 2Bi_{side}\lambda)T_{i=nx,j}^{t}, \quad (3.60)$$

top left corner BC:
$$\begin{aligned} T_{i=1,j=1}^{t+1} &= 2\lambda\left[T_{i+1,j}^{t} + T_{i,j+1}^{t} + T_\infty\left(Bi_{side} + Bi_{top}\right)\right] \\ &+ \left[1 - 4\lambda - 2\lambda(Bi_{side} + Bi_{top})\right]T_{i=1,j=1}^{t} \end{aligned}, \quad (3.61)$$

top right corner BC:
$$\begin{aligned} T_{i=nx,j=1}^{t+1} &= 2\lambda\left[T_{i-1,j}^{t} + T_{i,j+1}^{t} + T_\infty\left(Bi_{side} + Bi_{top}\right)\right] + \\ &\left[1 - 4\lambda - 2\lambda(Bi_{side} + Bi_{top})\right]T_{i=nx,j=1}^{t} \end{aligned}, \quad (3.62)$$

bottom left corner BC: $$\begin{aligned} T_{i=1,j=ny}^{t+1} &= 2\lambda\left[T_{i+1,j}^{t} + T_{i,j-1}^{t} + T_{\infty}\left(Bi_{side} + Bi_{bottom}\right)\right] \\ &+ \left[1 - 4\lambda - 2\lambda(Bi_{side} + Bi_{bottom})\right]T_{i=1,j=ny}^{t} \end{aligned}, \tag{3.63}$$

bottom right corner BC: $$\begin{aligned} T_{i=nx,j=ny}^{t+1} &= 2\lambda\left[T_{i-1,j}^{t} + T_{i,j-1}^{t} + T_{\infty}\left(Bi_{side} + Bi_{bottom}\right)\right] \\ &+ \left[1 - 4\lambda - 2\lambda(Bi_{side} + Bi_{bottom})\right]T_{i=nx,j=ny}^{t} \end{aligned}, \tag{3.64}$$

where T_{∞} is ambient temperature, Bi_{top} is Biot number at top lid, Bi_{side} is Biot number at side wall and Bi_{bottom} is Biot number at bottom wall.

Bi_{top}, Bi_{side} and Bi_{bottom} are given by:

$$Bi_{top} = \frac{h_{top}L}{k_{air}}, \tag{3.65}$$

$$Bi_{side} = \frac{h_{side}H}{k_{air}}, \tag{3.66}$$

$$Bi_{bottom} = \frac{h_{bottom}L}{k_{air}}, \tag{3.67}$$

where k_{air} is thermal conductivity of ambient air.

Convection heat transfer coefficient h_{top}, h_{side} and h_{bottom} are given by (Incropera et al., 2006):

$$h_{top} = \frac{0.54Ra_L^{1/4} \cdot k_{air}}{L}, \text{ for } 10^4 \le Ra_L \le 10^7, \tag{3.68}$$

$$h_{top} = \frac{0.15Ra_L^{1/3} \cdot k_{air}}{L}, \text{ for } 10^7 \le Ra_L \le 10^{11}, \tag{3.69}$$

Universiti Malaya

$$h_{side} = \left\{ 0.825 + \frac{0.387 Ra_L^{1/6}}{[1 + (0.492/\mathrm{Pr}_{air})^{9/16}]^{8/27}} \right\}^2 \cdot \frac{k_{air}}{H}, \tag{3.70}$$

$$h_{bottom} = \frac{0.27(Ra_L^{1/4}) \cdot k_{air}}{L}, \tag{3.71}$$

where Ra_L is Rayleigh number and Pr_{air} is Prandtl number of ambient air respectively.

The thermal analysis can be continued after the applied force at the top lid is removed. The fluid remains static and starts to cool down in this second step of analysis i.e. cooling process. Thus, value of stream function, $\psi = 0$. Equation (3.45) will be reduced to:

$$\frac{\partial T}{\partial t} = \frac{k}{\rho c}\left(\frac{\partial^2 T}{\partial x^2} + \frac{\partial^2 T}{\partial y^2} \right). \tag{3.72}$$

Equation (3.72) is known as two-dimensional transient heat conduction equation (Incropera et al., 2006). The resultant FDE for Equation (3.72) is given by:

$$\frac{T_{i,j}^{t+1} - T_{i,j}^{t}}{\Delta t} = \frac{k}{\rho c}\left(\frac{T_{i+1,j}^{t} + T_{i-1,j}^{t} + T_{i,j+1}^{t} + T_{i,j-1}^{t} - 4T_{i,j}^{t}}{h^2} \right). \tag{3.73}$$

Rearranging Equation (3.73) yields:

$$T_{i,j}^{t+1} = \Delta t \left[\frac{k}{\rho c}\left(\frac{T_{i+1,j}^{t} + T_{i-1,j}^{t} + T_{i,j+1}^{t} + T_{i,j-1}^{t}}{h^2} \right) \right] + \left(1 - 4\frac{k\Delta t}{\rho c h^2} \right) T_{i,j}^{t}. \tag{3.74}$$

From Equation (3.74), the criterion is determined by requiring that the coefficient associated with the node of interest at the previous time is greater than or equal to zero (Incropera et al., 2006), such that:

$$\left(1-\frac{4\mu\Delta t}{\rho h^2}\right)\geq 0 \text{ or } \Delta t \leq \frac{\rho h^2}{4\mu}. \tag{3.75}$$

3.7 Stability Criteria Analysis

Every forward finite difference equation has its own stability criterion. Equation 109, Equation (3.49) till Equation (3.56) and Equation (3.74) share the same stability criteria. Stability criterion of Equation (3.57) is given by:

$$\left(1-\frac{4k_{air}\Delta t}{\rho c h^2}-2Bi_{top}\frac{k_{air}\Delta t}{\rho c h^2}\right)\geq 0 \text{ or } \Delta t \leq \frac{\rho c h^2}{2k_{air}(2+Bi_{top})}, \tag{3.76}$$

stability criterion of Equation (3.58) is given by:

$$\left(1-\frac{4k_{air}\Delta t}{\rho c h^2}-2Bi_{bottom}\frac{k_{air}\Delta t}{\rho c h^2}\right)\geq 0 \text{ or } \Delta t \leq \frac{\rho c h^2}{2k_{air}(2+Bi_{bottom})}, \tag{3.77}$$

stability criterion of Equation (3.59) and Equation (3.60) are given by:

$$\left(1-\frac{4k_{air}\Delta t}{\rho c h^2}-2Bi_{side}\frac{k_{air}\Delta t}{\rho c h^2}\right)\geq 0 \text{ or } \Delta t \leq \frac{\rho c h^2}{2k_{air}(2+Bi_{side})}, \tag{3.78}$$

stability criterion of Equation (3.61) and Equation (3.62) are given by:

$$\left(1-\frac{4k_{air}\Delta t}{\rho c h^2}-2(Bi_{side}+Bi_{top})\frac{k_{air}\Delta t}{\rho c h^2}\right)\geq 0 \text{ or } \Delta t \leq \frac{\rho c h^2}{2k_{air}(2+Bi_{side}+Bi_{top})}, \tag{3.79}$$

and stability criterion of Equation (3.63) and Equation (3.64) are given by:

$$\left(1-\frac{4k_{air}\Delta t}{\rho ch^2}-2(Bi_{side}+Bi_{bottom})\frac{k_{air}\Delta t}{\rho ch^2}\right)\geq 0 \text{ or } \Delta t \leq \frac{\rho ch^2}{2k_{air}(2+Bi_{side}+Bi_{bottom})}. \tag{3.80}$$

Due to buoyancy effect of gravity in ambient air, it can be proved that (valid for square cavity only):

$$h_{top} > h_{side} > h_{bottom}. \tag{3.81}$$

The relation as shown in Equation (3.81) will be proven in Chapter 4. Based on Equation (3.76) till Equation (3.80), Equation (3.79) has the smallest maximum allowable step time, Δt.

However, the maximum allowable step time, Δt should be evaluated again so that it can fulfill Equation (3.21), Equation (3.47), Equation (3.49) till Equation (3.64) and Equation (3.74). Thus, the adopted maximum allowable step time, $\Delta t_{\max}$ is given by:

$$\Delta t_{\max} = \min\left(\frac{\rho h^2}{4\mu}, \frac{\rho ch^2}{4k}, \frac{\rho ch^2}{2k_{air}(2+Bi_{side}+Bi_{top})}\right), \tag{3.82}$$

where $\min(\ )$ means the smallest element is taken inside the bracket.

The maximum allowable step time, $\Delta t_{\max}$ which is evaluated based on Equation (3.82), will be employed along this two-steps analysis. However, if the thermal fluid analysis is carried out in Neumann BC, then the maximum allowable step time, $\Delta t_{\max}$ is given by:

$$\Delta t_{\max} = \min\left(\frac{\rho h^2}{4\mu}, \frac{\rho ch^2}{4k}\right). \tag{3.83}$$

3.8 Derivation and Discretization of non-Newtonian Governing Equations

NSEs are only limited to Newtonian fluid or linear stress-strain relation material. To study the fluid motion of non-Newtonian fluid, it is necessary to study the incompressible generalized Newtonian model (Bird et al., 2002).

$$\tau = -\eta(\dot{\gamma})\dot{\gamma}, \tag{3.84}$$

where $\eta(\dot{\gamma})$ is non-Newtonian viscosity or shear-rate dependent viscosity and $\dot{\gamma}$ is rate of shearing strain or rate of angular deformation.

Rate of shearing strain, $\dot{\gamma}$ is also defined by:

$$\dot{\gamma} = \nabla V + \nabla V^T, \tag{3.85}$$

where ∇V is gradient operator of velocity and ∇V^T is transpose of ∇V.

Then Equation (3.85) becomes:

$$\dot{\gamma} = \begin{pmatrix} \frac{\partial u}{\partial x} & \frac{\partial u}{\partial y} \\ \frac{\partial v}{\partial x} & \frac{\partial v}{\partial y} \end{pmatrix} + \begin{pmatrix} \frac{\partial u}{\partial x} & \frac{\partial v}{\partial x} \\ \frac{\partial u}{\partial y} & \frac{\partial v}{\partial y} \end{pmatrix} = \begin{pmatrix} 2\frac{\partial u}{\partial x} & \frac{\partial u}{\partial y} + \frac{\partial v}{\partial x} \\ \frac{\partial v}{\partial x} + \frac{\partial u}{\partial y} & 2\frac{\partial v}{\partial y} \end{pmatrix},$$

$$\begin{pmatrix} \dot{\gamma}_{xx} & \dot{\gamma}_{yx} \\ \dot{\gamma}_{xy} & \dot{\gamma}_{yy} \end{pmatrix} = \begin{pmatrix} 2\frac{\partial u}{\partial x} & \frac{\partial u}{\partial y} + \frac{\partial v}{\partial x} \\ \frac{\partial v}{\partial x} + \frac{\partial u}{\partial y} & 2\frac{\partial v}{\partial y} \end{pmatrix}. \tag{3.86}$$

The magnitude of the rate-of-strain tensor, $\dot{\gamma}$ is given by:

Universiti Malaya

$$\dot{\gamma} = \sqrt{\frac{1}{2}(\dot{\gamma} : \dot{\gamma})}$$

$$= \sqrt{\frac{1}{2}(\dot{\gamma}_{xx}^{2} + \dot{\gamma}_{yx}^{2} + \dot{\gamma}_{xy}^{2} + \dot{\gamma}_{yy}^{2})},$$

$$= \sqrt{2\left(\frac{\partial u}{\partial x}\right)^{2} + \left(\frac{\partial u}{\partial y} + \frac{\partial v}{\partial x}\right)^{2} + 2\left(\frac{\partial v}{\partial y}\right)^{2}} \quad . \tag{3.87}$$

By using this algebraic identity:

$$a^2 + b^2 = (a+b)^2 - 2ab$$

$$= \sqrt{2\left[\left(\frac{\partial u}{\partial x} + \frac{\partial v}{\partial y}\right)^{2} - 2\left(\frac{\partial u}{\partial x} \bullet \frac{\partial v}{\partial y}\right)\right] + \left(\frac{\partial u}{\partial y} + \frac{\partial v}{\partial x}\right)^{2}} \quad . \tag{3.88}$$

Then from Equation (2.11),

$\frac{\partial u}{\partial x} + \frac{\partial v}{\partial y} = 0$, (there is no component w) from (2.11)

$$= \sqrt{\left(\frac{\partial u}{\partial y} + \frac{\partial v}{\partial x}\right)^{2} - 4\left(\frac{\partial u}{\partial x} \bullet \frac{\partial v}{\partial y}\right)},$$

$$= \sqrt{\left(\frac{\partial u}{\partial y} + \frac{\partial v}{\partial x}\right)^{2} + 4\left(\frac{\partial u}{\partial x}\right)^{2}} \quad . \tag{3.89}$$

where „:“ is the Frobenius norm (Lyche, 2009).

Equation (3.89) it can be expressed as:

Universiti Malaya

$$\dot{\gamma} = \sqrt{\left(\frac{\partial u}{\partial y} + \frac{\partial v}{\partial x}\right)^2 + 4\left(\frac{\partial v}{\partial y}\right)^2}\,. \tag{3.90}$$

In this case,

$$\left(\frac{\partial u}{\partial y} + \frac{\partial v}{\partial x}\right)^2 - 4\left(\frac{\partial u}{\partial x} \bullet \frac{\partial v}{\partial y}\right) = \left(\frac{\partial u}{\partial y} + \frac{\partial v}{\partial x}\right)^2 + 4\left(\frac{\partial u}{\partial x}\right)^2 = \left(\frac{\partial u}{\partial y} + \frac{\partial v}{\partial x}\right)^2 + 4\left(\frac{\partial v}{\partial y}\right)^2 = A\,. \tag{3.91}$$

There are numerous non-Newtonian models (Krishnan & Deshpande, 2010) such as power law or Ostwald de Waele equation, Cross viscosity equation, Carreau-Yasuda model, Ellis fluid model, thixotropic, rheopectic model and etc. However, thixotropic and rheopectic models are time-dependent fluid behavior models. In this case, the power law model will be employed in this text. The non-Newtonian viscosity of power law model is given by:

$$\eta(\dot{\gamma}) = m\dot{\gamma}^{n-1}\,, \tag{3.92}$$

where is m consistency index and n is power-law index.

And the shear stress of power law model is given by:

$$\tau = m\dot{\gamma}^{n}\,. \tag{3.93}$$

To analogize Equation (3.93) with Equation (3.84), Equation (3.93) can be modified as:

$$\tau = -m\dot{\gamma}^{n-1}.\dot{\gamma}\,. \tag{3.94}$$

Power-law is the simplest and time-independent model, but it is unable to predict the zero shear-rate and infinite shear-rate region where they behave as Newtonian plateau. The momentum stress tensor or stress tensor, τ is given by:

$$\tau = \begin{pmatrix} \tau_{xx} & \tau_{yx} \\ \tau_{xy} & \tau_{yy} \end{pmatrix}. \tag{3.95}$$

Equation (3.95) is also known as constitutive equation.

The total stress tensor or total momentum flux tensor, π is given by:

$$\pi = -pI + \tau ,$$

$$= \begin{bmatrix} -p & 0 \\ 0 & -p \end{bmatrix} + \begin{bmatrix} \tau_{xx} & \tau_{yx} \\ \tau_{xy} & \tau_{yy} \end{bmatrix},$$

$$\begin{bmatrix} \pi_{xx} & \pi_{yx} \\ \pi_{xy} & \pi_{yy} \end{bmatrix} = \begin{bmatrix} -p + \tau_{xx} & \tau_{yx} \\ \tau_{xy} & -p + \tau_{yy} \end{bmatrix}. \tag{3.96}$$

Substituting Equation (3.87) into Equation (3.94) becomes:

$$\tau = -m\left[\frac{1}{2}(\dot{\gamma} : \dot{\gamma})\right]^{\frac{n-1}{2}} \bullet \dot{\gamma} . \tag{3.97}$$

The constitutive equation becomes:

$$\tau_{xx} = -m\left[\frac{1}{2}(\dot{\gamma} : \dot{\gamma})\right]^{\frac{n-1}{2}} \bullet \dot{\gamma}_{xx} ,$$

$$= -mA^{\frac{n-1}{2}} \bullet 2\frac{\partial u}{\partial x} . \tag{3.98}$$

Universiti Malaya

$$\tau_{yx} = \tau_{xy} = -mA^{\frac{n-1}{2}} \bullet \left(\frac{\partial u}{\partial y} + \frac{\partial v}{\partial x} \right), \tag{3.99}$$

$$\tau_{yy} = -mA^{\frac{n-1}{2}} \bullet 2\frac{\partial v}{\partial y}. \tag{3.100}$$

In matrix form,

$$\begin{pmatrix} \tau_{xx} & \tau_{yx} \\ \tau_{xy} & \tau_{yy} \end{pmatrix} = -mA^{\frac{n-1}{2}} \begin{pmatrix} 2\frac{\partial u}{\partial x} & \frac{\partial u}{\partial y} + \frac{\partial v}{\partial x} \\ \frac{\partial v}{\partial x} + \frac{\partial u}{\partial y} & 2\frac{\partial v}{\partial y} \end{pmatrix}. \tag{3.101}$$

The equation of motion or Cauchy momentum equation is given by Equation (3.102) and Equation (3.104).

In *x*-direction:

$$\rho g_x + \frac{\partial \pi_{xx}}{\partial x} + \frac{\partial \pi_{yx}}{\partial y} = \rho \left[\frac{\partial u}{\partial t} + u\frac{\partial u}{\partial x} + v\frac{\partial u}{\partial y} \right] \text{ (with absence of } w\text{-component)}, \tag{3.102}$$

From Equation (3.101),

$$\rho g_x + \frac{\partial(-p + \tau_{xx})}{\partial x} + \frac{\partial(\tau_{yx})}{\partial y} = \rho \left[\frac{\partial u}{\partial t} + u\frac{\partial u}{\partial x} + v\frac{\partial u}{\partial y} \right],$$

$$\rho g_x - \frac{\partial p}{\partial x} + \frac{\partial}{\partial x}\left(-2m\frac{\partial u}{\partial x} \bullet A^{\frac{n-1}{2}} \right) + \frac{\partial}{\partial y}\left[-m\left(\frac{\partial u}{\partial y} + \frac{\partial v}{\partial x} \right) \bullet A^{\frac{n-1}{2}} \right] = \rho \left[\frac{\partial u}{\partial t} + u\frac{\partial u}{\partial x} + v\frac{\partial u}{\partial y} \right],$$

$$\rho g_x - \frac{\partial p}{\partial x} - 2m\frac{\partial^2 u}{\partial x^2} A^{\frac{n-1}{2}} - 2m\frac{\partial u}{\partial x}\frac{\partial A^{\frac{n-1}{2}}}{\partial x} - mA^{\frac{n-1}{2}}\left(\frac{\partial^2 u}{\partial y^2} + \frac{\partial^2 v}{\partial x \partial y} \right) - m\frac{\partial A^{\frac{n-1}{2}}}{\partial y}\left(\frac{\partial u}{\partial y} + \frac{\partial v}{\partial x} \right),$$
$$= \rho \left[\frac{\partial u}{\partial t} + u\frac{\partial u}{\partial x} + v\frac{\partial u}{\partial y} \right]$$

Universiti Malaya

$$\rho g_x - \frac{\partial p}{\partial x} - mA^{\frac{n-1}{2}} \frac{\partial}{\partial x}\left(\frac{\partial u}{\partial x} + \frac{\partial v}{\partial y}\right) - 2m\frac{\partial u}{\partial x}\frac{\partial A^{\frac{n-1}{2}}}{\partial x} - mA^{\frac{n-1}{2}}\left(\frac{\partial^2 u}{\partial y^2} + \frac{\partial^2 u}{\partial x^2}\right) - m\frac{\partial A^{\frac{n-1}{2}}}{\partial y}\left(\frac{\partial u}{\partial y} + \frac{\partial v}{\partial x}\right) = \rho\left[\frac{\partial u}{\partial t} + u\frac{\partial u}{\partial x} + v\frac{\partial u}{\partial y}\right].$$

Then from Equation (2.11),

$$\frac{\partial u}{\partial x} + \frac{\partial v}{\partial y} = 0 \text{ (there is no component } w\text{)}, \qquad \text{from (2.11)}$$

$$\rho g_x - \frac{\partial p}{\partial x} - mA^{\frac{n-1}{2}}\left(\frac{\partial^2 u}{\partial x^2} + \frac{\partial^2 u}{\partial y^2}\right) - 2m\frac{\partial u}{\partial x}\frac{\partial A^{\frac{n-1}{2}}}{\partial x} - m\frac{\partial A^{\frac{n-1}{2}}}{\partial y}\left(\frac{\partial u}{\partial y} + \frac{\partial v}{\partial x}\right) = \rho\left[\frac{\partial u}{\partial t} + u\frac{\partial u}{\partial x} + v\frac{\partial u}{\partial y}\right]. \qquad (3.103)$$

Similarly in y-direction:

$$\rho g_y + \frac{\partial \pi_{xy}}{\partial x} + \frac{\partial \pi_{yy}}{\partial y} = \rho\left[\frac{\partial v}{\partial t} + u\frac{\partial v}{\partial x} + v\frac{\partial v}{\partial y}\right] \text{ (with absence of } w\text{-component)}, \qquad (3.104)$$

$$\rho g_y - \frac{\partial p}{\partial y} + mA^{\frac{n-1}{2}}\left(\frac{\partial^2 v}{\partial x^2} + \frac{\partial^2 v}{\partial y^2}\right) + 2m\frac{\partial v}{\partial y}\frac{\partial A^{\frac{n-1}{2}}}{\partial y} + m\frac{\partial A^{\frac{n-1}{2}}}{\partial x}\left(\frac{\partial u}{\partial y} + \frac{\partial v}{\partial x}\right) = \rho\left[\frac{\partial v}{\partial t} + u\frac{\partial v}{\partial x} + v\frac{\partial v}{\partial y}\right]. \qquad (3.105)$$

From Equation (2.68), the curl is given as:

$$Curl(NSEs) = \nabla \times \tilde{\omega} \times \tilde{r},$$

$$= \begin{vmatrix} i & j & k \\ \frac{\partial}{\partial x} & \frac{\partial}{\partial y} & \frac{\partial}{\partial z} \\ Eqn(3.103) & Eqn(3.105) & 0 \end{vmatrix},$$

$$= \left(\frac{\partial}{\partial x}\left(Eqn(3.105)\right) - \frac{\partial}{\partial y}\left(Eqn(3.103)\right) \right) k \,. \tag{3.106}$$

$$\frac{\partial}{\partial x}\left(Eqn(3.105)\right) \Rightarrow$$

$$\begin{aligned} &\frac{\partial(\rho g_y)}{\partial x} - \frac{\partial p}{\partial x \partial y} - m\frac{\partial A^{\frac{n-1}{2}}}{\partial x}\left(\frac{\partial^2 v}{\partial x^2} + \frac{\partial^2 v}{\partial y^2}\right) - mA^{\frac{n-1}{2}}\left(\frac{\partial^3 v}{\partial x^3} + \frac{\partial^3 v}{\partial x \partial y^2}\right) - 2m\frac{\partial^2 v}{\partial x \partial y}\frac{\partial A^{\frac{n-1}{2}}}{\partial y} \\ &- 2m\frac{\partial v}{\partial y}\frac{\partial^2 A^{\frac{n-1}{2}}}{\partial x \partial y} - m\frac{\partial^2 A^{\frac{n-1}{2}}}{\partial x^2}\left(\frac{\partial u}{\partial y} + \frac{\partial v}{\partial x}\right) - m\frac{\partial A^{\frac{n-1}{2}}}{\partial x}\left(\frac{\partial^2 u}{\partial x \partial y} + \frac{\partial^2 v}{\partial x^2}\right) \\ &= \rho\left[\frac{\partial^2 v}{\partial x \partial t} + \frac{\partial u}{\partial x}\frac{\partial v}{\partial x} + u\frac{\partial^2 v}{\partial x^2} + \frac{\partial v}{\partial x}\frac{\partial v}{\partial y} + v\frac{\partial^2 v}{\partial x \partial y}\right] \end{aligned} , \tag{3.107}$$

$$-\frac{\partial}{\partial y}\left(Eqn_165\right) \Rightarrow$$

$$\begin{aligned} &-\frac{\partial(\rho g_x)}{\partial y} + \frac{\partial p}{\partial x \partial y} + m\frac{\partial A^{\frac{n-1}{2}}}{\partial y}\left(\frac{\partial^2 u}{\partial x^2} + \frac{\partial^2 u}{\partial y^2}\right) + mA^{\frac{n-1}{2}}\left(\frac{\partial^3 u}{\partial x^2 \partial y} + \frac{\partial^3 u}{\partial y^3}\right) + 2m\frac{\partial^2 u}{\partial x \partial y}\frac{\partial A^{\frac{n-1}{2}}}{\partial x} \\ &+ 2m\frac{\partial u}{\partial x}\frac{\partial^2 A^{\frac{n-1}{2}}}{\partial x \partial y} + m\frac{\partial^2 A^{\frac{n-1}{2}}}{\partial y^2}\left(\frac{\partial u}{\partial y} + \frac{\partial v}{\partial x}\right) + m\frac{\partial A^{\frac{n-1}{2}}}{\partial y}\left(\frac{\partial^2 u}{\partial y^2} + \frac{\partial^2 v}{\partial x \partial y}\right) \\ &= -\rho\left[\frac{\partial^2 u}{\partial y \partial t} + \frac{\partial u}{\partial y}\frac{\partial u}{\partial x} + u\frac{\partial^2 u}{\partial x \partial y} + \frac{\partial v}{\partial y}\frac{\partial u}{\partial y} + v\frac{\partial^2 u}{\partial y^2}\right] \end{aligned} , \tag{3.108}$$

Combining Equation (3.107) and Equation (3.108) leads to:

Universiti Malaya

$$
\begin{aligned}
&\frac{\partial(\rho g_y)}{\partial x}-\frac{\partial(\rho g_x)}{\partial y}-\frac{\partial p}{\partial x\partial y}+\frac{\partial p}{\partial x\partial y}-m\frac{\partial A^{\frac{n-1}{2}}}{\partial x}\left(\frac{\partial^2 v}{\partial x^2}+\frac{\partial^2 v}{\partial y^2}\right)+m\frac{\partial A^{\frac{n-1}{2}}}{\partial y}\left(\frac{\partial^2 u}{\partial x^2}+\frac{\partial^2 u}{\partial y^2}\right)\\
&-mA^{\frac{n-1}{2}}\left(\frac{\partial^3 v}{\partial x^3}+\frac{\partial^3 v}{\partial x\partial y^2}\right)+mA^{\frac{n-1}{2}}\left(\frac{\partial^3 u}{\partial x^2\partial y}+\frac{\partial^3 u}{\partial y^3}\right)-2m\frac{\partial^2 v}{\partial x\partial y}\frac{\partial A^{\frac{n-1}{2}}}{\partial y}-2m\frac{\partial v}{\partial y}\frac{\partial^2 A^{\frac{n-1}{2}}}{\partial x\partial y}\\
&-m\frac{\partial^2 A^{\frac{n-1}{2}}}{\partial x^2}\left(\frac{\partial u}{\partial y}+\frac{\partial v}{\partial x}\right)-m\frac{\partial A^{\frac{n-1}{2}}}{\partial x}\left(\frac{\partial^2 u}{\partial x\partial y}+\frac{\partial^2 v}{\partial x^2}\right)+2m\frac{\partial^2 u}{\partial x\partial y}\frac{\partial A^{\frac{n-1}{2}}}{\partial x}+2m\frac{\partial u}{\partial x}\frac{\partial^2 A^{\frac{n-1}{2}}}{\partial x\partial y}\\
&+m\frac{\partial^2 A^{\frac{n-1}{2}}}{\partial y^2}\left(\frac{\partial u}{\partial y}+\frac{\partial v}{\partial x}\right)+m\frac{\partial A^{\frac{n-1}{2}}}{\partial y}\left(\frac{\partial^2 u}{\partial y^2}+\frac{\partial^2 v}{\partial x\partial y}\right)\\
&=\rho\left[\begin{array}{l}\frac{\partial}{\partial t}\left(\frac{\partial v}{\partial x}-\frac{\partial u}{\partial y}\right)+\frac{\partial u}{\partial x}\frac{\partial v}{\partial x}-\frac{\partial u}{\partial y}\frac{\partial u}{\partial x}+u\frac{\partial^2 v}{\partial x^2}-u\frac{\partial^2 u}{\partial x\partial y}+\frac{\partial v}{\partial x}\frac{\partial v}{\partial y}-\frac{\partial v}{\partial y}\frac{\partial u}{\partial y}+v\frac{\partial^2 v}{\partial x\partial y}\\ -v\frac{\partial^2 u}{\partial y^2}\end{array}\right],
\end{aligned}
$$

$$
\begin{aligned}
&-m\frac{\partial A^{\frac{n-1}{2}}}{\partial x}\frac{\partial^2 v}{\partial x^2}-m\frac{\partial A^{\frac{n-1}{2}}}{\partial x}\frac{\partial^2 v}{\partial y^2}+m\frac{\partial A^{\frac{n-1}{2}}}{\partial y}\frac{\partial^2 u}{\partial x^2}+m\frac{\partial A^{\frac{n-1}{2}}}{\partial y}\frac{\partial^2 u}{\partial y^2}-mA^{\frac{n-1}{2}}\frac{\partial^3 v}{\partial x^3}\\
&-mA^{\frac{n-1}{2}}\frac{\partial^3 v}{\partial x\partial y^2}+mA^{\frac{n-1}{2}}\frac{\partial^3 u}{\partial x^2\partial y}+mA^{\frac{n-1}{2}}\frac{\partial^3 u}{\partial y^3}-2m\frac{\partial^2 v}{\partial x\partial y}\frac{\partial A^{\frac{n-1}{2}}}{\partial y}-2m\frac{\partial v}{\partial y}\frac{\partial^2 A^{\frac{n-1}{2}}}{\partial x\partial y}\\
&-m\frac{\partial^2 A^{\frac{n-1}{2}}}{\partial x^2}\frac{\partial u}{\partial y}-m\frac{\partial^2 A^{\frac{n-1}{2}}}{\partial x^2}\frac{\partial v}{\partial x}-m\frac{\partial A^{\frac{n-1}{2}}}{\partial x}\frac{\partial^2 u}{\partial x\partial y}-m\frac{\partial A^{\frac{n-1}{2}}}{\partial x}\frac{\partial^2 v}{\partial x^2}+2m\frac{\partial^2 u}{\partial x\partial y}\frac{\partial A^{\frac{n-1}{2}}}{\partial x}.\\
&+2m\frac{\partial u}{\partial x}\frac{\partial^2 A^{\frac{n-1}{2}}}{\partial x\partial y}+m\frac{\partial^2 A^{\frac{n-1}{2}}}{\partial y^2}\frac{\partial u}{\partial y}+m\frac{\partial^2 A^{\frac{n-1}{2}}}{\partial y^2}\frac{\partial v}{\partial x}+m\frac{\partial A^{\frac{n-1}{2}}}{\partial y}\frac{\partial^2 u}{\partial y^2}+m\frac{\partial A^{\frac{n-1}{2}}}{\partial y}\frac{\partial^2 v}{\partial x\partial y}\\
&=\rho\left[\frac{\partial}{\partial t}\left(\frac{\partial v}{\partial x}-\frac{\partial u}{\partial y}\right)+v\frac{\partial}{\partial y}\left(\frac{\partial v}{\partial x}-\frac{\partial u}{\partial y}\right)+u\frac{\partial}{\partial x}\left(\frac{\partial v}{\partial x}-\frac{\partial u}{\partial y}\right)\right]
\end{aligned}
\tag{3.109}
$$

Equation (3.109) can be simplified by substituting Equation (2.11) and Equation (3.8). However, Equation (3.109) must to be manipulated and rearranged so that Equation (2.11) and Equation (3.8) appear. Rearranging Equation (3.109) and collecting all the terms in pairs will lead to:

$$
\begin{aligned}
&-mA^{\frac{n-1}{2}}\frac{\partial^2}{\partial x^2}\left(\frac{\partial v}{\partial x}-\frac{\partial u}{\partial y}\right)-mA^{\frac{n-1}{2}}\frac{\partial^2}{\partial y^2}\left(\frac{\partial v}{\partial x}-\frac{\partial u}{\partial y}\right)-2m\frac{\partial A^{\frac{n-1}{2}}}{\partial x}\frac{\partial}{\partial x}\left(\frac{\partial v}{\partial x}-\frac{\partial u}{\partial y}\right)\\
&-2m\frac{\partial A^{\frac{n-1}{2}}}{\partial y}\frac{\partial}{\partial y}\left(\frac{\partial v}{\partial x}-\frac{\partial u}{\partial y}\right)-m\frac{\partial A^{\frac{n-1}{2}}}{\partial x}\frac{\partial}{\partial y}\left(\frac{\partial u}{\partial x}+\frac{\partial v}{\partial y}\right)+m\frac{\partial A^{\frac{n-1}{2}}}{\partial y}\frac{\partial}{\partial x}\left(\frac{\partial u}{\partial x}+\frac{\partial v}{\partial y}\right)\\
&-m\frac{\partial u}{\partial y}\left(\frac{\partial^2 A^{\frac{n-1}{2}}}{\partial x^2}-\frac{\partial^2 A^{\frac{n-1}{2}}}{\partial y^2}\right)-m\frac{\partial v}{\partial x}\left(\frac{\partial^2 A^{\frac{n-1}{2}}}{\partial x^2}-\frac{\partial^2 A^{\frac{n-1}{2}}}{\partial y^2}\right)-2m\frac{\partial^2 A^{\frac{n-1}{2}}}{\partial x\partial y}\left(\frac{\partial v}{\partial y}-\frac{\partial u}{\partial x}\right)\\
&=\rho\left[\frac{\partial}{\partial t}\left(\frac{\partial v}{\partial x}-\frac{\partial u}{\partial y}\right)+v\frac{\partial}{\partial y}\left(\frac{\partial v}{\partial x}-\frac{\partial u}{\partial y}\right)+u\frac{\partial}{\partial x}\left(\frac{\partial v}{\partial x}-\frac{\partial u}{\partial y}\right)\right]
\end{aligned}
\quad . \tag{3.110}
$$

Then from Equation (3.8),

$$\zeta=\frac{\partial v}{\partial x}-\frac{\partial u}{\partial y},$$

$$
\begin{aligned}
&-mA^{\frac{n-1}{2}}\left(\frac{\partial^2\zeta}{\partial x^2}+\frac{\partial^2\zeta}{\partial y^2}\right)-2m\frac{\partial A^{\frac{n-1}{2}}}{\partial x}\frac{\partial\zeta}{\partial x}-2m\frac{\partial A^{\frac{n-1}{2}}}{\partial y}\frac{\partial\zeta}{\partial y}\\
&-m\left(\frac{\partial u}{\partial y}+\frac{\partial v}{\partial x}\right)\left(\frac{\partial^2 A^{\frac{n-1}{2}}}{\partial x^2}-\frac{\partial^2 A^{\frac{n-1}{2}}}{\partial y^2}\right)+4m\frac{\partial^2 A^{\frac{n-1}{2}}}{\partial x\partial y}\left(\frac{\partial u}{\partial x}\right).\\
&=\rho\left[\frac{\partial\zeta}{\partial t}+v\frac{\partial\zeta}{\partial y}+u\frac{\partial\zeta}{\partial x}\right]
\end{aligned}
\tag{3.111}
$$

where:

$$A^{\frac{n-1}{2}}=\left[\left(\frac{\partial u}{\partial y}+\frac{\partial v}{\partial x}\right)^2+4\left(\frac{\partial u}{\partial x}\right)^2\right]^{\frac{n-1}{2}}, \tag{3.112}$$

$$\frac{\partial A^{\frac{n-1}{2}}}{\partial x}=(n-1)A^{\frac{n-3}{2}}\left[\left(\frac{\partial u}{\partial y}+\frac{\partial v}{\partial x}\right)\left(\frac{\partial^2 u}{\partial x\partial y}+\frac{\partial^2 v}{\partial x^2}\right)+4\left(\frac{\partial u}{\partial x}\bullet\frac{\partial^2 u}{\partial x^2}\right)\right], \tag{3.113}$$

University Malaya

$$\frac{\partial A^{\frac{n-1}{2}}}{\partial y} = (n-1)A^{\frac{n-3}{2}}\left[\left(\frac{\partial u}{\partial y}+\frac{\partial v}{\partial x}\right)\left(\frac{\partial^2 u}{\partial y^2}+\frac{\partial^2 v}{\partial x \partial y}\right)+4\left(\frac{\partial v}{\partial y}\bullet\frac{\partial^2 v}{\partial y^2}\right)\right], \tag{3.114}$$

$$\begin{aligned}\frac{\partial^2 A^{\frac{n-1}{2}}}{\partial x^2} &= (n-1)(n-3)A^{\frac{n-5}{2}}\left[\left(\frac{\partial u}{\partial y}+\frac{\partial v}{\partial x}\right)\left(\frac{\partial^2 u}{\partial x \partial y}+\frac{\partial^2 v}{\partial x^2}\right)+4\left(\frac{\partial u}{\partial x}\right)\left(\frac{\partial^2 u}{\partial x^2}\right)\right]^2 \\ &+(n-1)A^{\frac{n-3}{2}}\left[\begin{array}{l}\left(\frac{\partial^2 u}{\partial x \partial y}+\frac{\partial^2 v}{\partial x^2}\right)^2+\left(\frac{\partial u}{\partial y}+\frac{\partial v}{\partial x}\right)\left(\frac{\partial^3 u}{\partial x^2 \partial y}+\frac{\partial^3 v}{\partial x^3}\right) \\ +4\left(\frac{\partial^2 u}{\partial x^2}\right)^2+4\left(\frac{\partial u}{\partial x}\right)\left(\frac{\partial^3 u}{\partial x^3}\right)\end{array}\right]^2,\end{aligned} \tag{3.115}$$

$$\begin{aligned}\frac{\partial^2 A^{\frac{n-1}{2}}}{\partial y^2} &= (n-1)(n-3)A^{\frac{n-5}{2}}\left[\left(\frac{\partial u}{\partial y}+\frac{\partial v}{\partial x}\right)\left(\frac{\partial^2 u}{\partial y^2}+\frac{\partial^2 v}{\partial x \partial y}\right)+4\left(\frac{\partial v}{\partial y}\right)\left(\frac{\partial^2 v}{\partial y^2}\right)\right]^2 \\ &+(n-1)A^{\frac{n-3}{2}}\left[\begin{array}{l}\left(\frac{\partial^2 u}{\partial y^2}+\frac{\partial^2 v}{\partial x \partial y}\right)^2+\left(\frac{\partial u}{\partial y}+\frac{\partial v}{\partial x}\right)\left(\frac{\partial^3 u}{\partial y^3}+\frac{\partial^3 v}{\partial x \partial y^2}\right) \\ +4\left(\frac{\partial^2 v}{\partial y^2}\right)^2+4\left(\frac{\partial v}{\partial y}\right)\left(\frac{\partial^3 v}{\partial y^3}\right)\end{array}\right]^2,\end{aligned} \tag{3.116}$$

$$\begin{aligned}\frac{\partial^2 A^{\frac{n-1}{2}}}{\partial x \partial y} &= (n-1)(n-3)A^{\frac{n-5}{2}}\left[\begin{array}{l}\left(\frac{\partial u}{\partial y}+\frac{\partial v}{\partial x}\right)\left(\frac{\partial^2 u}{\partial y^2}+\frac{\partial^2 v}{\partial x \partial y}\right)-2\left(\frac{\partial^2 u}{\partial x \partial y}\right)\left(\frac{\partial v}{\partial y}\right) \\ -2\left(\frac{\partial^2 v}{\partial y^2}\right)\left(\frac{\partial u}{\partial x}\right)\end{array}\right]\bullet \\ &\left[\left(\frac{\partial^2 u}{\partial x \partial y}+\frac{\partial^2 v}{\partial x^2}\right)\left(\frac{\partial u}{\partial y}+\frac{\partial v}{\partial x}\right)-2\left(\frac{\partial^2 v}{\partial x \partial y}\right)\left(\frac{\partial u}{\partial x}\right)-2\left(\frac{\partial^2 u}{\partial x^2}\right)\left(\frac{\partial v}{\partial y}\right)\right] \\ &+(n-1)A^{\frac{n-3}{2}}\left[\begin{array}{l}\left(\frac{\partial^2 u}{\partial y^2}+\frac{\partial^2 v}{\partial x \partial y}\right)\left(\frac{\partial^2 u}{\partial x \partial y}+\frac{\partial^2 v}{\partial x^2}\right)+\left(\frac{\partial u}{\partial y}+\frac{\partial v}{\partial x}\right)\left(\frac{\partial^3 u}{\partial x \partial y^2}+\frac{\partial^3 v}{\partial x^2 \partial y}\right) \\ -2\left(\frac{\partial^3 v}{\partial x \partial y^2}\right)\left(\frac{\partial u}{\partial x}\right)-2\left(\frac{\partial^2 v}{\partial x \partial y}\right)\left(\frac{\partial^2 u}{\partial x \partial y}\right)-2\left(\frac{\partial^3 u}{\partial x^2 \partial y}\right)\left(\frac{\partial v}{\partial y}\right) \\ -2\left(\frac{\partial^2 u}{\partial x^2}\right)\left(\frac{\partial^2 v}{\partial y^2}\right)\end{array}\right].\end{aligned} \tag{3.117}$$

From Equation (2.11),

Universiti Malaya

$\frac{\partial u}{\partial x}+\frac{\partial v}{\partial y}=0$. Hence, Equation (3.117) can be rewritten as:

$$\frac{\partial^2 A^{\frac{n-1}{2}}}{\partial x\partial y}=(n-1)(n-3)A^{\frac{n-5}{2}}\left[\left(\frac{\partial u}{\partial y}+\frac{\partial v}{\partial x}\right)\left(\frac{\partial^2 u}{\partial y^2}+\frac{\partial^2 v}{\partial x\partial y}\right)+4\left(\frac{\partial u}{\partial x}\right)\left(\frac{\partial^2 u}{\partial x\partial y}\right)\right]\bullet$$
$$\left[\left(\frac{\partial u}{\partial y}+\frac{\partial v}{\partial x}\right)\left(\frac{\partial^2 u}{\partial x\partial y}+\frac{\partial^2 v}{\partial x^2}\right)+4\left(\frac{\partial u}{\partial x}\right)\left(\frac{\partial^2 u}{\partial x^2}\right)\right] \quad , \qquad (3.118)$$
$$+(n-1)A^{\frac{n-3}{2}}\left[\begin{array}{l}\left(\frac{\partial^2 u}{\partial y^2}+\frac{\partial^2 v}{\partial x\partial y}\right)\left(\frac{\partial^2 u}{\partial x\partial y}+\frac{\partial^2 v}{\partial x^2}\right)+\left(\frac{\partial u}{\partial y}+\frac{\partial v}{\partial x}\right)\left(\frac{\partial^3 u}{\partial x\partial y^2}+\frac{\partial^3 v}{\partial x^2\partial y}\right)\\ +4\left(\frac{\partial u}{\partial x}\right)\left(\frac{\partial^3 u}{\partial x^2\partial y}\right)+4\left(\frac{\partial^2 u}{\partial x\partial y}\right)\left(\frac{\partial^2 u}{\partial x^2}\right)\end{array}\right]$$

or

$$\frac{\partial^2 A^{\frac{n-1}{2}}}{\partial x\partial y}=(n-1)(n-3)A^{\frac{n-5}{2}}\left[\left(\frac{\partial u}{\partial y}+\frac{\partial v}{\partial x}\right)\left(\frac{\partial^2 u}{\partial x\partial y}+\frac{\partial^2 v}{\partial x^2}\right)+4\left(\frac{\partial v}{\partial y}\right)\left(\frac{\partial^2 v}{\partial x\partial y}\right)\right]\bullet$$
$$\left[\left(\frac{\partial u}{\partial y}+\frac{\partial v}{\partial x}\right)\left(\frac{\partial^2 u}{\partial y^2}+\frac{\partial^2 v}{\partial x\partial y}\right)+4\left(\frac{\partial v}{\partial y}\right)\left(\frac{\partial^2 v}{\partial y^2}\right)\right] \quad . \qquad (3.119)$$
$$+(n-1)A^{\frac{n-3}{2}}\left[\begin{array}{l}\left(\frac{\partial^2 u}{\partial x\partial y}+\frac{\partial^2 v}{\partial x^2}\right)\left(\frac{\partial^2 u}{\partial y^2}+\frac{\partial^2 v}{\partial x\partial y}\right)+\left(\frac{\partial u}{\partial y}+\frac{\partial v}{\partial x}\right)\left(\frac{\partial^3 u}{\partial x\partial y^2}+\frac{\partial^3 v}{\partial x^2\partial y}\right)\\ +4\left(\frac{\partial^2 v}{\partial x\partial y}\right)\left(\frac{\partial^2 v}{\partial y^2}\right)+4\left(\frac{\partial v}{\partial y}\right)\left(\frac{\partial^3 v}{\partial x\partial y^2}\right)\end{array}\right]$$

From Equation (3.11) and Equation (3.12), using the stream function which relates the velocities. Equation (3.111) will become:

$$\frac{m}{\rho}A^{\frac{n-1}{2}}\left(\frac{\partial^2\zeta}{\partial x^2}+\frac{\partial^2\zeta}{\partial y^2}\right)+\frac{2m}{\rho}\frac{\partial A^{\frac{n-1}{2}}}{\partial x}\frac{\partial\zeta}{\partial x}+\frac{2m}{\rho}\frac{\partial A^{\frac{n-1}{2}}}{\partial y}\frac{\partial\zeta}{\partial y}+$$
$$\frac{m}{\rho}\left(\frac{\partial^2\psi}{\partial y^2}-\frac{\partial^2\psi}{\partial x^2}\right)\left(\frac{\partial^2 A^{\frac{n-1}{2}}}{\partial x^2}-\frac{\partial^2 A^{\frac{n-1}{2}}}{\partial y^2}\right)-\frac{4m}{\rho}\frac{\partial^2 A^{\frac{n-1}{2}}}{\partial x\partial y}\left(\frac{\partial^2\psi}{\partial x\partial y}\right)=\frac{\partial\zeta}{\partial t}-\frac{\partial\psi}{\partial x}\frac{\partial\zeta}{\partial y}+\frac{\partial\psi}{\partial y}\frac{\partial\zeta}{\partial x} \quad , \qquad (3.120)$$

Universiti Malaya

where:

$$A^{\frac{n-1}{2}} = \left[\left(\frac{\partial^2\psi}{\partial y^2} - \frac{\partial^2\psi}{\partial x^2}\right)^2 + 4\left(\frac{\partial^2\psi}{\partial x\partial y}\right)^2\right]^{\frac{n-1}{2}}, \tag{3.121}$$

$$\frac{\partial A^{\frac{n-1}{2}}}{\partial x} = (n-1)A^{\frac{n-3}{2}}\left[\left(\frac{\partial^2\psi}{\partial y^2} - \frac{\partial^2\psi}{\partial x^2}\right)\left(\frac{\partial^3\psi}{\partial x\partial y^2} - \frac{\partial^3\psi}{\partial x^3}\right) + 4\left(\frac{\partial^2\psi}{\partial x\partial y} \bullet \frac{\partial^3\psi}{\partial x^2\partial y}\right)\right], \tag{3.122}$$

$$\frac{\partial A^{\frac{n-1}{2}}}{\partial y} = (n-1)A^{\frac{n-3}{2}}\left[\left(\frac{\partial^2\psi}{\partial y^2} - \frac{\partial^2\psi}{\partial x^2}\right)\left(\frac{\partial^3\psi}{\partial y^3} - \frac{\partial^3\psi}{\partial x^2\partial y}\right) + 4\left(\frac{\partial^2\psi}{\partial x\partial y} \bullet \frac{\partial^3\psi}{\partial x\partial y^2}\right)\right], \tag{3.123}$$

$$\begin{aligned}\frac{\partial^2 A^{\frac{n-1}{2}}}{\partial x^2} &= (n-1)(n-3)A^{\frac{n-5}{2}}\left[\left(\frac{\partial^2\psi}{\partial y^2} - \frac{\partial^2\psi}{\partial x^2}\right)\left(\frac{\partial^3\psi}{\partial x\partial y^2} - \frac{\partial^3\psi}{\partial x^3}\right) + 4\left(\frac{\partial^2\psi}{\partial x\partial y}\right)\left(\frac{\partial^3\psi}{\partial x^2\partial y}\right)\right]^2 \\ &+ (n-1)A^{\frac{n-3}{2}}\left[\begin{array}{l}\left(\frac{\partial^3\psi}{\partial x\partial y^2} - \frac{\partial^3\psi}{\partial x^3}\right)^2 + \left(\frac{\partial^2\psi}{\partial y^2} - \frac{\partial^2\psi}{\partial x^2}\right)\left(\frac{\partial^4\psi}{\partial x^2\partial y^2} - \frac{\partial^4\psi}{\partial x^4}\right) \\ + 4\left(\frac{\partial^3\psi}{\partial x^2\partial y}\right)^2 + 4\left(\frac{\partial^2\psi}{\partial x\partial y}\right)\left(\frac{\partial^4\psi}{\partial x^3\partial y}\right)\end{array}\right]^2,\end{aligned} \tag{3.124}$$

$$\begin{aligned}\frac{\partial^2 A^{\frac{n-1}{2}}}{\partial y^2} &= (n-1)(n-3)A^{\frac{n-5}{2}}\left[\left(\frac{\partial^2\psi}{\partial y^2} - \frac{\partial^2\psi}{\partial x^2}\right)\left(\frac{\partial^3\psi}{\partial y^3} - \frac{\partial^3\psi}{\partial x^2\partial y}\right) + 4\left(\frac{\partial^2\psi}{\partial x\partial y}\right)\left(\frac{\partial^3\psi}{\partial x\partial y^2}\right)\right]^2 \\ &+ (n-1)A^{\frac{n-3}{2}}\left[\begin{array}{l}\left(\frac{\partial^3\psi}{\partial y^3} - \frac{\partial^3\psi}{\partial x^2\partial y}\right)^2 + \left(\frac{\partial^2\psi}{\partial y^2} - \frac{\partial^2\psi}{\partial x^2}\right)\left(\frac{\partial^4\psi}{\partial y^4} - \frac{\partial^4\psi}{\partial x^2\partial y^2}\right) \\ + 4\left(\frac{\partial^3\psi}{\partial x\partial y^2}\right)^2 + 4\left(\frac{\partial^2\psi}{\partial x\partial y}\right)\left(\frac{\partial^4\psi}{\partial x\partial y^3}\right)\end{array}\right]^2,\end{aligned} \tag{3.125}$$

Universiti Malaya

$$\frac{\partial^2 A^{\frac{n-1}{2}}}{\partial x \partial y} = (n-1)(n-3)A^{\frac{n-5}{2}}\left[\left(\frac{\partial^2\psi}{\partial y^2}-\frac{\partial^2\psi}{\partial x^2}\right)\left(\frac{\partial^3\psi}{\partial y^3}-\frac{\partial^3\psi}{\partial x^2\partial y}\right)+4\left(\frac{\partial^2\psi}{\partial x\partial y}\right)\left(\frac{\partial^3\psi}{\partial x\partial y^2}\right)\right]\bullet$$

$$\left[\left(\frac{\partial^2\psi}{\partial y^2}-\frac{\partial^2\psi}{\partial x^2}\right)\left(\frac{\partial^3\psi}{\partial x\partial y^2}-\frac{\partial^3\psi}{\partial x^3}\right)+4\left(\frac{\partial^2\psi}{\partial x\partial y}\right)\left(\frac{\partial^3\psi}{\partial x^2\partial y}\right)\right] \quad . \qquad (3.126)$$

$$+(n-1)A^{\frac{n-3}{2}}\left[\begin{array}{l}\left(\frac{\partial^3\psi}{\partial y^3}-\frac{\partial^3\psi}{\partial x^2\partial y}\right)\left(\frac{\partial^3\psi}{\partial x\partial y^2}-\frac{\partial^3\psi}{\partial x^3}\right)+\left(\frac{\partial^2\psi}{\partial y^2}-\frac{\partial^2\psi}{\partial x^2}\right)\left(\frac{\partial^4\psi}{\partial x\partial y^3}-\frac{\partial^4\psi}{\partial x^3\partial y}\right)\\ +4\left(\frac{\partial^2\psi}{\partial x\partial y}\right)\left(\frac{\partial^4\psi}{\partial x^2\partial y^2}\right)+4\left(\frac{\partial^3\psi}{\partial x\partial y^2}\right)\left(\frac{\partial^3\psi}{\partial x^2\partial y}\right)\end{array}\right]$$

3.8.1 Discretization of Non-Newtonian Governing Equations

Due to the fourth derivative of stream function exists in Equation (3.124) till Equation (3.126), 4×4 grids system will be used. Figure 3.22 shows the 4×4 grids system ($\Delta x = \Delta y = h$).

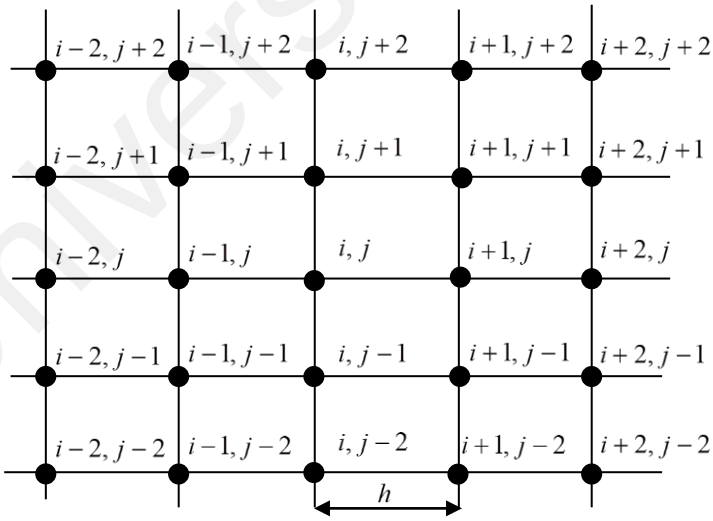

Figure 3.22: 4×4 grids system

Universiti Malaya

Table 3.2 shows the forward and centered finite difference formulas for first, second, third and fourth derivatives.

Table 3.2: Forward and centered finite difference formulas

Forward and centered finite difference formulas		
No.	Equations	Equivalent FDEs
1.	$\frac{\partial \psi}{\partial y}$	$\frac{\psi_{i,j+1}^{t} - \psi_{i,j-1}^{t}}{2h}$
2.	$\frac{\partial^2 \psi}{\partial y^2} - \frac{\partial^2 \psi}{\partial x^2}$	$\frac{\psi_{i,j+1}^{t} + \psi_{i,j-1}^{t} - \psi_{i+1,j}^{t} - \psi_{i-1,j}^{t}}{h^2}$
3.	$\frac{\partial^2 \psi}{\partial x \partial y}$	$\frac{\psi_{i+1,j+1}^{t} + \psi_{i-1,j-1}^{t} - \psi_{i+1,j-1}^{t} - \psi_{i-1,j+1}^{t}}{4h^2}$
4.	$\frac{\partial^3 \psi}{\partial x^3}$	$\frac{\psi_{i+2,j}^{t} - 2\psi_{i+1,j}^{t} + 2\psi_{i-1,j}^{t} - \psi_{i-2,j}^{t}}{2h^3}$
5.	$\frac{\partial^3 \psi}{\partial x \partial y^2}$	$\frac{\psi_{i+1,j+1}^{t} + \psi_{i+1,j-1}^{t} - 2\psi_{i+1,j}^{t} + 2\psi_{i-1,j}^{t} - \psi_{i-1,j+1}^{t} - \psi_{i-1,j-1}^{t}}{2h^3}$
6.	$\frac{\partial^3 \psi}{\partial x^2 \partial y}$	$\frac{\psi_{i+1,j+1}^{t} + \psi_{i-1,j+1}^{t} - 2\psi_{i,j+1}^{t} - \psi_{i+1,j-1}^{t} - \psi_{i-1,j-1}^{t} + 2\psi_{i,j-1}^{t}}{2h^3}$
7.	$\frac{\partial^4 \psi}{\partial x^4}$	$\frac{\psi_{i+2,j}^{t} - 4\psi_{i+1,j}^{t} + 6\psi_{i,j}^{t} - 4\psi_{i-1,j}^{t} + \psi_{i-2,j}^{t}}{h^4}$
8.	$\frac{\partial^4 \psi}{\partial x^2 \partial y^2}$	$\frac{\psi_{i+1,j+1}^{t} + \psi_{i+1,j-1}^{t} - 2\psi_{i+1,j}^{t} + \psi_{i-1,j+1}^{t} + \psi_{i-1,j-1}^{t} - 2\psi_{i-1,j}^{t} - 2\psi_{i,j+1}^{t} - 2\psi_{i,j-1}^{t} + 4\psi_{i,j}^{t}}{h^4}$
9.	$\frac{\partial^4 \psi}{\partial x \partial y^3}$	$\frac{\psi_{i+1,j+2}^{t} - 2\psi_{i+1,j+1}^{t} + 2\psi_{i+1,j-1}^{t} - \psi_{i+1,j-2}^{t} - \psi_{i-1,j+2}^{t} + 2\psi_{i-1,j+1}^{t} - 2\psi_{i-1,j-1}^{t} + \psi_{i-1,j-2}^{t}}{4h^4}$
10.	$\frac{\partial^4 \psi}{\partial x^3 \partial y}$	$\frac{\psi_{i+2,j+1}^{t} - 2\psi_{i+1,j+1}^{t} + 2\psi_{i-1,j+1}^{t} - \psi_{i-2,j+1}^{t} - \psi_{i+2,j-1}^{t} + 2\psi_{i+1,j-1}^{t} - 2\psi_{i-1,j-1}^{t} + \psi_{i-2,j-1}^{t}}{4h^4}$

Equation (3.120) can be transformed into a FDE using forward and centered finite-divided-difference formulas:

$$
\begin{aligned}
\frac{\zeta_{i,j}^{t+1}-\zeta_{i,j}^{t}}{\Delta t} &= -\left(\frac{\psi_{i,j+1}^{t}-\psi_{i,j-1}^{t}}{2h}\right)\left(\frac{\zeta_{i+1,j}^{t}-\zeta_{i-1,j}^{t}}{2h}\right)+\left(\frac{\psi_{i+1,j}^{t}-\psi_{i-1,j}^{t}}{2h}\right)\left(\frac{\zeta_{i,j+1}^{t}-\zeta_{i,j-1}^{t}}{2h}\right) \\
&+\frac{m}{\rho}A^{\frac{n-1}{2}}\left(\frac{\zeta_{i+1,j}^{t}+\zeta_{i-1,j}^{t}+\zeta_{i,j+1}^{t}+\zeta_{i,j-1}^{t}-4\zeta_{i,j}^{t}}{h^2}\right)+\frac{2m}{\rho}\frac{\partial A^{\frac{n-1}{2}}}{\partial x}\left(\frac{\zeta_{i+1,j}^{t}-\zeta_{i-1,j}^{t}}{2h}\right) \\
&+\frac{2m}{\rho}\frac{\partial A^{\frac{n-1}{2}}}{\partial y}\left(\frac{\zeta_{i,j+1}^{t}-\zeta_{i,j-1}^{t}}{2h}\right)+\frac{m}{\rho}\left(\frac{\partial^2 A^{\frac{n-1}{2}}}{\partial x^2}-\frac{\partial^2 A^{\frac{n-1}{2}}}{\partial y^2}\right)\left(\frac{\psi_{i,j+1}^{t}+\psi_{i,j-1}^{t}-\psi_{i+1,j}^{t}-\psi_{i-1,j}^{t}}{h^2}\right) \\
&-\frac{m}{\rho}\frac{\partial^2 A^{\frac{n-1}{2}}}{\partial x\partial y}\left(\frac{\psi_{i+1,j+1}^{t}+\psi_{i-1,j-1}^{t}-\psi_{i+1,j-1}^{t}-\psi_{i-1,j+1}^{t}}{4h^2}\right)
\end{aligned}
\quad . \tag{3.127}
$$

Rearranging Equation (3.127):

$$
\begin{aligned}
\zeta_{i,j}^{t+1} = \Delta t \Bigg[& -\left(\frac{\psi_{i,j+1}^{t}-\psi_{i,j-1}^{t}}{2h}\right)\left(\frac{\zeta_{i+1,j}^{t}-\zeta_{i-1,j}^{t}}{2h}\right)+\left(\frac{\psi_{i+1,j}^{t}-\psi_{i-1,j}^{t}}{2h}\right)\left(\frac{\zeta_{i,j+1}^{t}-\zeta_{i,j-1}^{t}}{2h}\right) \\
& +\frac{2m}{\rho}\frac{\partial A^{\frac{n-1}{2}}}{\partial x}\left(\frac{\zeta_{i+1,j}^{t}-\zeta_{i-1,j}^{t}}{2h}\right)+\frac{2m}{\rho}\frac{\partial A^{\frac{n-1}{2}}}{\partial y}\left(\frac{\zeta_{i,j+1}^{t}-\zeta_{i,j-1}^{t}}{2h}\right) \\
& +\frac{m}{\rho}\left(\frac{\partial^2 A^{\frac{n-1}{2}}}{\partial x^2}-\frac{\partial^2 A^{\frac{n-1}{2}}}{\partial y^2}\right)\left(\frac{\psi_{i,j+1}^{t}+\psi_{i,j-1}^{t}-\psi_{i+1,j}^{t}-\psi_{i-1,j}^{t}}{h^2}\right) \\
& -\frac{m}{\rho}\frac{\partial^2 A^{\frac{n-1}{2}}}{\partial x\partial y}\left(\frac{\psi_{i+1,j+1}^{t}+\psi_{i-1,j-1}^{t}-\psi_{i+1,j-1}^{t}-\psi_{i-1,j+1}^{t}}{4h^2}\right) \\
& +\frac{m}{\rho}A^{\frac{n-1}{2}}\left(\frac{\zeta_{i+1,j}^{t}+\zeta_{i-1,j}^{t}+\zeta_{i,j+1}^{t}+\zeta_{i,j-1}^{t}}{h^2}\right) \Bigg] \\
& +\left(1-\frac{4mA^{\frac{n-1}{2}}\Delta t}{\rho}\right)\zeta_{i,j}^{t}
\end{aligned}
\quad , \tag{3.128}
$$

where:

$$
A^{\frac{n-1}{2}} = \left[\left(\frac{\psi_{i,j+1}^{t}+\psi_{i,j-1}^{t}-\psi_{i+1,j}^{t}-\psi_{i-1,j}^{t}}{h^2}\right)^2 + \left(\frac{\psi_{i+1,j+1}^{t}+\psi_{i-1,j-1}^{t}-\psi_{i+1,j-1}^{t}-\psi_{i-1,j+1}^{t}}{2h^2}\right)^2\right]^{\frac{n-1}{2}} , \tag{3.129}
$$

Universiti Malaya

$$\frac{\partial A^{\frac{n-1}{2}}}{\partial x} = (n-1)A^{\frac{n-3}{2}} \left[\begin{array}{l} \left(\dfrac{\psi^t_{i,j+1} + \psi^t_{i,j-1} - \psi^t_{i+1,j} - \psi^t_{i-1,j}}{h^2} \right) \bullet \\ \left(\dfrac{\psi^t_{i+1,j+1} + \psi^t_{i+1,j-1} - \psi^t_{i-1,j+1} - \psi^t_{i-1,j-1} - \psi^t_{i+2,j} + \psi^t_{i-2,j}}{2h^3} \right) \\ + \left(\dfrac{\psi^t_{i+1,j+1} + \psi^t_{i-1,j-1} - \psi^t_{i+1,j-1} - \psi^t_{i-1,j+1}}{h^2} \right) \bullet \\ \left(\dfrac{\psi^t_{i+1,j+1} + \psi^t_{i-1,j+1} - 2\psi^t_{i,j+1} - \psi^t_{i+1,j-1} - \psi^t_{i-1,j-1} + 2\psi^t_{i,j-1}}{2h^3} \right) \end{array} \right], \tag{3.130}$$

$$\frac{\partial A^{\frac{n-1}{2}}}{\partial y} = (n-1)A^{\frac{n-3}{2}} \left[\begin{array}{l} \left(\dfrac{\psi^t_{i,j+1} + \psi^t_{i,j-1} - \psi^t_{i+1,j} - \psi^t_{i-1,j}}{h^2} \right) \bullet \\ \left(\dfrac{\psi^t_{i,j+2} - \psi^t_{i,j-2} - \psi^t_{i+1,j+1} - \psi^t_{i,-1\,j+1} + \psi^t_{i+1,j-1} + \psi^t_{i-1,j-1}}{2h^3} \right) \\ + \left(\dfrac{\psi^t_{i+1,j+1} + \psi^t_{i-1,j-1} - \psi^t_{i+1,j-1} - \psi^t_{i-1,j+1}}{h^2} \right) \bullet \\ \left(\dfrac{\psi^t_{i+1,j+1} + \psi^t_{i+1,j-1} - 2\psi^t_{i+1,j} + 2\psi^t_{i-1,j} - \psi^t_{i-1,j+1} - \psi^t_{i-1,j-1}}{2h^3} \right) \end{array} \right], \tag{3.131}$$

Universiti Malaya

$$
\begin{aligned}
\frac{\partial^2 A^{\frac{n-1}{2}}}{\partial x^2} = (n-1)(n-3)A^{\frac{n-5}{2}} & \left[\begin{array}{l} \left(\dfrac{\psi^t_{i,j+1} + \psi^t_{i,j-1} - \psi^t_{i+1,j} - \psi^t_{i-1,j}}{h^2} \right) \bullet \\ \left(\dfrac{\psi^t_{i-2,j} - \psi^t_{i+2,j} + \psi^t_{i+1,j+1} - \psi^t_{i-1,j+1} + \psi^t_{i+1,j-1} - \psi^t_{i-1,j-1}}{2h^3} \right) \\ + \left(\dfrac{\psi^t_{i+1,j+1} - \psi^t_{i-1,j+1} - \psi^t_{i+1,j-1} + \psi^t_{i-1,j-1}}{h^2} \right) \bullet \\ \left(\dfrac{\psi^t_{i+1,j+1} + \psi^t_{i-1,j+1} - 2\psi^t_{i,j+1} - \psi^t_{i+1,j-1} - \psi^t_{i-1,j-1} + 2\psi^t_{i,j-1}}{2h^3} \right) \end{array} \right]^2 \\
+ (n-1)A^{\frac{n-3}{2}} & \left[\begin{array}{l} \left(\dfrac{\psi^t_{i+1,j+1} + \psi^t_{i+1,j-1} - \psi^t_{i-1,j+1} - \psi^t_{i-1,j-1} - \psi^t_{i+2,j} + \psi^t_{i-2,j}}{2h^3} \right)^2 \\ + \left(\dfrac{\psi^t_{i,j+1} + \psi^t_{i,j-1} - \psi^t_{i+1,j} - \psi^t_{i-1,j}}{h^2} \right) \\ \bullet \left(\dfrac{\begin{array}{l} \psi^t_{i+1,j+1} + \psi^t_{i+1,j-1} + 2\psi^t_{i+1,j} + \psi^t_{i-1,j+1} + \psi^t_{i-1,j-1} + 2\psi^t_{i-1,j} - 2\psi^t_{i,j+1} \\ - 2\psi^t_{i,j-1} - 2\psi^t_{i,j} - \psi^t_{i+2,j} - \psi^t_{i-2,j} \end{array}}{h^4} \right) \\ + \left(\dfrac{\psi^t_{i+1\,j+1} + \psi^t_{i-1,j+1} - 2\psi^t_{i,j+1} - \psi^t_{i+1,j-1} - \psi^t_{i-1,j-1} + 2\psi^t_{i,j-1}}{h^3} \right)^2 \\ + \left(\dfrac{\psi^t_{i+1,j+1} + \psi^t_{i-1,j-1} - \psi^t_{i+1,j-1} - \psi^t_{i-1,j+1}}{h^2} \right) \\ \bullet \left(\dfrac{\begin{array}{l} \psi^t_{i+2,j+1} - 2\psi^t_{i+1,j+1} + 2\psi^t_{i-1,j+1} - \psi^t_{i-2,j+1} - \psi^t_{i+2,j-1} + 2\psi^t_{i+1,j-1} \\ - 2\psi^t_{i-1,j-1} + \psi^t_{i-2,j-1} \end{array}}{4h^4} \right) \end{array} \right]^2
\end{aligned}
\quad , \quad (3.132)
$$

Universiti Malaya

$$
\begin{aligned}
\frac{\partial^2 A^{\frac{n-1}{2}}}{\partial y^2} = (n-1)(n-3)A^{\frac{n-5}{2}} & \left[\begin{array}{l}
\left(\dfrac{\psi^t_{i,j+1} + \psi^t_{i,j-1} - \psi^t_{i+1,j} - \psi^t_{i-1,j}}{h^2} \right) \bullet \\
\left(\dfrac{\psi^t_{i,j+2} - \psi^t_{i,j-2} + \psi^t_{i+1,j-1} + \psi^t_{i-1,j-1} - \psi^t_{i+1,j+1} - \psi^t_{i-1,j+1}}{2h^3} \right) \\
+ \left(\dfrac{\psi^t_{i+1,j+1} - \psi^t_{i-1,j+1} - \psi^t_{i+1,j-1} + \psi^t_{i-1,j-1}}{h^2} \right) \bullet \\
\left(\dfrac{\psi^t_{i+1,j+1} + \psi^t_{i+1,j-1} - 2\psi^t_{i+1,j} - \psi^t_{i-1,j+1} - \psi^t_{i-1,j-1} + 2\psi^t_{i-1,j}}{2h^3} \right)
\end{array} \right]^2 \\
+ (n-1)A^{\frac{n-3}{2}} & \left[\begin{array}{l}
\left(\dfrac{\psi^t_{i,j+2} - \psi^t_{i,j-2} - \psi^t_{i+1,j+1} - \psi^t_{i-1,j+1} + \psi^t_{i+1,j-1} + \psi^t_{i-1,j-1}}{2h^3} \right)^2 \\
+ \left(\dfrac{\psi^t_{i,j+1} + \psi^t_{i,j-1} - \psi^t_{i+1,j} - \psi^t_{i-1,j}}{h^2} \right) \\
\bullet \left(\dfrac{\begin{array}{l} \psi^t_{i,j+2} - 2\psi^t_{i,j+1} + 2\psi^t_{i,j} - 2\psi^t_{i,j-1} + \psi^t_{i,j-2} - \psi^t_{i+1,j+1} - \psi^t_{i+1,j-1} \\ + 2\psi^t_{i+1,j} - \psi^t_{i-1,j+1} - \psi^t_{i-1,j-1} - 2\psi^t_{i-1,j} \end{array}}{h^4} \right) \\
+ \left(\dfrac{\psi^t_{i+1\,j+1} + \psi^t_{i+1,j-1} - 2\psi^t_{i+1,j} + 2\psi^t_{i-1,j} - \psi^t_{i-1,j+1} - \psi^t_{i-1,j-1}}{h^3} \right)^2 \\
+ \left(\dfrac{\psi^t_{i+1,j+1} + \psi^t_{i-1,j-1} - \psi^t_{i+1,j-1} - \psi^t_{i-1,j+1}}{h^2} \right) \\
\bullet \left(\dfrac{\begin{array}{l} \psi^t_{i+1,j+2} - 2\psi^t_{i+1,j+1} + 2\psi^t_{i+1,j-1} - \psi^t_{i+1,j-2} - \psi^t_{i-1,j+2} + 2\psi^t_{i-1,j+1} \\ - 2\psi^t_{i-1,j-1} + \psi^t_{i-1,j-2} \end{array}}{4h^4} \right)
\end{array} \right]^2
\end{aligned}
\quad , \qquad (3.133)
$$

Universiti Malaya

$$
\begin{aligned}
\frac{\partial^2 A^{\frac{n-1}{2}}}{\partial x \partial y} = (n-1)(n-3)A^{\frac{n-5}{2}} & \left[\begin{array}{l} \left(\dfrac{\psi^t_{i,j+1} + \psi^t_{i,j-1} - \psi^t_{i+1,j} - \psi^t_{i-1,j}}{h^2} \right) \\ \bullet \left(\dfrac{\psi^t_{i,j+2} - \psi^t_{i,j-2} - \psi^t_{i+1,j+1} - \psi^t_{i-1,j+1} + \psi^t_{i+1,j-1} + \psi^t_{i-1,j-1}}{2h^3} \right) \\ + \left(\dfrac{\psi^t_{i+1,j+1} - \psi^t_{i-1,j+1} - \psi^t_{i+1,j-1} + \psi^t_{i-1,j-1}}{h^2} \right) \bullet \\ \left(\dfrac{\psi^t_{i+1,j+1} + \psi^t_{i+1,j-1} - 2\psi^t_{i+1,j} - \psi^t_{i-1,j+1} - \psi^t_{i-1,j-1} + 2\psi^t_{i-1,j}}{2h^3} \right) \end{array} \right] \bullet \\
& \left[\begin{array}{l} \left(\dfrac{\psi^t_{i,j+1} + \psi^t_{i,j-1} - \psi^t_{i+1,j} - \psi^t_{i-1,j}}{h^2} \right) \left(\dfrac{\psi^t_{i+1,j+1} + \psi^t_{i+1,j-1} - \psi^t_{i-1,j+1} - \psi^t_{i-1,j-1} - \psi^t_{i+2,j} + \psi^t_{i-2,j}}{2h^3} \right) \\ + \left(\dfrac{\psi^t_{i+1,j+1} - \psi^t_{i-1,j+1} - \psi^t_{i+1,j-1} + \psi^t_{i-1,j-1}}{h^2} \right) \left(\dfrac{\psi^t_{i+1,j+1} + \psi^t_{i-1,j+1} - 2\psi^t_{i,j+1} - \psi^t_{i+1,j-1} - \psi^t_{i-1,j-1} + 2\psi^t_{i,j-1}}{2h^3} \right) \end{array} \right] \\
& + (n-1)A^{\frac{n-3}{2}} \left[\begin{array}{l} \left(\dfrac{\psi^t_{i,j+2} - \psi^t_{i,j-2} - \psi^t_{i+1,j+1} - \psi^t_{i-1,j+1} + \psi^t_{i+1,j-1} + \psi^t_{i-1,j-1}}{2h^3} \right) \\ \bullet \left(\dfrac{\psi^t_{i+1,j+1} + \psi^t_{i+1,j-1} - \psi^t_{i-1,j+1} - \psi^t_{i-1,j-1} - \psi^t_{i+2,j} + \psi^t_{i-2,j}}{2h^3} \right) \\ + \left(\dfrac{\psi^t_{i,j+1} + \psi^t_{i,j-1} - \psi^t_{i+1,j} - \psi^t_{i-1,j}}{h^2} \right) \\ \bullet \left(\dfrac{\psi^t_{i+1,j+2} - \psi^t_{i+1,j-2} - \psi^t_{i-1,j+2} + \psi^t_{i-1,j-2} - \psi^t_{i+2,j+1} + \psi^t_{i-2,j+1} + \psi^t_{i+2,j-1} - \psi^t_{i-2,j-1}}{4h^4} \right) \\ + \left(\dfrac{\psi^t_{i+1,j+1} - \psi^t_{i-1,j+1} - \psi^t_{i+1,j-1} + \psi^t_{i-1,j-1}}{h^2} \right) \\ \bullet \left(\dfrac{\psi^t_{i+1,j+1} + \psi^t_{i+1,j-1} - 2\psi^t_{i+1,j} + \psi^t_{i-1,j+1} + \psi^t_{i-1,j-1} - 2\psi^t_{i-1,j} - 2\psi^t_{i,j+1} - 2\psi^t_{i,j-1} + 4\psi^t_{i,j}}{h^4} \right) \\ + \left(\dfrac{\psi^t_{i+1,j+1} + \psi^t_{i+1,j-1} - 2\psi^t_{i+1,j} + 2\psi^t_{i-1,j} - \psi^t_{i-1,j+1} - \psi^t_{i-1,j-1}}{h^3} \right) \\ \bullet \left(\dfrac{\psi^t_{i+1,j+1} + \psi^t_{i-1,j+1} - 2\psi^t_{i,j+1} - \psi^t_{i+1,j-1} - \psi^t_{i-1,j-1} + 2\psi^t_{i,j-1}}{h^3} \right) \end{array} \right] . \qquad (3.134)
\end{aligned}
$$

Universiti Malaya

Explicit or forward FDM is conditionally stable and from Equation (3.128):

$$\left(1-\frac{4mA^{\frac{n-1}{2}}\Delta t}{\rho}\right)\geq 0 \text{ or } \Delta t\leq\frac{\rho}{4mA^{\frac{n-1}{2}}}, \tag{3.135}$$

where $A^{\frac{n-1}{2}}=\left[\begin{array}{l}\left(\dfrac{\psi_{i,j+1}^{t}+\psi_{i,j-1}^{t}-\psi_{i+1,j}^{t}-\psi_{i-1,j}^{t}}{h^2}\right)^2\\ +\left(\dfrac{\psi_{i+1,j+1}^{t}+\psi_{i-1,j-1}^{t}-\psi_{i+1,j-1}^{t}-\psi_{i-1,j+1}^{t}}{2h^2}\right)^2\end{array}\right]^{\frac{n-1}{2}}$ and it"s not a constant.

Thus, forward FDM is not suitable to be employed to solve Equation (3.128). Backward or implicit FDM will be tried to be employed here.

3.8.2 Discretization Using Implicit FDM

Since the maximum allowable value of Equation (3.135) cannot be evaluated, all other stream functions, ψ will be evaluated at the new step time, $t+1$. Thus from Equation (3.120),

$$\begin{aligned}\frac{\zeta_{i,j}^{t+1}-\zeta_{i,j}^{t}}{\Delta t}&=-\left(\frac{\psi_{i,j+1}^{t+1}-\psi_{i,j-1}^{t+1}}{2h}\right)\left(\frac{\zeta_{i+1,j}^{t+1}-\zeta_{i-1,j}^{t+1}}{2h}\right)+\left(\frac{\psi_{i+1,j}^{t+1}-\psi_{i-1,j}^{t+1}}{2h}\right)\left(\frac{\zeta_{i,j+1}^{t+1}-\zeta_{i,j-1}^{t+1}}{2h}\right)\\&+\frac{m}{\rho}A^{\frac{n-1}{2}}\left(\frac{\zeta_{i+1,j}^{t+1}+\zeta_{i-1,j}^{t+1}+\zeta_{i,j+1}^{t+1}+\zeta_{i,j-1}^{t+1}-4\zeta_{i,j}^{t+1}}{h^2}\right)+\frac{2m}{\rho}\frac{\partial A^{\frac{n-1}{2}}}{\partial x}\left(\frac{\zeta_{i+1,j}^{t+1}-\zeta_{i-1,j}^{t+1}}{2h}\right)\\&+\frac{2m}{\rho}\frac{\partial A^{\frac{n-1}{2}}}{\partial y}\left(\frac{\zeta_{i,j+1}^{t+1}-\zeta_{i,j-1}^{t+1}}{2h}\right)+\frac{m}{\rho}\left(\frac{\partial^2 A^{\frac{n-1}{2}}}{\partial x^2}-\frac{\partial^2 A^{\frac{n-1}{2}}}{\partial y^2}\right)\left(\frac{\psi_{i,j+1}^{t+1}+\psi_{i,j-1}^{t+1}-\psi_{i+1,j}^{t+1}-\psi_{i-1,j}^{t+1}}{h^2}\right)\\&-\frac{m}{\rho}\frac{\partial^2 A^{\frac{n-1}{2}}}{\partial x\partial y}\left(\frac{\psi_{i+1,j+1}^{t+1}+\psi_{i-1,j-1}^{t+1}-\psi_{i+1,j-1}^{t+1}-\psi_{i-1,j+1}^{t+1}}{4h^2}\right)\end{aligned}. \tag{3.136}$$

Rearranging Equation (3.136):

$$\zeta_{i,j}^{t} = \Delta t \left[\begin{array}{l} \left(\frac{\psi_{i,j+1}^{t+1} - \psi_{i,j-1}^{t+1}}{2h}\right)\left(\frac{\zeta_{i+1,j}^{t+1} - \zeta_{i-1,j}^{t+1}}{2h}\right) - \left(\frac{\psi_{i+1,j}^{t+1} - \psi_{i-1,j}^{t+1}}{2h}\right)\left(\frac{\zeta_{i,j+1}^{t+1} - \zeta_{i,j-1}^{t+1}}{2h}\right) \\ -\frac{m}{\rho} A^{\frac{n-1}{2}} \left(\frac{\zeta_{i+1,j}^{t+1} + \zeta_{i-1,j}^{t+1} + \zeta_{i,j+1}^{t+1} + \zeta_{i,j-1}^{t+1}}{h^2}\right) - \frac{2m}{\rho}\frac{\partial A^{\frac{n-1}{2}}}{\partial x}\left(\frac{\zeta_{i+1,j}^{t+1} - \zeta_{i-1,j}^{t+1}}{2h}\right) \\ -\frac{2m}{\rho}\frac{\partial A^{\frac{n-1}{2}}}{\partial y}\left(\frac{\zeta_{i,j+1}^{t+1} - \zeta_{i,j-1}^{t+1}}{2h}\right) - \frac{m}{\rho}\left(\frac{\partial^2 A^{\frac{n-1}{2}}}{\partial x^2} - \frac{\partial^2 A^{\frac{n-1}{2}}}{\partial y^2}\right)\left(\frac{\psi_{i,j+1}^{t+1} + \psi_{i,j-1}^{t+1} - \psi_{i+1,j}^{t+1} - \psi_{i-1,j}^{t+1}}{h^2}\right) \\ +\frac{m}{\rho}\frac{\partial^2 A^{\frac{n-1}{2}}}{\partial x \partial y}\left(\frac{\psi_{i+1,j+1}^{t+1} + \psi_{i-1,j-1}^{t+1} - \psi_{i+1,j-1}^{t+1} - \psi_{i-1,j+1}^{t+1}}{4h^2}\right) \end{array} \right], \quad (3.137)$$

$$+\left(1 + 4\frac{mA^{\frac{n-1}{2}}\Delta t}{\rho h}\right)\zeta_{i,j}^{t+1}$$

where:

$$A^{\frac{n-1}{2}} = \left[\begin{array}{l} \left(\frac{\psi_{i,j+1}^{t+1} + \psi_{i,j-1}^{t+1} - \psi_{i+1,j}^{t+1} - \psi_{i-1,j}^{t+1}}{h^2}\right)^2 \\ +\left(\frac{\psi_{i+1,j+1}^{t+1} + \psi_{i-1,j-1}^{t+1} - \psi_{i+1,j-1}^{t+1} - \psi_{i-1,j+1}^{t+1}}{2h^2}\right)^2 \end{array} \right]^{\frac{n-1}{2}}, \quad (3.138)$$

$$\frac{\partial A^{\frac{n-1}{2}}}{\partial x} = (n-1)A^{\frac{n-3}{2}} \left[\begin{array}{l} \left(\frac{\psi_{i,j+1}^{t+1} + \psi_{i,j-1}^{t+1} - \psi_{i+1,j}^{t+1} - \psi_{i-1,j}^{t+1}}{h^2}\right) \bullet \\ \left(\frac{\psi_{i+1,j+1}^{t+1} + \psi_{i+1,j-1}^{t+1} - \psi_{i-1,j+1}^{t+1} - \psi_{i-1,j-1}^{t+1} - \psi_{i+2,j}^{t+1} + \psi_{i-2,j}^{t+1}}{2h^3}\right) \\ +\left(\frac{\psi_{i+1,j+1}^{t+1} + \psi_{i-1,j-1}^{t+1} - \psi_{i+1,j-1}^{t+1} - \psi_{i-1,j+1}^{t+1}}{h^2}\right) \bullet \\ \left(\frac{\psi_{i+1,j+1}^{t+1} + \psi_{i-1,j+1}^{t+1} - 2\psi_{i,j+1}^{t+1} - \psi_{i+1,j-1}^{t+1} - \psi_{i-1,j-1}^{t+1} + 2\psi_{i,j-1}^{t+1}}{2h^3}\right) \end{array} \right], \quad (3.139)$$

Universiti Malaya

$$\frac{\partial A^{\frac{n-1}{2}}}{\partial y} = (n-1)A^{\frac{n-3}{2}} \left[\begin{array}{l} \left(\dfrac{\psi_{i,j+1}^{t+1} + \psi_{i,j-1}^{t+1} - \psi_{i+1,j}^{t+1} - \psi_{i-1,j}^{t+1}}{h^2} \right) \bullet \\ \left(\dfrac{\psi_{i,j+2}^{t+1} - \psi_{i,j-2}^{t+1} - \psi_{i+1,j+1}^{t+1} - \psi_{i,-1\,j+1}^{t+1} + \psi_{i+1,j-1}^{t+1} + \psi_{i-1,j-1}^{t+1}}{2h^3} \right) \\ + \left(\dfrac{\psi_{i+1,j+1}^{t+1} + \psi_{i-1,j-1}^{t+1} - \psi_{i+1,j-1}^{t+1} - \psi_{i-1,j+1}^{t+1}}{h^2} \right) \bullet \\ \left(\dfrac{\psi_{i+1,j+1}^{t+1} + \psi_{i+1,j-1}^{t+1} - 2\psi_{i+1,j}^{t+1} + 2\psi_{i-1,j}^{t+1} - \psi_{i-1,j+1}^{t+1} - \psi_{i-1,j-1}^{t+1}}{2h^3} \right) \end{array} \right], \tag{3.140}$$

Universiti Malaya

$$
\begin{aligned}
\frac{\partial^2 A^{\frac{n-1}{2}}}{\partial x^2} = (n-1)(n-3)A^{\frac{n-5}{2}} & \left[\begin{array}{l}
\left(\dfrac{\psi_{i,j+1}^{t+1} + \psi_{i,j-1}^{t+1} - \psi_{i+1,j}^{t+1} - \psi_{i-1,j}^{t+1}}{h^2} \right) \bullet \\
\left(\dfrac{\psi_{i-2,j}^{t+1} - \psi_{i+2,j}^{t+1} + \psi_{i+1,j+1}^{t+1} - \psi_{i-1,j+1}^{t+1} + \psi_{i+1,j-1}^{t+1} - \psi_{i-1,j-1}^{t+1}}{2h^3} \right) \\
+ \left(\dfrac{\psi_{i+1,j+1}^{t+1} - \psi_{i-1,j+1}^{t+1} - \psi_{i+1,j-1}^{t+1} + \psi_{i-1,j-1}^{t+1}}{h^2} \right) \bullet \\
\left(\dfrac{\psi_{i+1,j+1}^{t+1} + \psi_{i-1,j+1}^{t+1} - 2\psi_{i,j+1}^{t+1} - \psi_{i+1,j-1}^{t+1} - \psi_{i-1,j-1}^{t+1} + 2\psi_{i,j-1}^{t+1}}{2h^3} \right)
\end{array} \right]^2 \\
+ (n-1)A^{\frac{n-3}{2}} & \left[\begin{array}{l}
\left(\dfrac{\psi_{i+1,j+1}^{t+1} + \psi_{i+1,j-1}^{t+1} - \psi_{i-1,j+1}^{t+1} - \psi_{i-1,j-1}^{t+1} - \psi_{i+2,j}^{t+1} + \psi_{i-2,j}^{t+1}}{2h^3} \right)^2 \\
+ \left(\dfrac{\psi_{i,j+1}^{t+1} + \psi_{i,j-1}^{t+1} - \psi_{i+1,j}^{t+1} - \psi_{i-1,j}^{t+1}}{h^2} \right) \\
\bullet \left(\dfrac{\begin{array}{l} \psi_{i+1,j+1}^{t+1} + \psi_{i+1,j-1}^{t+1} + 2\psi_{i+1,j}^{t+1} + \psi_{i-1,j+1}^{t+1} + \psi_{i-1,j-1}^{t+1} + 2\psi_{i-1,j}^{t+1} - 2\psi_{i,j+1}^{t+1} \\ - 2\psi_{i,j-1}^{t+1} - 2\psi_{i,j}^{t+1} - \psi_{i+2,j}^{t+1} - \psi_{i-2,j}^{t+1} \end{array}}{h^4} \right) \\
+ \left(\dfrac{\psi_{i+1\,j+1}^{t+1} + \psi_{i-1,j+1}^{t+1} - 2\psi_{i,j+1}^{t+1} - \psi_{i+1,j-1}^{t+1} - \psi_{i-1,j-1}^{t+1} + 2\psi_{i,j-1}^{t+1}}{h^3} \right)^2 \\
+ \left(\dfrac{\psi_{i+1,j+1}^{t+1} + \psi_{i-1,j-1}^{t+1} - \psi_{i+1,j-1}^{t+1} - \psi_{i-1,j+1}^{t+1}}{h^2} \right) \\
\bullet \left(\dfrac{\begin{array}{l} \psi_{i+2,j+1}^{t+1} - 2\psi_{i+1,j+1}^{t+1} + 2\psi_{i-1,j+1}^{t+1} - \psi_{i-2,j+1}^{t+1} - \psi_{i+2,j-1}^{t+1} + 2\psi_{i+1,j-1}^{t+1} \\ - 2\psi_{i-1,j-1}^{t+1} + \psi_{i-2,j-1}^{t+1} \end{array}}{4h^4} \right)
\end{array} \right]^2
\end{aligned}
\quad , \quad (3.141)
$$

Universiti Malaya

$$
\begin{aligned}
\frac{\partial^2 A^{\frac{n-1}{2}}}{\partial y^2} = (n-1)(n-3)A^{\frac{n-5}{2}} & \left[\begin{array}{l}
\left(\dfrac{\psi_{i,j+1}^{t+1} + \psi_{i,j-1}^{t+1} - \psi_{i+1,j}^{t+1} - \psi_{i-1,j}^{t+1}}{h^2} \right) \bullet \\
\left(\dfrac{\psi_{i,j+2}^{t+1} - \psi_{i,j-2}^{t+1} + \psi_{i+1,j-1}^{t+1} + \psi_{i-1,j-1}^{t+1} - \psi_{i+1,j+1}^{t+1} - \psi_{i-1,j+1}^{t+1}}{2h^3} \right) \\
+ \left(\dfrac{\psi_{i+1,j+1}^{t+1} - \psi_{i-1,j+1}^{t+1} - \psi_{i+1,j-1}^{t+1} + \psi_{i-1,j-1}^{t+1}}{h^2} \right) \bullet \\
\left(\dfrac{\psi_{i+1,j+1}^{t+1} + \psi_{i+1,j-1}^{t+1} - 2\psi_{i+1,j}^{t+1} - \psi_{i-1,j+1}^{t+1} - \psi_{i-1,j-1}^{t+1} + 2\psi_{i-1,j}^{t+1}}{2h^3} \right)
\end{array} \right]^2 \\
+ (n-1)A^{\frac{n-3}{2}} & \left[\begin{array}{l}
\left(\dfrac{\psi_{i,j+2}^{t+1} - \psi_{i,j-2}^{t+1} - \psi_{i+1,j+1}^{t+1} - \psi_{i-1,j+1}^{t+1} + \psi_{i+1,j-1}^{t+1} + \psi_{i-1,j-1}^{t+1}}{2h^3} \right)^2 \\
+ \left(\dfrac{\psi_{i,j+1}^{t+1} + \psi_{i,j-1}^{t+1} - \psi_{i+1,j}^{t+1} - \psi_{i-1,j}^{t+1}}{h^2} \right) \\
\bullet \left(\dfrac{\begin{array}{l} \psi_{i,j+2}^{t+1} - 2\psi_{i,j+1}^{t+1} + 2\psi_{i,j}^{t+1} - 2\psi_{i,j-1}^{t+1} + \psi_{i,j-2}^{t+1} - \psi_{i+1,j+1}^{t+1} - \psi_{i+1,j-1}^{t+1} \\ + 2\psi_{i+1,j}^{t+1} - \psi_{i-1,j+1}^{t+1} - \psi_{i-1,j-1}^{t+1} - 2\psi_{i-1,j}^{t+1} \end{array}}{h^4} \right) \\
+ \left(\dfrac{\psi_{i+1\,j+1}^{t+1} + \psi_{i+1,j-1}^{t+1} - 2\psi_{i+1,j}^{t+1} + 2\psi_{i-1,j}^{t+1} - \psi_{i-1,j+1}^{t+1} - \psi_{i-1,j-1}^{t+1}}{h^3} \right)^2 \\
+ \left(\dfrac{\psi_{i+1,j+1}^{t+1} + \psi_{i-1,j-1}^{t+1} - \psi_{i+1,j-1}^{t+1} - \psi_{i-1,j+1}^{t+1}}{h^2} \right) \\
\bullet \left(\dfrac{\begin{array}{l} \psi_{i+1,j+2}^{t+1} - 2\psi_{i+1,j+1}^{t+1} + 2\psi_{i+1,j-1}^{t+1} - \psi_{i+1,j-2}^{t+1} - \psi_{i-1,j+2}^{t+1} + 2\psi_{i-1,j+1}^{t+1} \\ - 2\psi_{i-1,j-1}^{t+1} + \psi_{i-1,j-2}^{t+1} \end{array}}{4h^4} \right)
\end{array} \right]^2
\end{aligned}
\quad , \quad (3.142)
$$

Universiti Malaya

$$
\begin{aligned}
\frac{\partial^2 A^{\frac{n-1}{2}}}{\partial x \partial y} = (n-1)(n-3)A^{\frac{n-5}{2}} & \left[\begin{array}{l} \left(\dfrac{\psi_{i,j+1}^{t+1} + \psi_{i,j-1}^{t+1} - \psi_{i+1,j}^{t+1} - \psi_{i-1,j}^{t+1}}{h^2} \right) \\ \bullet \left(\dfrac{\psi_{i,j+2}^{t+1} - \psi_{i,j-2}^{t+1} - \psi_{i+1,j+1}^{t+1} - \psi_{i-1,j+1}^{t+1} + \psi_{i+1,j-1}^{t+1} + \psi_{i-1,j-1}^{t+1}}{2h^3} \right) \\ + \left(\dfrac{\psi_{i+1,j+1}^{t+1} - \psi_{i-1,j+1}^{t+1} - \psi_{i+1,j-1}^{t+1} + \psi_{i-1,j-1}^{t+1}}{h^2} \right) \bullet \\ \left(\dfrac{\psi_{i+1,j+1}^{t+1} + \psi_{i+1,j-1}^{t+1} - 2\psi_{i+1,j}^{t+1} - \psi_{i-1,j+1}^{t+1} - \psi_{i-1,j-1}^{t+1} + 2\psi_{i-1,j}^{t+1}}{2h^3} \right) \end{array} \right] \bullet \\
& \left[\begin{array}{l} \left(\dfrac{\psi_{i,j+1}^{t+1} + \psi_{i,j-1}^{t+1} - \psi_{i+1,j}^{t+1} - \psi_{i-1,j}^{t+1}}{h^2} \right) \left(\dfrac{\psi_{i+1,j+1}^{t+1} + \psi_{i+1,j-1}^{t+1} - \psi_{i-1,j+1}^{t+1} - \psi_{i-1,j-1}^{t+1} - \psi_{i+2,j}^{t+1} + \psi_{i-2,j}^{t+1}}{2h^3} \right) \\ + \left(\dfrac{\psi_{i+1,j+1}^{t+1} - \psi_{i-1,j+1}^{t+1} - \psi_{i+1,j-1}^{t+1} + \psi_{i-1,j-1}^{t+1}}{h^2} \right) \left(\dfrac{\psi_{i+1,j+1}^{t+1} + \psi_{i-1,j+1}^{t+1} - 2\psi_{i,j+1}^{t+1} - \psi_{i+1,j-1}^{t+1} - \psi_{i-1,j-1}^{t+1} + 2\psi_{i,j-1}^{t+1}}{2h^3} \right) \end{array} \right] \\
+ (n-1)A^{\frac{n-3}{2}} & \left[\begin{array}{l} \left(\dfrac{\psi_{i,j+2}^{t+1} - \psi_{i,j-2}^{t+1} - \psi_{i+1,j+1}^{t+1} - \psi_{i-1,j+1}^{t+1} + \psi_{i+1,j-1}^{t+1} + \psi_{i-1,j-1}^{t+1}}{2h^3} \right) \\ \bullet \left(\dfrac{\psi_{i+1,j+1}^{t+1} + \psi_{i+1,j-1}^{t+1} - \psi_{i-1,j+1}^{t+1} - \psi_{i-1,j-1}^{t+1} - \psi_{i+2,j}^{t+1} + \psi_{i-2,j}^{t+1}}{2h^3} \right) \\ + \left(\dfrac{\psi_{i,j+1}^{t+1} + \psi_{i,j-1}^{t+1} - \psi_{i+1,j}^{t+1} - \psi_{i-1,j}^{t+1}}{h^2} \right) \\ \bullet \left(\dfrac{\psi_{i+1,j+2}^{t+1} - \psi_{i+1,j-2}^{t+1} - \psi_{i-1,j+2}^{t+1} + \psi_{i-1,j-2}^{t+1} - \psi_{i+2,j+1}^{t+1} + \psi_{i-2,j+1}^{t+1} + \psi_{i+2,j-1}^{t+1} - \psi_{i-2,j-1}^{t+1}}{4h^4} \right) \\ + \left(\dfrac{\psi_{i+1,j+1}^{t+1} - \psi_{i-1,j+1}^{t+1} - \psi_{i+1,j-1}^{t+1} + \psi_{i-1,j-1}^{t+1}}{h^2} \right) \\ \bullet \left(\dfrac{\psi_{i+1,j+1}^{t+1} + \psi_{i+1,j-1}^{t+1} - 2\psi_{i+1,j}^{t+1} + \psi_{i-1,j+1}^{t+1} + \psi_{i-1,j-1}^{t+1} - 2\psi_{i-1,j}^{t+1} - 2\psi_{i,j+1}^{t+1} - 2\psi_{i,j-1}^{t+1} + 4\psi_{i,j}^{t+1}}{h^4} \right) \\ + \left(\dfrac{\psi_{i+1,j+1}^{t+1} + \psi_{i+1,j-1}^{t+1} - 2\psi_{i+1,j}^{t+1} + 2\psi_{i-1,j}^{t+1} - \psi_{i-1,j+1}^{t+1} - \psi_{i-1,j-1}^{t+1}}{h^3} \right) \\ \bullet \left(\dfrac{\psi_{i+1,j+1}^{t+1} + \psi_{i-1,j+1}^{t+1} - 2\psi_{i,j+1}^{t+1} - \psi_{i+1,j-1}^{t+1} - \psi_{i-1,j-1}^{t+1} + 2\psi_{i,j-1}^{t+1}}{h^3} \right) \end{array} \right] . \qquad (3.143)
\end{aligned}
$$

Rearranging Equation (3.137) in matrix form:

Universiti Malaya

For the 1st column,

$$\begin{pmatrix} \zeta_{1,1}^{t} \\ \zeta_{1,2}^{t} \\ \zeta_{1,3}^{t} \\ \zeta_{1,ny-1}^{t} \\ \zeta_{1,ny}^{t} \end{pmatrix} = \begin{pmatrix} A_{1,1}^{1} & A_{2,1}^{1} & A_{3,1}^{1} & A_{nx-1,1}^{1} & A_{nx,1}^{1} \\ A_{1,2}^{1} & A_{2,2}^{1} & A_{3,2}^{1} & A_{nx-1,2}^{1} & A_{nx,2}^{1} \\ A_{1,3}^{1} & A_{2,3}^{1} & A_{3,3}^{1} & A_{nx-1,3}^{1} & A_{nx,3}^{1} \\ A_{1,ny-1}^{1} & A_{2,ny-1}^{1} & A_{3,ny-1}^{1} & A_{nx-1,ny-1}^{1} & A_{nx,ny-1}^{1} \\ A_{1,ny}^{1} & A_{2,ny}^{1} & A_{3,ny}^{1} & A_{nx-1,ny}^{1} & A_{nx,ny}^{1} \end{pmatrix} \bullet \begin{pmatrix} \zeta_{1,1}^{t+1} \\ \zeta_{1,2}^{t+1} \\ \zeta_{1,3}^{t+1} \\ \zeta_{1,ny-1}^{t+1} \\ \zeta_{1,ny}^{t+1} \end{pmatrix}. \tag{3.144}$$

For the 2nd column,

$$\begin{pmatrix} \zeta_{2,1}^{t} \\ \zeta_{2,2}^{t} \\ \zeta_{2,3}^{t} \\ \zeta_{2,ny-1}^{t} \\ \zeta_{2,ny}^{t} \end{pmatrix} = \begin{pmatrix} A_{1,1}^{2} & A_{2,1}^{2} & A_{3,1}^{2} & A_{nx-1,1}^{2} & A_{nx,1}^{2} \\ A_{1,2}^{2} & A_{2,2}^{2} & A_{3,2}^{2} & A_{nx-1,2}^{2} & A_{nx,2}^{2} \\ A_{1,3}^{2} & A_{2,3}^{2} & A_{3,3}^{2} & A_{nx-1,3}^{2} & A_{nx,3}^{2} \\ A_{1,ny-1}^{2} & A_{2,ny-1}^{2} & A_{3,ny-1}^{2} & A_{nx-1,ny-1}^{2} & A_{nx,ny-1}^{2} \\ A_{1,ny}^{2} & A_{2,ny}^{2} & A_{3,ny}^{2} & A_{nx-1,ny}^{2} & A_{nx,ny}^{2} \end{pmatrix} \bullet \begin{pmatrix} \zeta_{2,1}^{t+1} \\ \zeta_{2,2}^{t+1} \\ \zeta_{2,3}^{t+1} \\ \zeta_{2,ny-1}^{t+1} \\ \zeta_{2,ny}^{t+1} \end{pmatrix}. \tag{3.145}$$

For the x-th column,

$$\begin{pmatrix} \zeta_{x,1}^{t} \\ \zeta_{x,2}^{t} \\ \zeta_{x,3}^{t} \\ \zeta_{x,ny-1}^{t} \\ \zeta_{x,ny}^{t} \end{pmatrix} = \begin{pmatrix} A_{1,1}^{x} & A_{2,1}^{x} & A_{3,1}^{x} & A_{nx-1,1}^{x} & A_{nx,1}^{x} \\ A_{1,2}^{x} & A_{2,2}^{x} & A_{3,2}^{x} & A_{nx-1,2}^{x} & A_{nx,2}^{x} \\ A_{1,3}^{x} & A_{2,3}^{x} & A_{3,3}^{x} & A_{nx-1,3}^{x} & A_{nx,3}^{x} \\ A_{1,ny-1}^{x} & A_{2,ny-1}^{x} & A_{3,ny-1}^{x} & A_{nx-1,ny-1}^{x} & A_{nx,ny-1}^{x} \\ A_{1,ny}^{x} & A_{2,ny}^{x} & A_{3,ny}^{x} & A_{nx-1,ny}^{x} & A_{nx,ny}^{x} \end{pmatrix} \bullet \begin{pmatrix} \zeta_{2,1}^{t+1} \\ \zeta_{2,2}^{t+1} \\ \zeta_{2,3}^{t+1} \\ \zeta_{2,ny-1}^{t+1} \\ \zeta_{2,ny}^{t+1} \end{pmatrix}. \tag{3.146}$$

Equation (3.144) till Equation (3.146) must be combined and solved simutanetously, such thart:

$$\zeta_{i,j}^{t} = A_{i,j}^{n} \bullet \zeta_{i,j}^{t+1}, \tag{3.147}$$

$$\zeta_{i,j}^{t+1} = \left(A_{i,j}^{n}\right)^{-1} \bullet \zeta_{i,j}^{t}$$

where $\zeta_{i,j}^{t}$ is a two-dimensional matrix of vorticity at current step time, $\zeta_{i,j}^{t+1}$ is a two-dimensional matrix of vorticity at new step time and $A_{i,j}^{n}$ is a three-dimensional matrix of stream function dependent material property.

However, Equation (3.137) consists of too many unknowns and it is not easy to form the three-dimensional matirx of stream function dependent matrial property.

3.9 Boundary Layer Model (Non-Newtonian Model)

The governing fluid flow equation that is used in lid-driven model can be reduced and used in boundary layer model by considering the boundary layer model for power law and considering Equation (3.103) for *x*-momentum equation:

$$\rho g_x - \frac{\partial p}{\partial x} - mA^{\frac{n-1}{2}}\left(\frac{\partial^2 u}{\partial x^2} + \frac{\partial^2 u}{\partial y^2}\right) - 2m\frac{\partial u}{\partial x}\frac{\partial}{\partial x}\left(A^{\frac{n-1}{2}}\right)$$
$$- m\frac{\partial}{\partial y}\left(A^{\frac{n-1}{2}}\right)\left(\frac{\partial u}{\partial y} + \frac{\partial v}{\partial x}\right) = \rho\left[\frac{\partial u}{\partial t} + u\frac{\partial u}{\partial x} + v\frac{\partial u}{\partial y}\right].$$

From Figure 3.11, there is only $\frac{\partial u}{\partial y}$ exists in boundary layer model and the rate of shearing strain is:

$$\dot{\gamma} = \begin{pmatrix} \dot{\gamma}_{xx} & \dot{\gamma}_{yx} \\ \dot{\gamma}_{xy} & \dot{\gamma}_{yy} \end{pmatrix} = \begin{pmatrix} 0 & \frac{\partial u}{\partial y} \\ \frac{\partial u}{\partial y} & 0 \end{pmatrix}. \tag{3.148}$$

From Equation (3.91),

$$A = \left(\frac{\partial u}{\partial y}\right)^2 . \tag{3.149}$$

From Equation (3.96), the total momentum flux tensor, π_{xx} and π_{yy} are equal to zero. Thus, pressure, p is equal to zero. For steady-state and without considering the gravitational force, Equation (3.103) will become:

$$-mA^{\frac{n-1}{2}}\left(\frac{\partial^2 u}{\partial y^2}\right) - m\frac{\partial}{\partial y}\left(A^{\frac{n-1}{2}}\right)\left(\frac{\partial u}{\partial y}\right) = \rho\left[u\frac{\partial u}{\partial x} + v\frac{\partial u}{\partial y}\right]. \tag{3.150}$$

Rearranging Equation (3.150):

$$u\frac{\partial u}{\partial x} + v\frac{\partial u}{\partial y} = -\frac{m}{\rho}A^{\frac{n-1}{2}}\left(\frac{\partial^2 u}{\partial y^2}\right) - \frac{m}{\rho}\frac{\partial}{\partial y}\left(A^{\frac{n-1}{2}}\right)\left(\frac{\partial u}{\partial y}\right). \tag{3.151}$$

Substituting Equation (3.149) into Equation (3.151) yields:

$$u\frac{\partial u}{\partial x} + v\frac{\partial u}{\partial y} = -\frac{m}{\rho}\left(\frac{\partial u}{\partial y}\right)^{2\times\frac{n-1}{2}}\left(\frac{\partial^2 u}{\partial y^2}\right) - \frac{m}{\rho}\frac{\partial}{\partial y}\left[\left(\frac{\partial u}{\partial y}\right)^{2\times\frac{n-1}{2}}\right]\left(\frac{\partial u}{\partial y}\right),$$

$$= -\left[\frac{m}{\rho}\left(\frac{\partial u}{\partial y}\right)^{n-1}\left(\frac{\partial^2 u}{\partial y^2}\right) + \frac{m}{\rho}\frac{\partial}{\partial y}\left(\frac{\partial u}{\partial y}\right)^{n-1}\left(\frac{\partial u}{\partial y}\right)\right],$$

$$= -\frac{m}{\rho}\left[\left(\frac{\partial u}{\partial y}\right)^{n-1}\left(\frac{\partial^2 u}{\partial y^2}\right) + \frac{\partial}{\partial y}\left(\frac{\partial u}{\partial y}\right)^{n-1}\left(\frac{\partial u}{\partial y}\right)\right],$$

$$= -\frac{m}{\rho}\left[\left(\frac{\partial u}{\partial y}\right)^{n-1}\frac{\partial}{\partial y}\left(\frac{\partial u}{\partial y}\right) + \frac{\partial}{\partial y}\left(\frac{\partial u}{\partial y}\right)^{n-1}\left(\frac{\partial u}{\partial y}\right)\right]. \tag{3.152}$$

Universiti Malaya

By using this calculus formula,

$$a \bullet b' + a' \bullet b = (a \bullet b)' \quad , \tag{3.153}$$

$$u\frac{\partial u}{\partial x} + v\frac{\partial u}{\partial y} = -\frac{m}{\rho}\left[\frac{\partial}{\partial y}\left(\frac{\partial u}{\partial y}\right)^{n}\right]. \tag{3.154}$$

Equation (3.154) was proposed (Jalil et al., 2013) to solve the boundary layer flow of power-law fluid over a stretching surface. The similar method can be used to derive lid-driven model for Sisko nanofluid and reduce the governing equation to boundary layer for Sisko nanofluid easily. The stress tensor for Sisko nanofluid (Hayat et al., 2017) is given by:

$$\tau = \left[a + b\left(\frac{1}{2}\dot{\gamma} : \dot{\gamma}\right)^{\frac{n-1}{2}}\right]\dot{\gamma}, \tag{3.155}$$

where a and b are constants, n is power law index, $\dot{\gamma}$ is rate of shearing strain and $\dot{\gamma} : \dot{\gamma}$ is magnitude of the rate-of-strain tensor.

3.10 Programming on Lid-driven Model

With reference to the methodology flow chart as shown in Figure 3.1, this part describes the programming part. Then all the involved equations will be written as a source code in Matlab® and a GUI has been designed to facilitate the analysis of 2D NSEs for Newtonian fluid flow. Figure 3.23 shows the computer programming steps in solving the FDE strategy.

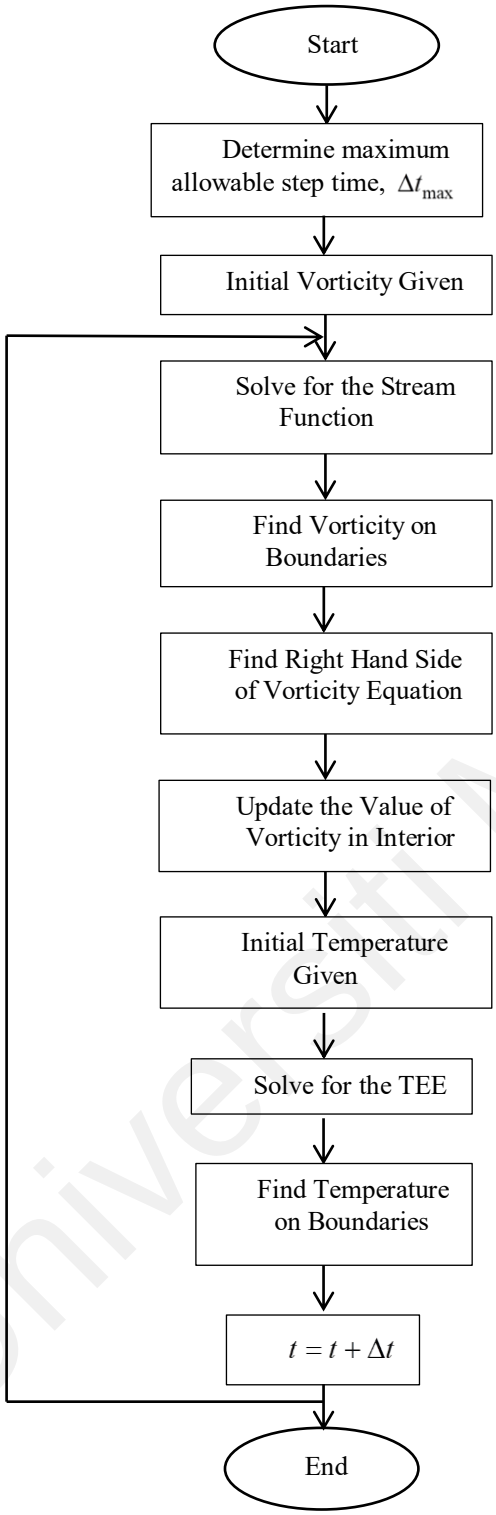

Figure 3.23: Computational solution strategy

Universiti Malaya

First of all, the maximum allowable step time, $\Delta t_{\max}$ is determined using Equation (3.82) or Equation (3.83). All the values of vorticity and stream function are set to zero at the beginning before the external force is imposed, thus velocity at the top moving boundary is zero at the beginning. Secondly, the stream function value at each of the nodes is computed using Equation (3.24) where the Poisson equation has been converted into a FDE. Equation (3.24) is solved at each of the nodes until the iteration converges. It can either be solved using Gauss-Seidel iteration method or Successive Over-Relaxation method (SOR method). If solving using SOR method, the accelerating factor should be taken between 1 and 2 (Dass, 1988).

Then is it followed by calculating the vorticity on four boundaries using Equation (3.32) till Equation (3.36). For free-slip BCs, Equation (3.39) till Equation (3.42) are utilized instead of Equation (3.32), Equation (3.35) and Equation (3.36). All these values of stream function and vorticity at the four boundaries are used to compute the Equation (3.21). Finally, all the values of vorticity at the interior are updated. This is followed by calculating the temperature at each of the nodes using Equation (3.47). Subsequently, temperatures at four boundaries are evaluated via Equation (3.49) till Equation (3.56) for Neumann BC while Equation (3.57) till Equation (3.64) are used for Robin BC. Consequently, all the calculations are done in current step time and continued for the next step time. Steady-state period can be found by setting the criterion (Moshkin & Poochinapan, 2010) as below once it is satisfied:

$$\frac{\max\left|\psi_{i,j}^{t+1}-\psi_{i,j}^{t}\right|}{\max\left|\psi_{i,j}^{t+1}\right|}\leq 10^{-8}. \tag{3.156}$$

3.11 Graphical User Interface (GUI)

Figure 3.24 shows the completed GUI which used for Newtonian fluid flow analysis only. The GUI built with multiple of buttons and columns to let the user to key-in the data. It facilitates the user to study the fluid flow distribution throughout the lid-driven cavity and to obtain the readings from the two-dimensional fluid flow profile. This GUI is consisted of three panels, four axes, seven buttons, ten columns and one radio button. However, there are two buttons remain disabled which means user cannot key-in any data into these columns. Once user has keyed-in the material properties and geometric properties of cavity lid-driven, only then these two columns are enabled. These four axes are consisted of stream function distribution, *u*-velocity distribution, *v*-velocity distribution and velocity vector distribution. From Equation (3.11) and Equation (3.12), their FDEs are:

$$u_{i,j} = \frac{\psi_{i,j+1} - \psi_{i,j-1}}{2h}, \tag{3.157}$$

$$v_{i,j} = -\frac{\psi_{i+1,j} - \psi_{i-1,j}}{2h}. \tag{3.158}$$

Velocity vector is given by:

$$V = \sqrt{u_{i,j}^2 + v_{i,j}^2}. \tag{3.159}$$

Direction of velocity vector, V is given by:

$$\theta = \tan^{-1}\left(\frac{v_{i,j}}{u_{i,j}}\right). \tag{3.160}$$

Universiti Malaya

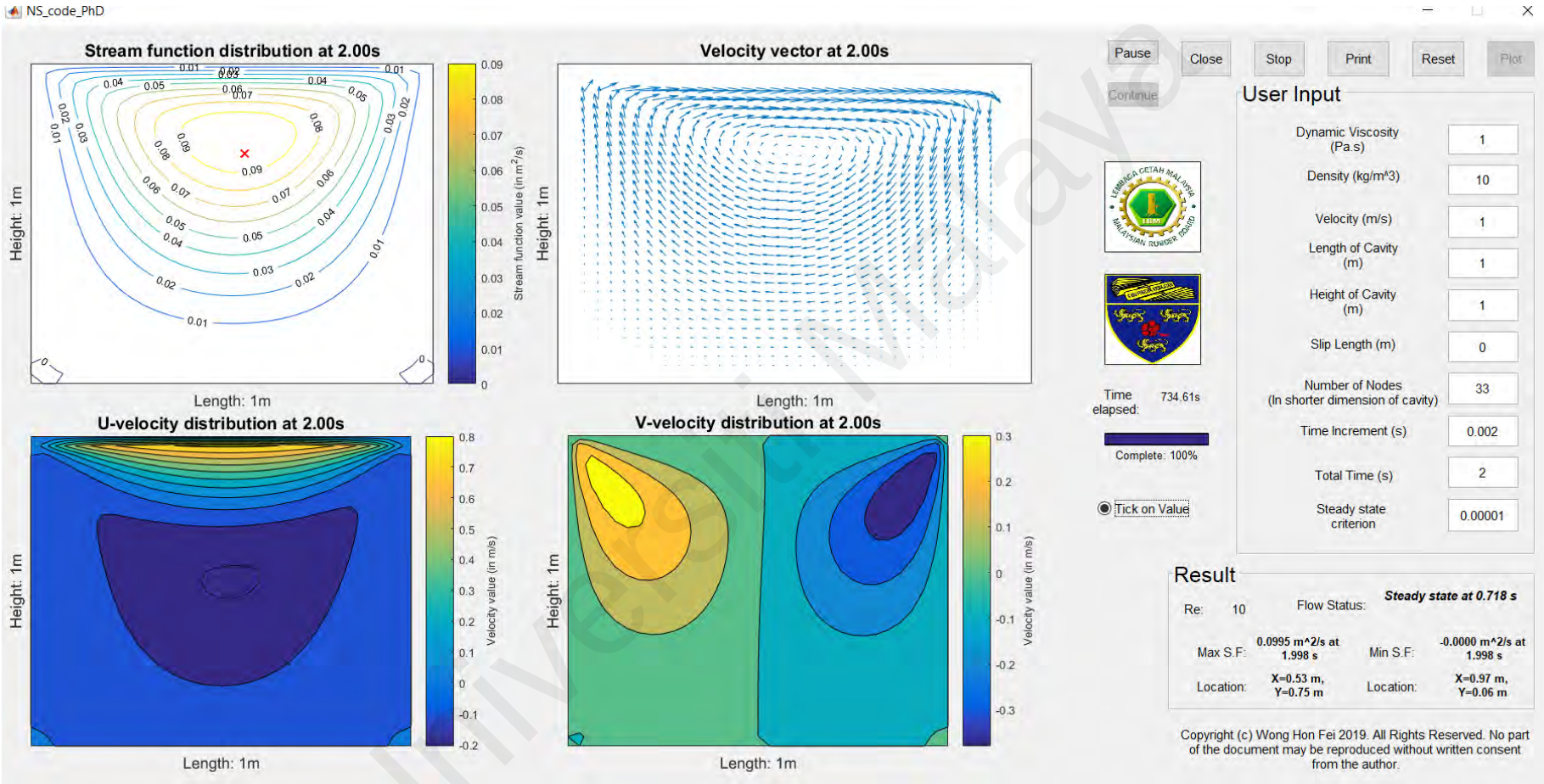

Figure 3.24: GUI

This GUI is consisted of three panels, four axes, seven buttons, one radio button. The panels are denoted as:

a) User input

b) Result

c) Time elapsed and percentage of analysis completed

Those four axes are consisted of:

a) Stream function distribution (contour plot)

b) Velocity vector distribution (vector plot)

c) u-velocity distribution (contour plot)

d) v-velocity distribution (contour plot)

Those seven buttons are consisted of:

a) Plot: Execute the analysis

b) Reset: Restart or reset all the columns and axes

c) Print: Print the whole layout

d) Stop: Abort or terminate the analysis

e) Close: Shut down the system/ interface

f) Pause: On hold the analysis

g) Continue: Resume back the analysis

Universiti Malaya

A radio button is used to request and to display the numeric data on those contour plots in stream function distribution. There are ten columns inside the user input panel. Initially the „time increment" and „total time" columns inside the user input panel remain status „disabled" which means it doesn't allow the user to key-in any data inside these columns. Figure 3.25 shows the user input panel.

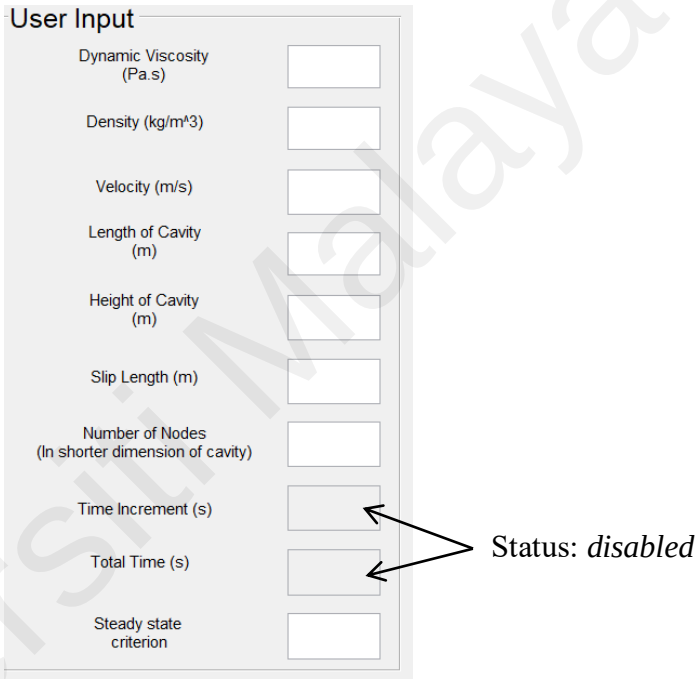

Figure 3.25: Input panel

User input panel is consisted of ten user input columns:

a) Dynamic viscosity (in unit *Pa.s*): Material property of cavity fluid

b) Density (in unit kg/m^3): Material property of cavity fluid

c) Velocity (in unit *m/s*): Velocity of the applied force at the top of lid-driven

d) Length of cavity (in unit *m*): Length of the cavity

e) Height of cavity (in unit *m*): Height of the cavity

f) Slip length (in unit *m*): Free length value if those stationary walls are pretty smooth. For no-slip BC, its value is zero.

g) Number of nodes: Number of nodes required to perform the calculation and results

h) Time increment (in unit *s*): The maximum allowable step time to run the analysis until the whole iteration is done.

i) Total time (in unit *s*): Total iteration period.

j) Steady-state criterion: The maximum steady-state criterion in is 10^{-5}.

All the data entries should be in SI unit. After the user has keyed-in these five columns (dynamics viscosity, density, length of cavity, height of cavity and number of nodes) above the „time increment" and „total time" columns, the „time increment" and „total time" columns will be switched to status „enabled" which means user is allowed to assign some values in these columns. The reason is because from Equation (3.22) where $\Delta t \leq \frac{h^2}{4\upsilon}$, and it is to make sure the user or to enforce the user to key-in a value of time increment based on the stated criteria. „Velocity" and „slip length" are not usable in Equation (3.22), thus user can key-in „time increment" with or without assigning any value to „velocity" and „slip length". After the user has keyed-in all the values inside the columns in the user input panel, user can tick on the radio button of „tick on value". So that all the numeric data can be displayed on all the axes after the analysis had been executed. User may turn off all the displayed numeric data in all the axes by ticking off the radio button.

This panel allows the user to key-in the material properties of the fluid, velocity of exerted force, dimension of the cavity, desired of number of nodes, time increment, total time of the simulation, steady-state criterion, slip length (in unit m). The unit of dynamic viscosity is in unit $Pa.s$ and density is in unit kg/m^3. The exerted velocity is in unit m/s. Since all the material properties are scalar quantites, thus this panel doesn't allow any negative and zero value. An error dialog box will pop-up to indicate that a negative or zero value of input data has been entered. This dialog box requests the user to re-enter an input which is in positive value. In the meanwhile, the word "Invalid" will appear inside the column which means that this current value is not accepted in this arithmetic calculation. If the user has entered a non-numeric input or empty input accidently, an error dialog box will pop-up as well to tell the user that an invalid input has been entered. Figure 3.26 and Figure 3.27 show the error message.

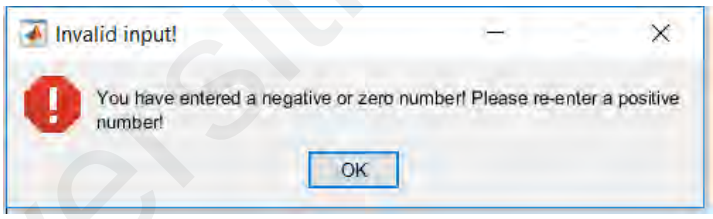

Figure 3.26: Error message of negative numeric data has been entered

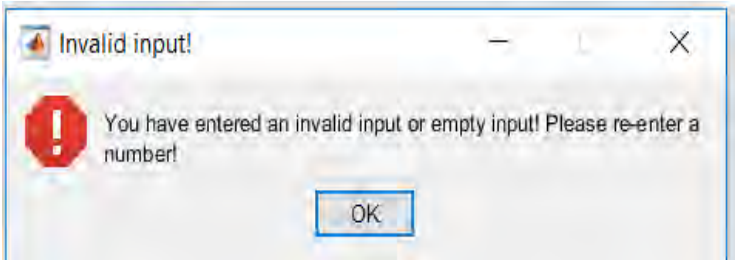

Figure 3.27: Error message of invalid or empty input has been entered

This panel also allows the user to enter the dimension of the cavity flow. Similarly, this panel doesn‟t allow any non-numeric input and non-positive input. Moreover, this panel offers more constraints if compare with material properties‟ panel. The schematic drawing of the finite difference nodes is shown in Figure 3.28:

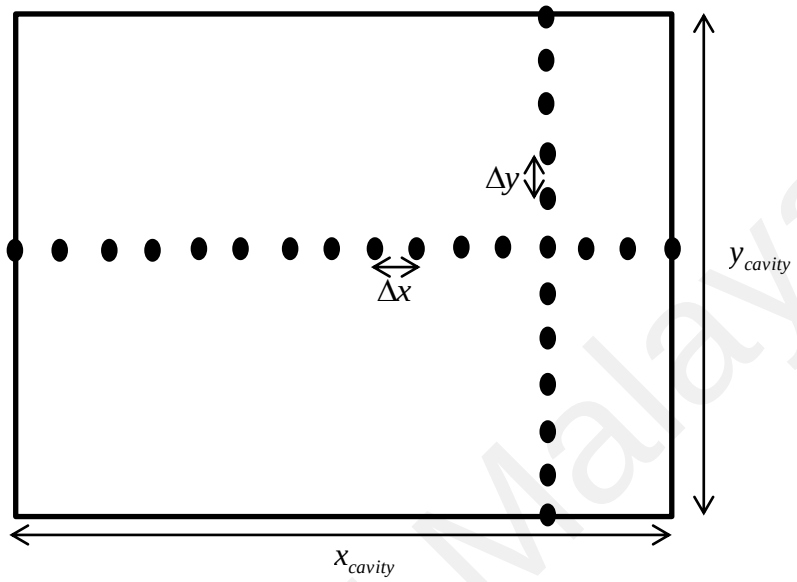

Figure 3.28: **Schematic drawing of nodes**

Typically, the finite difference nodes have been used to represent the drawing of the rectangular cavity flow. There are two inputs requested from the user such as length of cavity (x_{cavity}) and height of cavity (y_{cavity}). Step size, Δx is calculated based on the value of number of nodes, length of cavity and height of cavity. After the required data has been entered into this panel, the column of number of nodes is only revealed after the dimension of cavity has been entered correctly as shown in Figure 3.29:

Universiti Malaya

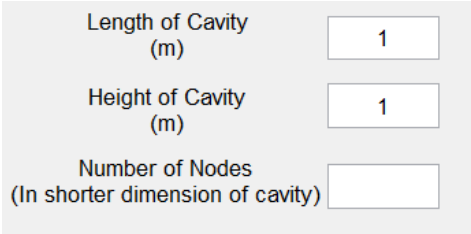

Figure 3.29: **Allow for data entry in number of nodes' column**

In order to guarantee an accurate result, this GUI will tell the user to enter the minimum number of nodes for this calculation"s algorithm. The figure below shows the pop-up warning dialog box when the user has entered a value in the number of nodes" column if the value is less than the calculated minimum value for this particular model. Figure 3.30 shows the warning message.

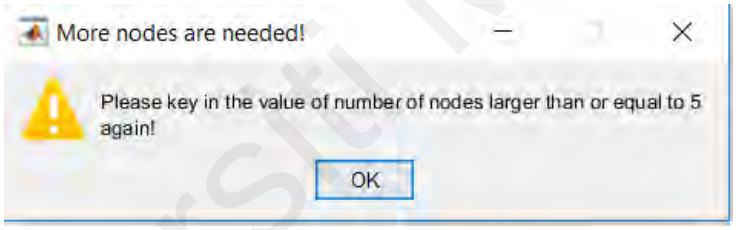

Figure 3.30: Minimum value of number of nodes

Moreover, the data entry for number of nodes should be in integral form. Any non-integral numeric input will cause another error dialog box to pop-up as shown in Figure 3.31:

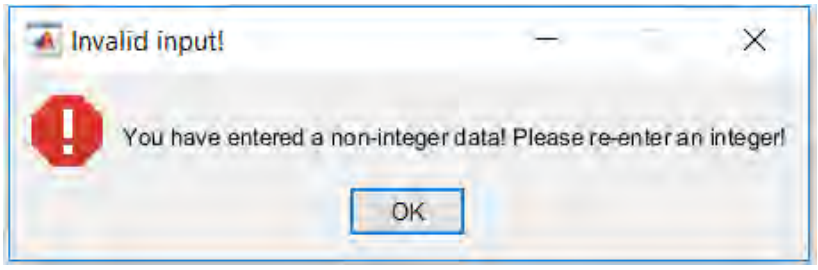

Figure 3.31: **Error dialog box (non-integer input)**

GUI will calculate the value for Δx and Δy and they will share the same value to simplify the calculation as shown in Equation (3.21). The same value of Δx and Δy has greatly simplified those FDEs discussed in Chapter 3 and made the algorithm easier. However, this will create some error as the calculated number of nodes will be used to represent the actual dimensions. The percentage error of representation of dimension by using number of nodes is given by equation below:

$$\%error_of_\max(x_{cavity}, y_{cavity}) = \frac{\max(x_{cavity}, y_{cavity}) - round\left[\frac{\max(x_{cavity}, y_{cavity})}{\Delta x}\right] \times \Delta x}{\max(x_{cavity}, y_{cavity})} \times 100\%, \quad (3.161)$$

where $\Delta x = \dfrac{\min(x_{cavity}, y_{cavity})}{nodes + 1}$. (3.162)

Note: $\max(x_{cavity}, y_{cavity})$ means the biggest element taken from x_{cavity} or y_{cavity}, $\min(x_{cavity}, y_{cavity})$ means the opposite of $\max(x_{cavity}, y_{cavity})$, $round\left[\dfrac{\max(x_{cavity}, y_{cavity})}{\Delta x}\right]$ means round the element inside it to the nearest integer.

Based on Equation (3.162), the larger the value of nodes will decrease the value of Δx. Thus, it will eventually reduce the percentage of error in $\max(x_{cavity}, y_{cavity})$ unless the division between $\max(x_{cavity}, y_{cavity})$ and Δx is an integer number, thus there will be no percentage of error. However, the larger the value of number of nodes will lead to a bigger computation time and effort. Note that the chosen number of nodes is as minimum as possible as allowed by this GUI.

Universiti Malaya

Time panel is the last data entry"s panel in this GUI. This panel is only enabled for data entry after the corrected inputs have been entered in these five columns above it as mentioned earlier. Figure 3.32 shows the sequence for data entry in these panels.

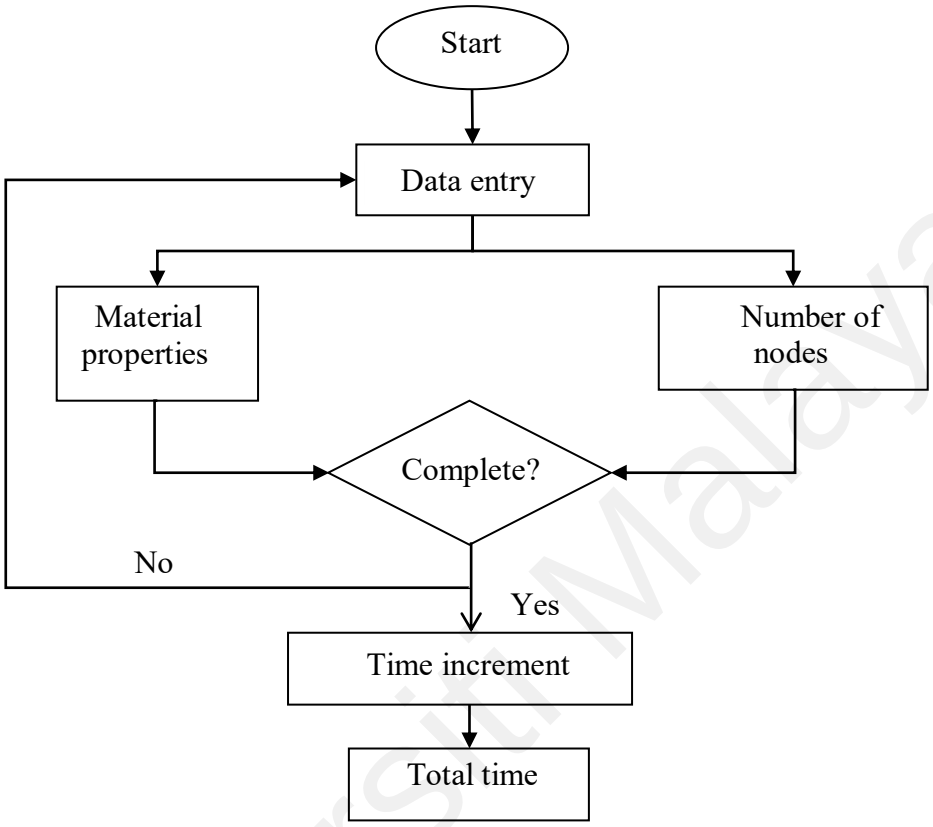

Figure 3.32: Sequence of data entry

The user can only enter data in this panel because the algorithm for „time increment" depends on the three parameters as shown in Equation (3.22). However, the value of exerted velocity and slip length are not needed in determining the maximum „time increment". If the entered „time increment" is bigger than the maximum calculated „time increment" based on Equation (3.22), the warning dialog box as shown in Figure 3.33 will appear and it will indicate the maximum value for the „time increment".

Universiti Malaya

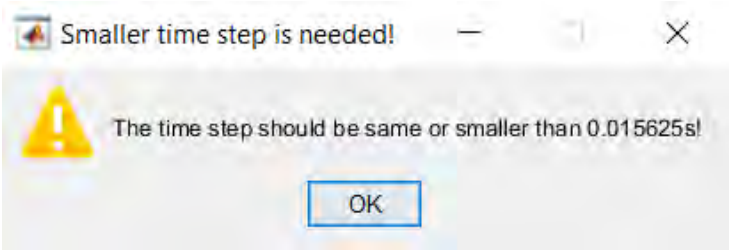

Figure 3.33: Warning dialog box (maximum time increment)

However, the column for „total time" is still disabled. It can only become enable after the correct (positive numeric data and not greater than the threshold value) data has been entered in the time increment"s column. After the value for „time increment" has been assigned with the correct data, the column of „total time" can only accept the positive number with multiple of „time increment". Any other value of „total time" which is not the multiple of „time increment", the warning dialog box will pop-up as shown in Figure 3.34:

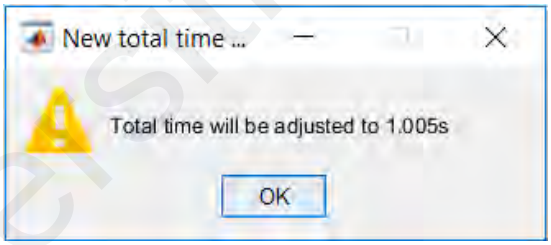

Figure 3.34: Warning dialog box (adjusted total time)

After all the required data have been entered, the push button can be pressed to execute the algorithm. The flowchart in Figure 3.35 shows the sequence on when the push button can be pressed:

Universiti Malaya

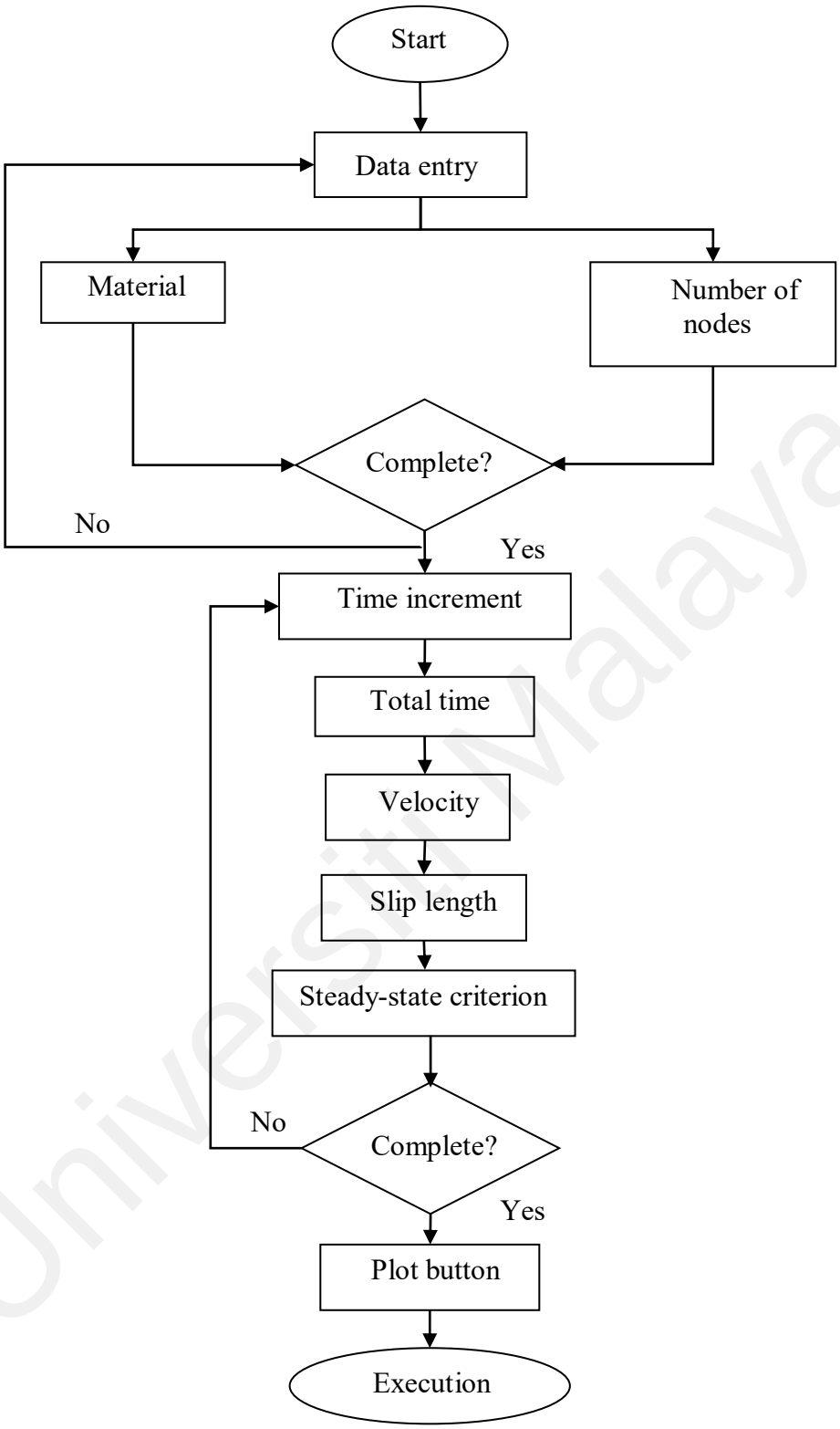

Figure 3.35: Sequence to push button

Universiti Malaya

If the push button is pressed when there is no enough inputs, an error dialog box will come out to warn the user that there is no enough inputs in order to execute the algorithm as shown in Figure 3.36.

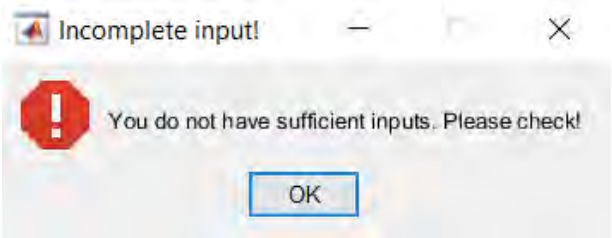

Figure 3.36: Error dialog box (plot button)

Besides, the result panel will also show a message and show the flow status as „insufficient input" as shown in Figure 3.37.

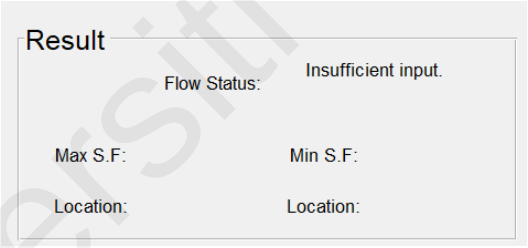

Figure 3.37: Flow status as insufficient input

After the user has keyed-in all the required and corrected input, the result panel will also show a message and show the flow status as „ready to flow" as shown in Figure 3.38.

Universiti Malaya

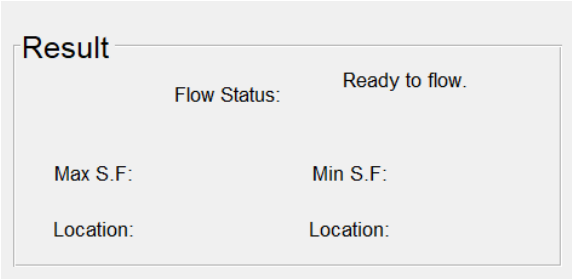

Figure 3.38: Flow status: Ready to flow

In this case, user can proceed to click the „plot" button to run the execution, while „continue" button remains disabled. The plot button is shown as Figure 3.39.

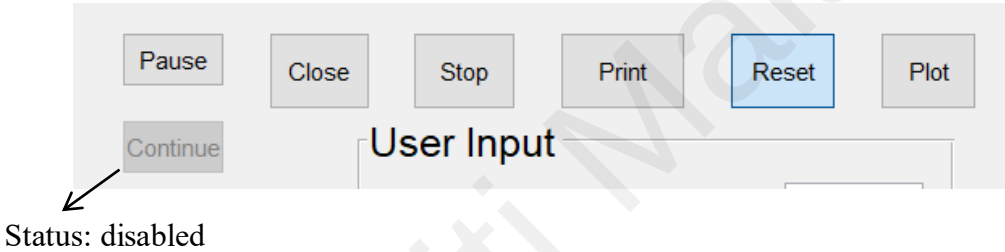

Figure 3.39: Plot button

During the program is being executed, user can click "tick on value" on this GUI so that the value of stream function (in unit m^2/s) can be shown on the contour plot. „Tick on value" function is shown in Figure 3.40.

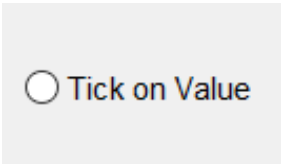

Figure 3.40: Radio button

Universiti Malaya

The „pause" button is to hold the simulation for certain period according to user requirement. Then user can click on „continue" to carry on the simulation. Figure 3.41 shows the contour plot of stream function distribution after the „tick on value" function is activated.

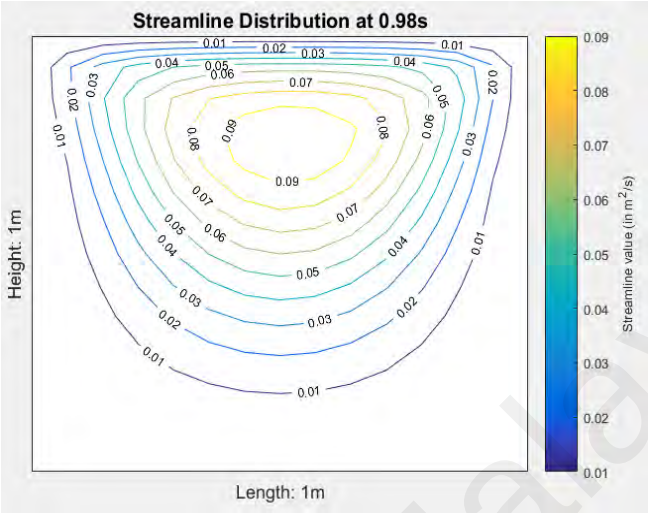

Figure 3.41: Contour plot of stream function distribution

Figure 3.42 shows the contour plot of *u*- and *v*-velocity distributions which plotted based on Equation (3.157) and Equation (3.158).

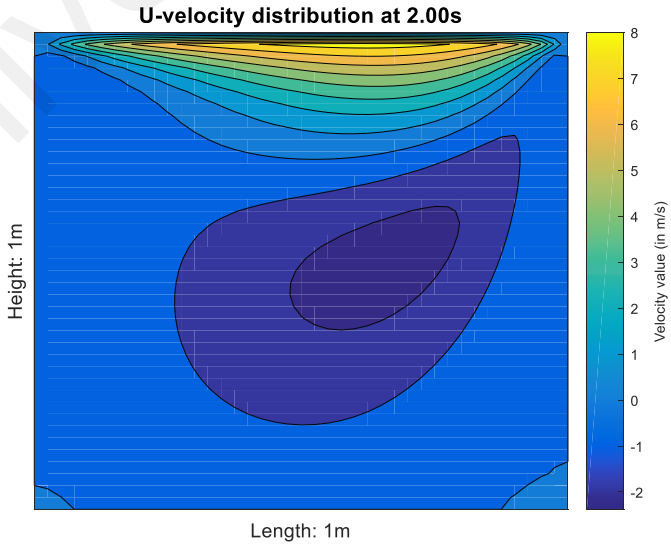

(a)

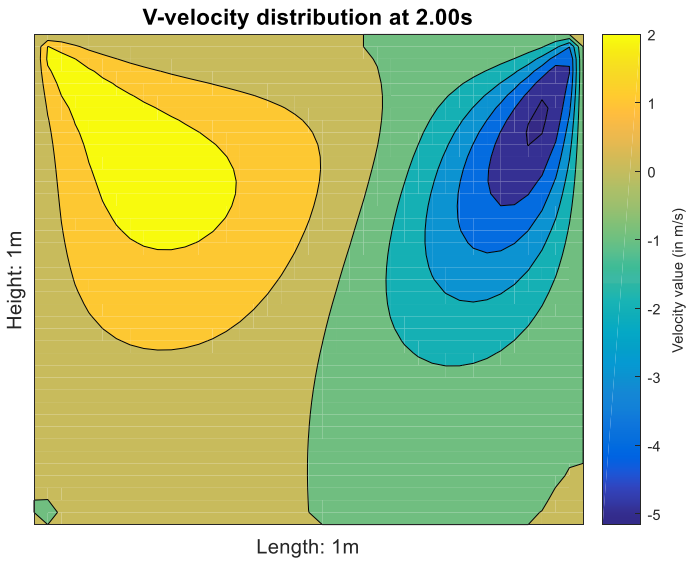

(b)

Figure 3.42: Contour plot of (a) *u*- and (b) *v*-velocity distribution

Figure 3.43 show the plot of velocity vector which plotted based on Equation (3.159) and Equation (3.160).

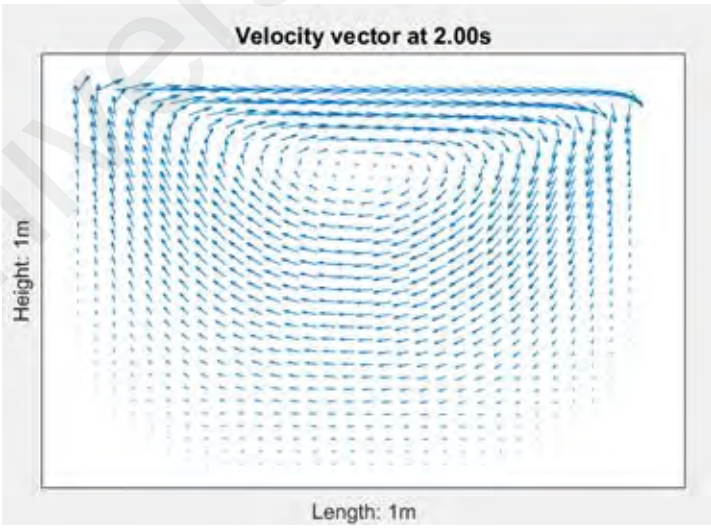

Figure 3.43: Velocity vector distribution

Universiti Malaya

Along the execution, the percentage of completion and time elapsed along the simulation are shown in the GUI as in Figure 3.44. So user would have some ideas on how long the time will be taken to accomplish a certain execution.

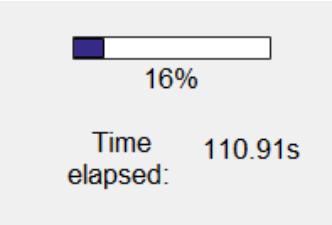

Figure 3.44: Computational time and percentage of completion

During the execution is running, the flow status will show „*Flowing...*". It means steady flow is yet to achieve as shown in Figure 3.45.

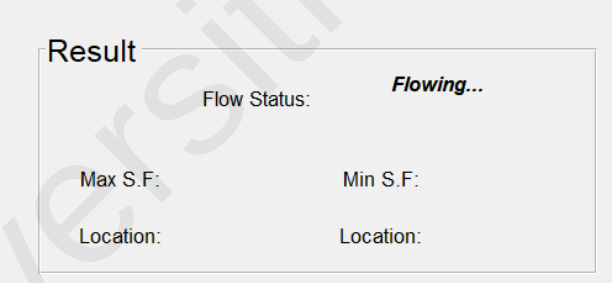

Figure 3.45: Simulation is running

After the execution is done, user can study the results as shown in result"s panel in Figure 3.46. This GUI can tell when steady state will take place, the location of maximum stream function value and when it happens.

Universiti Malaya

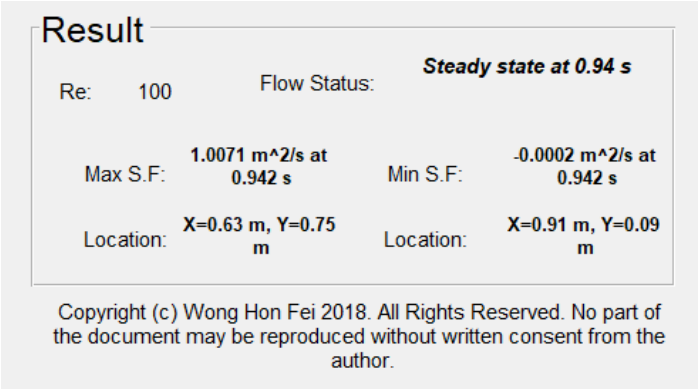

Figure 3.46: Result panel

3.12 Comparison with FEA Result

FEA is a computer-based simulation technique utilizing FEM that has been widely used in industries and elsewhere. Its most common use is for simulating the behavior of engineering components under external load. Such simulations are used to optimize the design geometry and thus reduce the requirement for prototype manufacture and testing. Standard engineering simulation software e.g. Ansys Fluent® can be used to model thermo fluid problem. The obtained transient history can be used to evaluate the performance of certain engineering applications.

In this project, a square model of lid-driven cavity fluid is simulated. The finite element model is shown in Figure 3.47:

Universiti Malaya

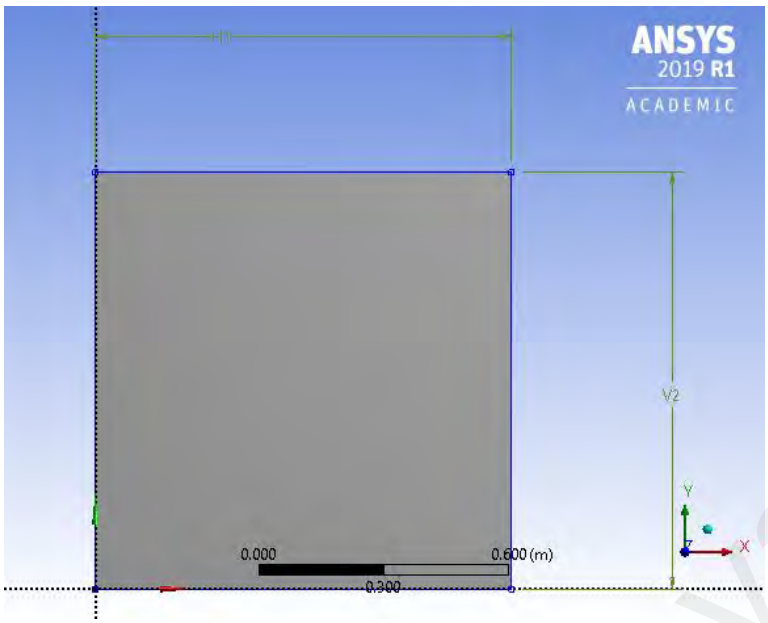

Figure 3.47: Finite element model

After the finite element model had been created, the material properties were assigned into the property module. Four BCs which are consisted of one moving top plate and three fixed walls have been created. This finite element model then splits into meshed model as shown in Figure 3.48.

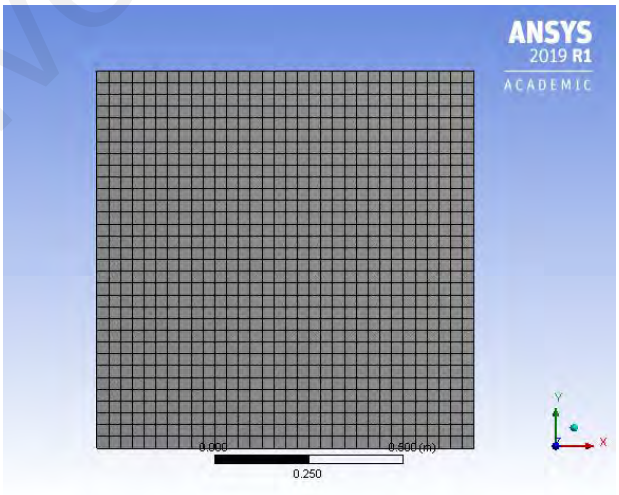

Figure 3.48: Meshing with about 1000 elements

Table 3.3 shows the mesh properties assigned to this finite element model.

Table 3.3: Mesh properties

Object Name	*Mesh*
State	Solved
Display	
Display Style	Use Geometry Setting
Defaults	
Physics Preference	CFD
Solver Preference	Fluent
Element Order	Linear
Element Size	3.125e-002 m
Export Format	Standard
Export Preview Surface Mesh	No
Sizing	
Use Adaptive Sizing	No
Growth Rate	Default (1.2)
Mesh Defeaturing	Yes
Defeature Size	3.5245e-004 m
Capture Curvature	Yes
Curvature Min Size	7.049e-004 m
Curvature Normal Angle	Default (18.0°)
Capture Proximity	Yes
Proximity Min Size	7.049e-004 m
Num Cells Across Gap	Default (3)
Proximity Size Function Sources	Faces and Edges
Bounding Box Diagonal	1.4142 m
Average Surface Area	1.0 m²
Minimum Edge Length	1.0 m
Quality	
Check Mesh Quality	Yes, Errors
Target Skewness	Default (0.900000)
Smoothing	Medium
Mesh Metric	Skewness
Min	1.3057e-010
Max	1.3059e-010
Average	1.3058e-010
Standard Deviation	0.
Inflation	
Use Automatic Inflation	None
Inflation Option	Smooth Transition
Transition Ratio	0.272
Maximum Layers	2
Growth Rate	1.2
Inflation Algorithm	Pre
View Advanced Options	No
Assembly Meshing	
Method	None
Advanced	
Number of CPUs for Parallel Part Meshing	Program Controlled

Universiti Malaya

Straight Sided Elements	
Rigid Body Behavior	Dimensionally Reduced
Triangle Surface Mesher	Program Controlled
Topology Checking	Yes
Use Sheet Thickness for Pinch	No
Pinch Tolerance	Default (6.3441e-004 m)
Generate Pinch on Refresh	No
Sheet Loop Removal	No
Statistics	
Nodes	1089
Elements	1024

Model (D3) > Mesh > Mesh Controls

Object Name	*Mapped Face Meshing*
State	Fully Defined
Scope	
Scoping Method	Geometry Selection
Geometry	1 Face
Definition	
Suppressed	No
Mapped Mesh	Yes
Method	Quadrilaterals
Constrain Boundary	No
Advanced	
Specified Sides	No Selection
Specified Corners	No Selection
Specified Ends	No Selection

Figure 3.49 shows the quadrilateral meshing was assigned to finite element model.

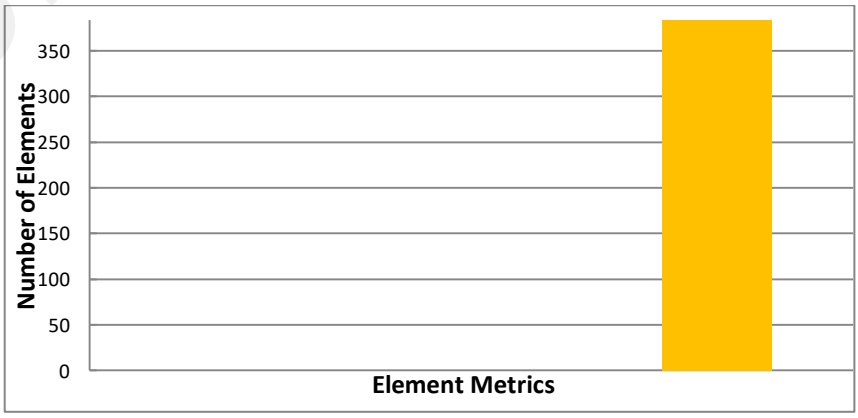

Figure 3.49: Quadrilateral meshing

Universiti Malaya

CHAPTER 4: RESULTS AND DISCUSSIONS

This chapter reviews the result and discussion obtained from this study. Section 4.1 demonstrates how certain fluid contained inside the lid-driven behaves when it is subject to different BCs and different AR in different steady-state criterion. Section 4.2 shows the dispersion of viscous-induced heat of fluid inside the insulated lid-driven cavity model in both no-slip and free-slip BCs. Section 4.3 exhibits a more complicated scenario where the model mentioned in Section 4.2 is subject to Robin BC and then subject to cooling process when the applied shear force at the top lid is removed. In this case, thermal analysis is extended in both no-slip and free-slip BCs. In each section, in-house Matlab® code has been verified using FEM employed in Ansys Fluent®. Some recommendations will be revealed based on this lid-driven model and the current completed GUI in Section 4.4.

4.1 Different BCs and Different AR in Different Steady-state Criterion

In this section, the square lid-driven cavity (1 m × 1 m) model used in Ref. 1 (Jingwei, 2014) will be served as a benchmark to verify the developed in-house Matlab® code. The iterative procedure of the numerical process can be performed at any period or until the flow is in a steady-state condition when criterion of $e \leq 10^{-9}$ is satisfied. The steady-state criterion is given by:

$$e = \frac{\left|\max(\psi_{i,j}^{n+1}) - \max(\psi_{i,j}^{n})\right|}{\left|\max(\psi_{i,j}^{n})\right|} \leq 10^{-9}, \tag{4.1}$$

where n is iterative time, $\psi_{i,j}^{n+1}$ is the stream function at current time and $\psi_{i,j}$ is the stream function at previous time.

The fluid density, ρ is set to 1 kg/m^3, dynamic viscosity, $\mu = 0.001$ $Pa.s$, applied velocity, U_{wall} = 0.2 m/s. Step time, Δt is set to 0.1 s, computation is performed on 40 × 40 uniform grids. Based on Equation 4.2, Reynolds number, Re is given by:

$$\mathrm{Re} = \frac{U_{wall}\rho L}{\mu}. \tag{4.2}$$

Thus, for Re = 200 and analysis was performed in no-slip BC. Then computational job is run until the steady-state criterion of $e \leq 10^{-9}$ is satisfied and those results are shown in Figure 4.1(a) and Figure 4.1(c). The steady-state results are then compared and verified by Ansys Fluent® as shown in Figure 4.1(b) and Figure 4.1(d). The results are interpreted in contour plots. Contour plot is a way to show a three-dimensional surface on a two-dimensional plane. It demonstrates two predictor variables x and y on the y-axis and a response variable z as contours. These contours are sometimes called z-slices or iso-response values. In this case, x and y are independent variables such as Δx and Δy respectively, whereas z variable means velocity, u or v, or stream-function, ψ or temperature, T or any dependent variable. Contour plot is useful and helpful to investigate how the dependent variable influenced by Δx and Δy. Moreover, it can be expressed in time-dependent contour plot and animation of contour plot can be envisaged. Colour-coded region can help to visualize 3D data in two dimensions. Two small eddies (which rotate in opposite directions with respect to primary main cell) are formed at both of the corners at the bottom, whereas the right bottom eddy seems bigger as shown in Figure 4.2. Thus, the value of stream function, ψ of the two small eddies is negative.

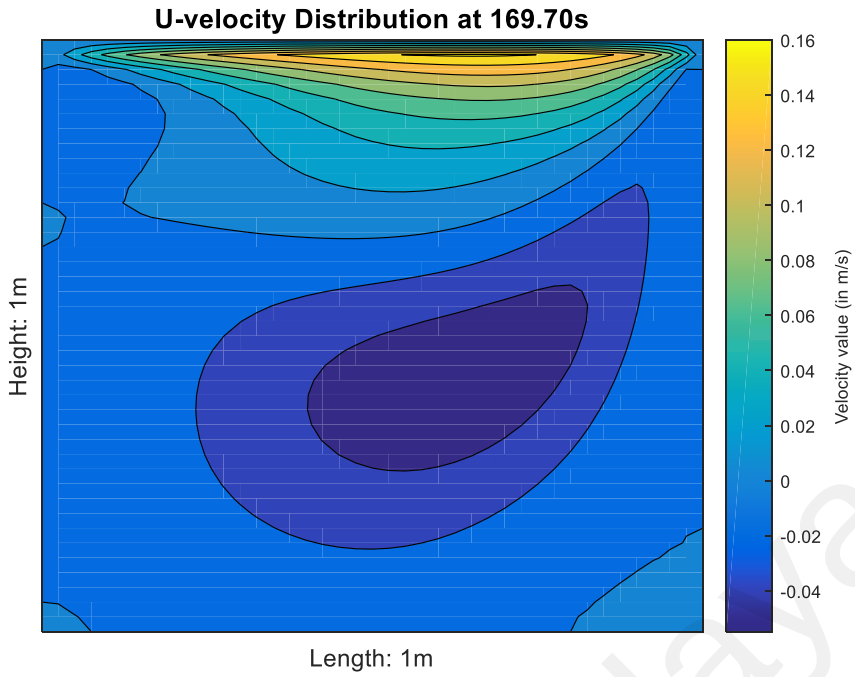

(a)

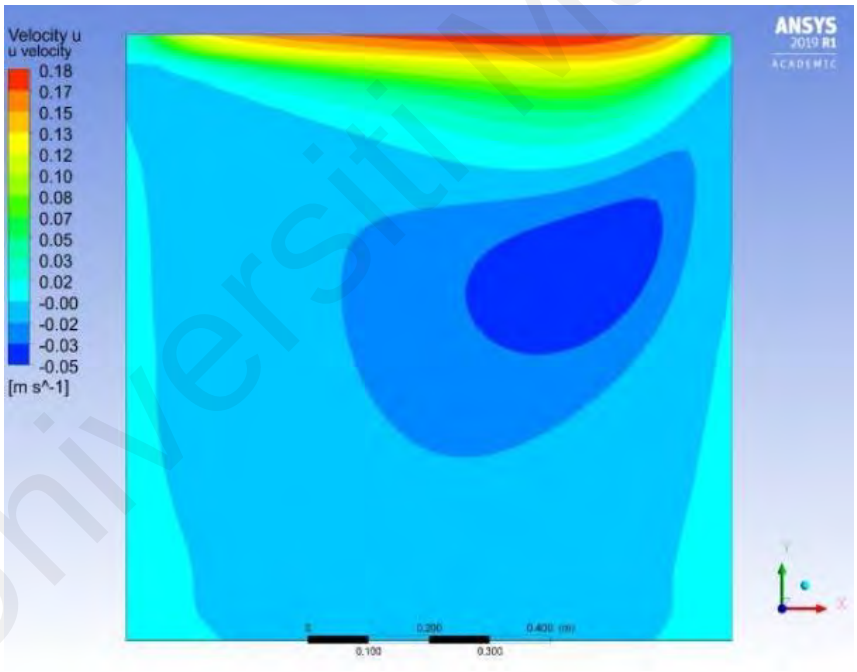

(b)

Universiti Malaya

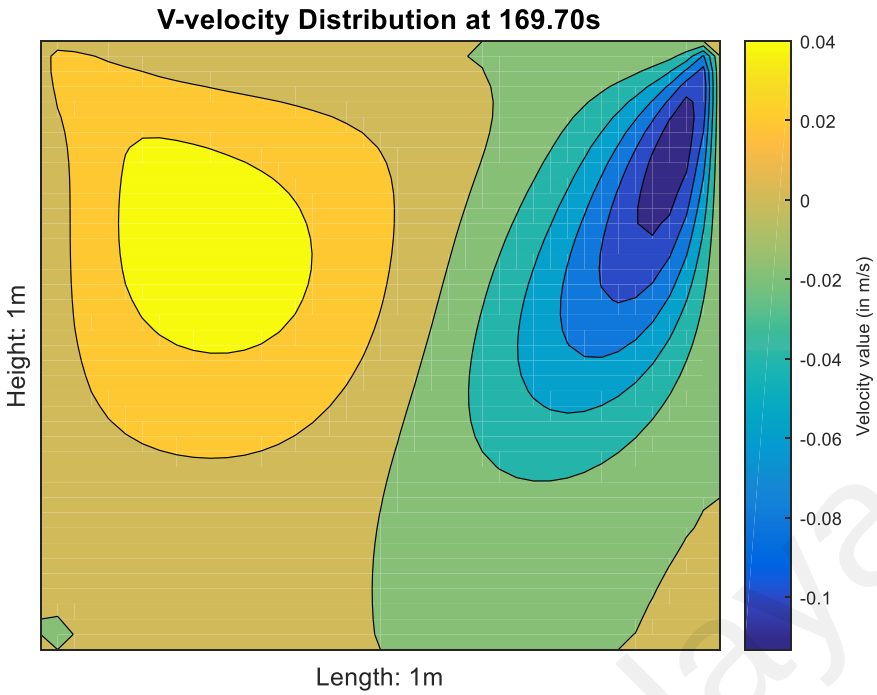

(c)

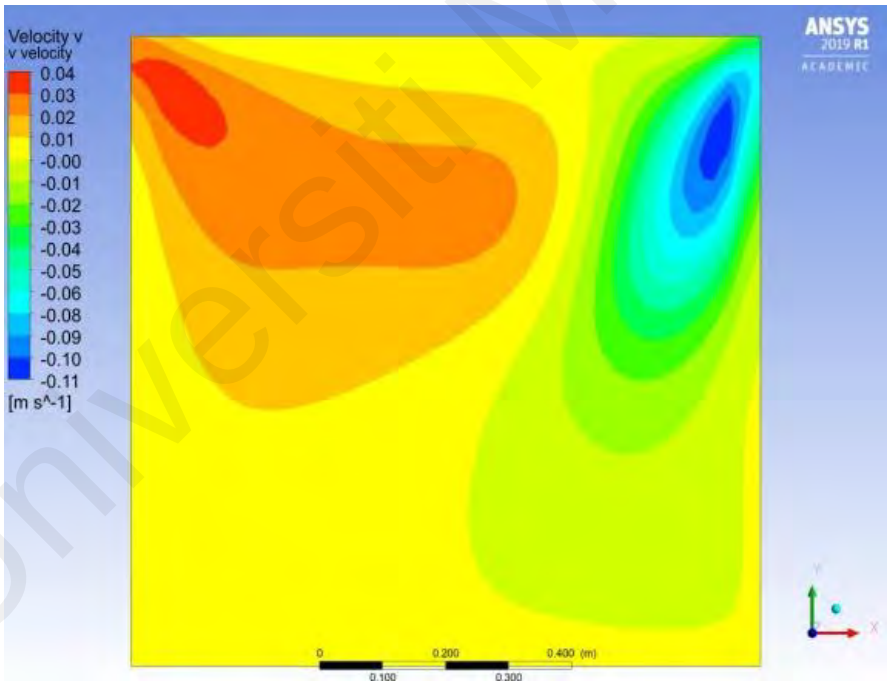

(d)

Figure 4.1: Comparison of contour plot at steady-state condition (a) *u*-velocity distribution via FDM (in-house Matlab® code) (b) *u*-velocity distribution via FEM (Ansys Fluent®) (c) *v*-velocity distribution via FDM (in-house Matlab® code) (d) *v*-velocity distribution via FEM (Ansys Fluent®)

Universiti Malaya

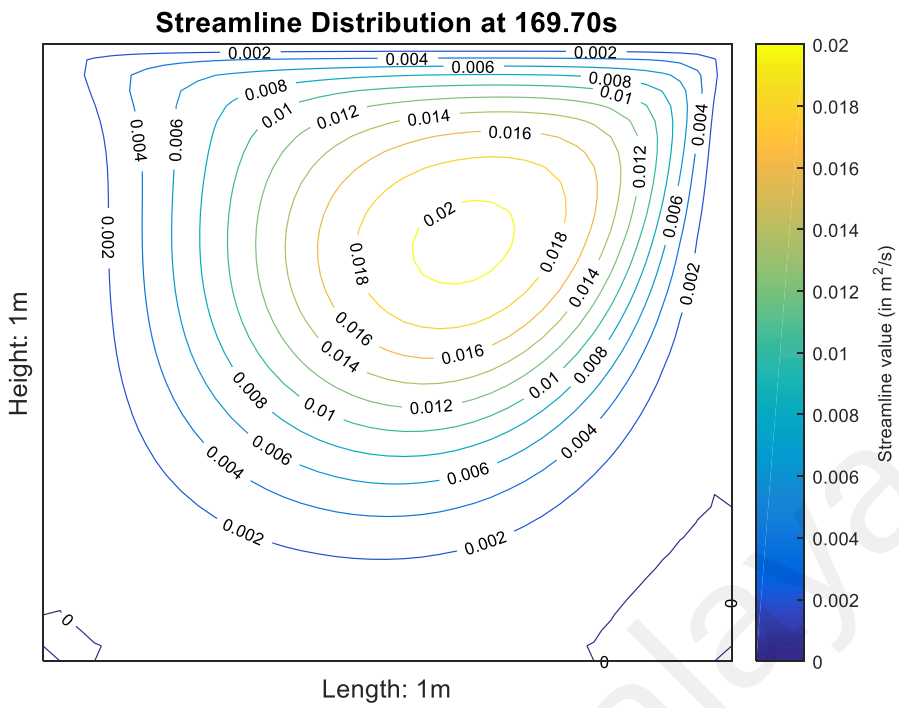

Figure 4.2: Contour plot of stream function distribution

In no-slip BC, both of the normal and tangential components of velocity are zero along the solid walls. However, an interesting phenomenon is observed when this iteration is subject to extremely high free-slip BC at $l_s = 1\ m$, the shape of the primary cell is being „stretched" to the corners at the bottom. In this scenario, there is no tangential shear force along the interface in between the fluid and solid walls. Thus, there is no velocity in the normal component along the solid wall but its tangential component is unrestricted. No corner eddies are able to be formed as observed in Figure 4.3 while contour plots of the streamlines of *u*- and *v*- velocity as shown in Figure 4.4. This extremely high free-slip BC model takes a longer period in order to achieve the steady-state condition of $e \leq 10^{-9}$.

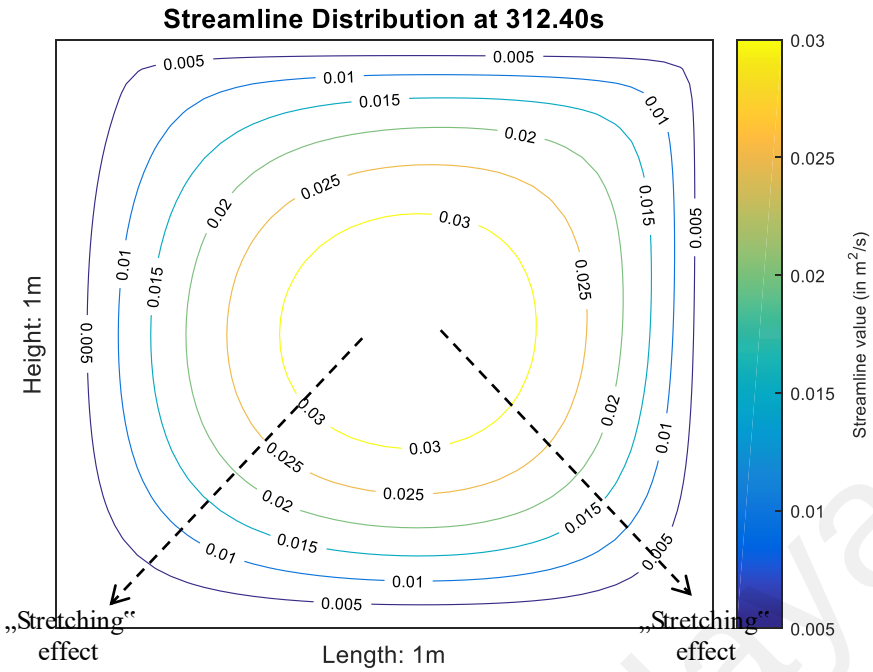

Figure 4.3: Contour plot of streamline distribution at steady-state condition (free-slip BC)

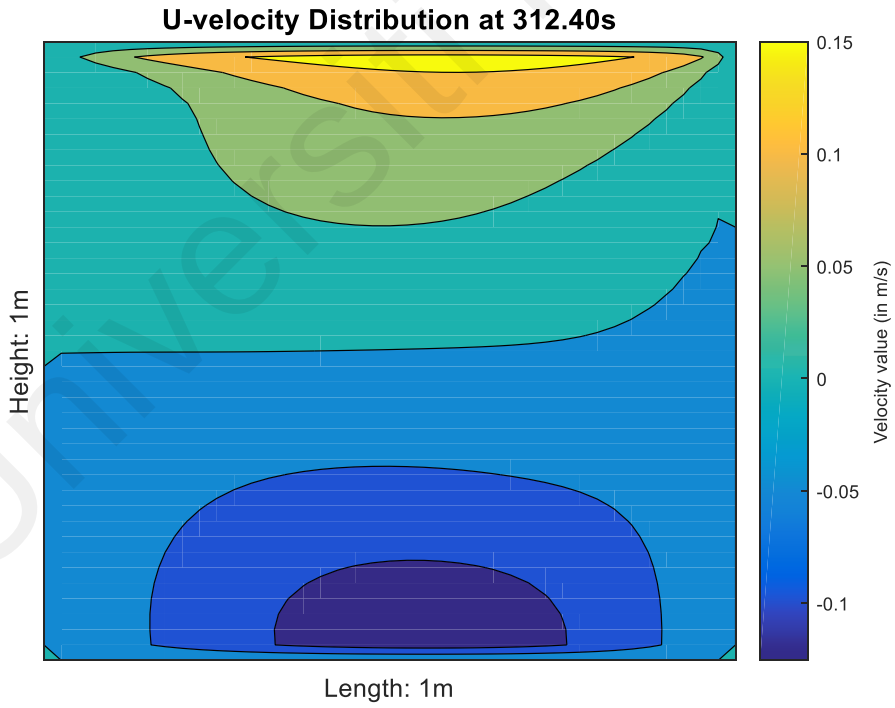

(a)

Universiti Malaya

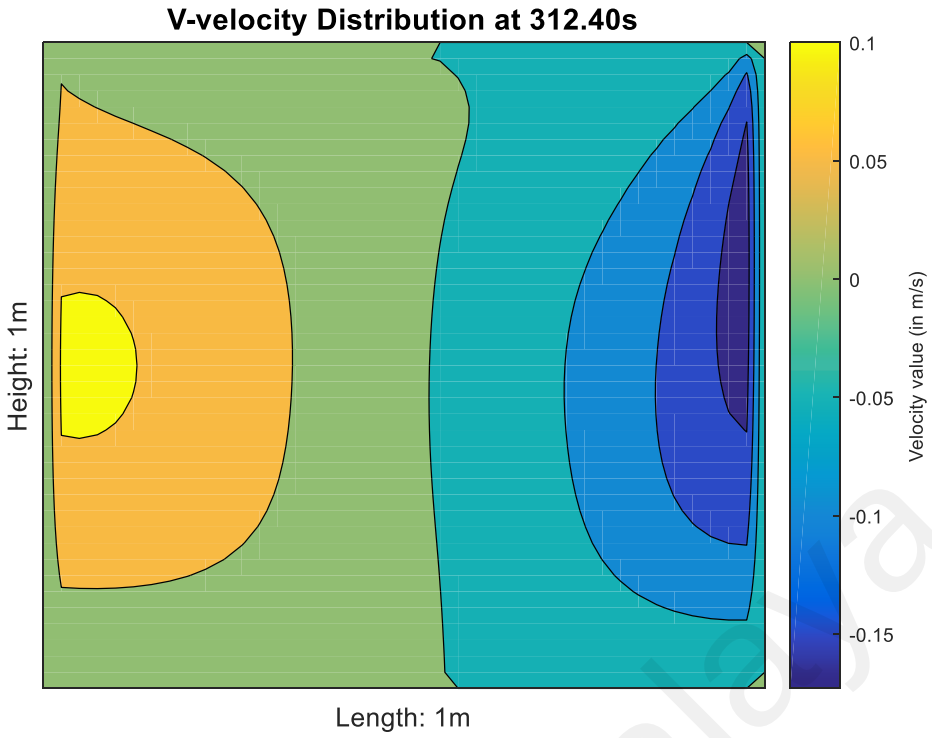

(b)

Figure 4.4: Contour plot of evolution of (a) *u*- and (b) *v*-velocity distribution at steady-state condition (free-slip BC)

The AR of the model is modified from AR = 1 to AR = 1.629 as suggested (Moffatt, 1964) in order to investigate how the two corner eddies at the bottom merge to form a secondary main cell at this critical AR in no-slip BC. A time series of contour plots of the evolution of the stream function distribution at different steady-state criteria (from $e \leq 10^{-2}$ to $e \leq 10^{-10}$) are shown in Figure 4.5. The value of maximum stream function, $\psi_{\max}$ in each step time is increasing along the iteration, then achieves plateau before approaching the highest point and drops in tiny quantity until the end of the iteration as shown in Figure 4.6.

Universiti Malaya

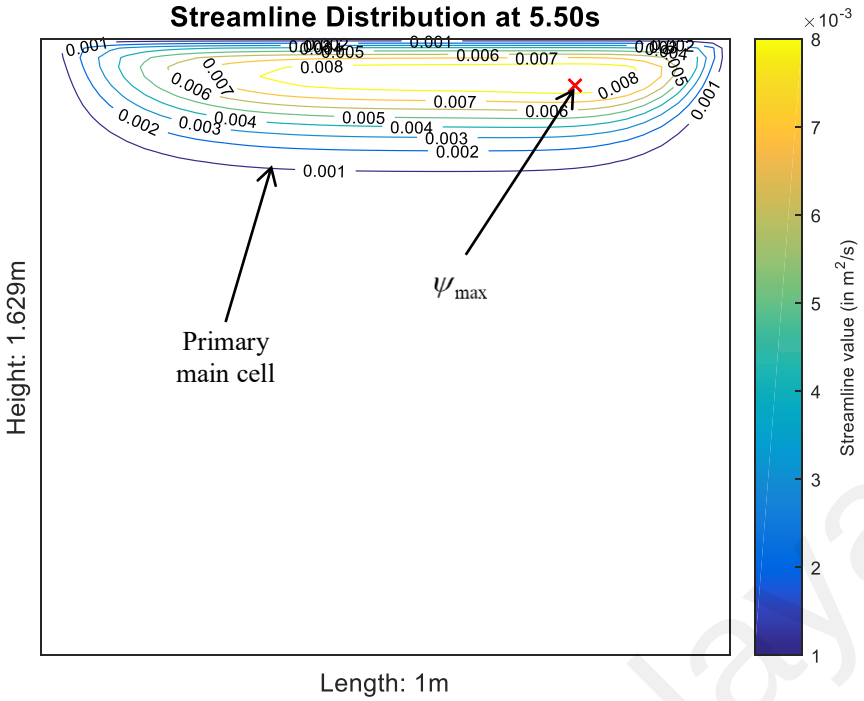

(a)

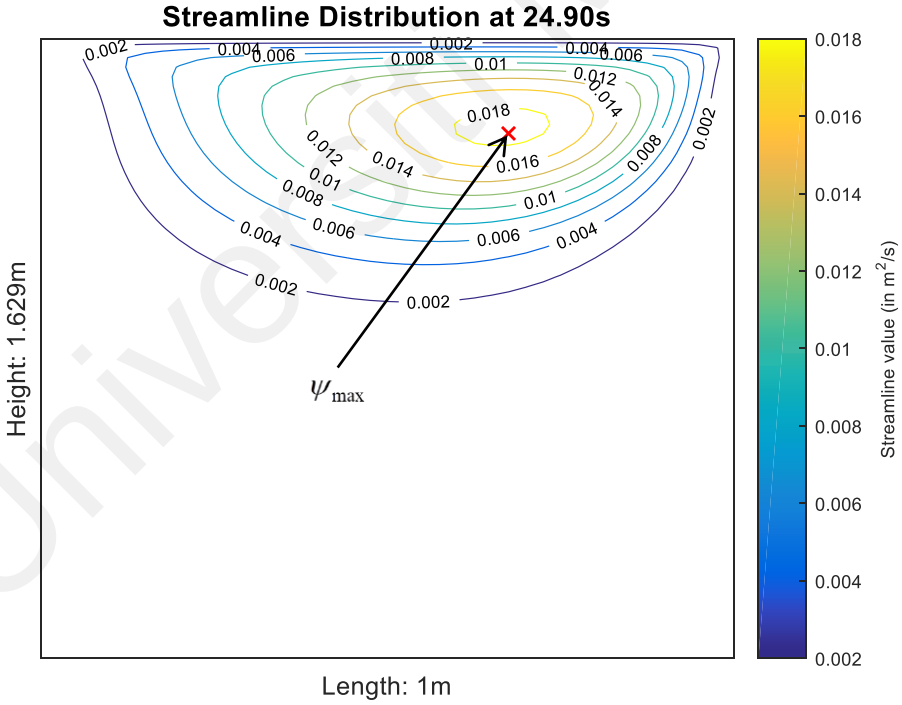

(b)

University of Malaya

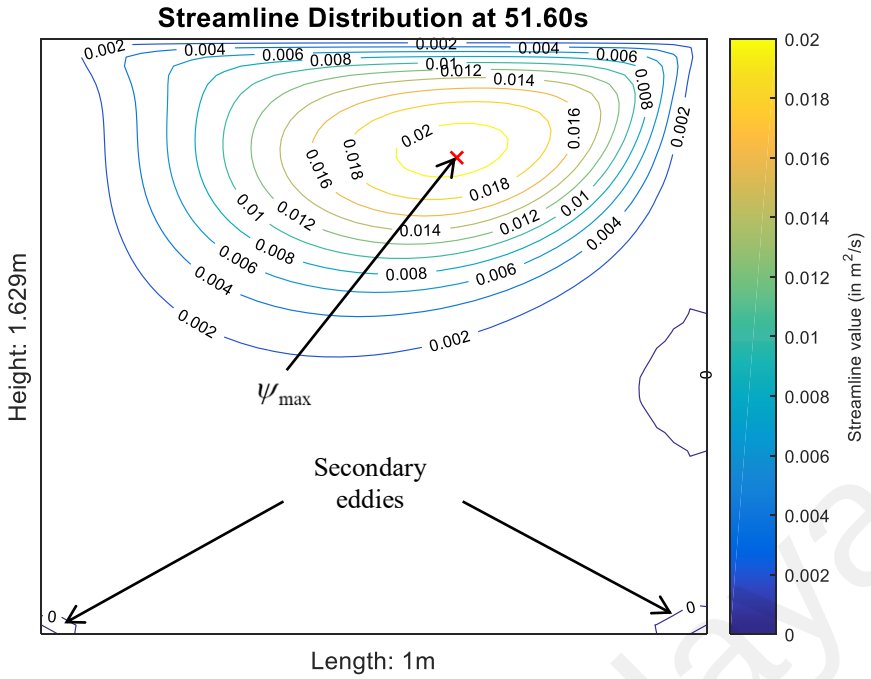

(c)

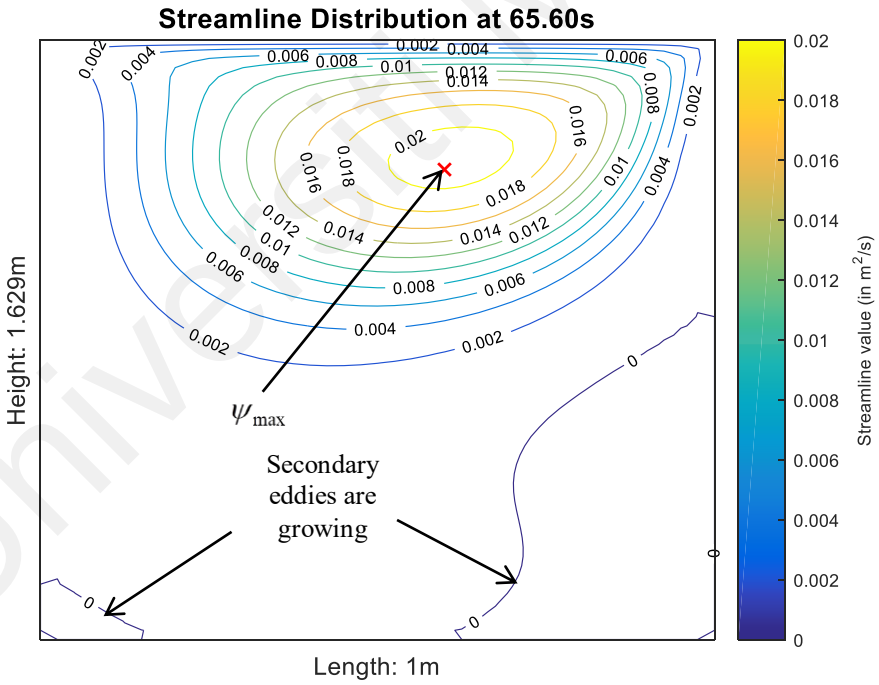

(d)

University of Malaya

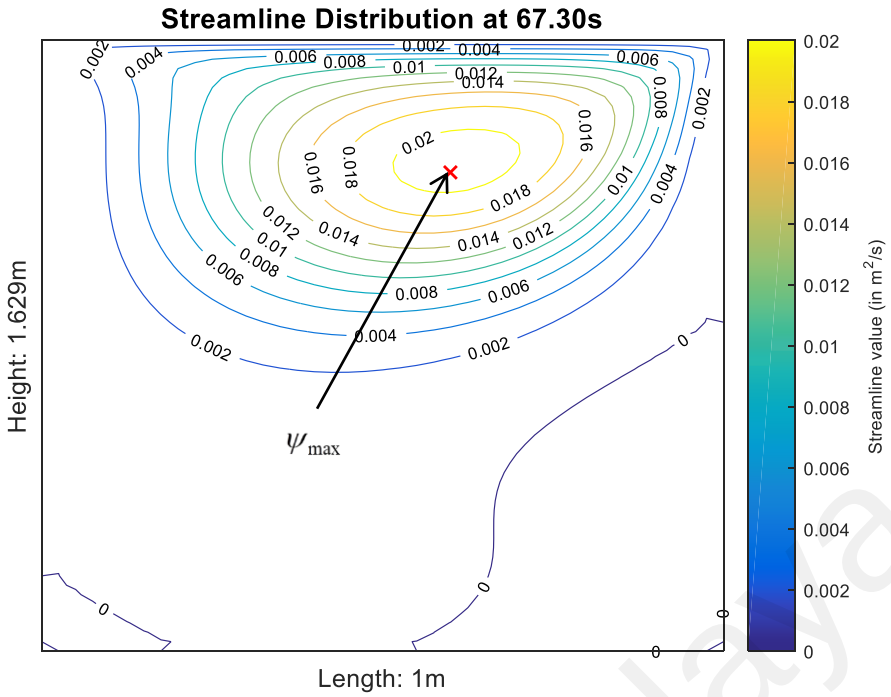

(e)

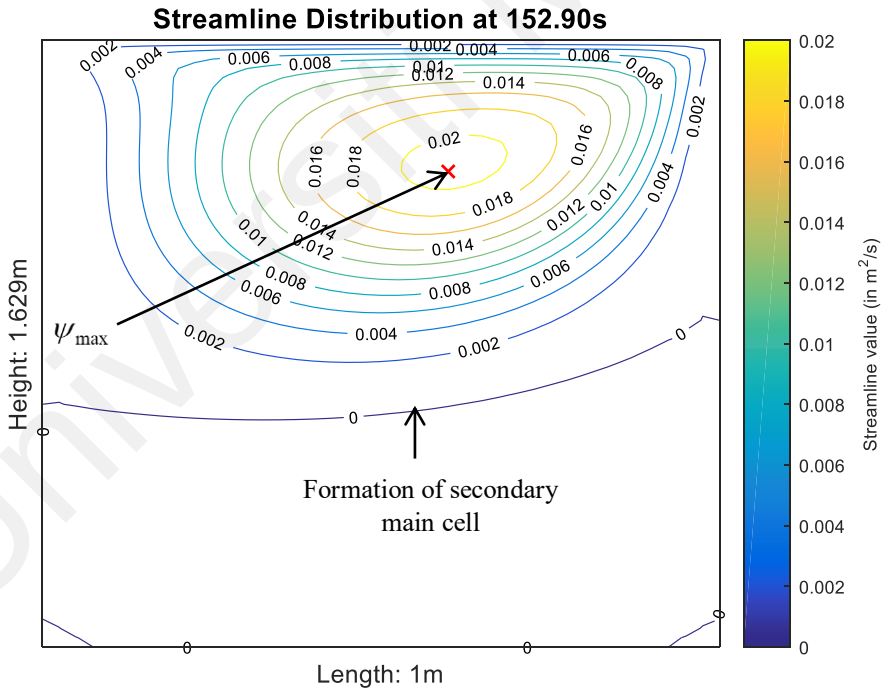

(f)

University of Malaya

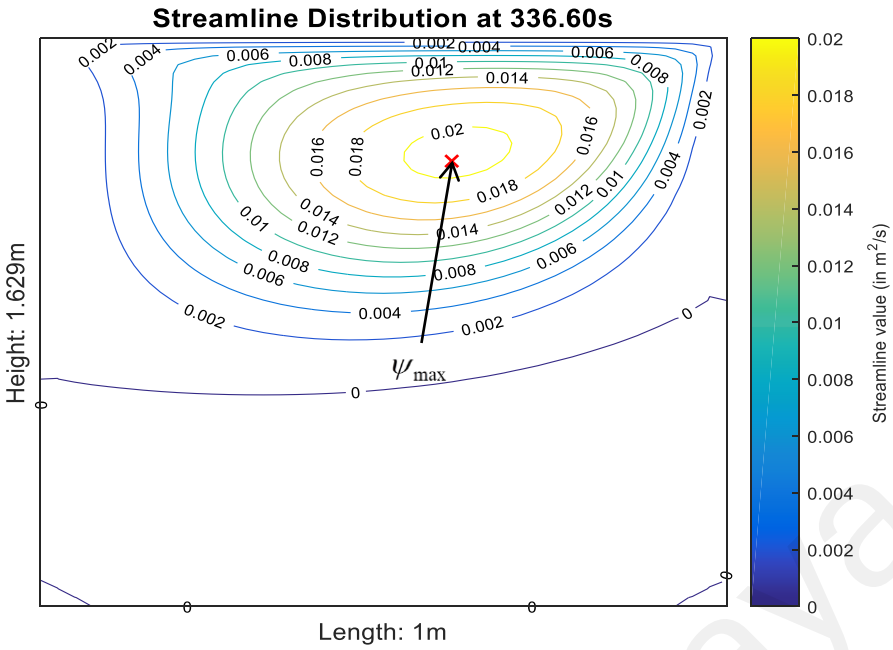

(g)

Figure 4.5: Contour plot of evolution of streamline distribution at (a) t = 5.50 s (b) t = 24.90 s (c) t = 51.60 s (d) t = 65.60 s (e) t = 67.30 s (f) t = 152.90 s and (g) t = 336.60 s (Re=325.8 with no-slip BC)

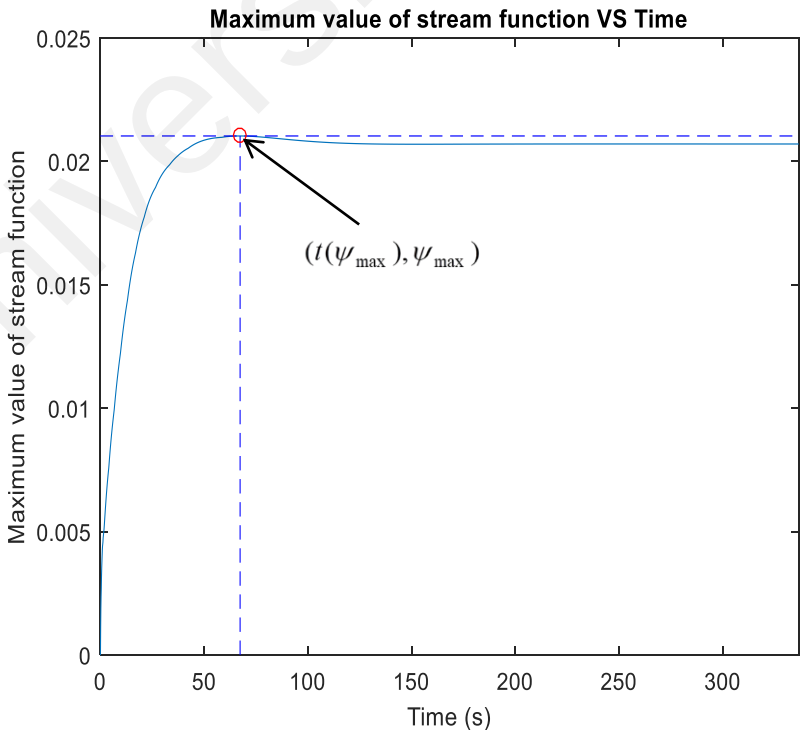

(a)

Universiti Malaya

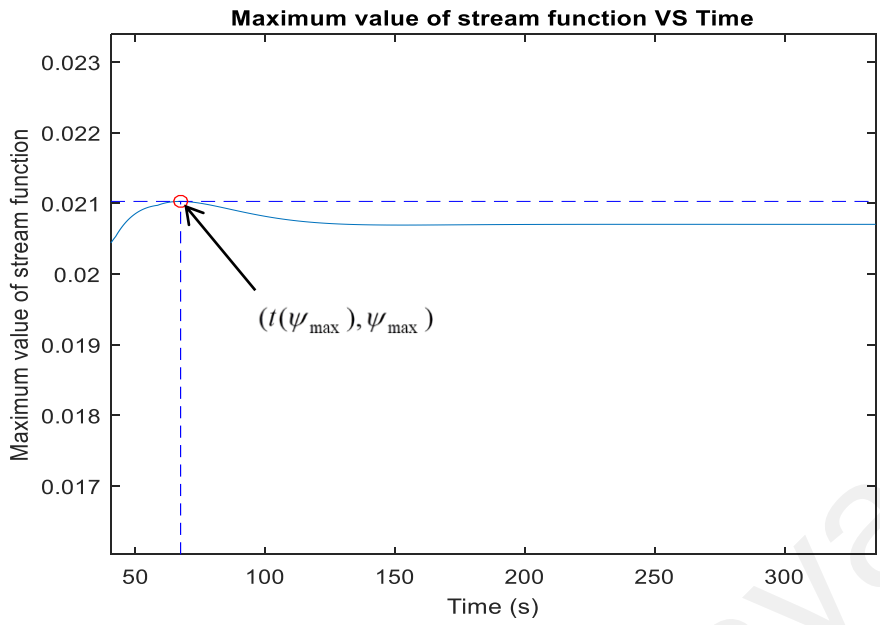

(b)

Figure 4.6: Maximum value of stream function along the iteration (a) Standard view (b) Zoomed view around coordinate $(t(\psi_{max}), \psi_{max})$

Based on Figure 4.6, the stream funtion distribution arrives the highest maximum value at $t = 65.6\ s$ (at about steady-state criterion of $e = 10^{-5}$). The location of maximum stream function, ψ_{max} is fixed in position and does not move anywhere after this steady-state criterion. Then the value of ψ_{max} begins to drop a little bit after $t = 65.6\ s$ due to numerical error. Secondary eddies were formed at $t = 51.6\ s$ and grow in size further. Then these two secondary eddies merged at $t = 152.9\ s$ (at about steady-state criterion of $e = 10^{-8}$) and the shape and size of the whole streamline distribution do not change at any further iteration as shown in Figure 11(g). According to Moshikin and Poochinapan (2010), they suggested the steady flow is achieved when the criterion, $e \le 10^{-8}$ is achieved. However, Abd-El-Hafiz et. al. (2004) proposed another criterion in which the iteration is repeated until the velocity profile (velocity and stream function are interrelated through Equation (3.11) and Equation (3.12) converges when criterion of $e \le 10^{-5}$ is reached. Secondary main cell is not able to form if iteration stops at steady-state criterion with

Universiti Malaya

$e \leq 10^{-5}$ is achieved. In addition to this, by performing iteration beyond the steady-state criterion, $e \leq 10^{-8}$ does not contribute any useful result. Due to iteration and round off errors (Marchi & Silva, 2002), the value of streamline distribution drops after achieving the steady-state criterion with $e \leq 10^{-5}$ as more iterations are needed in order to achieve the smaller criterion and the resultant steady-state period will be longer and causes a longer execution time. Table 4.1 shows the value and location of ψ_{max} at different steady-state criteria.

Table 4.1: Value and location of ψ_{max} at different steady-state criteria (AR= 1.629)

No.	Steady-state criteria, *e*	Period, *t* to achieve designated *e*	ψ_{max} (m^2/s) at designated *e*	Location of ψ_{max} (*m*) at designated *e*	Remark
1.	$e \leq 10^{-2}$	5.5 s	0.0089	$x = 0.775$, $y = 1.466$	Primary main cell is formed
2.	$e \leq 10^{-3}$	24.9 s	0.0186	$x = 0.675$, $y = 1.262$	Primary main cell is growing
3.	$e \leq 10^{-4}$	51.6 s	0.0209	$x = 0.625$, $y = 1.140$	Secondary eddies are formed
4.	$e \leq 10^{-5}$	65.6 s	0.0210	$x = 0.600$, $y = 1.100$ (location is fixed)	Secondary eddies are growing
5.	$e \leq 10^{-6}$	67.2 s	0.0210	$x = 0.600$, $y = 1.100$	/
6.	$e \leq 10^{-7}$	67.3 s	0.0210	$x = 0.600$, $y = 1.100$	/
7.	$e \leq 10^{-8}$	152.9 s	0.0207	$x = 0.600$, $y = 1.100$	Secondary main cell is formed and fixed in size
8.	$e \leq 10^{-10}$	336.6 s	0.0207	$x = 0.600$, $y = 1.100$	/

Universiti Malaya

The model with AR = 1.629 was analyzed again until the steady-state criterion, $e = 10^{-8}$ is achieved but in free-slip BC when the slip length, $l_s = 1$. The shape of the primary cell is being „*stretched*" to the corners at the bottom as shown in Figure 4.7 (similar with Figure 4.3). In the meanwhile, its associated contour plots of the streamline, $u-$ and $v-$velocity distributions are shown in Figure 4.8 (similar with Figure 4.4).

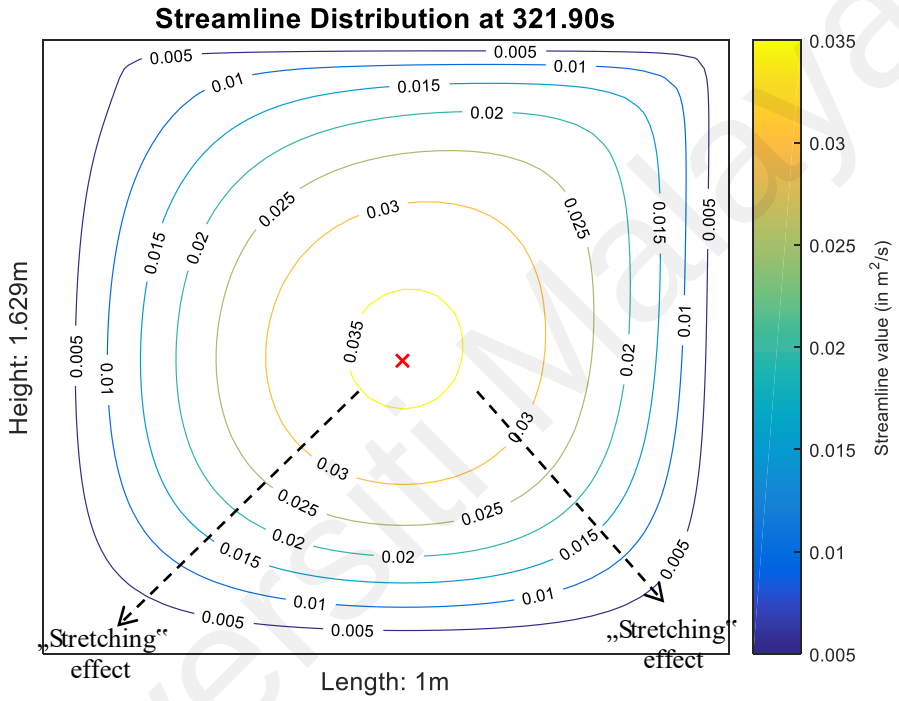

Figure 4.7: Contour plot of streamline distribution at steady-state condition (Re=325.8 with significant free-slip BC)

No eddies at the corners are observed based in Figure 4.7 as these eddies are eliminated by significant free-slip effect. Thus, the whole streamline is flowing in the same direction that is clockwise. Based on the contour plot of $u-$ and $v-$velocity distribution as shown in Figure 4.8, their shapes are not much different with AR =1.

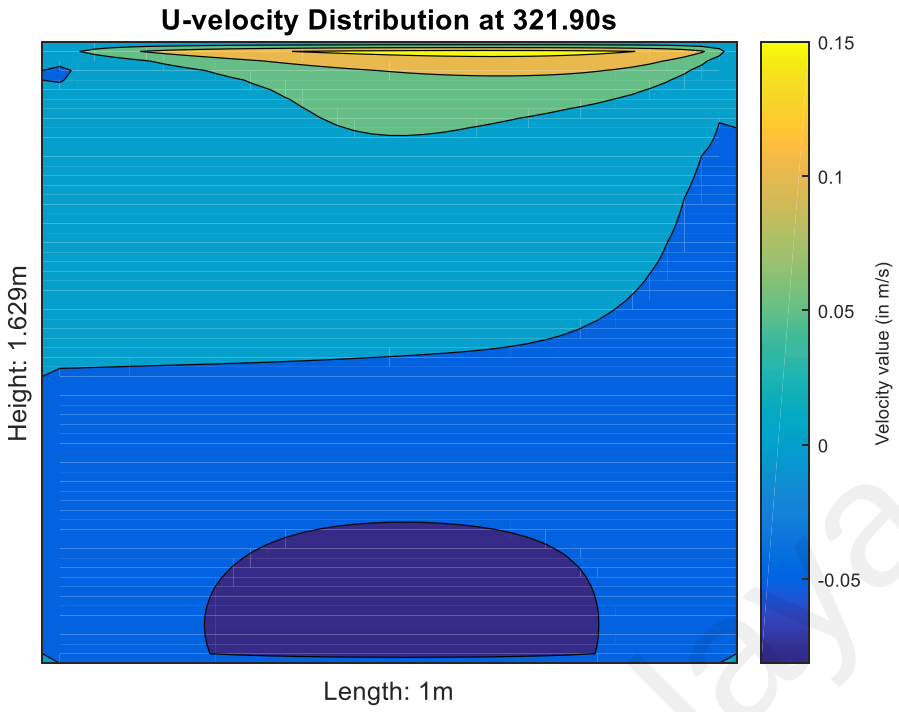

(a)

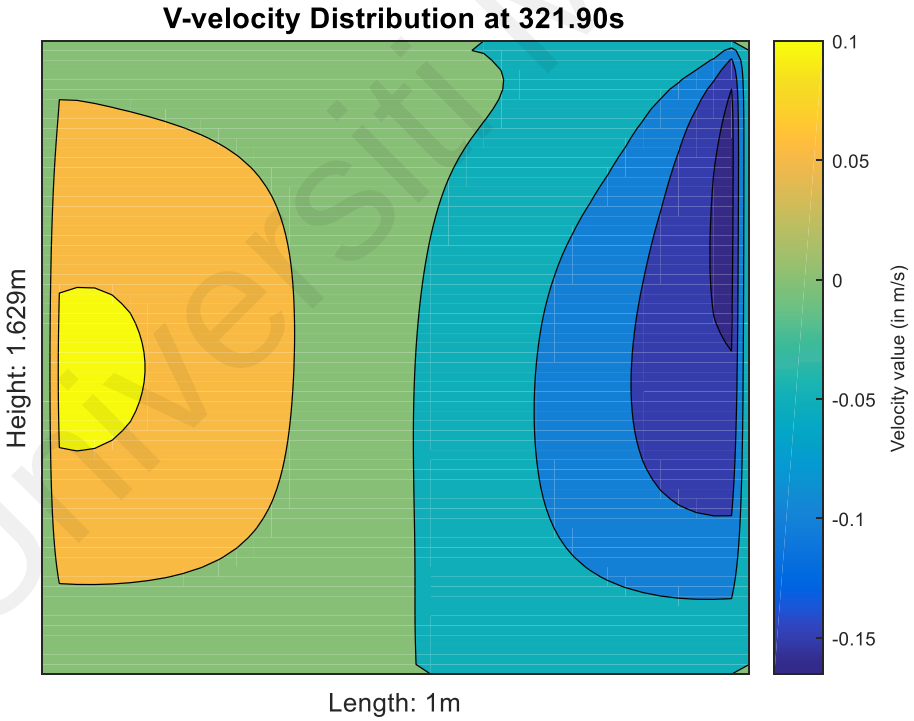

(b)

Figure 4.8: Contour plot of evolution of (a) *u*- and (b) *v*-velocity distributions at steady-state condition (Re=325.8 with significant free-slip BC)

Universiti Malaya

4.2 Lid-driven Cavity Fluid Subject to Neumann BC

A square lid-driven cavity with AR = 1 (1 m × 1 m) will be used in this section. There are six case studies to characterize the flow field and temperature distribution in a two-dimensional lid-driven with insulated walls considered in order to understand the effect of viscous heating in both no-slip and free-slip BCs. Six test cases with different fluid properties and flow conditions are performed in a laminar and unsteady iterative procedure until the analysis period, $t = 1.5\ s$ is achieved (longer than steady-state criterion of $e = 10^{-5}$). The applied velocity, U_{wall} = 10 m/s (except U_{wall} = 5 m/s in 3rd and 4th test case). The fluid density, ρ is set to 15 kg/m^3, dynamic viscosity, $\mu = 2\ Pa.s$, thermal conductivity, $k = 10\ W/m.K$, specific heat, c = 10 $J/kg.K$ (except c = 20 $J/kg.K$ in 5th and 6th case studies) and initial temperature, T_i of the whole fluid filled inside the lid driven is set to 25 ^oC. Step time, Δt is set to 0.001 s and computation is performed on uniform grids 40 × 40. The Prandtl number, $\Pr$ is defined as:

$$\Pr = \frac{\upsilon}{\alpha} = \frac{c\mu}{k}, \tag{4.3}$$

where υ is kinematic viscosity and α is thermal diffusivity.

Another important heat transfer parameter in evaluating the temperature profile of certain fluid is termed as thermal diffusivity, α and it is denoted by Equation (4.4):

$$\alpha = \frac{k}{\rho c}. \tag{4.4}$$

Then, free-slip BC with slip length value, $l_s = 1\ m$ is assigned in 2nd, 4th and 6th test cases while the no-slip BC is assigned with slip length value, $l_s = 0\ m$ in other test cases. Table 4.2 shows the value of $\Pr$, Re_L and α in all these test cases.

Table 4.2: Flow conditions of six test cases

Case	U_{wall} (m/s)	k $(W/m.K)$	c $(J/kg.K)$	l_s (m)	Pr	Re_L	$\alpha(m^2/s)$
1.	10	10	10	0	2	75	0.067
2.	10	10	10	1	2	75	0.067
3.	5	10	10	0	2	37.5	0.067
4.	5	10	10	1	2	35.5	0.067
5.	10	10	20	0	4	75	0.033
6.	10	10	20	1	4	75	0.033

In this section, the 1st and the 2nd test cases will serve as the benchmarks (both cases with identical Reynold number, Re_L, but subject to no-slip and free-slip BCs) for comparison with other test cases. First and foremost, the 1st test case results are compared with those results generated using commercial engineering software Ansys Fluent®. Figure 4.9 and Figure 4.10 show the comparison of contour plot of *u*- and *v*-velocity and temperature distribution respectively produced using in-house Matlab® code (FDM) and Ansys Fluent® (FEM). Stream function distribution at the end of iteration and the location of the maximum stream function value, $\psi_{\max}$ (designated as point A) in the stream function distribution for the 1st test case (no-slip BC) are shown in Figure 4.11. The steady-state criteria of $e = 10^{-5}$ and $e = 10^{-8}$ are shown in stream function profile of point A as shown in Figure 4.12. After achieving the steady-state of $e = 10^{-5}$, the flow parameter and streamline pattern does not change much with time.

Universiti Malaya

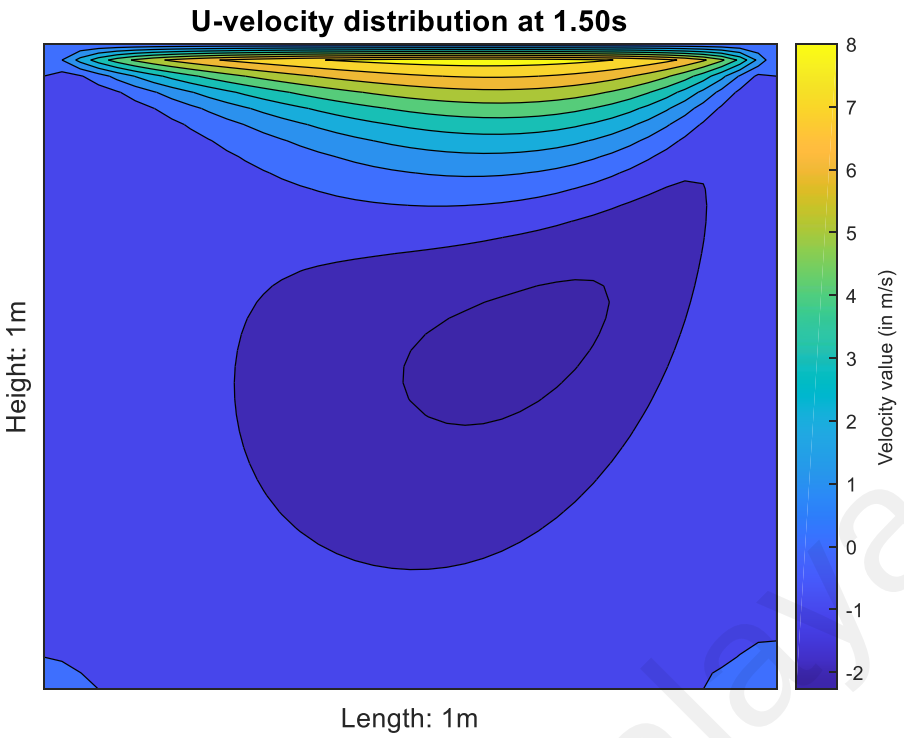

(a)

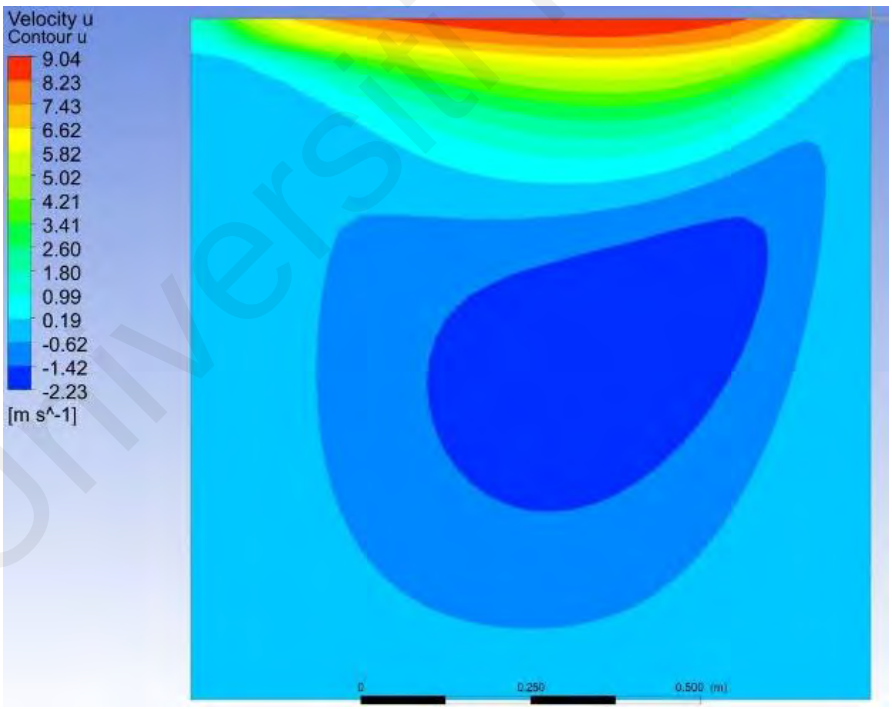

(b)

Universiti Malaya

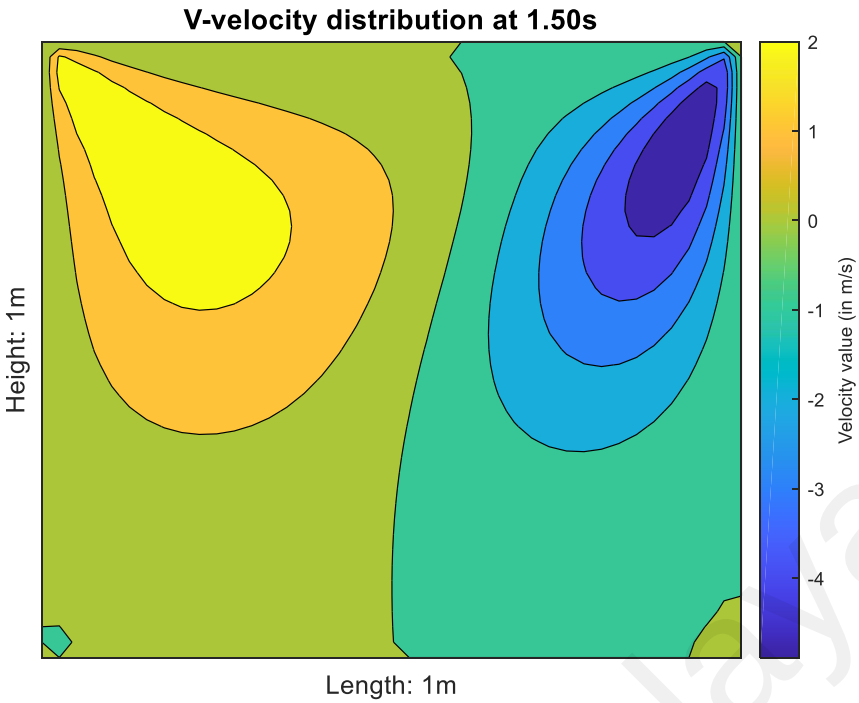

(c)

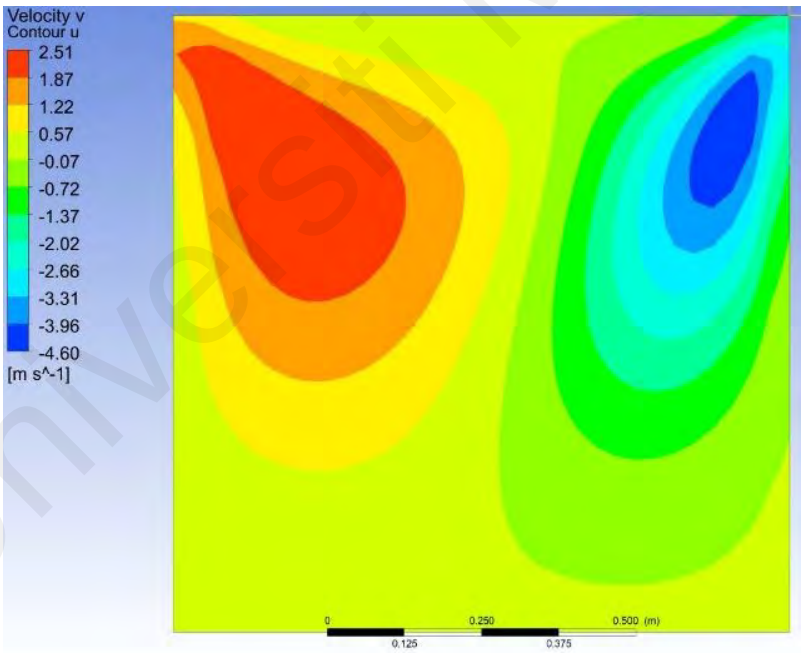

(d)

Figure 4.9: Comparison of contour plot at $t = 2.00\ s$ (a) *u*-velocity using FDM in Matlab® (b) *u*-velocity using FEM in Ansys Fluent® (c) *v*-velocity using FDM in Matlab® (d) *v*-velocity using FEM in Ansys Fluent®

Universiti Malaya

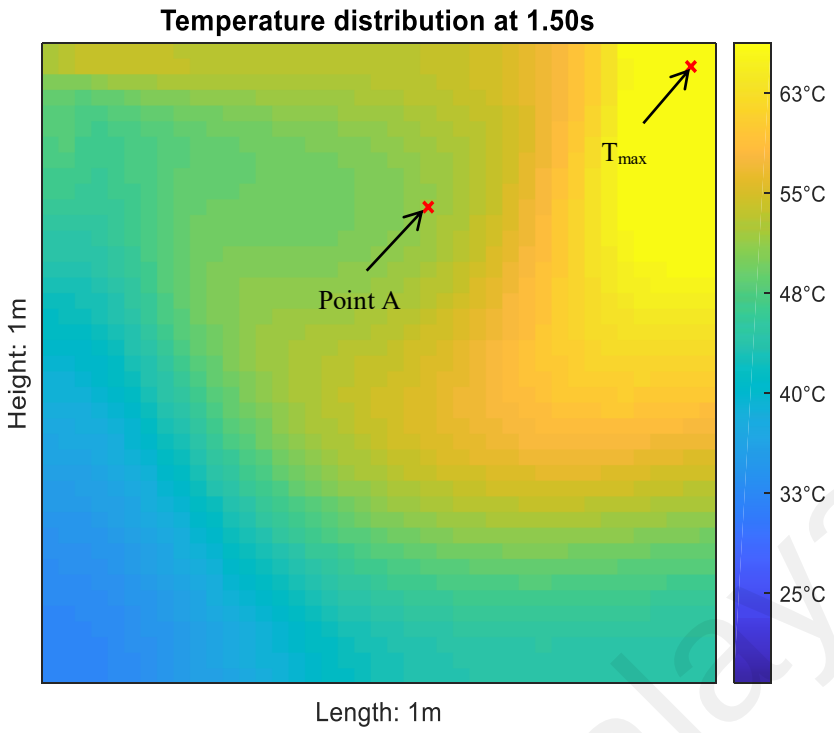

(a)

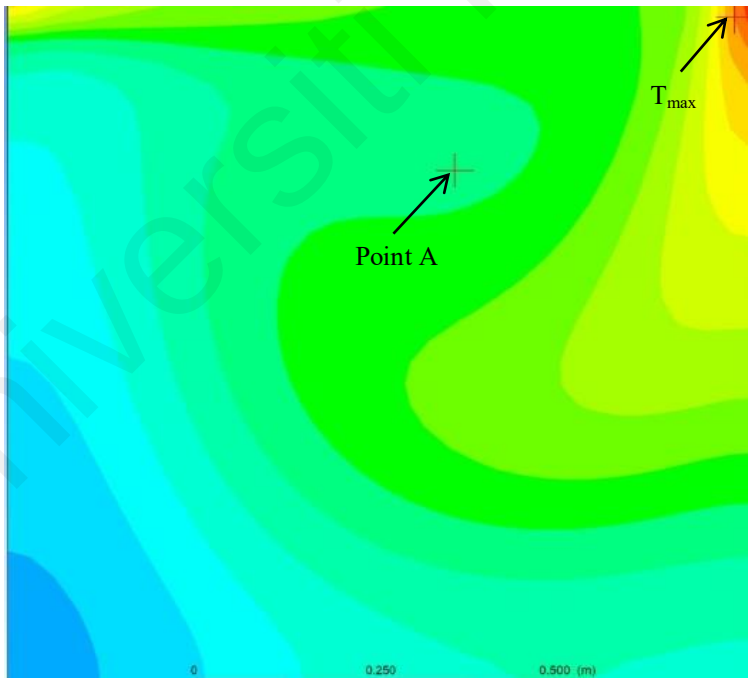

(b)

Figure 4.10: Comparison of image plot of temperature distribution at $t = 2.00$ s (a) using FDM in Matlab® (b) using FEM in Ansys Fluent®

Universiti Malaya

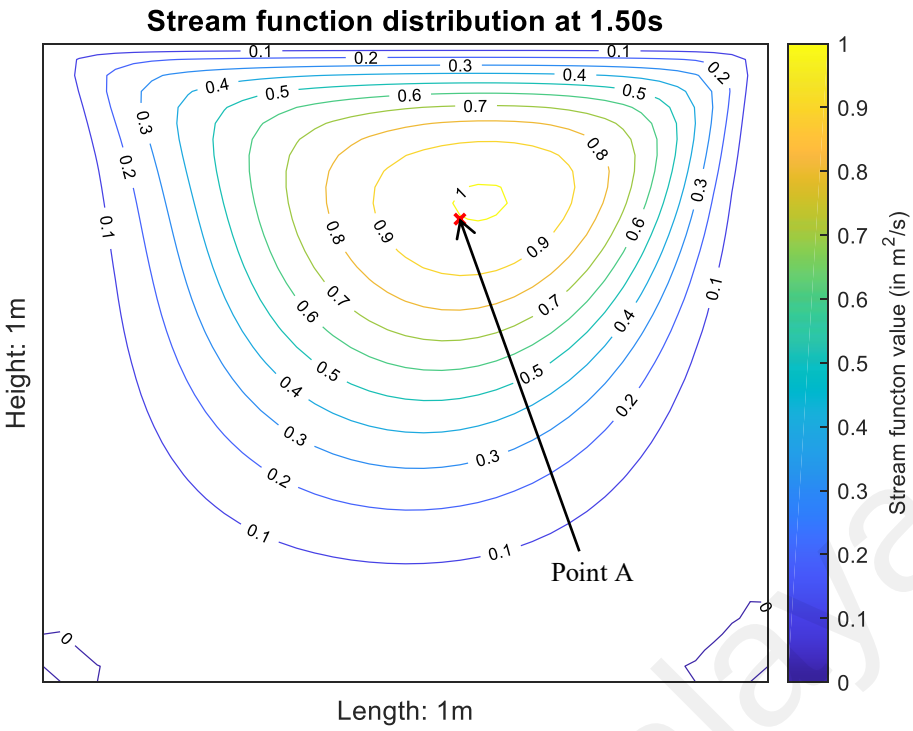

Figure 4.11: Stream function distribution at t = 1.50 *s*

Similarly, there are two small eddies are formed at corners which are flowing counter-rotating with respect to the primary main cell based on Figure 4.11. The point with maximum value of streamline is denoted as point A. Centre vertical line and centre horizontal line of the lid-driven model as shown in Figure 4.13 are used to create the comparison of u- and v-velocity profile using FDM (Matlab®) and FEM (Ansys Fluent®) at $t = 1.50$ s. Figure 4.14 shows a good agreement is achieved for u-velocity profile along the centre horizontal line and v-velocity profile along the centre vertical line at steady-state condition (at $t = 1.50$ s). A close agreement of comparison of temperature profile at point A is attained using FDM (Matlab®) and FEM (Ansys Fluent®) as shown in Figure 4.15.

Universiti Malaya

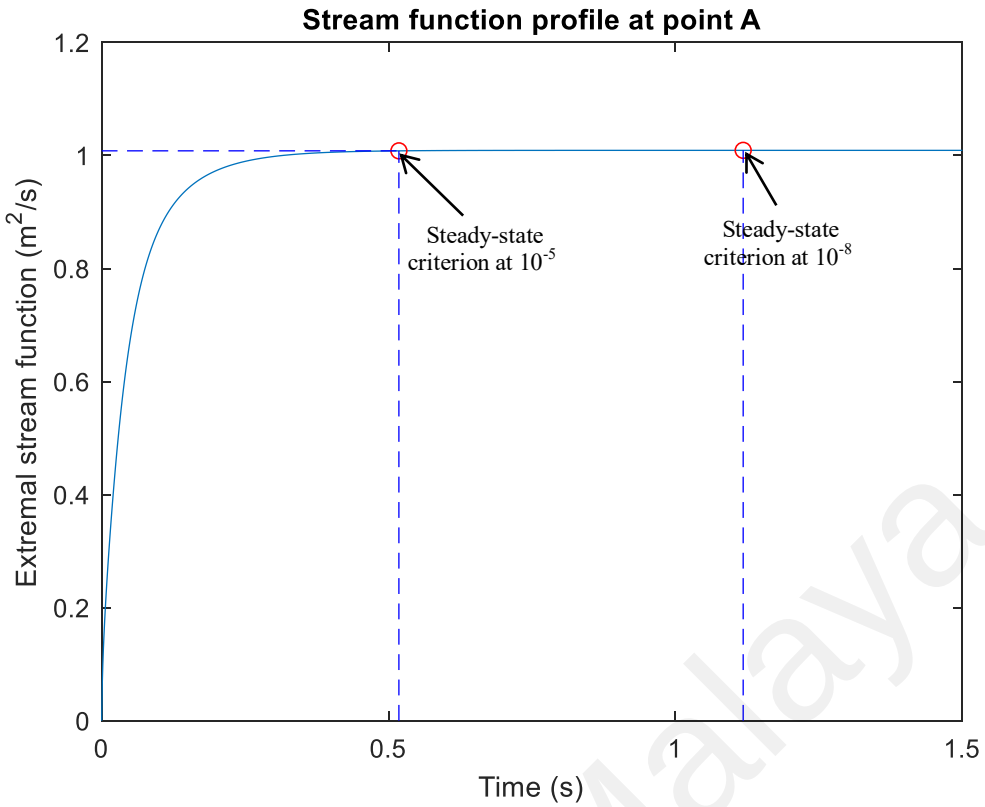

Figure 4.12: Stream function profile at point A

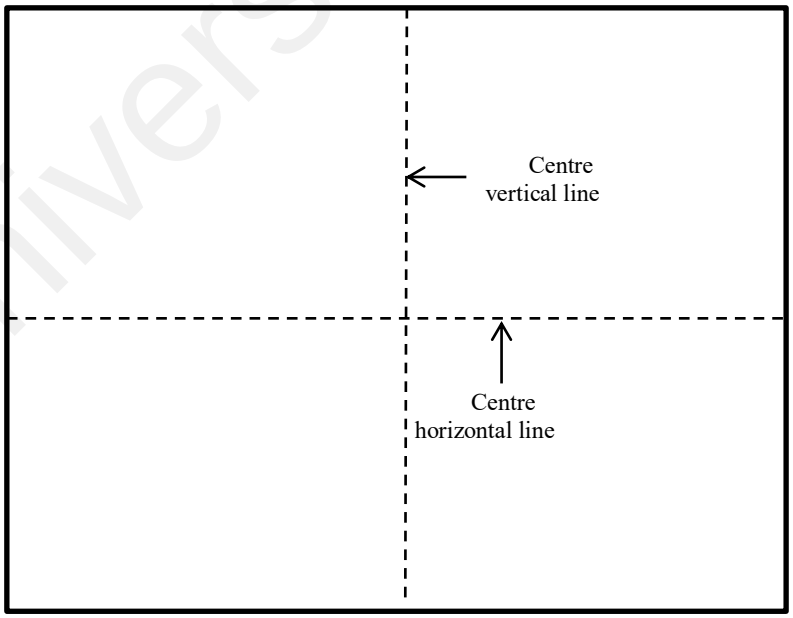

Figure 4.13: Centre vertical line and centre horizontal line

Universiti Malaya

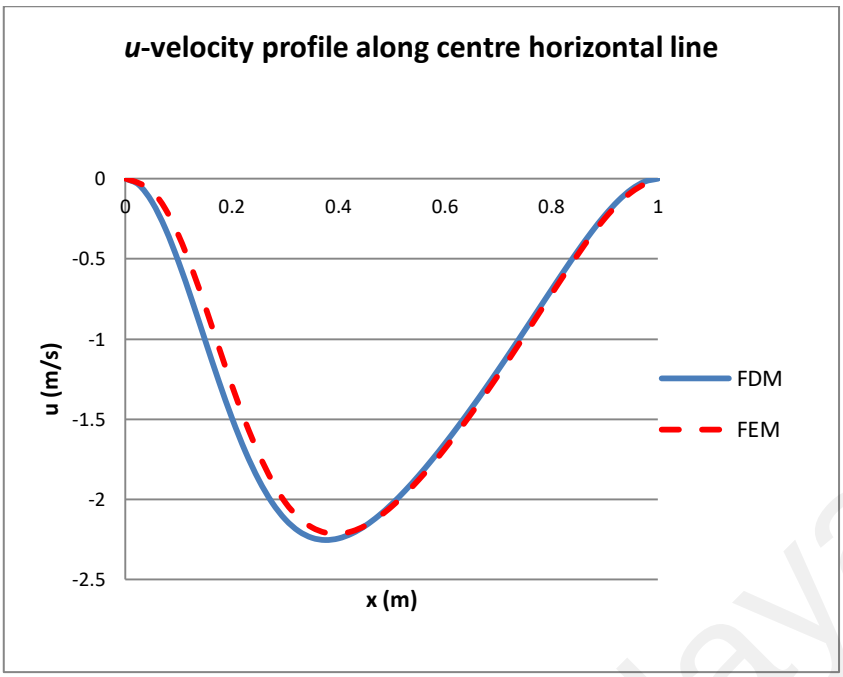

(a)

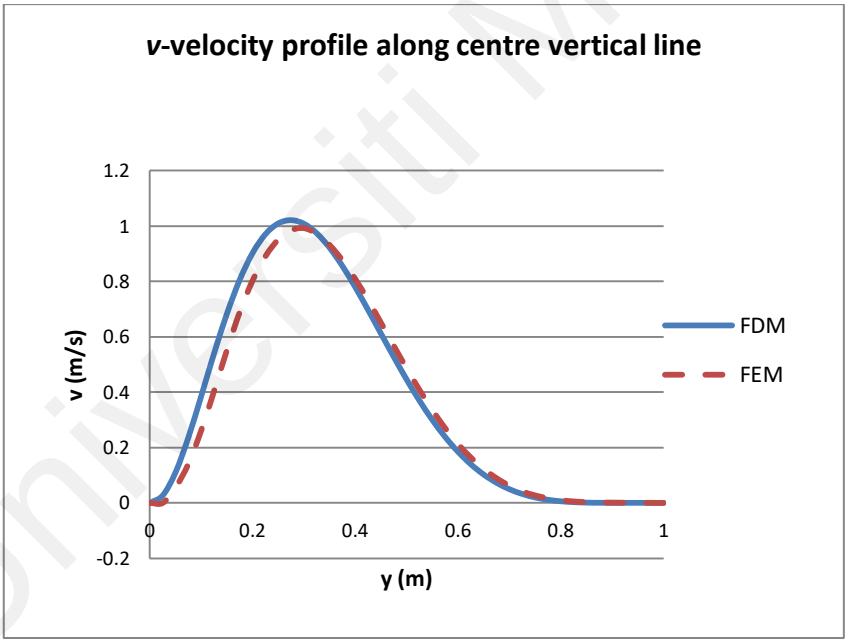

(b)

Figure 4.14: Comparison of results using FDM and FEM (a) *u*-velocity profile (b) *v*-velocity profile

Universiti Malaya

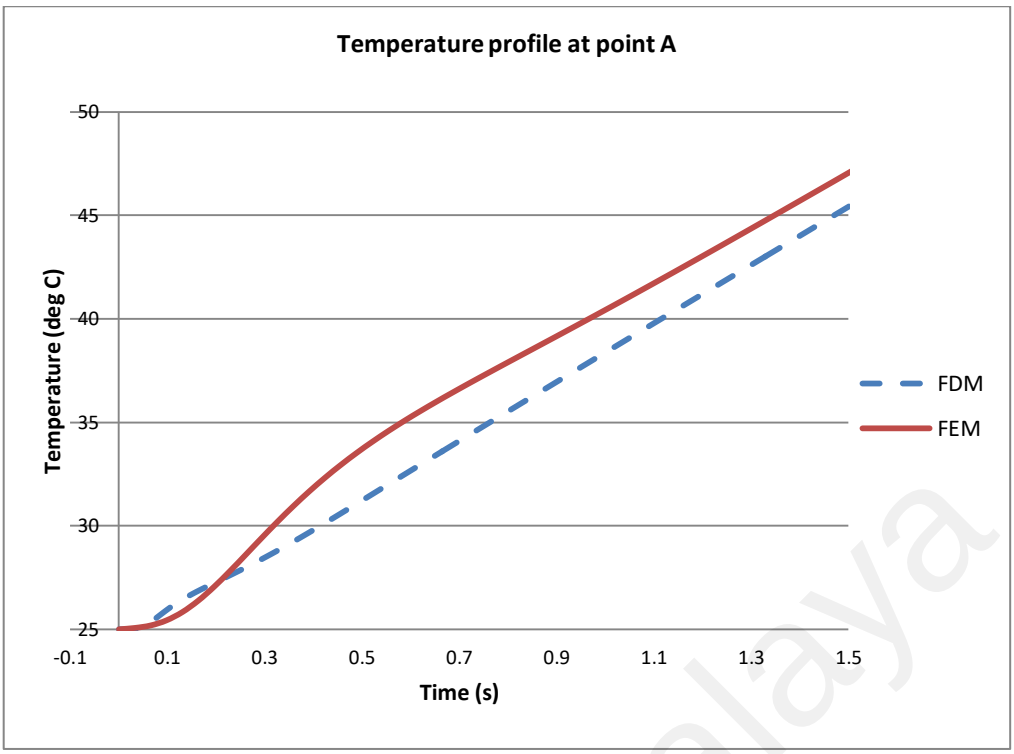

Figure 4.15: Comparison of temperature profile at point A between FDM and FEM

Once the in-house Matlab® code (FDM) is verified using Ansys Fluent®, 2nd test case (free-slip BC) is then simulated using FDM. Stream function, temperature distribution and location of maximum temperature, T_{max} for the 2nd test case are shown in Figure 4.16. Temperature distributions are quite similar in both no-slip (1st test case) and free-slip (2nd test case) BCs. The heat is generated from the moving top lid and concentrated at the top right corner first. Subsequently heat is slowly propagated to the right bottom corner and to the entire cavity. However, the overall temperature distribution is lower when the lid-driven flow is subject to free-slip BC. Comparison of temperature profile at point A for both test cases is shown in Figure 4.17.

Universiti Malaya

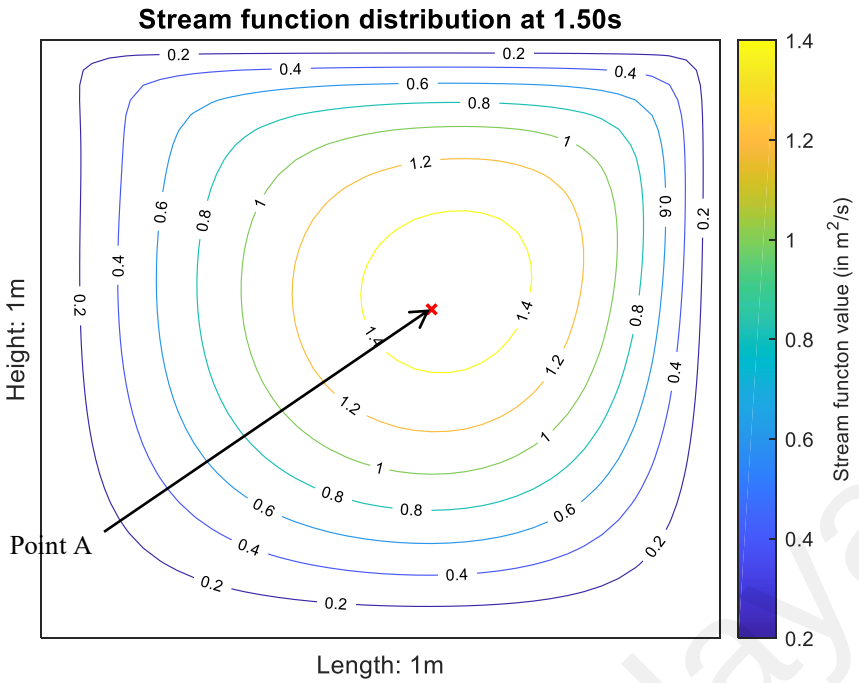

(a)

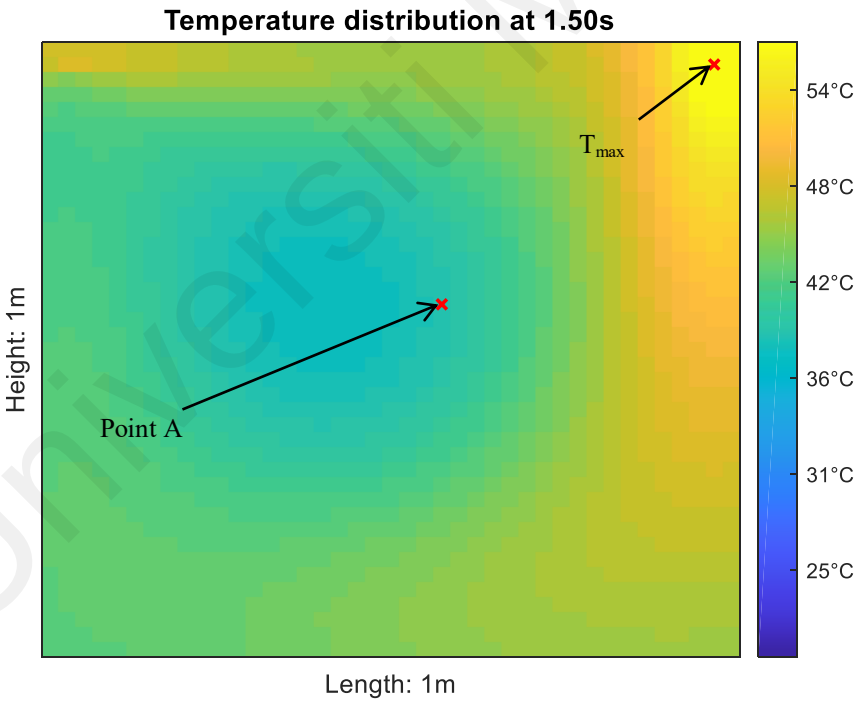

(b)

Figure 4.16: (a) Stream function and (b) temperature distribution for 2nd test case

Universiti Malaya

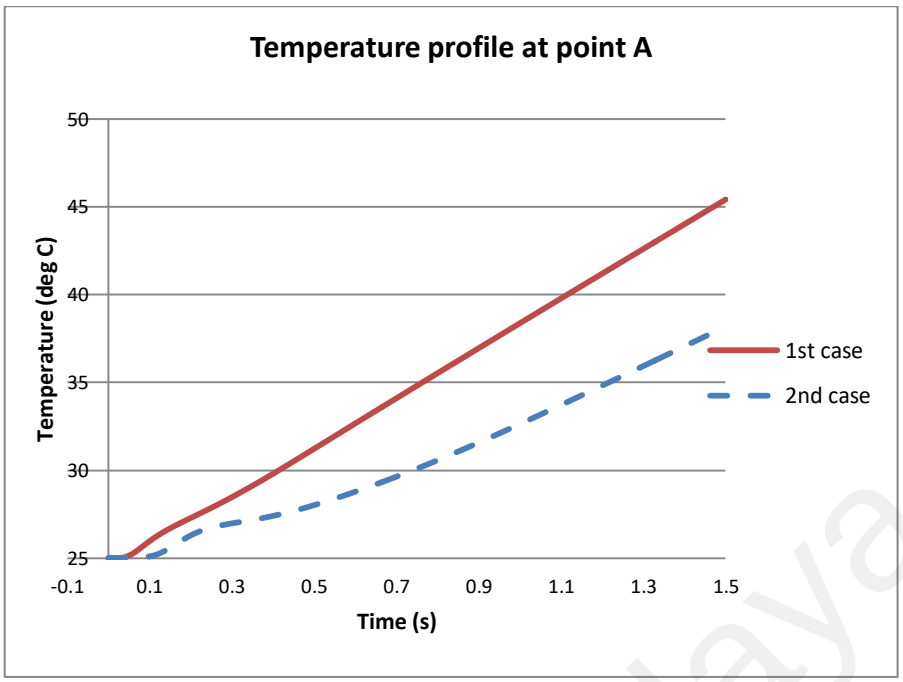

Figure 4.17: Temperature profile at point A along the iteration for the 1st test case (no-slip) and 2nd test case (free-slip)

Both BCs show the similar trend in temperature profile at point A and keep increasing, but no-slip BC gives an upper offset than free-slip BC as shown in Figure 4.17. This is due to the free-slip of the fluid at the wall or solid interface and no frictional heat can be generated at the wall. These two benchmarks (1st and 2nd test cases) are then compared with the 3rd and 4th test cases (with lower Reynold number, Re_L) as shown in Figure 4.18. The 3rd and 4th cases show a reduction in temperature profile due to the lower value of applied velocity, U_{wall} which will lead to a smaller stream function distribution in the whole lid-driven flow as prescribed by Equation (3.11) and Equation (3.12). Because of the last term on the right-hand side of TEE or Equation (3.45), the viscous heating term is much related to the stream function, $\psi_{\max}$ and the resultant viscous heating will bring about reduction in the temperature profile of point A, $T(\psi_{\max})$. Also, it is observed that the steady-state period at $e = 10^{-5}$ for 3rd and 4th test cases are longer than 1st and 2nd test case respectively.

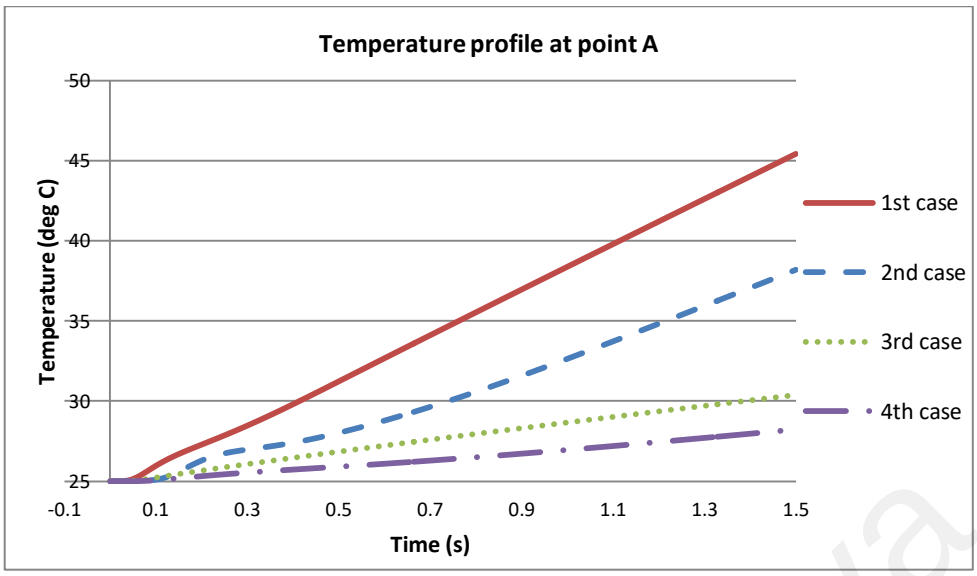

Figure 4.18: Temperature profile at point A ($\mathbf{Re}_L = 100$ VS $\mathbf{Re}_L = 50$)

The benchmarks of 1st and 2nd test cases are then compared with the 5th and the 6th test cases (with higher Prandtl number, Pr than those benchmarks) as shown in Figure 4.19.

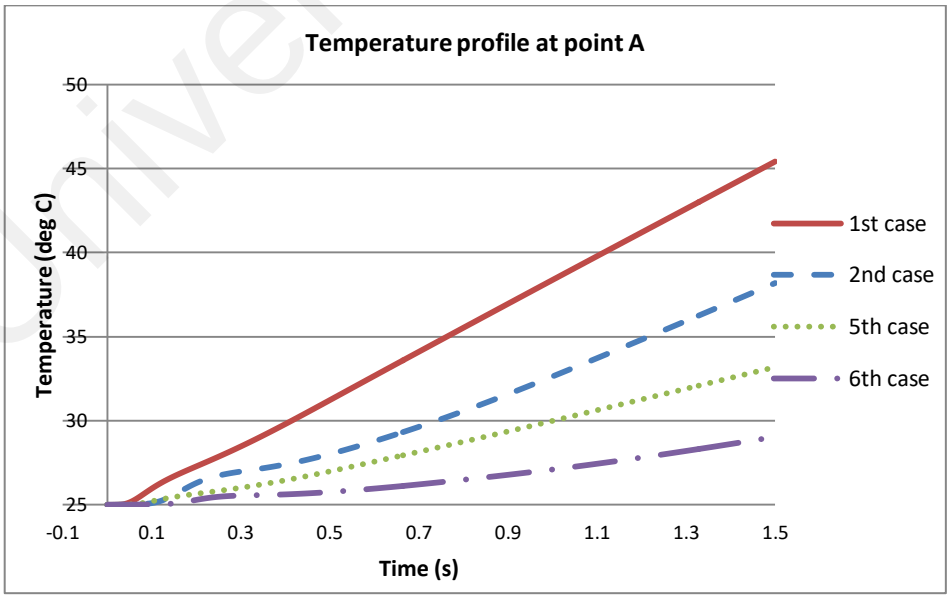

Figure 4.19: Temperature profile at point A ($Pr = 1$ VS $Pr = 2$)

Universiti Malaya

Both the test cases (no-slip and free-slip BCs) show lower temperature profiles at point A when they are compared with the benchmarks. This is due to the fact of Prandtl number, Pr where it is directly proportional with specific heat, c. Greater Prandtl number, Pr corresponds to a higher value of specific heat, c and hence will result a reduction in thermal boundary layer thickness. Recall that Prandtl number, Pr can be related to the relative thickness of momentum and energy transport by diffusion in the velocity and thermal boundary layers which is given by Equation (4.5) (Incropera F., Dewitt D., Bergman T., Lavine A., 2006):

$$\mathrm{Pr} = \frac{\delta}{\delta_t}, \tag{4.5}$$

where δ is thickness of the velocity boundary layer and δ_t is thickness of the thermal boundary layer.

It is also noticeable that the steady-state period at criterion of $e = 10^{-5}$ for the 5th and 6th test cases are the same with benchmarks. Although fluid flow has attained steady-state condition as elucidated in Figure 4.12, there is no steady-state condition can be observed in temperature profile in all test cases as shown in Figure 4.17 and Figure 4.18. Moreover, temperature profile increases in quasi-linear behaviour even though Equation (3.45) is an elliptic equation (Chapra S. C. & Canale R. P., 2006) due to the moving top lid provides finite heat flux to the entire lid-driven. Due to free-slip BC, the 2nd and the 4th test cases show a longer steady-state period of $e = 10^{-5}$ than the test cases with no-slip BC. It is also can be deduced that the temperature profile at point A (or even at any point inside the cavity fluid) will keep increasing if the iteration is extended at any period.

A schematic drawing which is showing the reason why temperature profile keeps increasing is shown in Figure 4.20. Each of the fluid layers is being sheared relative to each other and this will create viscous heating caused by the fluid viscosity. The heat is being trapped inside

Universiti Malaya

the cavity flow by the insulated walls and there is no way to escape. Thus, temperature profile at every point inside the cavity flow (or temperature distribution of the cavity flow) will keep increasing.

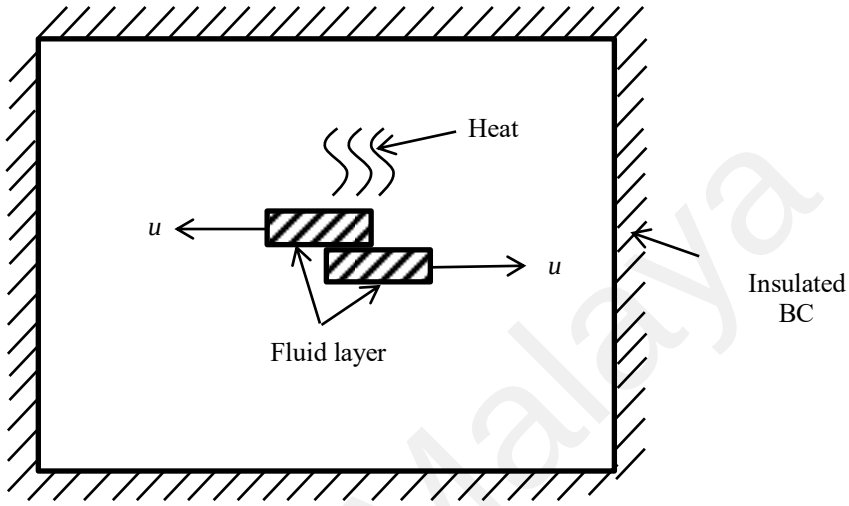

Figure 4.20: Schematic drawing of viscous heating inside the insulated BC

1st test case is rerun at unsteady-state condition for 3.00 s as shown in Figure 4.21 and it proves that temperature profile is increasing quasi-linearly. A good comparison is observed in between FDM and FEM. If the solution is extended to any period in this Neumann BC, the temperature at any point within the lid-driven model will keep increasing. If the value of applied force, dynamic viscosity and thermal conductivity is greater, then the whole temperature distribution of the lid-driven model will increase. The trapped heat in Neumann BC is useful for energy efficiency and heat insulation for building application such in to insulate the whole building during the winter season. Besides, the trapped heat is beneficial for energy renewable application.

Universiti Malaya

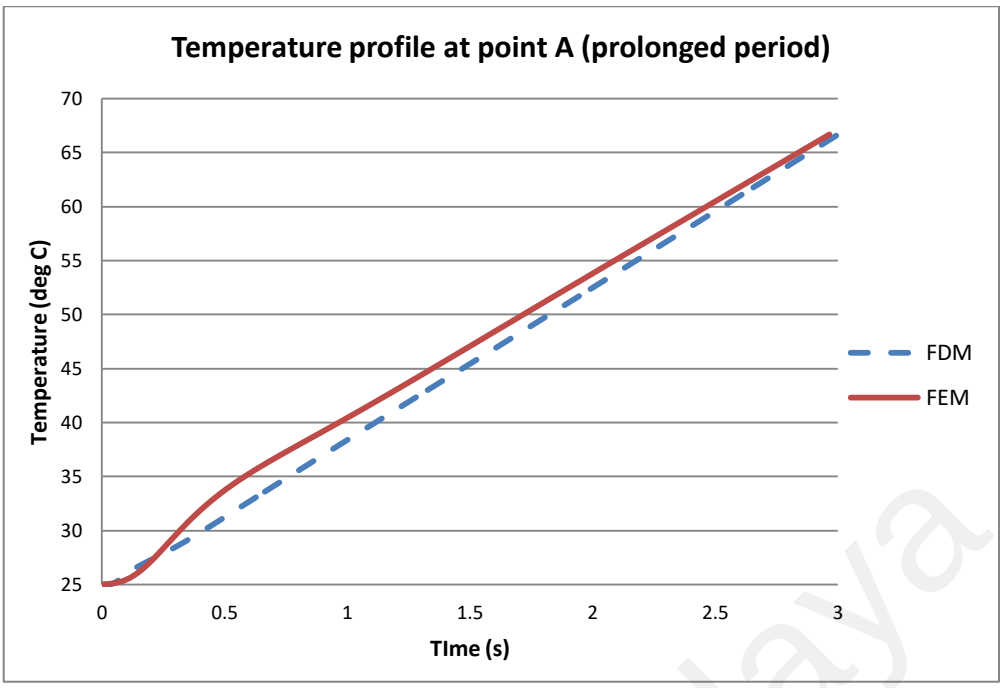

Figure 4.21: Temperature profile at point A (1st test case at prolonged period)

4.3 Lid-driven Cavity Fluid Subject to Robin BC

The model used in Section 4.2 (with different fluid properties i.e. fluid density, ρ is set to 10 kg/m^3, dynamic viscosity, $\mu = 1$ $Pa.s$,) is repeated but subject to Robin BC (third kind of BC) and subject to natural convection due to its ambient air. There are ten case studies to characterize the flow field and temperature distribution in a two-dimensional lid-driven model exposed to ambient air walls considered in order to understand the effects of viscous heating and cooling process in both no-slip and free-slip BCs. All test cases are subject to different flow conditions, different temperature, different thermal property and different size of square cavity are performed in a laminar and unsteady iterative procedure until the analysis period, $t = 2.0$ s is achieved in the first step (viscous heating) and second step (cooling process once the top shear force is removed) respectively in our analysis. Then, free-slip BC with slip length value, $l_s = 1$ m

is assigned in second, fourth, sixth, eighth and tenth test cases while the no-slip BC is assigned with slip length value, $l_s = 0\ m$ in other test cases. Table 4.3 shows the independent variables used in all these test cases.

Table 4.3: Flow conditions of ten test cases

Case	U_{wall} (m/s)	k $(W/m.K)$	size $(m \times m)$	l_s (m)	Pr	Re	Initial temperature (^oC)
1.	10	10	1×1	0	1	100	50
2.	10	10	1×1	1	1	100	50
3.	15	10	1×1	0	1	150	50
4.	15	10	1×1	1	1	150	50
5.	10	10	1×1	0	1	100	25
6.	10	10	1×1	1	1	100	25
7.	10	10	0.5×0.5	0	1	50	50
8.	10	10	0.5×0.5	1	1	50	50
9.	10	20	1×1	0	0.5	100	50
10.	10	20	1×1	1	0.5	100	50

In this section, the 1st and the 2nd test cases will serve as the benchmarks (both cases with identical fluid and thermal properties, identical thermal condition but subject to no-slip and free-slip BCs) for comparison with other test cases. Location of the center of whole lid-driven cavity is denoted as point A ($x = 0.5\ m$, $y = 0.5\ m$) as shown in Figure 4.22. In the meanwhile, T_{max} means the location of maximum temperature and T_{min} means the location of minimum temperature. Temperature distribution of lid-driven cavity at somewhere of second step at t = 2.80 s (cooling process) is shown in Figure 4.23.

Universiti Malaya

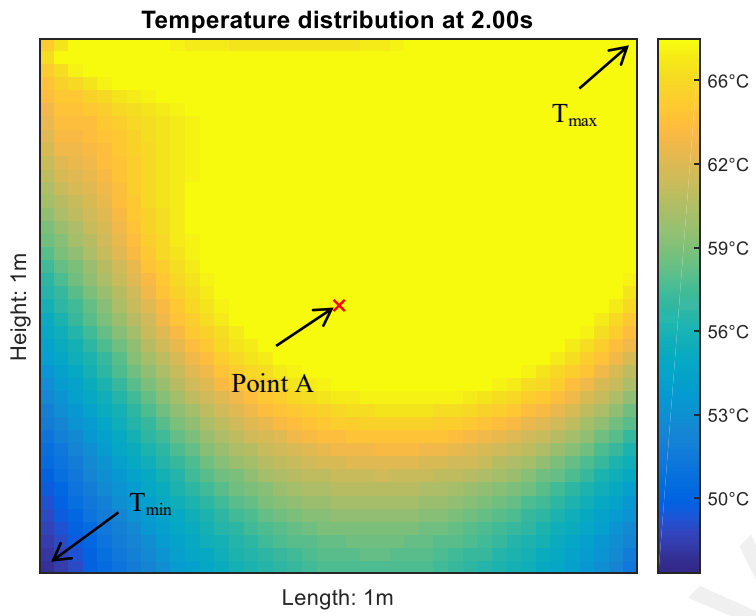

(a)

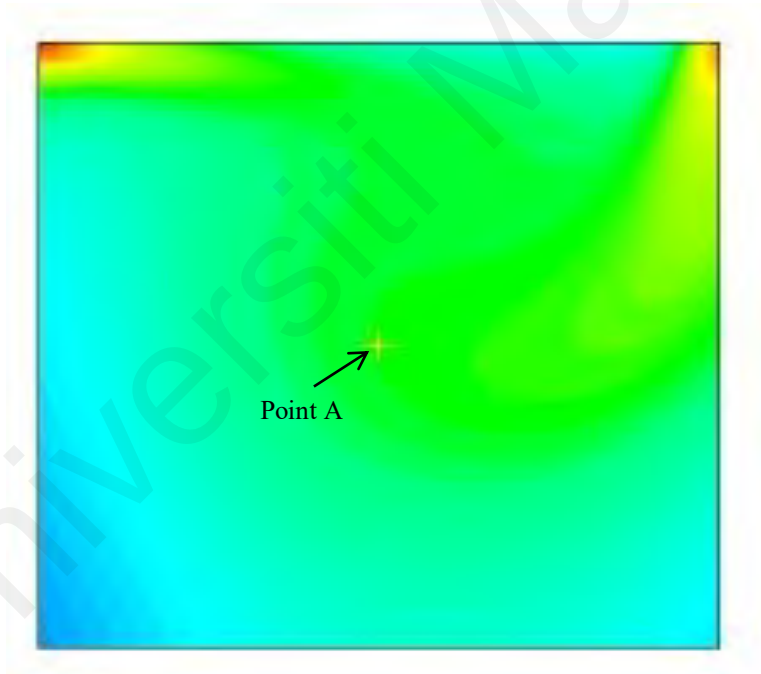

(b)

Figure 4.22: Comparison of image plot of temperature distribution at *t* = 2.00 *s* using (a) FDM in Matlab® (b) FEM in Ansys Fluent®

Universiti Malaya

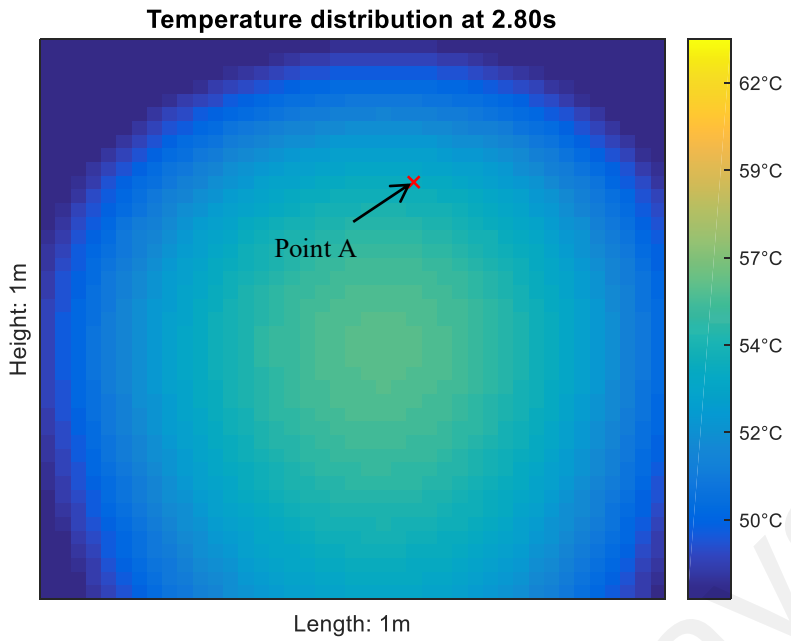

Figure 4.23: Temperature distribution at *t* = 2.80 *s*

Once the in-house Matlab® code (FDM) is verified using Ansys Fluent®, the 2nd test case (free-slip BC) is then simulated using FDM. Temperature profile at point A for the 1st and 2nd test cases are compared from viscous heating until cooling process as shown in Figure 4.24.

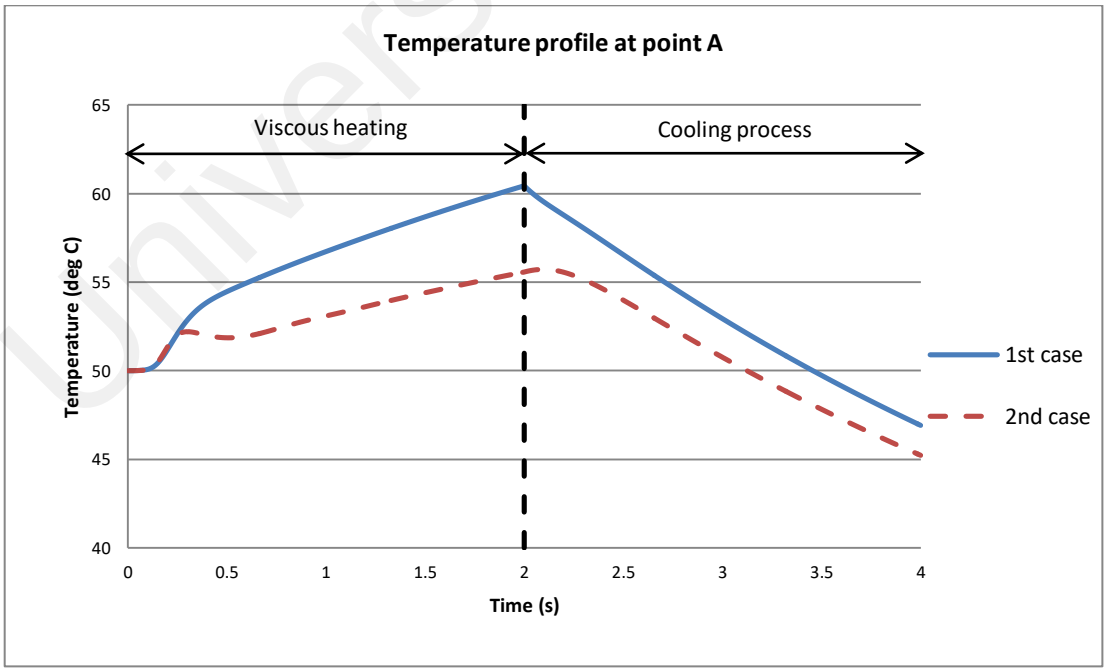

Figure 4.24: Comparison of temperature profile at point A for the 1st and 2nd test cases

Based on Figure 4.24, temperature profile at point A shows a lower profile when the lid-driven cavity flow is subject to free-slip BC. This is owing to the free-slip of the fluid at the wall or solid interface and no frictional heat can be generated at the wall. In no-slip BC, temperature profile shows an obvious reduction at the beginning of cooling process whereas it shows a blunted profile in free-slip BC. Temperature profile does not reduce abruptly in free-slip BC but it still increases once the cooling process is commencing. It reduces dawdlingly after sometimes when the cooling process is launched in free-slip BC. These two benchmarks are then compared with other test cases which subject to different flow and thermal conditions. Figure 4.25 shows the comparison of temperature profile at point A for the 3rd, 5th, 7th and 9th test cases with the benchmark (all test cases are in no-slip BC).

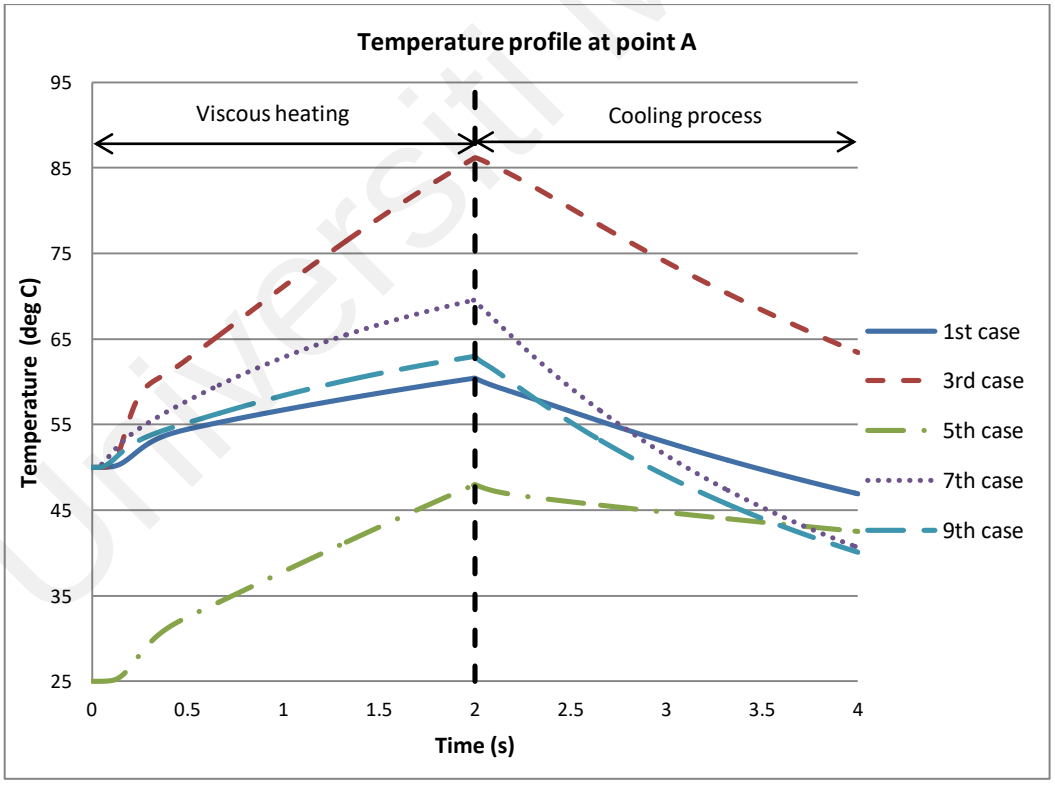

Figure 4.25: Comparison of temperature profile at point A for the 1st, 3rd, 5th, 7th and 9th test cases

In the 3rd test case, the flow is subject to higher shear velocity at the top lid and thus results in higher Reynolds number, *Re*. Temperature profile of 3rd test case increases by higher *Re* as it contributes to a higher value of stream function, ψ . Because of the last term on the right-hand side of TEE, the viscous heating term is much related to the stream function, ψ and the resultant viscous heating will bring up the temperature profile of point A. When initial temperature, T_i of the whole fluid inside the lid-driven cavity is reduced in the 5th test case, temperature profile at the point A shows a lower profile if compared with benchmark along the iteration. However, the temperature profile at point A does not reduce much in cooling process because the value of h_{top} , h_{side} and h_{bottom} are lower than benchmark. In as much as the value of T_i and T_∞ are the same, it will bring down the value of Rayleigh number, Ra_L as shown in Equation (3.68) till Equation (3.71). A lower value of convection heat transfer coefficient means the heat transfer rate from lid-driven cavity to its ambient environment is low. Table 4.4 shows the value of h_{top} , h_{side} and h_{bottom} for all test cases. Also, Table 4.4 proves the relation as shown in Equation (3.81) is correct provided the size of length, *L* is the same as size of height, *H*.

Table 4.4: Value of different type of convection heat transfer coefficient

No.	# of test cases	h_{top} $(W/m^2.K)$	h_{side} $(W/m^2.K)$	h_{bottom} $(W/m^2.K)$
1.	1st till 4th, 9th and 10th	6.36	5.05	1.81
2.	5th and 6th	2.82	2.38	0.98
3.	7th and 8th	6.36	5.27	2.15

In the 7th test case, the side of the lid-driven cavity is half of the benchmark and hence the amount of content fluid is a quarter of the benchmark. Although Reynolds number, *Re* for 7th test case is half of the benchmark, temperature profile does not reduce but higher than the benchmark during viscous heating step. The reason is the heat gain process by the quarter amount of fluid during the viscous heating is easier and faster. In cooling process, temperature profile at point A shows a higher reduction rate than benchmark due to higher value of h_{side} and h_{bottom}. A smaller value of length, *L* and height, *H* will increase the value of h_{side} and h_{bottom} as shown in Equation (3.70) and Equation (3.71) respectively. However, the value of h_{top} is the same as benchmark provided the value of $Ra_L \geq 10^7$. Rayleigh number, Ra_L is given by:

$$Ra_L = \frac{g\beta(T_s - T_\infty)L^3}{\nu_{air}\alpha_{air}}, \tag{4.6}$$

where β is volumetric thermal expansion coefficient, ν_{air} is kinematic viscosity and α_{air} is thermal diffusivity of ambient air respectively, T_s is surface temperature at wall.

By combining Equation (4.6) and Equation (3.69), h_{top} can be expressed as:

$$h_{top} = 0.15\left(\frac{g\beta[T_s - T_\infty]}{\nu\alpha}\right)^{1/3}.k_{air}. \tag{4.7}$$

Thus, h_{top} is independent of the size of length, *L*. The value of thermal conductivity, k of fluid in the 9th test case is doubled than benchmark. Hence, its Prandtl number, *Pr* is half of the benchmark. By recalling Equation (4.5), the smaller Prandtl number, Pr corresponds to a higher value of thermal conductivity, k and hence will result an increase in thermal boundary layer thickness and it helps to increase the temperature profile at point A during viscous heating. Because of higher value of thermal conductivity, k, it helps to transfer the heat from fluid inside

Universiti Malaya

the lid-driven cavity to ambient air and results an increase in reduction rate of temperature profile at point A during cooling process when compared to benchmark. Figure 4.26 shows the comparison of temperature profile at point A for the 4th, 6th, 8th and 10th test cases with the benchmark (all test cases are in free-slip BC).

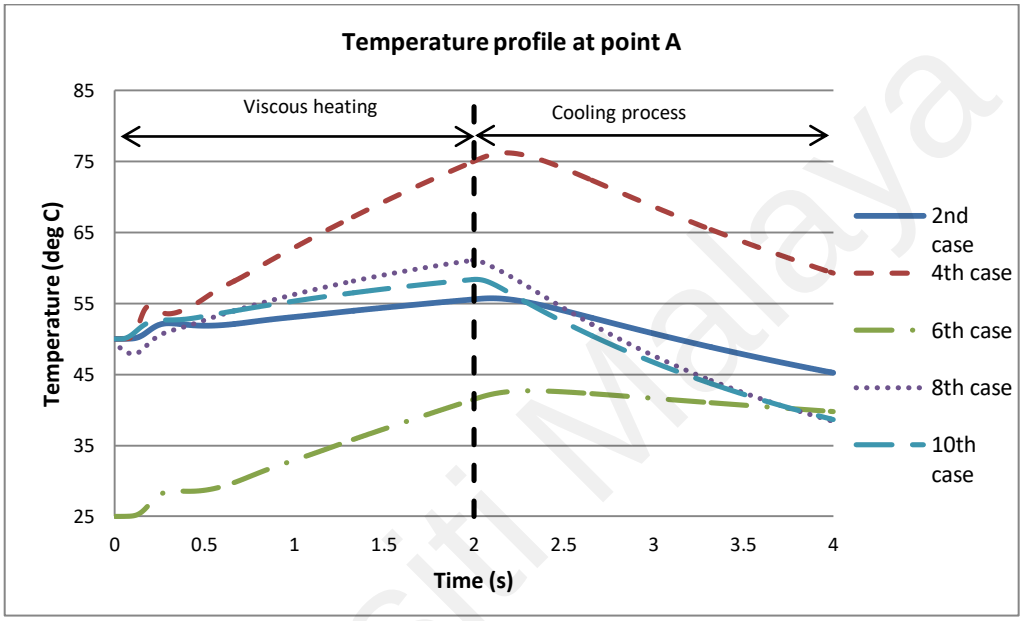

Figure 4.26: Comparison of temperature profile at point A for the 2nd, 4th, 6th, 8th and 10th test cases

Temperature profile at point A shows a similar trend in both Figure 4.25 and Figure 4.26 but all the temperature profiles at point A are lower as shown in Figure 4.26 if compared with Figure 4.25. The reason has been explained beforehand as no frictional heat can be generated along the walls. In free-slip BC, fluid is able to slip along the wall boundaries and does not stop instantaneously even though the applied shear force at the top lid is removed at the beginning of cooling process. Inertial behaviour of the fluid itself causes it to keep moving and only stop flowing after a while once the applied shear force is removed. The movement of fluid is still able to create viscous heating at the beginning of the cooling process especially at high Reynolds

number, *Re* (4th test case) during the viscous heating process. By definition, Reynolds number is also given by:

$$\mathrm{Re} = \frac{Inertial_force}{Viscous_force}. \tag{4.8}$$

Higher Reynolds number, *Re* corresponds to a higher inertial force. The effect of increasing temperature at the beginning of the cooling process ($t = 2\ s$) is shown as Figure 4.27.

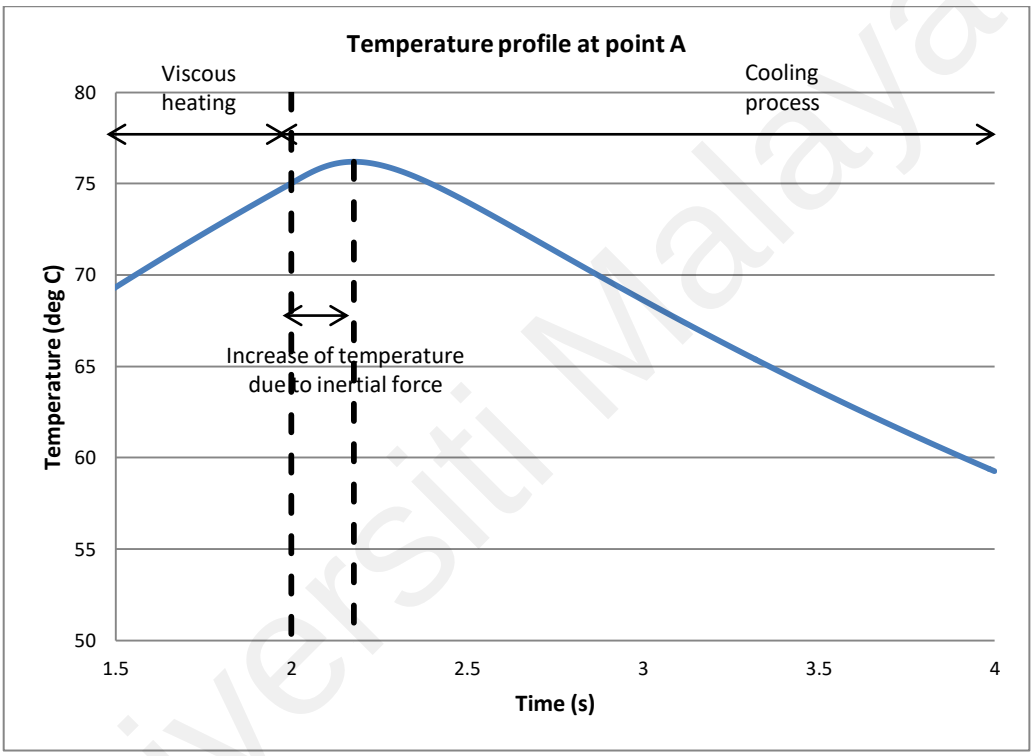

Figure 4.27: Increase of temperature due to inertial force (4th test case)

Fluid only stops flowing after sometimes at the beginning of the cooling process. Finally, fluid totally stops flowing as inertial force diminishes and stops creating viscous heating and eventually temperature profile at the point A starts reducing.

Universiti Malaya

4.4 Comments

Some comments have been made based on the results shown in section 4.1, section 4.2, section 4.3 and theories discussed in chapter 3.

a) A very good agreement of these results between explicit FDM used in this GUI and finite element method used in FEA software i.e. Ansys Fluent®.

b) Table 4.5 and Table 4.6 show some advantages and disadvantages between the usage of this GUI and FEA software respectively.

Table 4.5: Advantages of GUI and FEA

	GUI	FEA Software
Advantages	a) The knowledge of fundamental of heat transfer is not needed in using this software. b) No technical meshing is needed. c) Modeling is not needed. d) Be able to detect the error when entering the inputs. e) It will guide the user when entering the number of nodes in order to generate the accuracy result. f) Plot of stream function, *u*- and *v*-velocity and velocity vector are well-displayed.	a) Can simulate a lot of models. b) Can simulate the complicated boundary condition and geometry. c) Shorter computation time due to larger value of step time is allowed. d) Temperature-dependent material properties can be assigned.

Universiti Malaya

Table 4.6: Disadvantages of GUI and FEA

Disadvantages	a) Only limited to simple rectangular model. b) Only valid for lid-driven model. c) Long computation time due to limited value of step time increment. d) Limited to analysis with Re up to 300.	a) Some fundamentals of fluid mechanics and heat transfer are needed when using FEA software like calculation of convection coefficient. b) Technical meshing is needed. c) Modeling is needed. d) Can only detect the pre-processing error after the job has been submitted. e) The user has to decide how small the mesh in order to obtain the high accuracy result. f) The user has to manipulate the time-parameter graph.

Universiti Malaya

CHAPTER 5: CONCLUSION & RECOMMENDATIONS

This chapter reviews overall conclusions and recommendations made on the analysis of findings shown in previous chapters. Some discussions on the conclusion of the study and suggestion for future works are included in this section.

5.1 Conclusion

In this thesis, a simple user friendly GUI has been successfully developed after the literature and fundamental studies have been done. Basically, this thesis comprises the fundamental of fluid mechanics study, numerical method in solving the NSEs, programming and GUI design by using Matlab®, the use of Ansys Fluent® as FEA software in comparing the result obtained from in-house Matlab® code. The simple GUI was built based on some presumptions, approximation due to numerical method and simplification. The result shown by this GUI still agreeable with result obtained from Ansys Fluent®. Boussinesq approximation and TEE can also be included into this GUI easily. Accuracy in term of thermal analysis still can be increased by including the radiation or forced convection heat transfer, non-uniform convection or radiation heat transfer coefficient, non-constant value of thermal diffusivity and others can be taken into account in this GUI. One should bear in mind that inclusion of these effects will make the involved algorithm more complicated in this program.

Vorticity-stream function scheme was successfully derived and a simple forward FDM was formed to solve this scheme along this project. The fluid flow and thermal analyses of lid-driven cavity model were conducted using an in-house Matlab® code and verified by Ansys Fluent®. Although this scheme seems simple, it is manageable to feature and differentiate the flow pattern in both no-slip and free-slip BCs quantitatively by observing the stream function

Universiti Malaya

and temperature distributions. By executing iteration smaller than the steady-state criterion of $e \leq 10^{-8}$ it does not make any changes to the results and it would only bring about numerical error, longer computational effort and hence results in futile.

By assigning Neumann BC to the lid-driven model, temperature profile shows an increasing trend in all test cases as the produced constant heat flux is supplied continuously by the moving top lid. If the iteration period is prolonged to any other period, temperature profile of these test cases will keep increasing. This is the reason why the surface temperature of meteorite during its free-fall keep increasing although frictional heating or viscous heating due to the atmospheric air contributes very small portion of heat. The lower value of Reynolds number, *Re*, the lower value of thermal diffusivity, α and free-slip effect of the fluid flow can create a lower temperature distribution, while a greater value of Prandtl number, *Pr* can reduce the temperature distribution inside the lid-driven model.

In order to take into account the effect of natural convection of ambient air, Robin BC was assigned to this lid-driven model. Temperature profile of each test case in no-slip BC shows a similar trend in its free-slip BC respectively but in lower, blunted profile and reduces dawdlingly once top shear force at the top lid is removed as the cooling process is launched especially when subject to higher Reynolds number, *Re*. Inertial force is dominating and is still able to create viscous heating and hence contributes to increase of temperature until the inertial force diminishes. We have proved that higher convection heat transfer coefficient h_{top}, h_{side}, h_{bottom} and a higher thermal conductivity, k assist in increasing reduction rate of temperature profile during the cooling process and make lid-driven cavity cooled down faster. We do not make an assumption on the value of convection heat transfer coefficient, but the values of convection heat transfer coefficient are calculated meticulously based on empirical equation.

Besides, we have proved the relation of $h_{top} > h_{side} > h_{bottom}$ provided the size of length is same as the size of height of the cavity.

Finally, it can be concluded that free-slip BC will cause the fluid to flow faster but can entail a lower temperature profile and temperature distribution much alike as lubricant used in engineering application to lower the temperature during its operation. Last but not least, all the derived equations in Robin BC as shown in Equation (3.57) till Equation (3.64) can be used for Neumann BC by simply setting $h_{top} = h_{side} = h_{bottom} = 0$. Also, free-slip BC as shown in Equation (3.41) till Equation (3.43) can be catered for no-slip BC by simply assigning the slip length, $l_s = 0$.

5.2 Recommendations

Some of recommendations can be made to improve this current project and hopefully can give some ideas for any student or anyone who is keen and has enthusiasm to accept the challenge. The recommendations are shown as below:

a) Thermal analysis can be included into this GUI as shown in Section 3.11 by including TEE.

b) Newtonian fluid filled inside the lid-driven cavity flow in this project can be replaced by any non-Newtonian fluid. The governing non-Newtonian fluid flow equation can be derived and shown in Section 3.8. However, FDM is not feasible in solving the governing equation and its difficulty has been explained in Section 3.8.1 and Section 3.8.2. The suggested numerical method to solve the governing equation of non-Newtonian fluid flow is FEM.

Universiti Malaya

c) If the bottom wall of this lid-driven model is heated and has a temperature higher than top lid, then buoyancy effect will happen inside the cavity flow. Thus, Boussinesq approximation should be included in TEE.

d) A great suggestion can be proposed to analyze the mixed convection heat transfer lid-driven model under different multi-physical scenario.

e) Rotational lid-driven can be constructed and share some same ideas with this 2D lid-driven model. However, it will be 3D cylindrical model and all the governing equations should be expressed in cylindrical coordinate system. Figure 5.1 shows the suggested rotational lid-driven model:

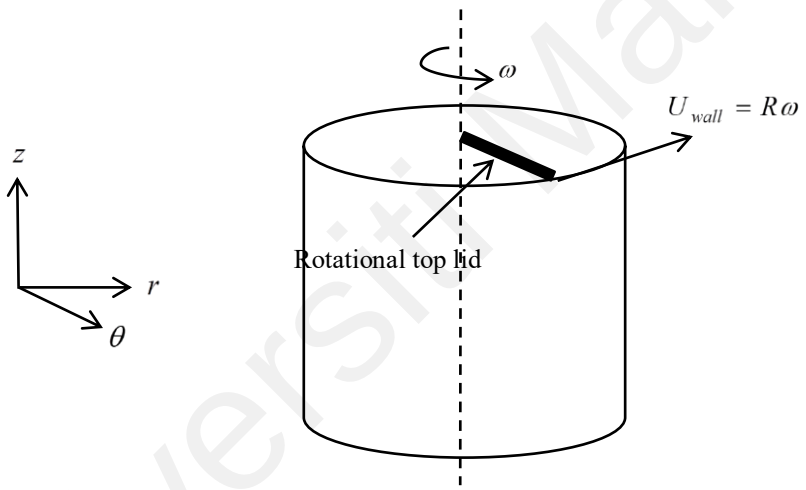

Figure 5.1: Rotational lid-driven model

Implementation of FDM to solve this model is still possible. All the governing equations are shown as below:

$$\frac{1}{r}\frac{\partial(rv_r)}{\partial r}+\frac{1}{r}\frac{\partial v_\theta}{\partial \theta}+\frac{\partial v_z}{\partial z}=0 \text{ (continuity equation)}, \tag{5.1}$$

$$\rho\left(\frac{\partial v_r}{\partial t}+v_r\frac{\partial v_r}{\partial r}+\frac{v_\theta}{r}\frac{\partial v_r}{\partial \theta}-\frac{v_\theta^2}{r}+v_z\frac{\partial v_r}{\partial z}\right)=-\frac{\partial p}{\partial r}+pg_r$$
$$+\mu\left[\frac{1}{r}\frac{\partial}{\partial r}\left(r\frac{\partial v_r}{\partial r}\right)-\frac{v_r}{r^2}+\frac{1}{r^2}\frac{\partial^2 v_r}{\partial \theta^2}-\frac{2}{r^2}\frac{\partial v_\theta}{\partial \theta}+\frac{\partial^2 v_r}{\partial z^2}\right] \quad \text{(in } r- \text{ direction)}, \tag{5.2}$$

$$\rho\left(\frac{\partial v_\theta}{\partial t}+v_r\frac{\partial v_\theta}{\partial r}+\frac{v_\theta}{r}\frac{\partial v_\theta}{\partial \theta}+\frac{v_r v_\theta}{r}+v_z\frac{\partial v_\theta}{\partial z}\right)=-\frac{1}{r}\frac{\partial p}{\partial \theta}+pg_\theta$$
$$+\mu\left[\frac{1}{r}\frac{\partial}{\partial r}\left(r\frac{\partial v_\theta}{\partial r}\right)-\frac{v_\theta}{r^2}+\frac{1}{r^2}\frac{\partial^2 v_\theta}{\partial \theta^2}+\frac{2}{r^2}\frac{\partial v_r}{\partial \theta}+\frac{\partial^2 v_\theta}{\partial z^2}\right] \quad \text{(in } \theta- \text{ direction)}, \tag{5.3}$$

$$\rho\left(\frac{\partial v_z}{\partial t}+v_r\frac{\partial v_z}{\partial r}+\frac{v_\theta}{r}\frac{\partial v_z}{\partial \theta}+v_z\frac{\partial v_z}{\partial z}\right)=$$
$$-\frac{\partial p}{\partial z}+pg_z+\mu\left[\frac{1}{r}\frac{\partial}{\partial r}\left(r\frac{\partial v_z}{\partial r}\right)+\frac{1}{r^2}\frac{\partial^2 v_z}{\partial \theta^2}+\frac{\partial^2 v_z}{\partial z^2}\right] \quad \text{(in } z- \text{ direction)}, \tag{5.4}$$

where v_r is velocity in $r-$direction, v_θ is velocity in $\theta-$direction, v_z is velocity in $z-$direction, $g_r = g_\theta = g_z = g$ is gravity acceleration and R is radius of the cylinder

Universiti Malaya

REFERENCES

Lecture 4: Finite difference method. (2017). TU Dortmund Universtiy. http://www.mathematik.unidortmund.de/~kuzmin/cfdintro/lecture4.pdf

Ababaei, A., Abbaszadeh, M., Arefmanesh, A., & Chamkha, A. J. (2018). Numerical simulation of double-diffusive mixed convection and entropy generation in a lid-driven trapezoidal enclosure with a heat source. *Numerical Heat Transfer; Part A: Applications*, *73*, 702-720.

Abd-El-Hafiz, S. K., Ismail, G.A. F., & Matit, B. S. (2004). Efficient numerical solution of 3D incompressible viscous Navier-Stokes equations. *International Journal of Pure and Applied Mathematics, 13*(3), 391-411.

Abu-Nada, E., & Chamkha, A. J. (2010). Mixed convection flow in a lid-driven inclined square enclosure filled with a nanofluid. *European Journal of Mechanics - B/Fluids*, *29*, 472-482.

Abu-Nada, E., & Chamkha, A. J. (2014). Mixed convection flow of a nanofluid in a lid driven cavity with a wavy wall. *International Communications in Heat and Mass Transfer*, *57*, 36-47.

Admin (2016). *Why is Rubber a Good Insulator?* Coruba. https://www.coruba.co.uk/blog/why-is-rubber-a-good-insulator/

Albright, M. D., Reed, R. J., & Ovens, D. W. (1995). Origin and structure of a numerically simulated polar low over Hudson bay. *Tellus A: Dynamic Meteorology and Oceanography, 47*, 834-848.

Alsabery, A. I., Ismael, M., Chamkha, A. J., & Hashim, I. (2018). Mixed convection of Al2O3-water nanofluid in a double lid-driven square cavity with a solid inner insert using Buongiorno's two-phase model. *International Communications in Heat and Mass Transfer, 119*, 939-961.

Alsabery, A. I., Ismael, M. A., Chamkha, A. J., & Hashim, I. (2019a). Effects of two-phase nanofluid model on MHD mixed convection in a lid-driven cavity in the presence of conductive inner block and corner heater. *Journal of Thermal Analysis and Calorimetry, 135*, 729-750.

Alsabery, A. I., Sheremet, M. A., Chamkha, A. J., & Hashim, I. (2019b). Impact of nonhomogeneous nanofluid model on transient mixed convection in a double lid-driven wavy cavity involving solid circular cylinder. *International Journal of Mechanical Sciences, 150*, 637-655.

Alsabery, A. I., Armaghani, T., Chamkha, A. J., Sadiq, M. A., & Hashim, I. (2019c). Effects of two-phase nanofluid model on convection in a lid-driven cavity in the presence of a magnetic field. *International Journal of Numerical Methods for Heat & Fluid Flow, 29*, 1272-1299.

Universiti Malaya

Alsabery, A. I., Armaghani, T., Chamkha, A. J., Sadiq, M. A., & Hashim, I. (2020a). Two-phase nanofluid model and magnetic field effects on mixed convection in a lid-driven cavity containing heated triangular wall. *Alexandria Engineering Journal*, *59*, 129-148.

Alsabery, A. I., Sheremet, M. A., Chamkha, A. J., & Hashim, I. (2020b). Energy transport of two-phase nanofluid approach inside a three-dimensional lid-driven cubic cavity containing solid cylinder and heat source. *Chemical Engineering and Processing*. *154*, Article 108010.

Aly, A. M., Chamkha, A. J., Lee, S. W., & AlMudhaf, A. F. (2016). On mixed convection in an inclined lid-driven cavity with sinusoidal heated walls using ISPH method. *Computational Thermal Sciences*, *8*, 337-354.

Anderson, J. D. (2003). *Modern compressible flow: with historical perspective* (3rd ed.). New York: McGraw-Hill.

Arthur, C. C. (2000, April). *Meteors burn up when they hit Earth's atmosphere. Why doesn't the space shuttle?* howstuffworks. https://science.howstuffworks.com/question308.htm

Aydin, O. (2005a). Effects of viscous dissipation on the heat transfer in a forced pipe flow. Part 2: Thermally developing flow. *Energy Conversion and Management, 46*, 3091-3102.

Aydin, O. (2005b). Effects of viscous dissipation on the heat transfer in forced pipe flow. Part 1: Both hydrodynamically and thermally fully developed flow. *Energy Convers. Manage., 46*, 757-769.

Aydin, O. & Avci, M. (2006). Heat and fluid flow characteristics of gases in micropipes. *International Journal of Heat and Mass Transfer, 49*, 1723-1730.

Aydin, O. & Avci, M. (2007). Analysis of laminar heat transfer in micro-poiseuille. *International Journal of Thermal Sciences, 46*, 30-37.

Basiri, E., Bryant, R., George, M., & Yerion, K. (2009). A finite difference method for modelling the formation of animal coat pattern. *Nonlinear Analysis Real World Application, 10,* 1730-1737.

Basak, T., Roy, S., & Chamkha, A. J. (2012). A Peclet number based analysis of mixed convection for lid-driven porous square cavities with various heating of bottom wall. *International Communications in Heat and Mass Transfer*, *39*, 657-664.

Black, W. B. (2000). *Wall slip and boundary effects in polymer shear flows (doctoral dissertation)*. University of Wisconsin, Madison, United States. https://grahamgroup.che.wisc.edu/pub/black_dissert.pdf

Bird, R. B., Steward, W. E., & Lightfoot, E. N. (2002). *Transport phenomena.* New York: John Wiley & Sons.

Biswas, N. & Manna, N. K. (2018). Magneto-hydrodynamic Marangoni flow in bottom-heated lid-driven cavity. *Journal of Molecular Liquids, 251*, 249-266.

Universiti Malaya

Botella, O. & Peyret, R. (1998). Benchmark spectral results on the lid-driven cavity flow. *Computers & Fluids, 27*, 421-433.

Bourke, J.D., & Chantler, C.T. (2010). Finite difference method calculations of long-range X-ray absorption structure for copper over k=20A-1. *Nuclear Instruments and Methods in Physics Research, 619*, 33-36.

Chamkha, A. J. (2002). Hydromagnetic combined convection flow in a vertical lid-driven cavity enclosure with internal heat generation or absorption. *Numerical Heat Transfer, Part A: Applications*, *41*, 529-546.

Chamkha, A. J. & Abu-Nada, E. (2012). Mixed convection flow in single- and double- lid driven square cavities filled with water-Al2O3 nanofluid: Effect of viscosity models. *European Journal of Mechanics - B/Fluids. 36*, 82-96.

Chamkha, A. J. & Ismael, M. A. (2016). Magnetic field effect on mixed convection in lid-driven trapezoidal cavities filled with a Cu-water nanofluid with an aiding or opposing side wall. *Journal of Thermal Science and Engineering Applications*, *8*, 031009-031009-12.

Chamkha, A. J., Rashad, A. M., Armaghani, T., & Mansour, M. A. (2017a). Effects of partial slip on entropy generation and MHD combined convection in a lid-driven porous enclosure saturated with a Cu-water nanofluid. *Journal of Thermal Analysis and Calorimetry*, *132*, 1291-1306.

Chamkha, A. J., Rashad, A. M., Mansour, M. A., Armaghani, T., & Ghalambaz, M. (2017b). Effects of heat sink and source and entropy generation and MHD mixed convective of a Cu-water nanofluid in a lid-driven square porous enclosure with partial slip. *Physics of Fluids*, *29*, 052001.

Chamkha, A. J., Selimefendigil, F., & Oztop, H. (2018). MHD mixed convection and entropy generation in a lid-driven triangular cavity for various electrical conductivity models. *Entropy*, 20 (003).

Chapra, S. C., & Canale, R. P. (2006). *Numerical methods for engineers* (5th ed.). New York: McGraw Hill.

Coelho, P. M., & Pinho, F. T. (2006). Fully-developed heat transfer in annuli with viscous dissipation. *International Journal of Heat and Mass Transfer, 49*, 3349-3359.

Dass, H. K. (1988). *Advanced engineering mathematics.* New Delhi: S. Chand & Company Ltd.

Deshpande, A. P, Krishnan, J. M., & Kumar, S. (2010). *Rheology of complex fluids.* New York: Springer-Verlag (eds).

Fang, Q., Tsuchiya, T., & Yamamoto, T. (2002). Finite difference, finite element and finite volume method applied to two-point boundary value problem. *Journal of Computational and Applied Mathematics, 139*, 9-19.

Gennady, V. M., Valeryi, A. S., Michael, B. P., & Ahmed, H. P. (2006). Application of finite-difference methods to membrane-mediated protein interactions and to heat and magnetics diffusion in plasmas. *Journal of Computational Physics, 212*, 25-51.

Universiti Malaya

Giudice, S. D., Nonino, C., & Savino, S. (2007). Effects of viscous dissipation and temperature dependent viscosity in thermally and simultaneously developing laminar flows in microchannels. *International Journal of Heat and Fluid Flow, 28*, 15-27.

Hayat, T., Aslam, N., Alsaedi, A., & Rafiq, M. (2017). Numerical study for MHD peristaltic transport of Sisko nanofluid in a curved channel. *International Journal of Heat and Mass Transfer, 109*, 1281-1288.

Incropera, F., Dewitt, D., Bergman, T., & Lavine, A. (2006). *Fundamentals of heat and mass Transfer* (6th ed.). New York: John Wiley & Sons.

Ismail, M. A., Armaghani, T., & Chamkha, A. J. (2018). Mixed convection and entropy generation in a lid-driven cavity filled with a hybrid nanofluid and heated by a triangular solid. *Heat Transfer Research. 49*, 1645-1665.

Ismail, M. A., Pop, L., & Chamkha, A. J. (2014). Mixed convection in a lid-driven square cavity with partial slip. *International Journal of Thermal Sciences, 82*(1), 47-61.

Jalil, M., Asghar, S., & Mushtaq, M. (2013). Analytical solutions of the boundary layer flow of power-law fluid. *Communications in Nonlinear Science and Numerical Simulation, 18*, 1143-1150.

Jingwei, Z. (2014). *Two-dimensional unsteady flow in a lid driven cavity with constant density and viscosity ME 412 Project 5.*

Kempe, T., Lennartz, M., Schwarz, S., & Fröhlich, J. (2015). Imposing the free-slip condition with a continuous forcing boundary method. *Journal of Computational Physics, 282*, 183-209.

Khanafer, K. M., & Chamkha, A. J. (1999). Mixed convection flow in a lid-driven enclosure filled with a fluid-saturated porous medium. *International Journal of Heat and Mass Transfer, 42,* 2465-2481.

Koo, J., & Kleinstreuer, C. (2004). Viscous dissipation effects in microtubes and microchannels. *International Journal of Heat and Mass Transfer, 47*, 3159-3169.

Kraus, E. B., & Businger, J. A. (1994). Atmosphere-ocean interaction. *Oxford University Press*, 362.

Kumar, K. G, Ramesh, G. K., Gireesha, B. J., & Gorla, R. S. R. (2017). Characteristics of Joule heating and viscous dissipation on three-dimensional flow of Oldroyd B nanofluid with thermal radiation. *Alexandria Eng. J.*, 1-11.

Kutluay, S., Bahadir, A. R., & Ozdes, A. (1999). Numerical solution of one-dimensional Burgers equation: explicit and exact explicit finite difference method. *Journal of Computational and Applied Mathematics, 103*, 251-261.

Lobbia, M. A. (2014). *1-D heat transfer in multilayer materials.* Los Angeles: The Aerospace Corporation.

Universiti Malaya

Lyche, T. (2009). *Matrix norms.* Centre of Mathematics for Application, Department of Informatics, University of Oslo.

Lynn, C. (2015). *Are meteorites hot or cold when they hit earth? (Intermediate).* Curious About Astronomy? http://curious.astro.cornell.edu/about-us/75-our-solar-system/comets-meteors-and-asteroids/meteorites/314-are-meteorites-hot-or-cold-when-they-hit-earth-intermediate

Mahdi, S. H., Jassim, W. H., Hamad, I. A., & Jasima, K. A. (2017). Epoxy/silicone rubber blends for voltage insulators and capacitors applications. *Energy Procedia, 119*, 501-506.

Manchanda, M., & Gangawane, K. M. (2018). Mixed convection in a two-sided lid-driven cavity containing heated triangular block for non-Newtonian power-law fluids. *International Journal of Mechanical Sciences, 144*, 235-248.

Manfred, G., Evis, K., & Giorgio, P. (2002). Solving finite difference schemes arising in trivariate option pricing. *Journal of Economic Dynamics & Control, 26*, 1499-1515.

Marchi, C. H., & Silva, A. F. C. (2002). Unidimensional numerical solution error estimation for convergent apparent order. *Numerical Heat Transfer, Part B, 42*, 167-188.

Marchi, C. H., Suero, R., & Araki, L. K. (2009). The lid-driven square cavity flow: numerical solution with a 1024 x 1024 grid. *Journal of the Brazilian Society of Mechanical Sciences and Engineering, XXXI*(3), 186-198.

Markus, B., & Mahamadi, W. (2009). The heat equation with nonlinear generalized Robin boundary conditions. *Journal of Differential Equations, 247*, 1949-1979.

Mirzakhanlari, S., Shiran, K. M., Mamourian, M., & Chamkha, A. J. (2017). Increment of mixed convection heat transfer and decrement of drag coefficient in a lid-driven nanofluid-filled cavity with a conductive rotating circular cylinder at different horizontal locations: a sensitivity analysis. *Advanced Powder Technology, 305,* 495-508.

Moffatt, H. K. (1964). Viscous and resistive eddies near a sharp corner. *Journal of Fluid Mechanics, 18*, 1-18.

Mohamed, G. (1999). The fluid mechanics of microdevices. *Journal of Fluids Engineering, 121*, 5-33.

Moshkin, N. P., & Poochinapan, K. (2009). Novel finite difference scheme for the numerical solution of two-dimensional incompressible Navier-Stokes equations. *International Journal of Numerical Analysis & Modeling, 7*(2), 321-329.

Munson, B. R., Young, D. F., & Okiishi, T. H. (2002). *Fundanmentals of fluid mechanics* (4th ed.). New York: John Wiley & Sons. Inc.

Muthukumar, S., Sureshkumar, S., Chamkha, A. J., Muthtamilselvan, M., & Prem, E. (2019). Combined MHD convection and thermal radiation of nanofluid in a lid-driven porous enclosure with irregular thermal source on vertical sidewalls. *Journal of Thermal Analysis and Calorimetry. 138*, 583-596.

Universiti Malaya

Nasrin, R., Chamkha, A. J., & Alim, M. A. (2014). Modeling of mixed convective heat transfer utilizing nanofluid in a double lid-driven chamber with internal heat generation. *International Journal of Numerical Methods for Heat & Fluid Flow, 24*, 36-57.

Oğlakkaya, F. S., & Bozkaya, C. (2018). Unsteady MHD mixed convection flow in a lid-driven cavity with a heated wavy wall. *International Journal of Mechanical Sciences, 148*, 231-245.

Qin, J. (2009). The new alternating direction implicit difference methods for the wave equations. *Journal of Computational and Applied Mathematics, 230*, 213-223.

Rahman, M., Oztop, H. F., Rahim, N., Saidur, R., & Al-Salem, K. (2011). MHD mixed convection with Joule heating effect in a lid-driven cavity with a heated semi-circular source using the finite element technique. *Numerical Heat Transfer, Part A: Applications, 60*(6), 543-600.

Ramos, J. J. (2006). Explicit finite difference methods for the EW and RLW equations. *Applied Mathematics and Computation, 179*, 622-638.

Rashad, A. M., Ismael, M., Chamkha, A. J., & Mansour, M. A. (2016). MHD mixed convection of localized heat sources in a nanofluid-filled lid-driven square cavity with partial slip. *Journal of the Taiwan Institute of Chemical Engineers, 68*, 173-186.

Rij, J. V., Ameel, A., & Harman, T. (2009). An evaluation of secondary effects on microchannel frictional and convective heat transfer characteristics. *International Journal of Heat and Mass Transfer, 52*, 2792-2801.

Sauli, Z., Taniselass, S., Ramasamy, T. K., Retnasamy, V., & Poopalan, P. (2010). No slip and free slip boundary conditions for liquid flow in obstructed straight microchannel. *Second International Conference on Computational Intelligence, Modelling and Simulation*, 565-569.

Selimefendigil, F., Oztop, H., & Chamkha A. J. (2017). Fluid-structure-magnetic field interaction in a nanofluid filled lid-driven cavity with flexible side wall. *European Journal of Mechanics - B/Fluids*. 61, 77-85.

Selimefendigil, F., & Chamkha, A. J. (2016). MHD mixed convection in a lid-driven cavity heating having a corrugated bottom wall and filled with a non-Newtonian power-law fluid under the influence of an inclined magnetic field. *Journal of Thermal Science and Engineering Applications, 8,* 021023-021023-8.

Shu, J. J., Melvin, J. B., & Chan, W. K. (2016). A new model for fluid velocity slip on a solid surface. *Soft Matter, 12*(40), 8388-8397.

Sousa, R. S., Poole, R. J., Afonso, A. M., Pinho, F. T., Oliveira, P. J., Morozov, A., & Alves M. A. (2016). Lid-driven cavity flow of viscoelastic liquids. *Journal of Non-Newtonian Fluid Mechanics, 234*, 129-138.

Tretheway, D. C., Liu, X., & Meinhart, C.D. (2002). Analysis of slip flow in microchannels. *University of California*.

Universiti Malaya

Veronique, H. R. (2004). A finite difference method to solve the forward problem in electroencephalography. *Journal of Computational and Applied Mathematics, 167*, 35-58.

Volgin, V.M., Volgina, O.V., & Davydov, A.D. (2003). Finite difference method of simulation of non-steady state ion transfer in electrochemical systems with allowance for migration. *Computational Biology and Chdemistry, 27*, 185-196.

Wang, H. (2005). Numerical studies on the split-step finite difference method for nonlinear schrodinger equation. *Applied Mathematics and Computation, 170*, 17-35.

Wu, B., & White, R. E. (2004). One implimentation variant of the finite difference method for solving ODEs/ DAEs. *Computers and Chemical Engineering, 28*, 303-309.

Wu, T. T. (1974). A cooling process according to two-temperature theory of heat conduction. *Journal of Mathematical Analysis and APplication, 45*, 23-31.

Yau, Y. H., Wong, H. F., & Ahmad, N. (2012). Numerical heat transfer study for a large rubber product. *International Journal of Heat and Mass Transfer, 55*, 2879–2888.

Yirka, B. (2017). *Meteorite impact casued the highest temperature ever recorded on Earth's surface*. Astronomy & Space. https://phys.org/news/2017-09-meteorite-impact-highest-temperature-earth.html

Zhang, T., Jia, L., Yang, L., & Jaluria, Y. (2010). Effect of viscous heating on heat transfer performance in microchannel slip. *International Journal of Heat and Mass Transfer, 53*, 4927-4934.

Zhang, Y. (2009). A finite difference method for fractional partial differential equation. *Applied Mathematics and Computation, 215*, 524-529.

Zhao, J., Matt, D., & Robert, M.C. (2007). Compact finite difference method for American option pricing. *Journal of Computational and Applied Mathematics, 206*, 306-321.

Zhao, P. (1996). An efficient computer program for wavefront calculation by the finite-difference method. *Computer and Geosciences, 22*, 239-251.

Zhou, W., Yan, Y., Liu, X., Chen, H., & Liu, B. (2018). Lattice Boltzmann simulation of mixed convection of nanofluid with different heat sources in a double lid-driven cavity. *Int. Commun. Heat Mass, 97*, 39-46.

Universiti Malaya